Hadronic Time-Reversal Violation in Effective Field Theory

This work is part of a research program funded in part by the Stichting voor Fundamenteel Onderzoek der Materie (FOM), which is financially supported by the Nederlandse Organisatie voor Wetenschappelijk Onderzoek (NWO).

PRINTED BY: Ipskamp Drukkers, Enschede, September 2012
COVER DESIGNED BY: Ivo de Kogel

RIJKSUNIVERSITEIT GRONINGEN

Hadronic Time-Reversal Violation in Effective Field Theory

Proefschrift

ter verkrijging van het doctoraat in de
Wiskunde en Natuurwetenschappen
aan de Rijksuniversiteit Groningen
op gezag van de
Rector Magnificus, dr. E. Sterken,
in het openbaar te verdedigen op
vrijdag 19 oktober 2012
om 14.30 uur

door

Jordy de Vries

geboren op 6 december 1986
te Zwolle

Promotor:	Prof. dr. R.G.E. Timmermans
Beoordelingscommissie:	Prof. dr. E.A. Bergshoeff
	Prof. dr. U. van Kolck
	Prof. dr. E. Laenen

ISBN: 978-94-6191-407-1 Printed version
ISBN: 978-94-6191-409-5 Electronic version

Contents

Chapter 1

Introduction

1.1 The concept of time-reversal violation

It appears to be obvious that the symmetry of time reversal is badly broken in nature. In our daily lives time flows forward, not backward, and any claim for a symmetry between the two sounds absurd. When shown a film of, for example, a collapsing house, we can easily tell whether the film is played normally or reversed and we would conclude that the laws of nature possess a clear direction of time. However, important physical equations such as Newton's second law and Maxwell's equations are symmetric under the transformation $t \to -t$. The reason why we observe a direction of time is of statistical nature and has to do with initial conditions. Systems containing a large number of particles, *i.e* macroscopic systems, have a much larger probability to flow from a complicated initial state (house) to a simple final state (rubble) than the other way around. The inverse process can, in principle, occur but is extremely unlikely. Since daily life involves macroscopic systems we can have an apparent direction of time, even though the fundamental, microscopic laws of physics work both ways.

Time reversal (T) is one of three important discrete symmetries in particle physics. The other two are parity (P), which reverses spatial coordinates $\vec{x} \to -\vec{x}$, and charge conjugation (C) which interchanges particles and antiparticles. For a long time it was thought that nature is symmetric under each of these discrete symmetries separately. This belief had to be abandoned when in 1957 it was found that P was broken by the weak interaction [1, 2]. Within a decade the violation of the combined symmetry CP was observed as well [3]. What about T violation? CP violation is intrinsically linked to T violation through the CPT theorem. This theorem states that any local Lorentz invariant (obeying special relativity) quantum field theory must be symmetric under the combined transformation of C, P, and T. The theorem implies that the observation of CP violation necessarily means that T is broken, unless Lorentz invariance is violated. There exists no experimental evidence for either CPT violation or Lorentz violation and in this thesis we take the CPT theorem to hold. Direct T violation has been more difficult to measure than CP violation, but it has been observed as well [4].

One of the great successes of the Standard Model (SM) of particle physics is the description of the violation of discrete symmetries. P and C violation arise because the weak interaction couples differently to left- and right-handed fermions. CP violation is described by a complex phase in the Cabibbo-Kobayashi-Maskawa (CKM) quark-mass matrix [5], which accounts for all measured CP violation so far.

Apart from CP violation in the electroweak sector, the SM contains an additional CP-violating source in the strong interaction [6]. In the theory of strong interactions, QCD, this CP violation is parametrized by the QCD vacuum angle $\bar{\theta}$. The $\bar{\theta}$ angle is one of the fundamental SM

parameters and, currently, cannot be calculated from first principles. The unique feature of strong *CP* violation is that it is flavor-conserving, in contrast with electroweak *CP* violation which occurs dominantly in flavor-changing interactions. The archetypical flavor-conserving *CP*-violating observable is a permanent electric dipole moment (EDM). An EDM is the interaction between the spin of a particle and a static external electric field. This should be compared with the magnetic dipole moment (MDM) which is the interaction between the spin and a magnetic field. The nonrelativistic Hamiltonian is given by

$$H = -(\mu\vec{B} + d\vec{E}) \cdot \vec{\sigma}, \tag{1.1}$$

where $\vec{E}$ denotes the electric field, $\vec{B}$ the magnetic field, $\vec{\sigma}$ the particle spin, and μ and d, respectively, the particle MDM and EDM. Under a P transformation, the electric field reverses, but the magnetic field and the spin are unchanged. Under a T transformation, the electric field is unaffected, but both the magnetic field and the spin flip sign. From these properties it is clear that a nonzero EDM indicates the simultaneous violation of both P and T, and by the *CPT* theorem of *CT* and *CP*. A nonzero MDM does not violate any discrete symmetries.

The first dedicated EDM experiment was performed on the neutron in 1957 [7], finding a result consistent with zero. At the time, decades before the invention of QCD and the associated $\bar{\theta}$ term, this came as no surprise since P and T were assumed to be symmetries of the strong interaction. However, with hindsight this experiment provides the first evidence of the so-called "strong *CP* problem". The upper bound set in 1957 amounts to a bound on the QCD vacuum angle $\bar{\theta} < 10^{-4}$ (in Chapter 4 we will discuss in detail how the neutron EDM depends on $\bar{\theta}$). Nowadays, the neutron EDM bound has been improved by six orders of magnitude [8] such that the limit is now $\bar{\theta} < 10^{-10}$. The strong *CP* problem is the problem of explaining why $\bar{\theta}$ is so extremely small. Several solutions have been proposed to explain in a natural way why $\bar{\theta} = 0$, but none of them have been experimentally verified.

Although the null-measurement of EDMs requires fine-tuning in the strong interaction, this is not the case for electroweak *CP* violation. Intuitively this can be understood by noticing that electroweak *CP* violation as described by the CKM mechanism requires the participation of all three generations of particles. Since an EDM is a flavor-conserving observable, a loop diagram with at least four electroweak vertices is required to get a nonzero contribution [9]. As a consequence, the SM with $\bar{\theta} = 0$ predicts a neutron EDM six orders of magnitude smaller than the current experimental upper bound [10, 11]. This smallness is a blessing because it means that, with current experimental accuracies, EDMs are "background-free" probes of unmeasured sources of *CP* violation (they are not SM-free probes because they could still be due to a nonzero $\bar{\theta}$). That is, for the foreseeable future any nonzero EDM measurement originates either in the SM $\bar{\theta}$ term or in some new, unknown source of *CP* and T violation. Both options are of great interest, and the latter may be even more so due to another problem of the standard models of particle physics and cosmology: the universal matter/antimatter asymmetry.

The current particle content of the universe can be summarized by stating that the number of antibaryons in the universe is much smaller than the number of baryons, which is much smaller than the number of photons. In fact, there is no evidence for an appreciable amount of antimatter in the universe at all. In 1967 Sakharov identified three conditions necessary to create such an asymmetry between matter and antimatter [12]. One of these conditions is that *CP* needs to be violated. However, detailed calculations show that the amount of *CP* violation in both the electroweak [13] and the strong sector [14] is not enough to explain the current matter/antimatter asymmetry. This failure strongly hints to a new source of *CP* violation not present in the SM. EDMs are excellent probes for these sources.

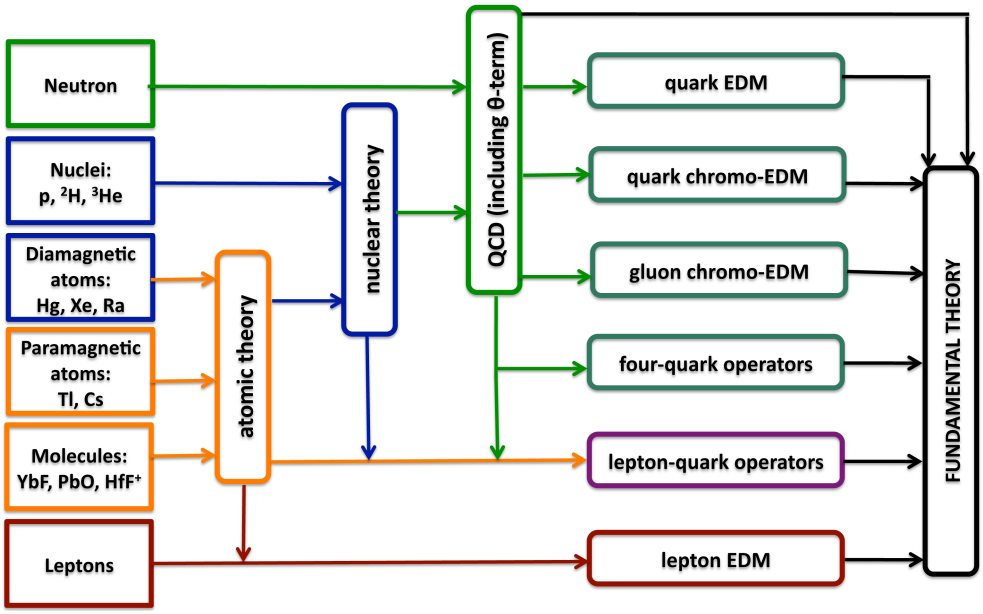

Figure 1.1: A schematic picture of the steps that need to be taken in order to connect experimental EDM results (left side) to the fundamental theory of *CP* violation (right side).

Apart from the matter/antimatter asymmetry there are additional reasons to conclude that the SM is incomplete. Examples are the lack of a dark matter candidate and, just as the strong *CP* problem, fine-tuning issues related to the Higgs mass. Many extensions of the SM, such as supersymmetry, invented to solve these problems generate, as a byproduct, much larger EDMs than the SM. EDMs are therefore complementary to direct accelerator-based searches of new physics. We will see in Chapters 4-6 that, based on dimensional arguments, current EDM searches probe energy scales up to 10^3 TeV, well beyond the reach of the LHC. These estimates can be offset by small dimensionless factors, but in any case they provide strong constraints on new physics models.

An observation of a nonzero EDM in any system would clearly be a major breakthrough. However, several EDM measurements are needed to unravel the microscopic source of *CP* violation. Theory is required to interpret any nonzero measurement in terms of more fundamental quantities like the $\bar{\theta}$ term or the quark EDM, and finally to the fundamental, microscopic theory of *CP* violation. This roadmap is illustrated in Fig. 1.1. Fortunately, because of its potential to discover new physics, the search for EDMs has turned into an active field of experiments on many different systems. So far, no evidence for a nonzero EDM of any particle or system has been found, but there are very stringent upper bounds. Ongoing experiments on the neutron EDM aim to improve the upper bound by one or two orders of magnitude [15]. Other experimental activity has focused on the search for EDMs of dia- and paramagnetic atoms or molecules. Diamagnetic atoms have closed electron shells and the atomic EDM is mostly sensitive to the nuclear EDM and *CP*-violating interactions between electrons and the nucleus. The bound on the EDM of the diamagnetic atom ^{199}Hg provides the best current limit on the proton EDM [16, 17]. Paramagnetic atoms, on the other hand, have an unpaired electron and the atomic EDM is mainly sensitive to the electron EDM. For some years the best electron EDM limit came from a measurement on the paramagnetic atom ^{205}Tl [18]. This limit was improved recently by setting a bound on the EDM of the molecule YbF [19].

Limits on the electron and proton EDM are inferred from atomic and molecular systems

Table 1.1: Present upper bounds (at 95% C.L.), expected accuracies of future measurements, and the Standard Model prediction with vanishing $\bar{\theta}$ angle of the EDMs of several particles. The units are $e\,\mathrm{cm}$.

System	Current limit	Expected improved limit	Standard Model ($\bar{\theta} = 0$)
electron	$1.4 \cdot 10^{-27}$ from YbF [19]	10^{-29} from ThO [23]	10^{-38} [24]
muon	$1.8 \cdot 10^{-19}$ [21]	10^{-24} [25]	10^{-36} [24]
neutron	$2.9 \cdot 10^{-26}$ [8]	10^{-28} [15]	10^{-32} [10]
^{199}Hg	$3.1 \cdot 10^{-29}$ [16]	10^{-29} [26]	10^{-33} [27]
proton	$7.9 \cdot 10^{-25}$ from ^{199}Hg [16, 17]	10^{-29} [22]	10^{-32} [10]

because the direct measurement of the EDM of a charged particle or system is difficult. An EDM measurement essentially consists in looking for a change in the precession of the spin of the system in the presence of electric and magnetic fields. A charged particle at rest in a strong electric field would quickly escape the experimental setup. This is not true for charged particles moving in a magnetic storage ring and it was realized that EDMs of charged particles could be directly measured in such a setup [20]. In its rest frame, the particle feels a strong electric field that interacts with the EDM which affects the spin precession. In this way, the strongest bound on the muon EDM has been set by the $g-2$ collaboration [21]. There are plans to use this technique to measure the EDMs of the muon, proton, deuteron, and helion (nucleus of ^{3}He atom) directly in dedicated storage rings [20, 22]. These experiments have an expected accuracy which exceeds the current neutron EDM limit by two to three orders of magnitude. One can think of measurements of the EDMs of other light nuclei such as the triton in a similar setup. Some information about the current status on EDMs of several particles is summarized in Table 1.1.

Triggered by the proposals to measure the EDMs of the proton and light nuclei directly, we focus in this thesis on the top part of Fig. 1.1. The main question we want to answer is whether it is possible to extract the fundamental *CP*-violating mechanism from these measurements. Can we separate the QCD $\bar{\theta}$ term from physics beyond the SM? If so, can we also differentiate between the various beyond-the-SM scenarios? We answer these questions by applying effective field theories.

1.2 Effective field theories

When we encounter in physics a problem with a clear separation of energy scales, it is often convenient to treat the problem in terms of an effective field theory (EFT). Very simply put, an EFT is based on the idea that physics at low energies (large distances) does not depend on details of physics at high energies (short distances) [28] (for an introduction to EFTs, see Ref. [29]). Although the SM is extremely successful there are, as mentioned above, reasons to believe that there should be additional sources of *CP* and *T* violation not contained in the SM. On the other hand, from many experiments we know that the SM works well up to, at least, the electroweak scale, such that any physics beyond the SM should originate at a scale considerably higher than that. This separation of scales suggests that we can look at the SM not as a fundamental theory of nature, but as an effective theory which is approximately correct at the electroweak scale. The SM contains only renormalizable interactions (of dimension four or less), but when seen as

an EFT the SM should be supplemented by all nonrenormalizable interactions (of dimension higher than four) allowed by the symmetry principles. This is similar to Fermi's theory of weak interaction in terms of local four-fermion operators. Although, in principle, the set of nonrenormalizable interactions is infinite, the interactions can be ordered by their dimension. The higher the dimension of the operator, the more suppressed its low-energy effects. In this way we parametrize our ignorance of the high-energy theory in a model-independent way.

A promising strategy to probe these higher-dimensional operators is to look for observables for which the SM contribution is extremely small or zero. Examples are rare processes such as $\mu \to e\gamma$ or neutrinoless double β-decay. This thesis focuses on hadronic and nuclear EDMs, which signal flavor-conserving CP violation and are insensitive to the CKM mechanism. The typical energy scale of hadronic and nuclear physics lies considerably lower than the electroweak scale. At these low energies additional complications arise due to the nonperturbative nature of QCD. We overcome this problem by applying another EFT called chiral perturbation theory (χPT). In χPT, instead of quarks and gluons, the effective degrees of freedoms are pions and nucleons (and heavier baryons) whose interactions are dictated by the symmetries of QCD and how they are (spontaneously and explicitly) broken. By extending χPT to include T violation, we end up with a chiral Lagrangian containing T-violating interactions among pions, nucleons, and photons. This Lagrangian can then be used to calculate T-violating hadronic and nuclear properties such as EDMs. A schematic picture of how T violation evolves through the different energy scales is shown in Fig. 1.2.

T violation in hadronic and nuclear systems has, of course, been studied before. These studies can globally be divided into two classes. The first class focuses on the high-energy part of T violation. These "top-down" studies look at a specific model (or classes of models) of new physics, *e.g.* supersymmetry, in which there exist new T-violating sources. The problem with this approach is that there exist a huge number of beyond-the-SM models and the parameter space of these models can be large as well. It is therefore not clear which model one should study. The advantage of the EFT approach outlined in this thesis is that it is not necessary to specify a particular model. After integrating out the heavy fields in any SM extension, their effects are absorbed in the coupling constants of the effective higher-dimensional operators that are added to the SM. If we do want to study a particular SM extension, we need to perform a matching calculation between the effective theory and the specific high-energy model.

The second class of studies has a "bottom-up" philosophy and focuses on the low-energy part of T violation. In this class one starts from a T-violating Lagrangian in terms of the relevant degrees of freedom for hadronic and nuclear systems: pions and nucleons. There are several problems with this approach. First of all, the hadronic Lagrangian considered is often not consistent with the symmetries, in particular chiral symmetry, of QCD. Second, as we will see, certain T-violating hadronic interactions which are important for EDMs are not taken into account. Finally, there is no direct link with the fundamental high-energy theory responsible for T violation. We overcome these problems by applying χPT to construct the complete T-violating hadronic Lagrangian consistent with the symmetries of QCD. An advantage of this approach is that for each source of T violation, *i.e.* the QCD $\bar{\theta}$ term and the effective higher-dimensional operators, we end up with a unique hadronic Lagrangian. Given enough observables it becomes possible to separate the various fundamental T-violating sources on the basis of the hadronic interactions that they generate.

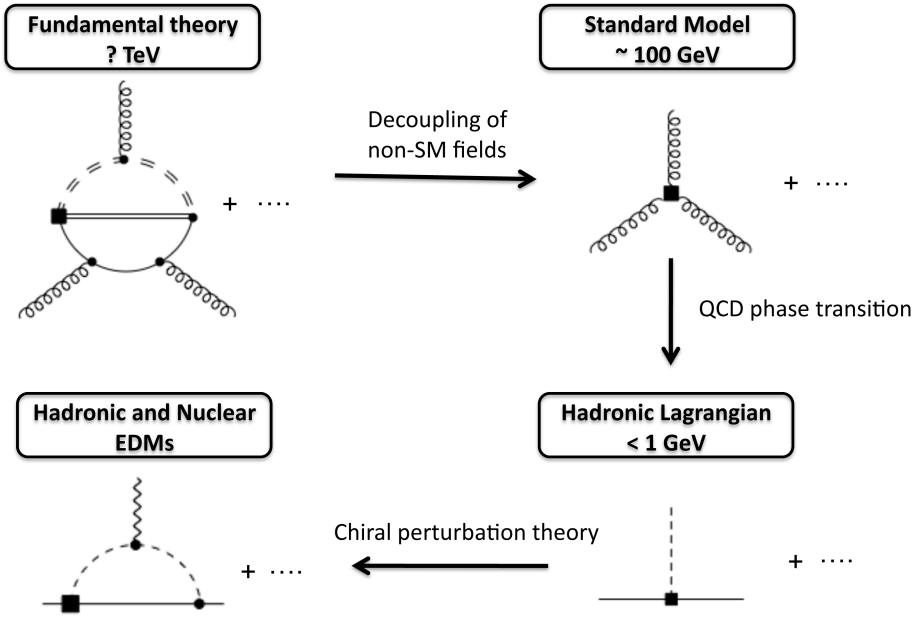

Figure 1.2: A schematic picture of how beyond-the-SM T violation is manifested at various energy scales. The square denotes a T-violating interaction and the arrows indicate the lowering of the energy scale. The top-left corner shows a loop diagram containing heavy virtual beyond-the-SM fields (denoted by double solid and dashed lines), quarks (single solid lines) and external gluons (curly lines). At the SM scale (100 GeV) such diagrams can be described by local T-violating interactions among SM fields, in this case a gluon chromo-EDM (top-right corner). By further lowering the energy at some point QCD undergoes a phase transition and T-violating interactions among pions (dashed lines) and nucleons (solid lines) appear (bottom right). These interactions induce hadronic and nuclear EDMs. In the bottom-left corner a contribution to the nucleon EDM is shown (the wavy line denotes a photon).

1.3 Outline of this thesis

This thesis can be globally divided into two parts. The first part, consisting of Chapters 2 and 3, can be seen as the theoretical fundament. In Chapter 2 we briefly review the SM, focusing on its T-violating parts. We interpret the SM as an EFT and extend it by adding higher-dimensional operators to the Lagrangian. Since EDM experiments are performed at much lower energies than the SM scale, the added operators are evolved down to this low scale. At very low energies, QCD becomes nonperturbative and the Lagrangian in terms of quarks and gluons stops being useful for calculational purposes. By extending χPT to include T violation, in Chapter 3 we recast the quark-gluon Lagrangian into a hadronic Lagrangian in terms of pions and nucleons.

The second part of this thesis consists of Chapters 4, 5, and 6 and is based on the Lagrangians derived in the first part. In Chapter 4 we study the T-violating properties of the proton and neutron, setting limits on the various T-violating sources. In Chapters 5 and 6 we extend these calculations to the lightest bound nuclei. These calculations are significantly more difficult due to the appearance of the internucleon interaction. In Chapter 5 we apply a so-called perturbative-pion approach to the deuteron T-violating form factors. In this approach one-pion exchange between nucleons is treated in perturbation theory. In Chapter 6 we relax the assumption of perturbative pions and the calculations are redone with an approach that treats one-pion exchange to all orders. In this chapter we also study the EDMs of nuclei consisting of three

nucleons: the helion (^{3}He) and the triton (^{3}H). We end with a detailed discussion of an exotic T-violating property of the spin-1 deuteron, its magnetic quadrupole moment (MQM). The results in these chapters show that measuring the EDMs and MQMs of several light nuclei would shed a lot of light on the fundamental mechanism of CP and T violation. We summarize, conclude, and give an outlook in Chapter 7. Several Appendices are devoted to technical issues.

Chapter 2

Sources of Time-Reversal Violation

2.1 Introduction

The description of CP violation in the kaon and B-meson systems is one of the many successful features of the Standard Model (SM). So far the complex phase in the CKM matrix is able to quantitatively describe all experimental results in the mesonic sectors. On the other hand, as discussed in the previous chapter, there exist a few caveats in the current knowledge of CP violation. First of all, there should theoretically be a second source of CP violation in the SM, the QCD $\bar{\theta}$ term. However, neutron EDM experiments constrain the associated $\bar{\theta}$ angle to be extremely small. This unnatural suppression of the angle demands a satisfying explanation which is currently lacking. Second, it appears that the CKM mechanism is unable to explain the matter/antimatter asymmetry, such that a successful description of the evolution of the universe requires additional sources of CP violation.

EDM measurements are good probes of new CP-violating, or equivalently T-violating ($\not{T}$), sources, because EDMs are sensitive to flavor-diagonal CP violation while the CKM mechanism causes dominantly flavor-changing CP violation. Therefore, EDMs do not suffer from a CKM background which is present for searches of new physics in mesonic systems. Here we focus mainly on the EDMs of hadronic and nuclear systems for which there does exist a SM background generated by the aforementioned $\bar{\theta}$ term, which might be very small but nonzero. This implies that a finite experimental result in any of the upcoming EDM experiments does not necessarily imply physics beyond the SM. In this thesis, the main question we want to answer is whether it is possible to extract the fundamental $\not{T}$ mechanism from hadronic and nuclear EDM measurements. To answer this question it is first necessary to identify the possible different $\not{T}$ mechanisms. This is the topic of this chapter.

We know that the SM works well all the way up to at least the electroweak scale $\sim 100\,\mathrm{GeV}$ and it is important to use this information when we study low-energy T violation. On the other hand, we have little information about physics at energies higher than the electroweak scale. Picking a specific model amounts to a theoretical bias which can be misleading. Therefore, we choose to start our analysis at the electroweak scale. At this scale we have, of course, the SM Lagrangian consisting of all renormalizable, *i.e.* dimension-four and lower, operators obeying Lorentz and the $SU(3)_c \times SU(2)_L \times U(1)_Y$ gauge symmetries. Since the SM works so well any new physics must arise at a scale considerably higher than the electroweak scale. At the electroweak scale it is possible, in the EFT spirit, to integrate out the new dynamics and the effects can be captured by adding higher-dimensional operators to the SM Lagrangian. In this chapter we identify these possible higher-dimensional interactions and estimate their size in terms of the unknown scale of new physics. In order to study their effects at low energy we bring these new

	q_L	u_R	d_R	l_L	e_R	φ
Y	$\frac{1}{6}$	$\frac{2}{3}$	$-\frac{1}{3}$	$-\frac{1}{2}$	-1	$\frac{1}{2}$

Table 2.1: Hypercharge assignment of Standard Model particles.

interactions to a scale of a few GeV where T violation is captured by interactions between light quarks, gluons, and photons (and leptons, but they are not considered in this thesis).

This chapter is organized as follows. In Sec. 2.2 we briefly review the SM focusing on the only $\not{T}$ source in the SM relevant for EDMs; the QCD $\bar{\theta}$ term. In Sec. 2.3 we list all $\not{T}$ terms at the electroweak scale up to dimension six and discuss their relevance for low-energy T violation. The typical scale of hadronic and nuclear EDMs lies way below the electroweak scale. We discuss the matching to this low scale in Sec. 2.4. We summarize the effective Lagrangian we have obtained in Sec. 2.5. At this point we are armed with an effective low-energy $\not{T}$ Lagrangian consistent with the SM symmetries in terms of light-quark, gluon, and photon fields. This Lagrangian is the starting point of this thesis from which the results in Chapters 3, 4, 5, and 6 are systematically derived.

2.2 The Standard Model

The SM of particle physics is an extremely successful and well-tested theory. Its Lagrangian is dictated by gauge symmetry, with gauge group $SU_c(3)\times SU_L(2)\times U_Y(1)$, by the matter content, three generations of leptons and quarks and one scalar doublet, and by requiring the theory to be renormalizable. Therefore, before spontaneous symmetry breaking, the SM Lagrangian is expressed in terms of all the possible dimension-four gauge-invariant operators:

$$\begin{aligned}
\mathcal{L}_{SM} &= -\frac{1}{4}G^a_{\mu\nu}G^{a\,\mu\nu} - \frac{1}{4}W^i_{\mu\nu}W^{i\,\mu\nu} - \frac{1}{4}B_{\mu\nu}B^{\mu\nu} && (2.1)\\
&\quad +\bar{q}_L i\not{D}\, q_L + \bar{u}_R i\not{D}\, u_R + \bar{d}_R i\not{D}\, d_R + \bar{l}_L i\not{D}\, l_L + \bar{e}_R i\not{D}\, e_R && (2.2)\\
&\quad +D_\mu\varphi^\dagger D^\mu\varphi + \mu^2\varphi^\dagger\varphi - \lambda(\varphi^\dagger\varphi)^2 && (2.3)\\
&\quad -\bar{q}_L Y^u\tilde{\varphi}u_R - \bar{q}_L Y^d\varphi d_R - \bar{l}_L Y^e\varphi e_R + \text{h.c.} && (2.4)\\
&\quad -\theta\frac{g_s^2}{64\pi^2}\varepsilon^{\mu\nu\alpha\beta}G^a_{\mu\nu}G^a_{\alpha\beta} - \theta_W\frac{g^2}{64\pi^2}\varepsilon^{\mu\nu\alpha\beta}W^i_{\mu\nu}W^i_{\alpha\beta} - \theta_B\frac{g'^2}{64\pi^2}\varepsilon^{\mu\nu\alpha\beta}B_{\mu\nu}B_{\alpha\beta}. && (2.5)
\end{aligned}$$

Eq. (2.1) contains the kinetic terms and self-interactions of the $SU_c(3)$, $SU_L(2)$ and $U_Y(1)$ gauge bosons, expressed in terms of the gauge-covariant gluon field strength $G^a_{\mu\nu}$ and of the field strengths of the $SU_L(2)$ and hypercharge gauge bosons,

$$\begin{aligned}
G^a_{\mu\nu} &= \partial_\mu A^a_\nu - \partial_\mu A^a_\mu - g_s f^{abc}A^b_\mu A^c_\nu,\\
W^i_{\mu\nu} &= \partial_\mu W^i_\nu - \partial_\nu W^i_\mu - g\varepsilon^{ijk}W^j_\mu W^k_\nu, \qquad B_{\mu\nu} = \partial_\mu B_\nu - \partial_\nu B_\mu, && (2.6)
\end{aligned}$$

where f^{abc} and ε^{ijk} are the $SU_c(3)$ and $SU_L(2)$ structure constants and g_s and g, respectively, the $SU_c(3)$ and $SU_L(2)$ coupling constant.

The left-handed fields q_L and l_L are doublets of quark and lepton fields

$$q_L = \begin{pmatrix} u_L \\ d_L \end{pmatrix}, \qquad l_L = \begin{pmatrix} \nu_L \\ e_L \end{pmatrix}, \tag{2.7}$$

while the right-handed fields u_R, d_R and e_R are singlet under $SU(2)$. Left- and right-handed quarks are in the fundamental representation of $SU_c(3)$, with hypercharge assignments summarized in Table 2.1. Quark and lepton fields carry a generation index, which we left implicit,

running over the three generations of up-type quarks $u = (u, c, t)$, down-type quarks $d = (d, s, b)$, charged leptons $e = (e, \mu, \tau)$ and neutrinos $\nu = (\nu_e, \nu_\mu, \nu_\tau)$. The field φ denotes a doublet of scalar fields, singlet under $SU_c(3)$.

Eq. (2.2) and the first term of Eq. (2.3) contain the kinetic energy and the gauge couplings of fermions and scalars. These couplings are completely determined by gauge invariance, and they proceed through the covariant derivative

$$D_\mu = \partial_\mu - ig_s\, A^a_\mu t^a - i\frac{g}{2}\, W^i_\mu \tau^i - ig' Y B_\mu, \tag{2.8}$$

where g' is the hypercharge coupling constant, and t^a and τ^i are $SU(3)$ and $SU(2)$ generators in the representation of the field on which the derivative acts. For example, for left-handed quarks $t^a = \lambda^a/2$, with λ^a the Gell-Mann matrices, and τ^i are the Pauli matrices.

The second and third term of Eq. (2.3) are the scalar potential. For $\mu^2 > 0$, the scalar field acquires a vacuum expectation value,

$$\langle \varphi \rangle = \frac{1}{\sqrt{2}} \begin{pmatrix} 0 \\ v \end{pmatrix}, \tag{2.9}$$

with $v = \sqrt{\mu^2/\lambda}$. The Higgs boson represents fluctuations around this vacuum,

$$\varphi = \frac{1}{\sqrt{2}} U(x) \begin{pmatrix} 0 \\ v + h(x) \end{pmatrix}, \tag{2.10}$$

where $U(x)$ is an $SU(2)$ matrix, which encodes the three Goldstone bosons. The Goldstone bosons are not physical degrees of freedom and with a particular choice of gauge, the unitarity gauge, $U(x)$ can be set to one. In this gauge, the Goldstone bosons are "eaten" by the longitudinal polarizations of the massive vector bosons. We will use this gauge to discuss the structure of dimension-six operators.

After electroweak symmetry breaking (EWSB), the scalar field kinetic energy provides a mass term for the weak gauge bosons. It is convenient to express the fields W^i_μ and B_μ in terms of the physical charged $W^\pm$ fields

$$W^\pm_\mu = \frac{1}{\sqrt{2}}(W^1_\mu \mp i W^2_\mu), \tag{2.11}$$

the physical photon and Z fields

$$\begin{aligned} W^3_\mu &= \cos\theta_w Z_\mu + \sin\theta_w A_\mu, \\ B_\mu &= \cos\theta_w A_\mu - \sin\theta_w Z_\mu, \end{aligned} \tag{2.12}$$

and the couplings g and g' in terms of the proton charge $e > 0$ and of weak mixing angle θ_w

$$g = -\frac{e}{\sin\theta_w}, \qquad g' = -\frac{e}{\cos\theta_w}. \tag{2.13}$$

The next dimension-four operators one can write are the Yukawa couplings of the fermions to the scalar boson in Eq. (2.4), which, after EWSB, generate the quark and lepton masses. In Eq. (2.4) we denote $\tilde{\varphi}^I = \varepsilon^{IJ}(\varphi^J)^*$, where ε^{IJ} is the antisymmetric tensor in two dimensions. By means of unitary transformations on the quark and lepton fields, it is always possible to render the fermion-mass matrices diagonal and real, up to a common phase. For leptons, these transformations do not leave any trace, while for quarks the price to pay for the diagonalization

of the mass matrix is that the interaction of the $W^\pm$ boson with the quarks is no longer flavor diagonal, an effect that can be obtained by replacing q_L in Eq. (2.2) by

$$q_L^r = \begin{pmatrix} u_L^r \\ V_{rs} d_L^s \end{pmatrix}, \tag{2.14}$$

where V_{rs} is the unitary Cabibbo-Kobayashi-Maskawa (CKM) matrix. For three generations of quarks, the CKM matrix has one complex phase which is responsible for the observed CP violation in the kaon and B meson systems. However, the contribution of the CKM phase to nuclear EDMs is orders of magnitude smaller than the current experimental sensitivity, and we will neglect it in the rest of the thesis. The second $\not{T}$ parameter in the SM Lagrangian is the global phase of the quark-mass matrices. It can be eliminated by an axial rotation of all the quark fields $q_L \to e^{i\rho} q_L$, $q_R \to e^{-i\rho} q_R$. Such a transformation is anomalous and its net effect is to shift the coefficients of the $\not{T}$ operators in Eq. (2.5). These operators are total derivatives, but for non-Abelian gauge fields they contribute to the action through extended field configurations, the instantons [6]. The contribution of the instantons to the actions is proportional to $\exp(-1/g_i^2)$. For QCD instantons, the coupling constant g_s is large at low energy, $g_s \approx 1$, and the instanton contribution to the action cannot be neglected. On the other hand, the electroweak coupling g is small and electroweak instantons are extremely suppressed, negligible for all practical purposes. We will neglect the terms in Eq. (2.5) containing $SU_L(2)$ and $U_Y(1)$ gauge bosons.

The dimension-four $\not{T}$ Lagrangian relevant for our study can therefore be summarized by

$$\mathcal{L}_4 = -\theta \frac{g_s^2}{64\pi^2} \varepsilon^{\mu\nu\alpha\beta} G^a_{\mu\nu} G^a_{\alpha\beta} - e^{i\rho} \left(1 + \frac{h}{v}\right) \left(\bar{u}_L M^u u_R + \bar{d}_L M^d d_R\right) + \text{h.c.}, \tag{2.15}$$

where $\varepsilon^{\mu\nu\alpha\beta}$ is the totally antisymmetric symbol in four dimensions ($\varepsilon^{0123} = 1$) and M^u and M^d are the diagonal quark-mass matrices.

In the last forty years, the SM has successfully passed the test of numerous experiments. In the CP-even sector, for a long time, the only ingredient that had yet to be directly observed was the Higgs boson. This situation changed when recently a particle consistent with the Higgs boson was discovered at the LHC [30]. More tests are needed to verify that this particle is indeed the long-sought Higgs boson.

Our work focuses on electric dipole moments (EDMs) which signal $\not{T}$ in the flavor-diagonal sector and are insensitive to the phase of the CKM matrix. Current bounds on the neutron EDM constrain the QCD vacuum angle to be unnaturally small, $\bar{\theta} \lesssim 10^{-10}$ [31]. It is therefore possible that $\not{T}$ operators of higher dimension are competitive with the $\bar{\theta}$ term. These higher-dimensional operators eventually need to be linked to an underlying ultraviolet complete theory. Because we focus on $\not{T}$ physics, we denote the scale characteristic of this theory by $M_{\not{T}}$. Well below the scale $M_{\not{T}}$ we expect $\not{T}$ effects to be captured by the lowest-dimension interactions among SM fields that respect the theory's gauge symmetry [32, 33, 34, 35, 36]. In general, operators of dimension $(4+n)$ at the SM scale M_W, where M_W is the mass of the W boson, are suppressed by powers of $M_{\not{T}}^{-n}$. In the next section we list the relevant operators of dimension six.

2.3 Dimension-six operators at the electroweak scale

In Ref. [36] all operators in terms of SM fields and obeying the SM symmetries up to dimension six have been constructed. There is only one gauge-invariant dimension-five operator [37]. It violates lepton number conservation and, after EWSB, gives rise to neutrino masses and mixing. Since we are interested in $\not{T}$ in strongly interacting systems we ignore this operator.

Following Ref. [36], we organize the dimension-six operators according to their field content: two gauge bosons and two scalars (XX$\varphi\varphi$), two fermions, a scalar, and a vector boson ($qq\varphi$X), three vector bosons (XXX), two quarks and two scalars ($qq\varphi\varphi$), and four quarks ($qqqq$). We ignore (semi-)leptonic operators.

At the electroweak scale the dimension-six operators relevant for our goals are

$$\begin{aligned}
\mathcal{L}_{6,\,\mathrm{XX}\varphi\varphi} &= -\left(\theta' \frac{g_s^2}{32\pi^2}\varepsilon^{\mu\nu\alpha\beta}\, G^a_{\mu\nu}G^a_{\alpha\beta} + \theta'_W \frac{g^2}{32\pi^2}\varepsilon^{\mu\nu\alpha\beta}\, W^i_{\mu\nu}W^i_{\alpha\beta} + \theta'_B \frac{g'^2}{32\pi^2}\varepsilon^{\mu\nu\alpha\beta}\, B_{\mu\nu}B_{\alpha\beta}\right)\frac{\varphi^\dagger\varphi}{v^2} \\
&\quad +\theta'_{WB}\frac{gg'}{32\pi^2}\varepsilon^{\mu\nu\alpha\beta}\, W^i_{\mu\nu}B_{\alpha\beta}\frac{\varphi^\dagger\tau^i\varphi}{v^2} - 2\frac{\varphi^\dagger\varphi}{v^2}\left(\bar q_L Y'^u\tilde\varphi u_R + \bar q_L Y'^d\tilde\varphi d_R\right), \qquad (2.16)\\
\mathcal{L}_{6,\,qq\varphi X} &= -\frac{1}{\sqrt{2}}\bar q_L\sigma^{\mu\nu}\tilde\Gamma^u\lambda^a\frac{\tilde\varphi}{v}\,u_R G^a_{\mu\nu} - \frac{1}{\sqrt{2}}\bar q_L\sigma^{\mu\nu}\tilde\Gamma^d\lambda^a\frac{\varphi}{v}\,d_R G^a_{\mu\nu} \\
&\quad -\frac{1}{\sqrt{2}}\bar q_L\sigma^{\mu\nu}\left(\Gamma^u_B B_{\mu\nu} + \Gamma^u_W\boldsymbol{\tau}\cdot\mathbf{W}_{\mu\nu}\right)\frac{\tilde\varphi}{v}\,u_R \\
&\quad -\frac{1}{\sqrt{2}}\bar q_L\sigma^{\mu\nu}\left(\Gamma^d_B B_{\mu\nu} + \Gamma^d_W\boldsymbol{\tau}\cdot\mathbf{W}_{\mu\nu}\right)\frac{\varphi}{v}d_R + \mathrm{h.c.}\,, \qquad (2.17)\\
\mathcal{L}_{6,\,\mathrm{XXX}} &= \frac{d_W}{6}f^{abc}\varepsilon^{\mu\nu\alpha\beta}G^a_{\alpha\beta}G^b_{\mu\rho}G^{c\,\rho}_{\nu} + \frac{d_{W,\mathrm{weak}}}{6}\varepsilon^{ijk}\varepsilon^{\mu\nu\alpha\beta}W^i_{\alpha\beta}W^j_{\mu\rho}W^{k\,\rho}_{\nu}, \qquad (2.18)\\
\mathcal{L}_{6,\,qq\varphi\varphi} &= \Xi\,\bar u_R\gamma^\mu d_R\left(\tilde\varphi^\dagger i D_\mu\varphi\right) + \mathrm{h.c.}, \qquad (2.19)\\
\mathcal{L}_{6,\,qqqq} &= \Sigma_1\left(\bar q^J_L u_R\right)\,\varepsilon_{JK}\,\left(\bar q^K_L d_R\right) + \Sigma_8\left(\bar q^J_L\lambda^a u_R\right)\,\varepsilon_{JK}\,\left(\bar q^K_L\lambda^a d_R\right) + \mathrm{h.c.} \qquad (2.20)
\end{aligned}$$

The coefficients of the operators in Eqs. (2.16)-(2.20) are all proportional to $M_{\not T}^{-2}$.

In principle there are additional $\not T$ operators not listed here. These operators involve at least two generations of quark fields and are not flavor conserving. Such operators will have little effect on hadronic EDMs because they require additional weak interactions to make them flavor diagonal. Their low-energy EDM contributions are suppressed with respect to those in Eqs. (2.16-2.20) by the electroweak gauge coupling in the combination $g^2/(4\pi)^2 = \alpha_{\mathrm{w}}/4\pi \simeq 10^{-3}$ and off-diagonal CKM elements. Flavor-changing operators are important for experiments such as LHCb where flavor-changing $\not T$ observables are measured in, for example, heavy-meson decays. It would be interesting to study these effects simultaneously, starting from the most general dimension-six operators at the electroweak scale. However, this is beyond the scope of this thesis and we focus on flavor-diagonal $\not T$ terms only.

The angles θ', $\theta'_{W,\,B,\,WB}$, and the Yukawa couplings $Y'^{u,d}$ scale as

$$\theta', \theta_{W,\,B,\,WB} = \mathcal{O}\left(\frac{v^2}{M_{\not T}^2}\right), \qquad Y'^{u,d} = \mathcal{O}\left(\frac{v^2}{M_{\not T}^2}\right). \qquad (2.21)$$

Eq. (2.16) is closely reminiscent of Eqs. (2.4) and (2.5). Indeed, for the first three operators and the Yukawa couplings, one can rewrite $2\varphi^\dagger\varphi/v^2 = 1 + (2\varphi^\dagger\varphi/v^2 - 1)$. The piece that does not contain the Higgs boson can be absorbed in a redefinition of the couplings θ, $\theta_{W,B}$, and $Y^{u,d}$ in Eqs. (2.4) and (2.5). In some sense this aggravates the strong *CP* problem since even if the "bare" QCD parameter is tuned to zero, we need to explain why the electroweak corrections are small as well. Only the operator θ_{WB} obtains after EWSB a nontopological piece without a Higgs boson [34]

$$i\theta_{WB}\,\varepsilon^{\mu\nu\alpha\beta}W^+_\mu W^-_\nu\left(\cos\theta_w F_{\alpha\beta} - \sin\theta_w Z_{\alpha\beta}\right), \qquad (2.22)$$

in terms of physical field strengths. These terms can contribute through loop diagrams to quark electric, chromo-electric, and weak dipole moments which will be introduced shortly. An example

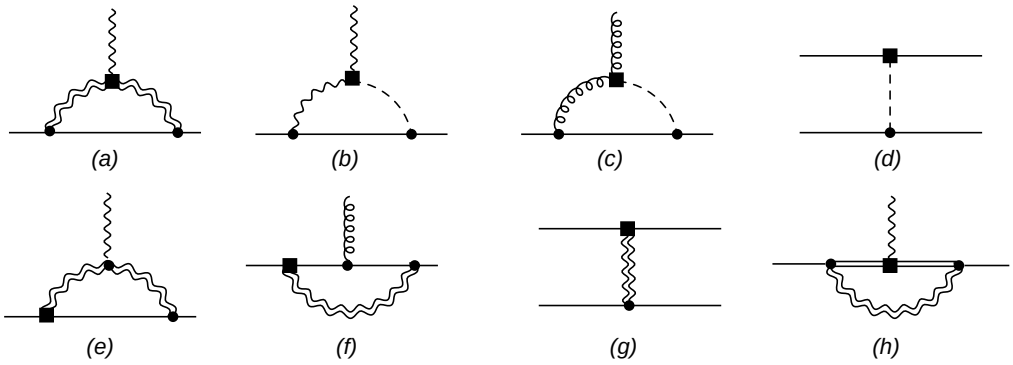

Figure 2.1: Some examples of tree-level and one-loop diagrams involving heavy gauge or scalar bosons that induce quark (C)EDMs and $\not{T}$ four-quark operators. Single (double) straight lines denote light (heavy) quark propagators, single wiggly lines photon propagators, double wiggly lines W or Z propagators, curly lines gluon propagators, and dashed lines scalar field propagators. The square denotes a $\not{T}$ vertex originating in one of the effective operators discussed in the text. The circles denotes SM T-conserving vertices. These diagrams represent only a few possibilities of the complete set of diagrams.

of such a loop diagrams is depicted in Diagram 2.1(a). Such contributions are suppressed by $\alpha_w/4\pi$ [34] and can be absorbed into the coupling constants of the various dipole moments.

The remainder of the terms in Eq. (2.16) then include operators with at least one Higgs boson. In the unitarity gauge,

$$\begin{aligned}\mathcal{L}_{6,\,\mathrm{XX}\varphi\varphi} &= -\Big\{\frac{h}{64\pi^2 v}\varepsilon^{\mu\nu\alpha\beta}(g_s^2\theta'\,G^a_{\mu\nu}G^a_{\alpha\beta}+g^2\theta'_W\,W^i_{\mu\nu}W^i_{\alpha\beta}\\ &\quad +g'^2\theta'_B\,B_{\mu\nu}B_{\alpha\beta}+gg'\theta_{WB}\,W^3_{\mu\nu}B_{\alpha\beta})\\ &\quad +\frac{h}{\sqrt{2}}\left(1+\frac{h}{v}\right)\left(\bar{u}_L Y'^u u_R+\bar{d}_L Y'^d d_R\right)\Big\}2\left(1+\frac{h}{2v}\right). \qquad (2.23)\end{aligned}$$

The first two lines of Eq. (2.23) contain $\not{T}$ interactions of the Higgs boson to two gluons, two photons, or two weak bosons. At low energy the Higgs is integrated out, and these interactions again result in loop corrections to the quark electric, chromo-electric, and weak dipole moments. Such loop corrections are shown in Diagrams 2.1(b,c). The Yukawa couplings $Y'^{u,d}$ in the third line of Eq. (2.23) are complex matrices in flavor space. The imaginary part generates flavor-diagonal and flavor-changing $\not{T}$ Higgs-quark interactions. At tree level, $\not{T}$ Higgs-quark interactions generate $\not{T}$ four-quark operators as depicted in Diagram 2.1(d). Since the Higgs boson couples to the mass, the contribution to operators that only contain light flavors are suppressed not only by two powers of $M_{\not{T}}$, but also by the ratio of the quark mass to the Higgs vacuum expectation value. Such operators are effectively dimension seven and we neglect them.

In the most general case, the couplings in Eq. (2.17) $\Gamma^u_{B,W}$, $\Gamma^d_{B,W}$, $\tilde{\Gamma}^u$, and $\tilde{\Gamma}^d$ are 3×3 complex-valued matrices. Since these operators flip the chirality of the quark field, we assume these matrices to be proportional to the Yukawa coupling in the SM Lagrangian

$$\Gamma^u_{W(B)} = \mathcal{O}\left(g^{(\prime)}\delta_u^{(\prime)}\frac{vY^u}{M^2_{\not{T}}}\right),\quad \Gamma^d_{W(B)} = \mathcal{O}\left(g^{(\prime)}\delta_d^{(\prime)}\frac{vY^d}{M^2_{\not{T}}}\right), \qquad (2.24)$$

$$\tilde{\Gamma}^u = \mathcal{O}\left(4\pi\tilde{\delta}_u\frac{vY^u}{M^2_{\not{T}}}\right),\quad \tilde{\Gamma}^d = \mathcal{O}\left(4\pi\tilde{\delta}_d\frac{vY^d}{M^2_{\not{T}}}\right), \qquad (2.25)$$

where $\tilde{\delta}_{u,d}$ and $\delta^{(\prime)}_{u,d}$ are dimensionless constants that parameterize any deviation from this assumption and they contain information on beyond-the-SM physics.

After EWSB, the operators in Eq. (2.17) can be expressed in terms of dipole moment operators,

$$\begin{aligned}\mathcal{L}_{qq\varphi X} &= -\frac{1}{2}\bar{q}_L\sigma^{\mu\nu}\left(\tilde{\Gamma}_0+\tilde{\Gamma}_3\tau_3\right)\lambda^a q_R\, G^a_{\mu\nu} - \frac{1}{2}\bar{q}_L\sigma^{\mu\nu}\left(\Gamma_0+\Gamma_3\tau_3\right) q_R\, F_{\mu\nu} \\ &\quad -\frac{1}{2}\bar{q}_L\sigma^{\mu\nu}\left(\Gamma_{Z\,0}+\Gamma_{Z\,3}\tau_3\right) q_R\, Z_{\mu\nu} \\ &\quad -\frac{1}{\sqrt{2}}\bar{d}_L\sigma^{\mu\nu}\Gamma^u_W u_R\, W^+_{\mu\nu} - \frac{1}{\sqrt{2}}\bar{u}_L\sigma^{\mu\nu}\Gamma^d_W d_R\, W^-_{\mu\nu} + \text{h.c.} \end{aligned} \tag{2.26}$$

where, for notational convenience, we grouped the right-handed up and down-type quark in a doublet q_R. The couplings Γ are complex-valued matrices in flavor space. They are linear combination of the matrices in Eq. (2.17),

$$\Gamma_{0,3} = \frac{1}{2}\left(\left(\Gamma^u_B \pm \Gamma^d_B\right)\cos\theta_W + \left(\Gamma^u_W \mp \Gamma^d_W\right)\sin\theta_W\right) \tag{2.27}$$

$$\Gamma_{Z\,0,3} = \frac{1}{2}\left(\left(\Gamma^u_W \mp \Gamma^d_W\right)\cos\theta_W - \left(\Gamma^u_B \pm \Gamma^d_B\right)\sin\theta_W\right), \tag{2.28}$$

and

$$\tilde{\Gamma}_{0,3} = \frac{1}{2}\left(\tilde{\Gamma}^u \pm \tilde{\Gamma}^d\right), \tag{2.29}$$

where the relations (2.27) and (2.29) are understood to be valid at a renormalization scale $\mu \approx M_W$.

The first two operators in Eq. (2.26) are the most interesting for low-energy applications. The imaginary part of the diagonal entries of $\Gamma_{0,3}$ and $\tilde{\Gamma}_{0,3}$ generates the quark electric and chromo-electric dipole moments (qEDM and qCEDM). The nondiagonal entries are also of considerable interest, since they produce flavor-changing neutral currents. In the *CP*-odd sector, for example, the *uc* entries were found to be the least constrained dimension-six operators that contribute to the recently observed *CP* violation in charm decays [38]. Since the flavor-changing operators contribute to nuclear EDMs only via additional loops involving weak-boson exchange, their contributions are suppressed by $\alpha_w/4\pi$ and off-diagonal CKM elements. We neglect these operators. The remaining three operators in Eq. (2.26) are weak dipole moments. Their contributions to the qEDM and qCEDM, via loops such as those in 2.1(e,f), are also suppressed by $\alpha_w/4\pi$. Weak dipole moments generate through tree-level diagrams dimension-seven four-quark operators containing one derivative. At low energies the effects of such operators are additionally suppressed by Qm_q/M_W^2 where Q is the energy exchanged by the quarks. For our purposes we can neglect such terms.

The first operator in Eq. (2.18) is the Weinberg three-gluon operator [33] which can be interpreted as the gluon chromo-electric dipole moment (gCEDM) [39]. Similarly, the second operator is the W boson weak-electric dipole moment. After ESWB, this operator generates interactions containing at least two heavy gauge bosons [34], which can contribute to quark (C)EDMs through loop diagrams like 2.1(a). Again these contributions are suppressed by $\alpha_w/4\pi$ [34] and we neglect the weak-electric dipole moment of the W boson. We keep only

$$\mathcal{L}_{ggg} = \frac{d_W}{6} f^{abc}\varepsilon^{\mu\nu\alpha\beta} G^a_{\alpha\beta} G^b_{\mu\rho} G^{c\,\rho}_{\nu}. \tag{2.30}$$

The coupling constant in Eq. (2.30) is proportional to two inverse powers of the new physics scale $M_{\not T}$

$$d_W = \mathcal{O}\left(4\pi \frac{w}{M_{\not T}^2}\right), \tag{2.31}$$

with w a dimensionless constant.

The next class of dimension-six operators consists of operators containing a quark bilinear and two scalars. They are shown in Eq. (2.19), where we limited ourselves to the flavor-diagonal case. Ξ is a diagonal complex 3×3 matrix. After EWSB only the bosonic part of the derivative survives and Eq. (2.19) can be written as

$$\begin{aligned} \mathcal{L}_{6,\,qq\varphi\varphi} &= g\frac{\mathrm{Re}[\Xi]v^2}{2\sqrt{2}}\left(W_\mu^+ \bar{u}_R\gamma^\mu d_R + W_\mu^- \bar{d}_R\gamma^\mu u_R\right) \\ &\quad + ig\frac{\mathrm{Im}[\Xi]v^2}{2\sqrt{2}}\left(W_\mu^+ \bar{u}_R\gamma^\mu d_R - W_\mu^- \bar{d}_R\gamma^\mu u_R\right), \end{aligned} \tag{2.32}$$

in terms of the physical positively (negatively) charged W_μ^+ (W_μ^-) boson. Contrary to the operators in Eq. (2.17), the operators in Eq. (2.32) do not change chirality and we do not expect them to be proportional to the quark mass, so we parameterize

$$\Xi = \mathcal{O}\left((4\pi)^2 \frac{\xi}{M_{\not T}^2}\right). \tag{2.33}$$

At low energy, after we integrate out the W boson, see Diagram 2.1(g), the imaginary part of Ξ contributes to $\not T$ four-quark operators, which are particularly interesting because they are not suppressed by the light-quark mass [40]. As detailed in the next section, $\mathrm{Im}[\Xi]$ generates four-quark operators of the same importance as the four-quark operators that are generated directly at the electroweak scale, which we introduced in Eq. (2.20).

The couplings $\Sigma_{1,8}$ in Eq. (2.20) are 3×3, diagonal, complex matrices, and ε^{IJ} is the antisymmetric Levi-Civita tensor in two dimensions. The four-quark coupling scales as

$$\Sigma_{1,8} = \mathcal{O}\left(\frac{(4\pi)^2\sigma_{1,8}}{M_{\not T}^2}\right), \tag{2.34}$$

where $\sigma_{1,8}$ are dimensionless constants. Just as in Eq. (2.32) there is no mass enhancement for heavy-quark operators. The operators in Eq. (2.20) are not affected by EWSB. For later convenience, we rewrite Eq. (2.20) in terms of quark doublets $q = q_L + q_R$, and focus on the $\not T$ terms only,

$$\begin{aligned} \mathcal{L}_{6,\,qqqq} &= \frac{1}{4}\mathrm{Im}\Sigma_1\left(\bar{q}q\,\bar{q}i\gamma^5 q - \bar{q}\boldsymbol{\tau}q\cdot\bar{q}\boldsymbol{\tau}i\gamma^5 q\right) \\ &\quad + \frac{1}{4}\mathrm{Im}\Sigma_8\left(\bar{q}\lambda^a q\,\bar{q}i\gamma^5\lambda^a q - \bar{q}\boldsymbol{\tau}\lambda^a q\cdot\bar{q}\boldsymbol{\tau}i\gamma^5\lambda^a q\right). \end{aligned} \tag{2.35}$$

2.4 Matching onto the QCD scale

The dimension-four and -six $\not T$ Lagrangian relevant for the calculation of hadronic and nuclear EDMs is summarized in Eqs. (2.15), (2.23), (2.26), (2.32), and (2.35). For low-energy applications, it is important to evolve the $\not T$ Lagrangian from the electroweak scale down to the

typical hadronic scale $\mu \sim M_{QCD} \approx 1$ GeV. In the process, one has to integrate out the effects of heavy SM particles [34, 41, 42], and, at the same time, evaluate the running the coupling constants and account for the possible mixing of the dimension-six operators [39, 43, 44, 45] through renormalization group equations (RGE). A detailed account of the matching and evolution of the complete dimension-six $\not{T}$ Lagrangian is beyond the scope of this work. Here we limit ourselves to tree-level matching onto operators involving only light, *i.e.* up and down, quarks. A full calculation including QCD corrections is work in progress. Being interested in EDMs of hadrons consisting of the lightest two quarks only, we do not take into account the strange quark although its mass lies below the QCD scale. All work in this thesis can straightforwardly be extended to include the effects of the strange quark. From now on q denotes the light-quark doublet (and similarly u and d the up and down quark).

We start from the dimension-four Lagrangian. At low energy we keep only the light quark, gluon, and photon kinetic terms,

$$\mathcal{L}_{\rm cl} = -\frac{1}{4}\left(G^a_{\mu\nu}G^{a\,\mu\nu} + F_{\mu\nu}F^{\mu\nu}\right) + \bar{q}\left(i\partial\!\!\!/ + \frac{g_s}{2}A\!\!\!/^a\lambda^a\right)q. \tag{2.36}$$

We can neglect the effects of the Higgs and the heavy quarks to rewrite Eq. (2.15) as

$$\mathcal{L}_4 \;=\; -e^{i\rho}\bar{q}_L M q_R - e^{-i\rho}\bar{q}_R M q_L - \theta\frac{g_s^2}{64\pi^2}\varepsilon^{\mu\nu\alpha\beta}\,G^a_{\mu\nu}G^a_{\alpha\beta}\;, \tag{2.37}$$

with

$$M = \begin{pmatrix} m_u & 0 \\ 0 & m_d \end{pmatrix} = \bar{m}\,(1-\varepsilon\tau_3)\,, \tag{2.38}$$

and the real parameters ρ and $m_{u,d}$, or alternatively

$$\bar{m} = \frac{m_u + m_d}{2}, \qquad \varepsilon = \frac{m_d - m_u}{m_u + m_d}. \tag{2.39}$$

The $\not{T}$ parameters θ and ρ are not independent and $\not{T}$ observables only depend on $\bar{\theta} = \theta + 2\rho$. For a χPT treatment, it is more convenient to eliminate the θ term with an axial $U(1)$ rotation on the quark field, moving all $\not{T}$ to the quark-mass term [46]. After vacuum alignment the QCD $\bar{\theta}$ term becomes [47]

$$\mathcal{L}_4 \;=\; \bar{m}r(\bar{\theta})\bar{q}q - \varepsilon\bar{m}\,r^{-1}(\bar{\theta})\bar{q}\tau_3 q - m_*\sin\bar{\theta}\,r^{-1}(\bar{\theta})\bar{q}i\gamma^5 q, \tag{2.40}$$

where we introduced the reduced quark mass

$$m_* = \frac{m_u m_d}{m_u + m_d} = \frac{\bar{m}}{2}(1-\varepsilon^2), \tag{2.41}$$

and $r(\bar{\theta})$ is a function that goes to 1 in the limit of small $\bar{\theta}$,

$$r(\bar{\theta}) \;=\; \left(\frac{1+\varepsilon^2\tan^2\frac{1}{2}\bar{\theta}}{1+\tan^2\frac{1}{2}\bar{\theta}}\right)^{1/2} \approx 1 + \mathcal{O}(\bar{\theta}^2). \tag{2.42}$$

The terms in Eq. (2.36) are invariant under a global $SU(2)\times SU(2) \sim SO(4)$ chiral transformation

$$q \to \exp\left[i\boldsymbol{\theta}_V\cdot\boldsymbol{t} + i\boldsymbol{\theta}_A\cdot\boldsymbol{x}\right]q, \tag{2.43}$$

where $\boldsymbol{\theta}_{V,A}$ are real parameters and

$$\boldsymbol{t} = \boldsymbol{\tau}/2, \qquad \boldsymbol{x} = \gamma_5\boldsymbol{\tau}/2, \tag{2.44}$$

are the group generators. The symmetry is explicitly broken by the terms in Eq. (2.40). The way these terms break the $SO(4)$ symmetry is important and we keep track of this by writing the symmetry breaking terms as components of $SO(4)$ vectors and tensors. We will come back to this in detail the next chapter. We rewrite Eq. (2.40) as

$$\mathcal{L}_4 \;=\; \bar{m} r(\bar{\theta}) S_4 - \varepsilon \bar{m}\, r^{-1}(\bar{\theta}) P_3 - m_* \sin\bar{\theta}\, r^{-1}(\bar{\theta}) P_4 \;, \tag{2.45}$$

where we introduced two $SO(4)$ vectors

$$S = \begin{pmatrix} -i\bar{q}\gamma^5 \boldsymbol{\tau} q \\ \bar{q} q \end{pmatrix}, \qquad P = \begin{pmatrix} \bar{q}\boldsymbol{\tau} q \\ i\bar{q}\gamma^5 q \end{pmatrix}. \tag{2.46}$$

From Eq. (2.45), we see that the quarks have obtained an imaginary mass proportional to $\sin\bar{\theta}$. It is clear that a nonzero value of $\bar{\theta}$ causes $\not{P}\not{T}$, since P_4 is a Lorentz pseudoscalar. Moreover, isospin violation from the quark-mass difference transforms as another component, P_3, of the *same* $SO(4)$ vector. This implies that isospin violation coming from the quark-mass difference is closely linked to $\not{P}\not{T}$ coming from the $\bar{\theta}$ term. The low-energy implications of this link have been studied in detail in Ref. [48]. The most important example of this connection is discussed in Sec. 3.3.2.

For the construction of $\not{T}$ electromagnetic operators in the chiral Lagrangian it is necessary to consider the chiral properties of the T-conserving electromagnetic couplings of the quarks. The quark-photon Lagrangian is

$$\mathcal{L}_e \;=\; -eA_\mu \bar{q}_L \gamma^\mu Q q_L - eA_\mu \bar{q}_R \gamma^\mu Q q_R = -eA_\mu \left(\frac{I^\mu}{6} + \frac{1}{2} T^\mu_{34} \right), \tag{2.47}$$

where Q is the quark-charge matrix

$$Q = \frac{1}{6} + \frac{1}{2}\tau_3. \tag{2.48}$$

Eq. (2.47) contains a chiral-invariant piece I^μ and an antisymmetric $SO(4)$ tensor

$$I^\mu = \bar{q}\gamma^\mu q, \qquad T^\mu = \begin{pmatrix} \varepsilon_{ijk}\bar{q}\gamma^\mu\gamma^5\tau_k q & \bar{q}\gamma^\mu\tau_i q \\ -\bar{q}\gamma^\mu\tau_i q & 0 \end{pmatrix}. \tag{2.49}$$

We now turn to the dimension-six Lagrangian. As explained above, the operators in Eq. (2.16) either can be absorbed in the $\bar{\theta}$ term or they contribute to the quark (C)EDMs. The light-flavor components of the dipole operators in Eq. (2.26) match onto the light-quark qEDM and qCEDM.

$$\mathcal{L}_{6,\,qqX} \;=\; -\frac{1}{2}\,\bar{q}\, i\sigma^{\mu\nu}\gamma^5 \left(d_0 + d_3\tau_3\right) q\, F_{\mu\nu} - \frac{1}{2}\,\bar{q}\, i\sigma^{\mu\nu}\gamma^5 \left(\tilde{d}_0 + \tilde{d}_3\tau_3\right) \lambda^a q\, G^a_{\mu\nu}, \tag{2.50}$$

where, at tree level,

$$d_0 = \mathrm{Im}(\Gamma_0)_{11}, \qquad d_3 = \mathrm{Im}(\Gamma_3)_{11}, \tag{2.51}$$

and similar relations hold for $\tilde{d}_{0,3}$. From Eqs. (2.24, 2.25) we see that d_i and $\tilde{d}_i$ depend linearly on the light-quark mass. The heavier-quark components of the EDM and CEDM operators in Eq. (2.26) correct Eq. (2.51) at the loop level. Since these operators depend on the heavy-quark mass, one might think that the top q(C)EDM gives important contribution to light q(C)EDMs. A heavy q(C)EDM induces light q(C)EDMs through weak interactions, see Diagram 2.1(h). This contribution is suppressed by a typical factor [42]

$$(d_q,\, \tilde{d}_q) \;=\; \left(\frac{\alpha_{\rm em}}{4\pi}\right) \left(\frac{|V_{qQ}|^2}{\sin^2\theta_w}\right) \frac{m_q m_Q}{M_W^2} f(m_q, m_Q)(d_Q,\, \tilde{d}_Q), \tag{2.52}$$

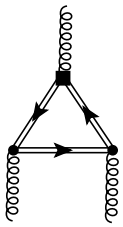

Figure 2.2: A diagram that induces a gluon chromo-EDM due to integrating out a heavy quark chromo-EDM. The notation is as in Fig. 2.1.

where $q = u$ or d, $Q = b$ or t, V_{Qq} is the associated CKM element, and $f(m_q, m_Q) = \mathcal{O}(1)$. For example, in the case of $Q = t$ and $q = d$ (such that $(d_t,\, \tilde{d}_t) \simeq 10^5 (d_d,\, \tilde{d}_d)$) the induced light-quark (C)EDM is suppressed by seven orders of magnitude compared to Eq. (2.51), due to the smallness of $V_{td} \sim 7 \cdot 10^{-3}$. A larger effect comes from integrating out a heavy qCEDM between external gluons, see Fig. 2.2. This induces a threshold correction to the gCEDM [39] of order

$$\delta d_W(m_Q) \;=\; \frac{g_s^2(m_Q)}{32\pi^2}\frac{\tilde{d}_Q}{m_Q}. \tag{2.53}$$

The induced gCEDM will, in turn, mix into a light qCEDM through QCD RGE. The resulting qCEDM is, however, still suppressed by three orders of magnitude compared to Eq. (2.51) [41]. We conclude that, despite the mass enhancement of heavy q(C)EDMs, their low-energy effects can be safely neglected for our purposes.

The gCEDM in Eq. (2.30) and the four-quark operators in Eq. (2.35) match onto themselves. Through QCD RGE they will mix into the q(C)EDMs [39, 43, 44, 45]. Since the four-quark operators are not dependent on the quark mass, we ignore the operators involving heavy quarks.

To infer the low-energy effects of the operator in Eq. (2.32), we need to integrate out the heavy gauge boson. The largest effect comes from an exchange, shown in Diagram 2.1(g), of a W boson between light quarks giving rise to the effective $\not{T}$ operator

$$\begin{aligned}\mathcal{L}_{\rm LR} &= i\mathrm{Im}[\Xi]\frac{g^2v^2}{4M_W^2}V_{ud}\left(\bar{u}_R\gamma^\mu d_R\bar{d}_L\gamma_\mu u_L - \bar{d}_R\gamma^\mu u_R\bar{u}_L\gamma_\mu d_L\right)\\ &= i\mathrm{Im}[\Xi]V_{ud}\left(\bar{u}_R\gamma^\mu d_R\bar{d}_L\gamma_\mu u_L - \bar{d}_R\gamma^\mu u_R\bar{u}_L\gamma_\mu d_L\right),\end{aligned} \tag{2.54}$$

where $V_{ud} \simeq 1$ is the CKM element. Due to its left-right mixing we abbreviate this four-quark operator as FQLR. In terms of light-quark doublets, we can rewrite Eq. (2.54) as

$$\mathcal{L}_{\rm LR} = \frac{1}{4}\,\mathrm{Im}[\Xi]\varepsilon^{3ij}\,\bar{q}\gamma^\mu\tau^i q\,\bar{q}\tau^j\gamma_\mu\gamma^5 q, \tag{2.55}$$

which can be brought to a form more similar to Eq. (2.35) by a Fierz rearrangement,

$$\mathcal{L}_{\rm LR} = \frac{1}{4}\,\mathrm{Im}[\Xi]\left\{\bar{q}q\,\bar{q}i\gamma^5\tau_3 q - \bar{q}\tau_3 q\,\bar{q}i\gamma^5 q - 6(\bar{q}t^a q\,\bar{q}i\gamma^5\tau_3 t^a q - \bar{q}\tau_3 t^a q\,\bar{q}i\gamma^5 t^a q)\right\}. \tag{2.56}$$

This operator was studied in Ref. [49] in the framework of left-right models. Although a large list of four-quark operators is presented there, only one combination is generated at the electroweak scale. This combination is identical to Eq. (2.56). It is interesting to point out that we could have coupled the operator in Eq. (2.32) to the left-handed lepton current. The operator created this way causes $\not{T}$ in β-decay through contributions to the triple correlation $\sim D\,\vec{J}\cdot(\vec{p}_e\times\vec{p}_\nu)$. In Ref. [40] it is argued that, with current experimental accuracies, the best limit on FQLR comes from EDM experiments.

2.5 Summary

In summary, the $\not{T}$ Lagrangian at the QCD scale up to dimension six is

$$\begin{aligned}\mathcal{L}_{4-6} &= \bar{\theta} m_* \,\bar{q} i\gamma^5 q - \frac{i}{2}\bar{q}\left(d_0 + d_3\tau_3\right)\sigma^{\mu\nu}\gamma_5 q\, F_{\mu\nu} - \frac{i}{2}\bar{q}\left(\tilde{d}_0 + \tilde{d}_3\tau_3\right)\sigma^{\mu\nu}\gamma_5\lambda^a q\, G^a_{\mu\nu} \\ &+\frac{d_W}{6} f^{abc}\varepsilon^{\mu\nu\alpha\beta} G^a_{\alpha\beta} G^b_{\mu\rho} G^{c\,\rho}_{\nu} + \frac{\mathrm{Im}[\Xi]}{4}\varepsilon^{3ij}\bar{q}\tau^i\gamma^\mu q\,\bar{q}\tau^j\gamma_\mu\gamma^5 q \\ &+\frac{1}{4}\mathrm{Im}\Sigma_1\left(\bar{q}q\,\bar{q}i\gamma^5 q - \bar{q}\boldsymbol{\tau}q\cdot\bar{q}\boldsymbol{\tau}i\gamma^5 q\right) \\ &+\frac{1}{4}\mathrm{Im}\Sigma_8\left(\bar{q}\lambda^a q\,\bar{q}i\gamma^5\lambda^a q - \bar{q}\boldsymbol{\tau}\lambda^a q\cdot\bar{q}\boldsymbol{\tau}i\gamma^5\lambda^a q\right), \end{aligned} \tag{2.57}$$

where all coupling constants have been redefined in order to absorb effects from operator mixing and QCD renormalization group running. The redefined constants scale as

$$\begin{aligned} d_{0,3} &= \mathcal{O}\left(\frac{e\delta_{0,3}\bar{m}}{M_{\not{T}}^2}\right), & \tilde{d}_{0,3} &= \mathcal{O}\left(4\pi\frac{\tilde{\delta}_{0,3}\bar{m}}{M_{\not{T}}^2}\right), & d_W &= \mathcal{O}\left(4\pi\frac{w}{M_{\not{T}}^2}\right), \\ \Xi &= \mathcal{O}\left(\frac{(4\pi)^2\xi}{M_{\not{T}}^2}\right), & \Sigma_{1,8} &= \mathcal{O}\left(\frac{(4\pi)^2\sigma_{1,8}}{M_{\not{T}}^2}\right), \end{aligned} \tag{2.58}$$

in terms of dimensionless numbers $\delta_{0,3}$, $\tilde{\delta}_{0,3}$, w, ξ, and $\sigma_{1,8}$. In principle, one can imagine additional $\not{T}$ four-quark operators, however such operators require additional loops and are suppressed by factors of $\alpha_w/4\pi$, small off-diagonal CKM elements, or are higher-dimensional operators in disguise and suppressed by powers of m_q/M_W. We expect the operators in Eq. (2.57) to capture the dominant part of flavor-conserving T violation in hadronic and nuclear systems at low energy. It is interesting to note that all dimension-four and -six terms break not only T, but also P. The first $P\not{T}$ terms enter at the electroweak scale at dimension seven [50].

The sizes of $\delta_{0,3}$, $\tilde{\delta}_{0,3}$, w, ξ, and $\sigma_{1,8}$ depend on the exact mechanisms of electroweak and P and T breaking and on the running to the low energies where nonperturbative QCD effects take over. The minimal assumption is that they are $\mathcal{O}(1)$, $\mathcal{O}(g_s/4\pi)$, $\mathcal{O}((g_s/4\pi)^3)$, $\mathcal{O}(1)$, and $\mathcal{O}(1)$, respectively, with g_s the strong coupling constant. However, they can be much smaller or much larger (depending on the parameters encoding $\not{P}\not{T}$ beyond the SM). In the SM itself, where $M_{\not{T}} = M_W$, δ, $\tilde{\delta}$ and w are suppressed not only by the Jarlskog parameter $J_{CP} \simeq 3\cdot 10^{-5}$ [51], but also by additional powers of the $\not{P}\not{T}$ scale, in this case equal to M_W, and by small gauge coupling constants. For example, in the SM, the qEDM and gCEDM both receive their first contribution at three loops [9, 11, 52]

$$\delta = \frac{2}{27} J_{CP}\frac{\alpha_{\mathrm{em}}^2}{(4\pi)^2\sin^4\theta_w}\frac{\alpha_s}{4\pi}\frac{m_c^2}{M_W^2}\ln^2\frac{m_b^2}{m_c^2}\,\ln\frac{M_W^2}{m_b^2}, \tag{2.59}$$

$$w = \frac{1}{12}\left(\frac{g_s}{4\pi}\right)^3 J_{CP}\frac{\alpha_{\mathrm{em}}^2}{(4\pi)^2\sin^4\theta_w}\frac{m_b^2 m_c^2 m_s^2}{M_W^6}\ln\frac{m_b^2}{m_s^2}\,\ln\frac{M_W^2}{m_b^2}, \tag{2.60}$$

and therefore δ and w are much smaller than the naive expectation.

In supersymmetric models with various simplifying, universality assumptions of a soft-breaking sector with a common scale M_{SUSY}, one has $M_{\not{T}} = M_{\mathrm{SUSY}}$ and the size of the dimensionless parameters is given by the minimal assumption times a factor which is [9, 53], roughly (neglecting electroweak parameters), $A_{CP} = (g_s/4\pi)^2\sin\phi$, with ϕ a phase encoding T violation. Allowing for nondiagonal terms in the soft-breaking sfermion mass matrices, enhancements of the type

$m_b/m_d \sim 10^3$ or even $m_t/m_u \sim 10^5$ are possible, although they are usually associated with other, smaller phases [9].

These considerations indicate that the (relative) size of the dimensionless coefficients $\bar{\theta}$, $\delta_{0,3}$, $\tilde{\delta}_{0,3}$, w, ξ, and $\sigma_{1,8}$ depends on what model of beyond-the-SM physics we are studying. This dependence makes it hard to compare, in a model-independent way, the contributions from the different $\not{P}\not{T}$ sources to the same observable. To overcome this problem we do not assume any hierarchy between the various sources and construct the low-energy $\not{P}\not{T}$ Lagrangian for each source separately. As we will see in the next chapter, the different dimension-four and -six $\not{P}\not{T}$ sources induce, due to their different field content and their transformation properties under chiral symmetry, different hadronic $\not{P}\not{T}$ Lagrangians. The different Lagrangians give rise to a different pattern of hadronic observables. Given enough measurements on, for example, nucleon and nuclear EDMs, we can search for these patterns and effectively identify the dominant $\not{P}\not{T}$ mechanism at the QCD scale. Once this is known, the next step would be to pinpoint the dominant mechanism at the electroweak scale.

Our framework, however, is flexible enough to study specific models of new physics. At the electroweak scale such models can be matched to the SM extended with the effective dimension-six operators. After running to $M_{\rm QCD}$, specific values are obtained for $\delta_{0,3}$, $\tilde{\delta}_{0,3}$, w, ξ and $\sigma_{1,8}$. These values can be used in the scaling of the interactions constructed in the next chapter. In such a way we can study the low-energy implications of various extensions of the SM.

Below the hadronic scale $M_{\rm QCD}$, the dimension-six $\not{P}\not{T}$ sources generate further effective interactions, which break chiral symmetry in their own ways. Introducing the $SO(4)$ singlets

$$I_W = \frac{1}{6} f^{abc} \varepsilon^{\mu\nu\alpha\beta} G^a_{\alpha\beta} G^b_{\mu\rho} G^{c\,\rho}_{\nu}, \tag{2.61}$$

$$I^{(1)}_{qq} = \frac{1}{4}\left(\bar{q}q\,\bar{q}i\gamma^5 q - \bar{q}\boldsymbol{\tau}q\cdot\bar{q}\boldsymbol{\tau}i\gamma^5 q\right), \tag{2.62}$$

$$I^{(8)}_{qq} = \frac{1}{4}\left(\bar{q}\lambda^a q\,\bar{q}i\gamma^5\lambda^a q - \bar{q}\boldsymbol{\tau}\lambda^a q\cdot\bar{q}\boldsymbol{\tau}i\gamma^5\lambda^a q\right), \tag{2.63}$$

the $SO(4)$ vectors

$$W = \tfrac{1}{2}\begin{pmatrix} -i\bar{q}\sigma^{\mu\nu}\gamma^5\boldsymbol{\tau}q \\ \bar{q}\sigma^{\mu\nu}q \end{pmatrix} F_{\mu\nu}, \qquad V = \tfrac{1}{2}\begin{pmatrix} \bar{q}\sigma^{\mu\nu}\boldsymbol{\tau}q \\ i\bar{q}\sigma^{\mu\nu}\gamma^5 q \end{pmatrix} F_{\mu\nu}, \tag{2.64}$$

and

$$\tilde{W} = \tfrac{1}{2}\begin{pmatrix} -i\bar{q}\sigma^{\mu\nu}\gamma^5\boldsymbol{\tau}\lambda^a q \\ \bar{q}\sigma^{\mu\nu}\lambda^a q \end{pmatrix} G^a_{\mu\nu}, \qquad \tilde{V} = \tfrac{1}{2}\begin{pmatrix} \bar{q}\sigma^{\mu\nu}\boldsymbol{\tau}\lambda^a q \\ i\bar{q}\sigma^{\mu\nu}\gamma^5\lambda^a q \end{pmatrix} G^a_{\mu\nu}, \tag{2.65}$$

and the symmetric $SO(4)$ tensor

$$X = \frac{1}{4}\begin{pmatrix} \bar{q}\tau^i\gamma^\mu q\,\bar{q}\tau^j\gamma_\mu q - \bar{q}\tau^i\gamma^\mu\gamma^5 q\,\bar{q}\tau^j\gamma_\mu\gamma^5 q & -\varepsilon^{ikl}\bar{q}\tau^k\gamma^\mu q\,\bar{q}\tau^l\gamma_\mu\gamma^5 q \\ -\varepsilon^{jkl}\bar{q}\tau^k\gamma^\mu q\,\bar{q}\tau^l\gamma_\mu\gamma^5 q & (\bar{q}\boldsymbol{\tau}\gamma^\mu q)\cdot(\bar{q}\boldsymbol{\tau}\gamma_\mu q) - (\bar{q}\boldsymbol{\tau}\gamma^\mu\gamma^5 q)\cdot(\bar{q}\boldsymbol{\tau}\gamma_\mu\gamma^5 q) \end{pmatrix}, \tag{2.66}$$

we summarize the $\not{P}\not{T}$ Lagrangian by

$$\begin{aligned}\mathcal{L}_{\not{P}\not{T},6} = {} & m_*\bar{\theta}P_4 - d_0 V_4 + d_3 W_3 - \tilde{d}_0\tilde{V}_4 + \tilde{d}_3\tilde{W}_3 \\ & + d_W I_W - \mathrm{Im}[\Xi]X_{34} + \mathrm{Im}\Sigma_1\, I^{(1)}_{qq} + \mathrm{Im}\Sigma_8\, I^{(8)}_{qq}.\end{aligned} \tag{2.67}$$

The next chapter is devoted to the construction of the hadronic Lagrangian induced by the operators in Eq. (2.67).

Chapter 3

The Effective Parity- and Time-Reversal-Violating Chiral Lagrangian

3.1 Introduction[1]

In the previous chapter we investigated possible sources of time-reversal violation up to dimension six. We concluded that at energies around the QCD scale there are seven different operators up to dimension six that capture the dominant flavor-conserving $\not{T}$ physics in hadronic and nuclear systems. All these operators simultaneously violate P as well. The set of operators consists of the QCD $\bar{\theta}$ term, the quark electric dipole moment (qEDM) which couples quarks and photons, the quark chromo-electric dipole moment (qCEDM) which couples quarks and gluons, the gluon chromo-electric dipole moment (gCEDM) which couples three-or more gluons, a chiral- and isospin-breaking four-quark operator (FQLR), and two chiral-invariant (χI) four-quark operators.

The next logical step would be the calculation of observables from these operators. In principle, properties of hadrons and nuclei are described by QCD, the theory of the strong interaction. Unfortunately, due to the nonperturbative nature of QCD at low energies, actual calculations are problematic. Although a perturbative expansion in the strong coupling constant α_s is lost, QCD still provides strong symmetry requirements on low-energy physics. Focusing on the two lightest quarks and in the limit of zero quark masses and charges, the QCD Lagrangian has a global chiral symmetry consisting of two $SU(2)$ symmetries, *i.e* axial and isospin symmetry. Only isospin symmetry is realized in the spectrum of hadrons. The other symmetry, axial symmetry, is spontaneously broken in the QCD ground state resulting in the existence of three massless Goldstone bosons. However, because the original symmetries are not exact, being broken by the small quark masses, the Goldstone bosons obtain a relatively small mass. The three Goldstone bosons are identified with the pion triplet. The interaction between pions and heavier degrees of freedom, such as baryons (most importantly the nucleon and Delta-isobar) and heavier mesons (ρ, ω, ...) are strongly constrained by consistently enforcing the QCD symmetries. These symmetry requirements allow us to formulate an effective field theory (EFT) between pions, nucleons, and heavier baryons, which is called chiral perturbation theory (χPT) [54]. χPT provides a new expansion in $Q/M_{\rm QCD}$, where Q is the typical energy scale of the physical process and $M_{\rm QCD} \approx 1\,\text{GeV}$ the typical QCD scale. We briefly review χPT in Sec. 3.2.

[1] This chapter is based on J. de Vries, E. Mereghetti, R. G. E. Timmermans, and U. van Kolck, in preparation.

χPT has been successfully applied to many processes such as pion-nucleon (πN) scattering and the pion and nucleon electromagnetic form factors [55]. It has also been used to systematically derive a nucleon-nucleon (NN) potential which can be used to calculate nuclear properties [56].

In this thesis we extend χPT to include time-reversal violation. The effective chiral Lagrangian includes not only interactions that stem from spontaneous chiral symmetry breaking and are therefore χI, but also interactions that break chiral symmetry in the same way as chiral-symmetry-breaking operators at the QCD level. While they all break P and T, the dimension-six operators break chiral symmetry differently from each other and from the $\bar{\theta}$ term and therefore give rise to different effective interactions. Given enough observables it should be possible to separate the various $\not{P}\not{T}$ sources on the basis of the hadronic interactions that they generate.

In addition to constructing the Lagrangian, we need to organize in leading order (LO), next-to-leading order (NLO), *etc.* the various effective $\not{P}\not{T}$ structures that appear. This is done according to the estimated size of their contributions to observables. In order to get a consistent, manifest power counting we work in a heavy-baryon framework [57] wherein the nucleon mass has been eliminated from the nucleon propagator. This framework has a transparent power counting and it greatly simplifies the loop calculations, but there are some complications when one goes to subleading orders in the Lagrangian. These problems can be solved by demanding that the Lagrangian obeys reparametrization invariance (RPI) [58, 59, 60]. This puts constraints on certain coefficients of operators, which we calculate up to next-to-next-to-leading order (NNLO).

This chapter is organized as follows. In Sec. 3.2 we briefly discuss $SU(2) \times SU(2)$ χPT and the parity- and time-reversal-conserving (PT) chiral Lagrangian. The bulk of the chapter is in Sec. 3.3, where we construct the effective $\not{P}\not{T}$ Lagrangian for the different sources discussed in Chapter 2. (Details about RPI are relegated to App. A). Time-reversal violation in combination with isospin breaking can lead to pion tadpoles which destabilize the vacuum. We discuss these tadpoles and their removal in Sec. 3.4. In Sec. 3.5 we use the constructed Lagrangian by calculating the $\not{P}\not{T}$ πN form factor. The obtained results are discussed in Sec. 3.6.

3.2 Chiral perturbation theory

At low momentum $Q \sim m_\pi \ll M_{QCD}$ the effects of the Lagrangian in Eqs. (2.36), (2.45), (2.47), and (2.67) on the interactions among pions and nucleons (and heavier baryons) are described by χPT, the EFT of QCD. At momenta Q comparable to the pion mass, interactions among nucleons and pions are described by the most general Lagrangian that involves these degrees of freedom and that has the same symmetries as QCD. A particularly important role at low energy is played by the approximate symmetry of QCD under the chiral group $SU_L(2) \times SU_R(2) \sim SO(4)$. Since it is not manifest in the spectrum (there exists no partner of the nucleon with odd parity), which instead exhibits an approximate isospin symmetry, chiral symmetry must be spontaneously broken down to the isospin subgroup $SU_{L+R}(2) \sim SO(3)$. The corresponding Goldstone bosons can be identified with the pions, which provide a nonlinear realization of chiral symmetry.

Chiral symmetry and its spontaneous breaking strongly constrain the form of the interactions among nucleons and pions. In particular, in the limit of vanishing quark masses and charges, when chiral symmetry is exact, pion interactions proceed through a covariant derivative, which in stereographic coordinates $\boldsymbol{\pi}$ for the pions is [61]

$$D_\mu \boldsymbol{\pi} = D^{-1} \partial_\mu \boldsymbol{\pi}, \tag{3.1}$$

with $F_\pi \simeq 186$ MeV, the pion decay constant, and

$$D = 1 + \frac{\boldsymbol{\pi}^2}{F_\pi^2}. \tag{3.2}$$

Similarly, we can use an isospin-1/2 nucleon field N that transforms in an analogous way, and a nucleon covariant derivative

$$\mathcal{D}_\mu N = \left(\partial_\mu + \frac{i}{F_\pi^2}\boldsymbol{\tau}\cdot\boldsymbol{\pi}\times D_\mu\boldsymbol{\pi}\right) N. \tag{3.3}$$

We define $\mathcal{D}^\dagger$ through $\bar{N}\mathcal{D}^\dagger \equiv \overline{\mathcal{D}N}$, and use the shorthand notation,

$$\begin{aligned} \mathcal{D}^\mu_\pm &\equiv \mathcal{D}^\mu \pm \mathcal{D}^{\dagger\mu}, & \mathcal{D}^\mu_\pm\mathcal{D}^\nu_\pm &\equiv \mathcal{D}^\mu\mathcal{D}^\nu + \mathcal{D}^{\dagger\mu}\mathcal{D}^{\dagger\nu} \pm \mathcal{D}^{\dagger\mu}\mathcal{D}^\nu \pm \mathcal{D}^{\dagger\nu}\mathcal{D}^\mu, \\ \tau_i\mathcal{D}^\mu_\pm &\equiv \tau_i\mathcal{D}^\mu \pm \mathcal{D}^{\dagger\mu}\tau_i, & \tau_i\mathcal{D}^\mu_\pm\mathcal{D}^\nu_\pm &\equiv \tau_i\mathcal{D}^\mu\mathcal{D}^\nu + \mathcal{D}^{\dagger\mu}\mathcal{D}^{\dagger\nu}\tau_i \pm \mathcal{D}^{\dagger\mu}\tau_i\mathcal{D}^\nu \pm \mathcal{D}^{\dagger\nu}\tau_i\mathcal{D}^\mu. \end{aligned} \tag{3.4}$$

Covariant derivatives of covariant derivatives can be constructed similarly, for example

$$(\mathcal{D}_\mu D_\nu \pi)_i = \left(\partial_\mu\delta_{ij} - \frac{2}{F_\pi^2}\varepsilon^{ikj}(\boldsymbol{\pi}\times D_\mu\boldsymbol{\pi})_k\right) D_\nu\pi_j. \tag{3.5}$$

For simplicity we omit the Δ-isobar here, but one can introduce an isospin-3/2 field for it along completely analogous lines [62].

The construction of the low-energy effective Lagrangian involves an infinite number of interactions. We need a method to order these interactions according to the expected size of their contributions to physical processes (such a method is called a power-counting scheme). Here we will label interactions by the even number of nucleon fields f and an integer "chiral index" Δ

$$\mathcal{L} = \sum_{\Delta=0}^{\infty}\sum_{f/2}\mathcal{L}_f^{(\Delta)}. \tag{3.6}$$

We will first neglect quark masses and charges, the $\bar{\theta}$ term, and the dimension-six operators, and focus on the chiral-invariant part of the QCD Lagrangian. The EFT Lagrangian includes all Lorentz-covariant, chiral-, isospin-, C-, P-, and T-invariant interactions made out of $D_\mu\boldsymbol{\pi}$, N, and their covariant derivatives. In this case, the chiral index of interactions with $f \leq 2$ depends only on the number of nucleon fields and covariant derivatives (d) in the operator [54]

$$\Delta = d + f/2 - 2 \geq 0. \tag{3.7}$$

The coefficients of the effective operators, the so-called low-energy constants (LECs), can be estimated using naive dimensional analysis (NDA) [63, 33], in which case the index Δ tracks the number of inverse powers of $M_{\rm QCD}$ associated with an interaction. NDA is discussed in App. B. Better estimates could be given with lattice-QCD calculations.

The most important terms in the chiral-symmetric Lagrangian are given by

$$\mathcal{L}^{(0)} = \frac{1}{2}D_\mu\boldsymbol{\pi}\cdot D^\mu\boldsymbol{\pi} + \bar{N}\left(i\not{\mathcal{D}} - m_N - \frac{g_A}{F_\pi}(\boldsymbol{\tau}\cdot D_\mu\boldsymbol{\pi})\gamma^\mu\gamma_5\right) N, \tag{3.8}$$

in terms of the nucleon mass m_N and the πN axial-vector coupling g_A. From NDA we expect $g_A = \mathcal{O}(1)$, in fair agreement with the experimental value $g_A \simeq 1.267$.

Since nucleons are essentially nonrelativistic for $Q \ll m_N$ we work in the heavy-baryon framework [57] where, instead of gamma matrices, it is the nucleon velocity v^μ and spin S_μ

($S = (\vec{\sigma}/2, 0)$ in the rest frame $v = (\vec{0}, 1)$) that appear in interactions. In the heavy-baryon framework, see App. A, Eq. (3.8) becomes

$$\mathcal{L}^{(0)} = \frac{1}{2} D_\mu \boldsymbol{\pi} \cdot D^\mu \boldsymbol{\pi} + \bar{N} \left(iv \cdot \mathcal{D} - \frac{2g_A}{F_\pi} S^\mu \boldsymbol{\tau} \cdot D_\mu \boldsymbol{\pi} \right) N + \mathcal{O}\left(\frac{1}{m_N} \right), \tag{3.9}$$

where we only kept the LO terms. At this order the nucleon is static; kinetic corrections have relative size $\mathcal{O}(Q/m_N)$ and appear in $\mathcal{L}^{(1)}$. We use RPI [58, 59, 60] to incorporate Lorentz invariance in an expansion in powers of Q/m_N. Below we use a subscript $\perp$ to denote the component of a four-vector perpendicular to the velocity, for example

$$\mathcal{D}^\mu_\perp = \mathcal{D}^\mu - v^\mu v \cdot \mathcal{D}. \tag{3.10}$$

For processes where only a single nucleon is involved, the momenta and energies of the particles in the process are all of order $\sim Q$. That means that each derivative in a vertex contributes one power of Q to a diagram, each nucleon propagator in the heavy-baryon framework $1/Q$, each pion propagator $1/Q^2$, and each loop Q^4. A general diagram makes a contribution of order Q^ν, where the counting index ν is [61]

$$\nu = 4 - 2C - A + 2L + \sum_i \Delta_i. \tag{3.11}$$

Here, $C = 1$ and L are respectively the number of connected pieces and loops in the diagrams, $A \leq 1$ the number of nucleons, and i counts the number of insertions of vertices from $\mathcal{L}_f^{(\Delta)}$. Because Q is small compared to $M_{\rm QCD}$, a larger ν implies a more suppressed diagram. Since ν grows with the number of loops, the most important diagrams are those with the smallest number of loops, *i.e.* tree-level diagrams. Loop integrals involve the characteristic factor $1/(2\pi)^2$ and pions are associated with inverse powers of F_π, such that $M_{QCD} \sim 2\pi F_\pi \simeq 1.2$ GeV. The above discussion can be neatly summarized by the following power-counting rules from which the size of a diagram can easily be obtained

- a factor $Q^4/(2\pi)^2$ for each loop integral;
- a factor $1/Q$ for each nucleon propagator;
- a factor $1/Q^2$ for each pion propagator;
- the NDA estimates for the LECs corresponding to the interactions in the diagram.

These rules only apply for diagrams with zero or one nucleon in the intermediate state. Diagrams with multiple intermediate nucleons require a more complicated power counting [64, 65, 66]. We come back to this in Chapters 5 and 6.

So far we have talked about the chiral-symmetric part of the QCD Lagrangian. The formalism to include chiral-symmetry-breaking operators in the $SU(2) \times SU(2)$ χPT Lagrangian has been developed in Refs. [61, 62]. Operators that break the symmetry as components of chiral tensors can be obtained by rotating operators constructed with non-Goldstone fields Ψ such as nucleons, nucleon and pion covariant derivatives, and photons,

$$\mathcal{O}_{ij\cdots z}[\pi, \Psi] = R_{i\alpha} R_{j\beta} \cdots R_{z\xi} \mathcal{O}_{\alpha\beta\cdots\xi}[0, \Psi]. \tag{3.12}$$

In stereographic coordinates, the chiral rotation R is given by

$$R_{\alpha\beta} = \begin{pmatrix} \delta_{ij} - \frac{2}{D}\frac{\pi_i \pi_j}{F_\pi^2} & \frac{2}{D}\frac{\pi_i}{F_\pi} \\ -\frac{2}{D}\frac{\pi_j}{F_\pi} & \frac{1}{D}\left(1 - \frac{\boldsymbol{\pi}^2}{F_\pi^2}\right) \end{pmatrix}. \tag{3.13}$$

Due to the chiral rotation, chiral-breaking terms in the QCD Lagrangian induce effective interactions involving $\boldsymbol{\pi}$ directly. The effective interactions are proportional to powers of the symmetry-breaking parameters. As an example, consider the quark mass in Eq. (2.45) which transforms as the fourth component of the $SO(4)$ vector S defined in Eq. (2.46). From Eqs. (3.12) and (3.13)

$$S_4[\pi,\Psi] \;=\; \frac{1}{D}\left(1-\frac{\boldsymbol{\pi}^2}{F_\pi^2}\right) S_4[0,\Psi] - \frac{2\boldsymbol{\pi}}{F_\pi D}\cdot \boldsymbol{S}[0,\Psi], \tag{3.14}$$

and since the quark mass is a Lorentz scalar and the pion field a Lorentz pseudoscalar, $S_4[0,\Psi]$ has to be P and T even, while $\boldsymbol{S}[0,\Psi]$ has to be P and T odd. A particular choice would be $S[0,0]=\bar{m}(\mathbf{0},\ v_0)$, where v_0 is a real number depending on the details of the spontaneous breaking of chiral symmetry. This choice generates

$$S_4[\pi,0] = \frac{1}{D}\left(1-\frac{\boldsymbol{\pi}^2}{F_\pi^2}\right) v_0 = \bar{m}(v_0 - v_0\frac{2\boldsymbol{\pi}^2}{DF_\pi^2}). \tag{3.15}$$

The first term in Eq. (3.15) is an irrelevant constant, but the second term denotes a contribution to the pion mass

$$\mathcal{L}^{(0)}_{m_\pi} = -\frac{m_\pi^2}{2D}\boldsymbol{\pi}^2, \tag{3.16}$$

where we redefined the constants. The size of the pion mass can be estimated by applying NDA $m_\pi^2 = \mathcal{O}(\bar{m}M_{\rm QCD})$, such that the pion mass squared is proportional to the average light-quark mass. From this relation we see that the quark mass scales as $m_\pi^2/M_{\rm QCD}$ and is associated with one inverse power of $M_{\rm QCD}$. We generalize the index Δ in Eq. (3.7) by letting d count the powers of the quark mass as well.

A different choice would be $S[0,N]=\bar{m}(\mathbf{0},\ v_1\bar{N}N)$ which generates

$$\mathcal{L}^{(1)}_{\Delta m_N} = \Delta m_N\left(1-\frac{2\boldsymbol{\pi}^2}{DF_\pi^2}\right)\bar{N}N. \tag{3.17}$$

The shift in the nucleon mass, the so-called σ term, is related through chiral symmetry to a $\pi\pi N$ vertex. NDA gives $\Delta m_N = \mathcal{O}(\bar{m}) = \mathcal{O}(m_\pi^2/M_{\rm QCD})$.

In a similar way, one can incorporate in the EFT the $\varepsilon\bar{m}$ term in Eq. (2.45), which leads to isospin violation as P_3 [62]. The most important term is

$$\mathcal{L}^{(1)}_{\delta m_N} \;=\; \frac{\delta m_N}{2}\bar{N}\left(\tau_3 - \frac{2\pi_3}{F_\pi^2 D}\boldsymbol{\tau}\cdot\boldsymbol{\pi}\right)N, \tag{3.18}$$

where the nucleon-mass splitting $\delta m_N = \mathcal{O}(\varepsilon\bar{m}) = \mathcal{O}(\varepsilon m_\pi^2/M_{\rm QCD})$ reflects the small neutron-proton mass difference. For simplicity in the power counting, we count $\varepsilon \simeq 1/3 = \mathcal{O}(1)$.

Other isospin-violating hadronic operators and interactions with the photon field A_μ come from $\mathcal{L}_e$ in Eq. (2.47). Gauge-invariant interactions containing an explicit photon field A_μ appear by modifying the covariant derivatives of the pion and nucleon fields

$$\begin{aligned}
(D_\mu\boldsymbol{\pi})_a \;&\to\; (D_\mu\boldsymbol{\pi})_a = \frac{1}{D}\left(\partial_\mu\delta_{ab} + eA_\mu\varepsilon_{3ab}\right)\pi_b,\\
\mathcal{D}_\mu N \;&\to\; \mathcal{D}_{\mu,\rm em}N = \left[\partial_\mu + \frac{i}{F_\pi^2}\boldsymbol{\tau}\cdot(\boldsymbol{\pi}\times D_\mu\boldsymbol{\pi}) + ieA_\mu\frac{1}{2}\left(1+\tau_3\right)\right]N,
\end{aligned} \tag{3.19}$$

in terms of the proton charge e. The other possibility is to construct operators that contain the electromagnetic field strength $F_{\mu\nu}$. Such operators transform as $I^\mu/6 + T^\mu_{34}/2$ or its tensor products. Because photon fields have dimension one, we generalize the index Δ defined in Eq. (3.7) by letting d count the number of photon fields as well. The term I^μ in Eq. (2.47) generates χI interactions, the simplest example being

$$\mathcal{L}^{(1)}_{\rm em} = c_{s,{\rm em}}\,\varepsilon^{\alpha\beta\mu\nu} v_\alpha \bar{N} S_\beta N\, eF_{\mu\nu}, \tag{3.20}$$

where $c_{s,{\rm em}} = \mathcal{O}(1/M_{\rm QCD})$ and we define $\varepsilon^{0123} = 1$. The operators generated by T_{34} are more complicated and transform as the 3-4 component of an antisymmetric tensor. From Eqs. (3.12) and (3.13)

$$\begin{aligned} T_{34}[\pi,\Psi] &= (R_{3\alpha}R_{4\beta} - R_{3\beta}R_{4\alpha})T_{\alpha\beta}[0,\Psi] \\ &= \left[\left(1 - \frac{2\boldsymbol{\pi}^2}{DF_\pi^2}\right)\delta^{i3} + \frac{2\pi_i\pi_3}{F_\pi^2 D}\right] T_{i4}[0,\Psi] + \frac{2}{F_\pi D}(\pi_i\delta_{j3} - \pi_j\delta_{i3})T_{ij}[0,\Psi]. \end{aligned} \tag{3.21}$$

Picking the tensor $T_{ij}[0,\Psi] = T_{44}[0,\Psi] = 0$, and $T_{i4}[0,\Psi] = -T_{4i}[0,\Psi] = \varepsilon^{\alpha\beta\mu\nu} v_\alpha \bar{N} S_\beta \tau^i N\, eF_{\mu\nu}$ generates

$$\mathcal{L}^{(1)}_{\rm em} = c_{v,{\rm em}}\,\varepsilon^{\alpha\beta\mu\nu} v_\alpha \bar{N}\left[\tau^3 - \frac{2}{F_\pi^2 D}\left(\boldsymbol{\pi}^2\tau^3 - \pi_3\boldsymbol{\pi}\cdot\boldsymbol{\tau}\right)\right] S_\beta N\, eF_{\mu\nu}. \tag{3.22}$$

The two operators constructed in Eqs. (3.20) and (3.22) are the dominant contribution to the isoscalar and isovector magnetic dipole moments of the nucleon. We redefine $c_{s,v,{\rm em}} = -(1+\kappa_{0,1})/4m_N$ and interpret $\kappa_{0,1}$ as the anomalous magnetic dipole moments. From NDA we expect $c_{s,v,{\rm em}} = \mathcal{O}(1/M_{\rm QCD})$, in reasonable agreement with the experimental values $\kappa_0 = -0.12$ and $\kappa_1 = 3.7$.

Finally, integrated-out hard photons (with momenta larger than $M_{\rm QCD}$) give rise to purely hadronic operators that also transform as $I^\mu/6 + T^\mu_{34}/2$ or as its tensor products. From NDA we infer that operators created this way are proportional to $(e/4\pi)^2 = \alpha_{\rm em}/4\pi$. The numerical value of $\alpha_{\rm em}/4\pi$ is close to that of $m_\pi^3/M_{\rm QCD}^3$ such that integrating out a hard photon increases Δ by 3. An example of such an operator is the dominant contribution to the pion-mass splitting

$$\mathcal{L}^{(1)}_{\breve{\delta}m_\pi} = -\frac{\breve{\delta}m_\pi^2}{2D^2}\left(\boldsymbol{\pi}^2 - \pi_3^2\right), \tag{3.23}$$

which arises from the tensor product $T_{34}\otimes T_{34}$ and $\breve{\delta}m_\pi^2 = \mathcal{O}(\alpha_{\rm em}M_{\rm QCD}^2/4\pi)$, in fair agreement with experiment: $m^2_{\pi^\pm} - m^2_{\pi^0} = \breve{\delta}m_\pi^2 = (35.5\ {\rm MeV})^2$ [67].

3.2.1 The time-reversal-conserving chiral Lagrangian

The strategy outlined in the previous section, combined with the method of dealing with relativistic corrections described in App. B, can be used to construct, in principle, the chiral PT Lagrangian up to any given order. For practical purposes, only the first few orders are necessary. Here we summarize the PT interactions used in this thesis (A more complete list can be found in, for example, Refs. [55, 56, 62, 68, 69].) Some of the operators were mentioned as examples in the previous section, but for completeness we list them here as well.

The leading PT chiral Lagrangian has chiral index $\Delta = 0$ and is given by

$$\mathcal{L}^{(0)}_{f\le 2,PT} = \frac{1}{2}D_\mu\boldsymbol{\pi}\cdot D^\mu\boldsymbol{\pi} - \frac{m_\pi^2}{2D}\boldsymbol{\pi}^2 + \bar{N}iv\cdot\mathcal{D}N - \frac{2g_A}{F_\pi}D_\mu\boldsymbol{\pi}\cdot\bar{N}\boldsymbol{\tau}S^\mu N, \tag{3.24}$$

where g_A is the πN axial coupling, $g_A \simeq 1.27$. The pion mass term originates in explicit chiral-symmetry breaking by the average quark mass $\bar{m} = (m_u + m_d)/2$ and, by NDA, $m_\pi^2 = \mathcal{O}(\bar{m} M_{QCD})$. Neglecting for the moment isospin-breaking operators, at chiral order $\Delta = 1$ the relevant Lagrangian consists of

$$\mathcal{L}^{(1)}_{f\leq 2,PT} = -\frac{1}{2m_N}\bar{N}\mathcal{D}_\perp^2 N + \frac{g_A}{F_\pi m_N}(iv\cdot D\boldsymbol{\pi})\cdot\bar{N}\boldsymbol{\tau}\, S\cdot\mathcal{D}_- N + \Delta m_N\left(1-\frac{2\boldsymbol{\pi}^2}{F_\pi^2 D}\right)\bar{N}N. \quad (3.25)$$

Here the first two terms are the nucleon kinetic energy and a relativistic correction to the πN coupling, the coefficients of both operators being fixed by Galilean invariance. The third term is the nucleon sigma term with a coefficient $\Delta m_N = \mathcal{O}(m_\pi^2/M_{QCD})$. At the next chiral order, $\Delta = 2$,

$$\begin{aligned}\mathcal{L}^{(2)}_{f\leq 2,PT} &= -\frac{\Delta m_\pi^2}{2D^2}\boldsymbol{\pi}^2 + \frac{g_A}{4F_\pi m_N^2} D_\mu\boldsymbol{\pi}\cdot\bar{N}\boldsymbol{\tau}\left(S^\mu\mathcal{D}^2_{\perp,-} - \mathcal{D}^\mu_{\perp,-}\, S\cdot\mathcal{D}_{\perp,-}\right)N \\ &\quad -\frac{2g_A}{F_\pi}\left[c_A\mathcal{D}_\perp^2 D_\mu\boldsymbol{\pi} - d_A\left(1-\frac{2\boldsymbol{\pi}^2}{F_\pi^2 D}\right)D_\mu\boldsymbol{\pi}\right]\cdot\bar{N}\boldsymbol{\tau}S^\mu N. \end{aligned} \quad (3.26)$$

The first term is a correction to the pion mass, $\Delta m_\pi^2 = \mathcal{O}(m_\pi^4/M_{QCD}^2)$. The second term represents further relativistic corrections to the g_A term in Eq. (3.24). The constraints imposed by Lorentz invariance on Eqs. (3.25) and (3.26) agree with the results of Ref. [68], once a field redefinition is used to eliminate time derivatives acting on the nucleon field from the subleading $\Delta = 1$ and $\Delta = 2$ Lagrangians. The operator with coefficient $c_A = \mathcal{O}(1/M_{QCD}^2)$ in Eq. (3.26) is a contribution to the square radius of the πN form factor, while $d_A = \mathcal{O}(m_\pi^2/M_{QCD}^2)$ is a chiral-symmetry-breaking correction to g_A [70], which provides the Goldberger-Treiman discrepancy.

Isospin-breaking operators in the chiral Lagrangian [62] stem from the quark-mass difference $m_d - m_u = 2\bar{m}\varepsilon$ and from quark coupling to photons through the fine-structure constant $\alpha_{\rm em} = e^2/4\pi$. Isospin-violating terms first contribute to the $\Delta = 1$ Lagrangian,

$$\mathcal{L}^{(1)}_{f\leq 2,PTI} = -\frac{\breve{\delta}m_\pi^2}{2D^2}\left(\boldsymbol{\pi}^2 - \pi_3^2\right) + \frac{\delta m_N}{2}\bar{N}\left(\tau_3 - \frac{2\pi_3}{F_\pi^2 D}\boldsymbol{\pi}\cdot\boldsymbol{\tau}\right)N, \quad (3.27)$$

while at order $\Delta = 2$,

$$\begin{aligned}\mathcal{L}^{(2)}_{f\leq 2,PTI} &= -\frac{\delta m_\pi^2}{2D^2}\pi_3^2 + \frac{\breve{\delta}m_N}{2}\bar{N}\left[\tau_3 + \frac{2}{F_\pi^2 D}\left(\pi_3\boldsymbol{\pi}\cdot\boldsymbol{\tau} - \boldsymbol{\pi}^2\tau_3\right)\right]N \\ &\quad +\frac{\beta_1}{F_\pi}\left(D_\mu\pi_3 - \frac{2\pi_3}{F_\pi^2 D}\boldsymbol{\pi}\cdot D_\mu\boldsymbol{\pi}\right)\bar{N}S^\mu N. \end{aligned} \quad (3.28)$$

Here $\breve{\delta}m_\pi^2 = \mathcal{O}(\alpha_{\rm em} M_{QCD}^2/4\pi)$ is the leading electromagnetic contribution to the pion-mass splitting, while the quark-mass-difference contribution, $\delta m_\pi^2 = \mathcal{O}(\varepsilon^2 m_\pi^4/M_{QCD}^2)$, is smaller by a power of $\varepsilon^2 m_\pi/M_{QCD}$. Therefore, the pion-mass splitting, $m_{\pi^\pm}^2 - m_{\pi^0}^2 = \breve{\delta}m_\pi^2 - \delta m_\pi^2 = (35.5\ \text{MeV})^2$ [67], is dominated by the electromagnetic contribution. The nucleon-mass splitting, $m_n - m_p = \delta m_N + \breve{\delta}m_N = 1.29$ MeV [67] also receives contributions from electromagnetism and from the quark masses. In this case, the quark-mass contribution δm_N is expected to be the largest. By dimensional analysis $\delta m_N = \mathcal{O}(\varepsilon m_\pi^2/M_{QCD})$, and lattice simulations estimate it to be $\delta m_N = 2.26 \pm 0.57 \pm 0.42 \pm 0.10$ MeV [71], which is in agreement with an extraction from charge-symmetry breaking in the $pn \to d\pi^0$ reaction [72]. The electromagnetic contribution is $\breve{\delta}m_N = \mathcal{O}(\alpha_{\rm em} M_{QCD}/4\pi)$, that is, $\mathcal{O}(\varepsilon m_\pi^3/M_{QCD}^2)$ and about 20% of δm_N. Using the

Cottingham sum rule, $\breve{\delta}m_N = -(0.76 \pm 0.30)$ MeV [73], which is consistent with dimensional analysis. The operator with coefficient $\beta_1 = \mathcal{O}(\varepsilon m_\pi^2/M_{QCD}^2)$ is an isospin-violating πN coupling. At present there are only bounds on β_1 from isospin violation in NN scattering. For example, a phase-shift analysis of two-nucleon data gives $\beta_1 = (0 \pm 9) \cdot 10^{-3}$ [70, 74], which is comparable to estimates of β_1 from π-η mixing.

For calculational purposes, it is convenient to eliminate the nucleon mass difference $m_n - m_p$ from the nucleon propagator and from asymptotic states. This result can be accomplished through a field redefinition, defined in Ref. [69]. After the field redefinition, Eqs. (3.27) and (3.28) become

$$\begin{aligned}\mathcal{L}^{(1,2)}_{f\leq 2,PT\not{I}} &= -\frac{1}{2D^2}\left(\breve{\delta}m_\pi^2 - \delta m_N^2\right)\left(\boldsymbol{\pi}^2 - \pi_3^2\right) - \frac{\delta m_\pi^2}{2D^2}\pi_3^2 - \left(\delta m_N + \breve{\delta}m_N\right)\left(\boldsymbol{\pi}\times v\cdot D\boldsymbol{\pi}\right)_3 \\ &\quad + \frac{g_A \delta m_N}{F_\pi m_N} i\varepsilon_{3ab}\pi_a \bar{N}\tau_b S\cdot\mathcal{D}_- N + \frac{\beta_1}{F_\pi}\left(D_\mu\pi_3 - \frac{2\pi_3}{F_\pi^2 D}\boldsymbol{\pi}\cdot D_\mu\boldsymbol{\pi}\right)\bar{N}S^\mu N. \qquad (3.29)\end{aligned}$$

We will incorporate isospin-breaking effects using the Lagrangian (3.29).

Finally we list the relevant operators containing the electromagnetic field strength

$$\mathcal{L}^{(1)}_{f\leq 2,PT,\mathrm{em}} = -\frac{1}{4m_N}\varepsilon^{\alpha\beta\mu\nu} v_\alpha \bar{N}S_\beta\left[(1+\kappa_0) + (1+\kappa_1)\tau_3\right] N e F_{\mu\nu} \qquad (3.30)$$

ignoring terms containing pions, and with $\varepsilon^{0123} = 1$. The LECs $\kappa_0 = -0.12$ and $\kappa_1 = 3.7$ are the leading contributions to respectively, the isoscalar and isovector anomalous magnetic moments. At $\Delta = 2$ we find a relativistic correction [75] to the electromagnetic coupling of the nucleon

$$\mathcal{L}^{(2)}_{f\leq 2,PT,\mathrm{em}} = \frac{i}{16m_N^2}\varepsilon^{\alpha\beta\mu\nu}\bar{N}S_\alpha\left[(1+2\kappa_0) + (1+2\kappa_1)\tau_3\right]\mathcal{D}_{\beta,\perp,-}]N\, e F_{\mu\nu}. \qquad (3.31)$$

3.3 The parity- and time-reversal-violating chiral Lagrangian

In this section we construct the $\not{P}\not{T}$ effective Lagrangian stemming from the dimension-six operators in Eq. (2.67). The Lagrangian from the dimension-four $\bar{\theta}$ term has been constructed in Ref. [48] from which we take the most important results. The interactions stemming from the dimension-six $\not{P}\not{T}$ sources can be organized according to a chiral index analogous to Eq. (3.7) (which can be used for the $\bar{\theta}$ term), with the only difference that the coefficients of low-energy interactions must contain two powers of the high-energy scale $M_{\not{T}}$, which replace two powers of M_{QCD}. The powers of M_{QCD} in a coefficient are therefore counted by

$$\Delta_6 = d + f/2 - 4, \qquad (3.32)$$

where d counts derivatives, powers of the quark mass, and photon fields as described above. We will find that for the qEDM, qCEDM, gCEDM and χI four-quark operators $\Delta_6 > -2$, while for the FQLR operator $\Delta_6 > -4$. The $\not{P}\not{T}$ Lagrangian can be constructed by writing down all terms that transform in the same way under Lorentz, P, T, and chiral symmetry as the terms in Eq. (2.67).

The gCEDM and the two four-quark operators in Eq. (2.67) with coefficients $\mathrm{Im}\Sigma_{1,8}$ conserve chiral symmetry, *i.e.* they are $SO(4)$ scalars. This implies that they induce identical chiral Lagrangians. From now on we refer to these as χI sources and use the symbol w ($\bar{I}$) to denote collectively the dimensionless constants w and $\sigma_{1,8}$ (the invariants I_w, $I_{qq}^{(1)}$, and $I_{qq}^{(8)}$) in Eq.

(2.58) (Eq. (2.67)):

$$\{w, \sigma_1, \sigma_8\} \rightarrow w \tag{3.33}$$

$$\left\{I_w, I_{qq}^{(1)}, I_{qq}^{(8)}\right\} \rightarrow \bar{I}. \tag{3.34}$$

As discussed in Sect. 2.5, the dimensionless coefficients $\bar{\theta}$, $\delta_{0,3}$, $\tilde{\delta}_{0,3}$, w, and ξ are model dependent and we construct the low-energy $\not{P}\not{T}$ Lagrangian for each source separately. The question now is to what order, for each separate source, do we need to construct the $\not{P}\not{T}$ chiral Lagrangian. This obviously depends on what observable one wants to calculate. In this thesis we calculate the $\not{P}\not{T}$ electromagnetic moments and form factors of light nuclei which requires the use of the most important $\not{P}\not{T}$ πN, NN, nucleon-photon ($N\gamma$), and pion-nucleon-photon ($\pi N\gamma$) interactions. In order to compare our EFT approach to more traditional approaches where $\not{P}\not{T}$ is implemented through three nonderivative $\not{P}\not{T}$ πN interactions, we construct the πN Lagrangian for each source up to the order where all three of these interactions appear. As we will see, the $\not{P}\not{T}$ NN interactions are, depending on the source, of the same order or subleading with respect to $\not{P}\not{T}$ one-pion exchange between nucleons and we only construct the LO operators in the NN sector. We construct the electromagnetic sector until, for each source, we find the first momentum dependence of the nucleon electric dipole form factor, the Schiff moment, which is important for the evaluation of atomic EDMs [76]. Since operators with two explicit photons give small contributions even to atomic EDMs [77], we do not construct here operators with more than a single soft photon. Not all operators we construct here are actually used in the calculations performed in later chapters. However, since other observables might depend on these unused operators we list them here for completeness.

Time-reversal violation in combination with isospin breaking leads to operators consisting of a single neutral pion, *i.e.* pion tadpoles. These tadpoles complicate calculations because additional Feynman diagrams including tadpoles need to be taken into account. In principle this can be done [48], but it is more convenient to perform a field redefinition which eliminates the pion tadpoles in favor of additional interactions in the other sectors. We first construct the Lagrangian with pion tadpoles explicit. In Sect. 3.4 we perform the field redefinition to eliminate them. This has important consequences for the effective Lagrangian originating in isospin-breaking $\not{P}\not{T}$ sources such as the qCEDM and FQLR.

We start with the construction of operators in the purely mesonic sector in Sec. 3.3.1. After that we construct the πN and NN sectors in, respectively, Secs. 3.3.2 and 3.3.3. We extend our analysis to include electromagnetism in Sec. 3.3.4.

3.3.1 Pion sector

$\bar{\theta}$ term and quark chromo-EDM

The qCEDM consists of two independent components. The isoscalar and isovector qCEDM transform, respectively, as the fourth and third component of the $SO(4)$ vectors $\tilde{V}$ and $\tilde{W}$ defined in Eq. (2.64). Since the QCD $\bar{\theta}$ term transforms as the fourth component of an $SO(4)$ vector as well, the $\bar{\theta}$ term and isoscalar qCEDM generate identical chiral operators with different strengths. As was found in Ref. [48], without any nucleon fields it is not possible to construct an operator that transforms as the fourth component of an $SO(4)$ vector. The isovector qCEDM, however, breaks isospin symmetry and generates a pion tadpole with chiral index $\Delta_6 = -2$,

$$\mathcal{L}_{\tilde{q},f=0}^{(-2)} = \tilde{\Delta}^{(-2)} \frac{F_\pi \pi_3}{2D}. \tag{3.35}$$

By NDA the LEC scales as

$$\tilde{\Delta}^{(-2)} = \mathcal{O}\left(\tilde{\delta}_3 \frac{m_\pi^2 M_{\rm QCD}^2}{M_T^2}\right). \tag{3.36}$$

The tadpole causes the vacuum to become unstable because it can create neutral pions to lower its energy. Since the tadpole is small compared to the pion mass it can, in principle, be treated in perturbation theory, but a more convenient way of handling the tadpole is to rotate it away by performing a field redefinition [48]; we do so in Sec. 3.4.

The next operators appear two orders higher in the chiral expansion, and apart from operators containing two derivatives there are contributions from the combined effect of the quark mass and the qCEDM. This produces pionic operators with the same chiral properties as the tensor products $\bar{m}S_4 \otimes \tilde{d}_3\tilde{W}_3$ and $\bar{m}\varepsilon P_3 \otimes (m_*\bar{\theta}P_4 - \tilde{d}_0\tilde{V}_4)$,

$$\mathcal{L}^{(0)}_{\tilde{q},f=0} = \vartheta_1 \frac{\pi_3}{F_\pi D}(D_\mu\boldsymbol{\pi}\cdot D^\mu\boldsymbol{\pi}) + \tilde{\Delta}^{(0)}\frac{F_\pi\pi_3}{2D^2}\left(1-\frac{\boldsymbol{\pi}^2}{F_\pi^2}\right), \tag{3.37}$$

where

$$\vartheta_1 = \mathcal{O}\left(\tilde{\delta}_3\frac{m_\pi^2}{M_T^2}\right), \qquad \tilde{\Delta}^{(0)} = \mathcal{O}\left(\varepsilon\bar{\theta}\frac{m_\pi^4}{M_{\rm QCD}^2}, (\varepsilon\tilde{\delta}_0+\tilde{\delta}_3)\frac{m_\pi^4}{M_T^2}\right). \tag{3.38}$$

The + appearing in the scaling of $\tilde{\Delta}^{(0)}$ should not be taken literally, but as an indication that the LECs get contributions from two different sources.

Four-quark left-right operator

The FQLR operator has the most complicated chiral structure, transforming as the 3-4 component of the symmetric tensor X defined in Eq. (2.66). In the pionic sector this leads to a tadpole operator

$$\mathcal{L}^{(-4)}_{{\rm LR},f=0} = \bar{\Delta}^{(-4)}\frac{F_\pi\pi_3}{2D^2}\left(1-\frac{\boldsymbol{\pi}^2}{F_\pi^2}\right), \tag{3.39}$$

with coefficient

$$\bar{\Delta}^{(-4)} = \mathcal{O}\left(\xi\frac{M_{\rm QCD}^4}{M_T^2}\right). \tag{3.40}$$

Eq. (3.39) contains three-pion vertices different from those in Eq. (3.35). This difference is important because the elimination of the pion tadpole does not completely cancel the operator in Eq. (3.39), but leaves some three-pion couplings behind. We will discuss them in Secs. 3.4 and 3.5.

Two orders down we find terms with two derivatives and terms transforming as $X_{34}\otimes\bar{m}S_4$,

$$\begin{aligned}\mathcal{L}^{(-2)}_{{\rm LR},f=0} = {}& \vartheta_2\frac{\pi_3}{F_\pi D^2}(D_\mu\boldsymbol{\pi}\cdot D^\mu\boldsymbol{\pi})\left(1-\frac{\boldsymbol{\pi}^2}{F_\pi^2}\right) + \vartheta_3\frac{\boldsymbol{\pi}\cdot D_\mu\boldsymbol{\pi}}{F_\pi D}\left(D^\mu\pi_3 - \frac{2\pi_3\boldsymbol{\pi}\cdot D^\mu\boldsymbol{\pi}}{F_\pi^2 D}\right)\\ &+\frac{F_\pi\pi_3}{2D}\left[\bar{\Delta}_1^{(-2)} + \bar{\Delta}_2^{(-2)}\left(1-\frac{2\boldsymbol{\pi}^2}{F_\pi^2 D}\right)^2\right],\end{aligned} \tag{3.41}$$

with the scaling

$$\vartheta_{2,3} = \mathcal{O}\left(\xi\frac{M_{\rm QCD}^2}{M_T^2}\right), \qquad \bar{\Delta}_{1,2}^{(-2)} = \mathcal{O}\left(\xi\frac{m_\pi^2 M_{\rm QCD}^2}{M_T^2}\right). \tag{3.42}$$

Quark electric dipole moment

The qEDM contributes to the pionic sector through photon exchange and the LECs are suppressed by $\alpha_{\rm em}/4\pi$. The induced operators transform as $(d_3W_3 + d_0V_4) \otimes e(I^\mu/6 + T^\mu_{34}/2)$ and are given by

$$\mathcal{L}^{(1)}_{q,f=0} \quad = \quad \bar{\Delta}^{(1)} \frac{F_\pi \pi_3}{2D}, \tag{3.43}$$

where the LEC scales as

$$\bar{\Delta}^{(1)} = \mathcal{O}\left(\frac{\alpha_{\rm em}}{4\pi}(\delta_0 + \delta_3) \frac{m_\pi^2 M_{\rm QCD}^2}{M_{\not T}^2} \right). \tag{3.44}$$

Again the + in the scaling of the LEC should not be taken literally.

Chiral-invariant sources

In the mesonic sector it is not possible to write down $\not P\not T$ χI operators. Operators in this sector can be constructed by combining the effects of χI operators with chiral-symmetry breaking from the quark-mass difference,

$$\mathcal{L}^{(-2)}_{w,f=0} \quad = \quad \bar{\Delta}^{(-2)}_w \frac{F_\pi \pi_3}{2D}, \tag{3.45}$$

with

$$\bar{\Delta}^{(-2)}_w = \mathcal{O}\left(w\varepsilon \frac{m_\pi^2 M_{\rm QCD}^2}{M_{\not T}^2} \right). \tag{3.46}$$

At $\Delta_6 = 0$, we get operators with two covariant derivatives and operators transforming as $\bar{m}S_4 \otimes \bar{m}\varepsilon P_3 \otimes d_w \bar{I}$,

$$\mathcal{L}^{(0)}_{w,f=0} \quad = \quad \vartheta_1 \frac{\pi_3}{F_\pi D}(D_\mu \boldsymbol{\pi} \cdot D^\mu \boldsymbol{\pi}) + \bar{\Delta}^{(0)}_w \frac{\pi_3 F_\pi}{2D^2}\left(1 - \frac{\boldsymbol{\pi}^2}{F_\pi^2}\right), \tag{3.47}$$

where the LECs scale as

$$\vartheta_1 = \mathcal{O}\left(w\varepsilon \frac{m_\pi^2}{M_{\not T}^2} \right), \qquad \bar{\Delta}^{(0)}_w = \mathcal{O}\left(w\varepsilon \frac{m_\pi^4}{M_{\not T}^2} \right). \tag{3.48}$$

3.3.2 Pion-nucleon sector

$\bar{\theta}$ term and quark chromo-EDM

We start with operators coming from the $\bar{\theta}$ term and the isoscalar qCEDM. They both transform as fourth components of an $SO(4)$ vector and they generate identical chiral operators (of course with different strengths). The lowest-order contributions of the $\bar{\theta}$ term and isoscalar qCEDM to the πN Lagrangian arise at chiral order $\Delta_6 = -1$ ($\Delta = 1$) and consist of the isospin-conserving πN coupling,

$$\mathcal{L}^{(-1)}_{\bar{\theta},\tilde{q},f=2} \quad = \quad -\frac{\bar{g}_0}{F_\pi D} \bar{N} \boldsymbol{\tau} \cdot \boldsymbol{\pi} N. \tag{3.49}$$

This operator is induced by both sources directly and by NDA the LEC scales as

$$\bar{g}_0 = \mathcal{O}\left(\bar{\theta}\frac{m_\pi^2}{M_{\rm QCD}},\ \tilde{\delta}_0\frac{m_\pi^2 M_{\rm QCD}}{M_T^2}\right). \tag{3.50}$$

Before continuing with the construction of other operators it is useful to study in more detail the operator in Eq. (3.49) induced by the $\bar{\theta}$ term. As shown in Eq. (2.45), the $\bar{\theta}$ term transforms as the fourth component of the $SO(4)$ vector P whose third component is responsible for isospin breaking from the quark-mass difference [48]. That is, for each $\not{P}\not{T}$ operator induced by the $\bar{\theta}$ term there is an associated PT isospin-breaking operator. As explained in Sec. 3.2, the chiral operators induced by the vector P are constructed by rotating an operator involving non-Goldstone fields Ψ only

$$P_\alpha[\boldsymbol{\pi},\Psi] \;=\; R_{\alpha\beta}P_\beta[0,\Psi]. \tag{3.51}$$

By using $P_\beta[0,\Psi] = v(\bar{N}\tau_i N\ 0)$, where v is a real number determined by the dynamics of spontaneous chiral symmetry breaking, the PT isospin-breaking and $\not{P}\not{T}$ operators become

$$v\left\{(\varepsilon\bar{m})\bar{N}\left(\tau_3 - \frac{2\pi_3}{F_\pi^2 D}\boldsymbol{\tau}\cdot\boldsymbol{\pi}\right)N - (m_*\bar{\theta})\frac{2}{F_\pi D}\bar{N}\boldsymbol{\pi}\cdot\boldsymbol{\tau}N\right\}. \tag{3.52}$$

The first term in this equation is the nucleon mass difference in Eq. (3.18) with the identification $\delta m_N = 2v\,\varepsilon\bar{m}$ and the second term is the $\not{P}\not{T}$ isospin-conserving πN vertex in Eq. (3.49) with the identification $\bar{g}_0 = 2v\,m_*\bar{\theta}$. In this case, $\bar{g}_0$ and δm_N depend on the same number v, such that the ratio $\bar{g}_0/\delta m_N = m_*\bar{\theta}/\varepsilon\bar{m} \approx \bar{\theta}/(2\varepsilon)$ is independent of v. Using the lattice-QCD value $\delta m_N/(2\varepsilon) = 2.8\,\text{MeV}$ [71] we find

$$\bar{g}_0 \;\simeq\; (2.8\,\text{MeV})\,\bar{\theta}, \tag{3.53}$$

which provides a more accurate estimation of $\bar{g}_0$ than Eq. (3.50). For other operators induced by the $\bar{\theta}$ term there are similar links between PT and $\not{P}\not{T}$ operators. Unfortunately, in these cases there is no precise lattice calculation or experimental extraction of the corresponding isospin-breaking PT LEC, such that we cannot do better than NDA. These additional relations can be found in Ref. [48].

Contrary to the $\bar{\theta}$ term the qCEDM has an isovector component. This component transforms as the third component of an $SO(4)$ vector, and therefore breaks chiral and isospin symmetry. At LO the isovector qCEDM generates

$$\mathcal{L}^{(-1)}_{\tilde{q},f=2} \;=\; -\frac{\bar{g}_1}{F_\pi D}\pi_3\bar{N}N, \tag{3.54}$$

where

$$\bar{g}_1 = \mathcal{O}\left(\tilde{\delta}_3\frac{m_\pi^2 M_{\rm QCD}}{M_T^2}\right). \tag{3.55}$$

Eqs. (3.49) and (3.54) show the first important difference between $\not{P}\not{T}$ from dimension-six operators and the QCD $\bar{\theta}$ term, namely the presence of the $\not{P}\not{T}$ isospin-breaking interaction $\bar{g}_1$ at leading order in the $f = 2$ Lagrangian. The $\bar{\theta}$ term also generates this interaction but, as we will see, it is suppressed by two powers of $m_\pi/M_{\rm QCD}$ compared to the $\not{P}\not{T}$ isospin-conserving interaction $\bar{g}_0$ [48]. This difference is particularly relevant for the $\not{P}\not{T}$ moments of the deuteron.

Increasing Δ_6 by one, we find operators with one covariant derivative,

$$\begin{aligned}\mathcal{L}^{(0)}_{\bar\theta,\tilde q,f=2} &= \frac{2\bar\beta_1}{F_\pi^2 D}(\boldsymbol{\pi}\cdot\mathcal{D}_\mu\boldsymbol{\pi})\bar N S^\mu N + \frac{2\bar\beta_2}{F_\pi^2 D}(\pi_3\mathcal{D}_\mu\boldsymbol{\pi})\cdot\bar N S^\mu\boldsymbol{\tau}N\\ &\quad+\frac{\bar\beta_3}{F_\pi}\left(\delta^{i3}-\frac{2\pi_i\pi_3}{F_\pi^2 D}\right)\bar N(\boldsymbol{\tau}\times v\cdot D\boldsymbol{\pi})_i N,\end{aligned}\tag{3.56}$$

with LECs scaling as

$$\bar\beta_1=\mathcal{O}\left(\bar\theta\frac{m_\pi^2}{M_{\rm QCD}^2},\ \tilde\delta_0\frac{m_\pi^2}{M_T^2}\right),\qquad \bar\beta_{2,3}=\mathcal{O}\left(\tilde\delta_3\frac{m_\pi^2}{M_T^2}\right).\tag{3.57}$$

With two covariant derivatives we find the following interactions originating from the $\bar\theta$ term and isoscalar qCEDM

$$\begin{aligned}\mathcal{L}^{(1)}_{\bar\theta,\tilde q,f=2} &= \left\{\frac{\bar\zeta_1}{2F_\pi}(D_\nu\boldsymbol{\pi})\cdot\bar N[S^\mu,S^\nu]\boldsymbol{\tau}\mathcal{D}_{\mu,-}N+\frac{\bar\zeta_2}{F_\pi}(v\cdot\mathcal{D}v\cdot D\boldsymbol{\pi})\cdot\bar N\boldsymbol{\tau}N\right.\\ &\quad\left.+\frac{\bar\zeta_3}{F_\pi}(\mathcal{D}_{\mu,\perp}D^\mu_\perp\boldsymbol{\pi})\cdot\bar N\boldsymbol{\tau}N+\frac{\bar\zeta_4}{F_\pi^2}(D_\mu\boldsymbol{\pi}\times v\cdot D\boldsymbol{\pi})\cdot\bar N S^\mu\boldsymbol{\tau}N\right\}\frac{1}{D}\left(1-\frac{\boldsymbol{\pi}^2}{F_\pi^2}\right)\\ &\quad-\left\{-\frac{\bar\zeta_5}{4}\bar N\boldsymbol{\tau}(v\cdot\mathcal{D}_-)^2N-\frac{\bar\zeta_6}{4}\bar N\boldsymbol{\tau}\mathcal{D}^2_{\perp,-}N+\frac{\bar\zeta_7}{F_\pi}\bar N S^\mu(\boldsymbol{\tau}\times(v\cdot\mathcal{D}D_\mu\boldsymbol{\pi}))N\right.\\ &\quad+\frac{i\bar\zeta_8}{F_\pi}(v\cdot D\boldsymbol{\pi})\bar N S\cdot\mathcal{D}_-N+2\frac{i\bar\zeta_9}{F_\pi^2}(D_\mu\boldsymbol{\pi}\times D_\nu\boldsymbol{\pi})\bar N[S^\mu,S^\nu]N\\ &\quad+\frac{\bar\zeta_{10}}{F_\pi^2}D_\mu\boldsymbol{\pi}((D^\mu\boldsymbol{\pi})\cdot\bar N\boldsymbol{\tau}N)+\frac{\bar\zeta_{11}}{F_\pi^2}v\cdot D\boldsymbol{\pi}((v\cdot D\boldsymbol{\pi})\cdot\bar N\boldsymbol{\tau}N)\\ &\quad\left.+\frac{\bar\zeta_{12}}{F_\pi^2}(D_\mu\boldsymbol{\pi})^2\bar N\boldsymbol{\tau}N+\frac{\bar\zeta_{13}}{F_\pi^2}(v\cdot D\boldsymbol{\pi})^2\bar N\boldsymbol{\tau}N\right\}\cdot\frac{\boldsymbol{\pi}}{F_\pi D},\end{aligned}\tag{3.58}$$

and originating from the isovector qCEDM

$$\begin{aligned}\mathcal{L}^{(1)}_{\tilde q,f=2} &= \left\{\frac{\bar\xi_1}{F_\pi}D_\nu\pi_i\bar N[S^\mu,S^\nu]\mathcal{D}_{\mu,-}N+\frac{\bar\xi_2}{F_\pi}(v\cdot\mathcal{D}v\cdot D\pi_i)\bar N N\right.\\ &\quad+\frac{\bar\xi_3}{F_\pi}(\mathcal{D}_{\mu,\perp}D^\mu_\perp\pi_i)\bar N N+2\frac{\bar\xi_4}{F_\pi^2}(D_\mu\boldsymbol{\pi}\times v\cdot D\boldsymbol{\pi})_i\bar N S^\mu N\\ &\quad\left.+\frac{i\bar\xi_5}{F_\pi}\bar N((D_\mu\boldsymbol{\pi})\times\boldsymbol{\tau})_i\mathcal{D}^\mu_{\perp,-}N\right\}\left(\delta_{i3}-\frac{2\pi_3\pi_i}{F_\pi^2 D}\right)\\ &\quad+\left\{-\frac{\bar\xi_6}{4}\bar N(v\cdot\mathcal{D}_-)^2N-\frac{\bar\xi_7}{4}\bar N\mathcal{D}^2_{\perp,-}N+\frac{i\bar\xi_8}{2F_\pi}(v\cdot D\boldsymbol{\pi})\cdot\bar N\boldsymbol{\tau}S\cdot\mathcal{D}_-N\right.\\ &\quad+\frac{i\bar\xi_9}{2F_\pi^2}(D_\mu\boldsymbol{\pi}\times D_\nu\boldsymbol{\pi})\cdot\bar N[S^\mu,S^\nu]\boldsymbol{\tau}N+\frac{\bar\xi_{10}}{F_\pi^2}(D_\mu\boldsymbol{\pi})^2\bar N N\\ &\quad\left.+\frac{\bar\xi_{11}}{F_\pi^2}(v\cdot D\boldsymbol{\pi})^2\bar N N\right\}\frac{2\pi_3}{F_\pi D}.\end{aligned}\tag{3.59}$$

The scaling of the LECs $\bar\zeta_i$ and $\bar\xi_i$ are

$$\bar\zeta_i=\mathcal{O}\left(\bar\theta\frac{m_\pi^2}{M_{\rm QCD}^3},\ \tilde\delta_0\frac{m_\pi^2}{M_T^2}\frac{1}{M_{\rm QCD}}\right),\qquad \bar\xi_i=\mathcal{O}\left(\tilde\delta_3\frac{m_\pi^2}{M_T^2}\frac{1}{M_{\rm QCD}}\right).\tag{3.60}$$

The heavy-baryon χPT Lagrangian is not manifestly Lorentz invariant, but Lorentz covariance is realized order by order in the $1/m_N$ expansion by relating the coefficients of power-suppressed operators to low-energy constants in the leading Lagrangian. We used RPI [58, 60] specialized to χPT (see App. A) to find the following relations

$$\begin{aligned}
&\bar{\zeta}_1 = \bar{\zeta}_6 = \frac{\bar{g}_0}{2m_N^2}, \qquad \zeta_8 = \frac{g_A\bar{g}_0}{m_N^2} - \frac{\bar{\beta}_1}{m_N}, \\
&\bar{\xi}_1 = -\bar{\xi}_7 = \frac{\bar{g}_1}{4m_N^2}, \qquad \bar{\xi}_5 = -\frac{\bar{\beta}_3}{2m_N}, \qquad \bar{\xi}_8 = -\frac{g_A\bar{g}_1}{m_N^2} - \frac{\bar{\beta}_2}{m_N}.
\end{aligned} \tag{3.61}$$

At the same order interactions arise from the combined effect of $\bar{\theta}$ or the qCEDM and the QCD mass terms. The resulting operators transform as $(\bar{m}S_4 - \varepsilon\bar{m}P_3)\otimes(m_*\bar{\theta}P_4 - \tilde{d}_0\tilde{V}_4 + \tilde{d}_3\tilde{W}_3)$. The isoscalar $\not{P}\not{T}$ sources generate

$$\mathcal{L}^{(1)}_{\bar{\theta},\tilde{q},f=2} = -\frac{\bar{g}_1}{F_\pi D}\pi_3\left(1 - \frac{2\boldsymbol{\pi}^2}{F_\pi^2}\right)\bar{N}N - \delta\bar{g}_0\frac{1}{F_\pi D}\left(1 - \frac{2\boldsymbol{\pi}^2}{F_\pi^2}\right)\bar{N}\boldsymbol{\tau}\cdot\boldsymbol{\pi}N, \tag{3.62}$$

while the isovector qCEDM generates

$$\mathcal{L}^{(1)}_{\tilde{q},f=2} = -\frac{\delta\bar{g}_1}{F_\pi D}\pi_3\left(1 - \frac{2\boldsymbol{\pi}^2}{F_\pi^2}\right)\bar{N}N - \frac{\bar{g}_2}{F_\pi D}\pi_3\bar{N}\left(\tau_3 - \frac{2\pi_3}{F_\pi^D}\boldsymbol{\tau}\cdot\boldsymbol{\pi}\right)N., \tag{3.63}$$

The first operator in Eq. (3.62) is the dominant contribution from the $\bar{\theta}$ term and isoscalar qCEDM to the isovector $\not{P}\not{T}$ πN coupling, from which it differs only by terms containing three or more pions. The required isospin violation is brought in by the quark-mass difference. The LEC scales as

$$\bar{g}_1 = \mathcal{O}\left(\varepsilon\bar{\theta}\frac{m_\pi^4}{M_{\rm QCD}^3},\ \varepsilon\tilde{\delta}_0\frac{m_\pi^4}{M_{\not{T}}^2}\frac{1}{M_{\rm QCD}}\right), \tag{3.64}$$

such that for these sources $\bar{g}_1/\bar{g}_0 = \mathcal{O}(\varepsilon m_\pi^2/M_{\rm QCD}^2)$. The second operator in Eq. (3.62) is a correction to the isoscalar $\not{P}\not{T}$ coupling in Eq. (3.49), and again it differs only by terms with three or more pions. Similarly the first term in Eq. (3.63) is a correction to $\bar{g}_1$, which for the isovector qCEDM already appears at $\Delta_6 = -1$. The corrections scale as

$$\delta\bar{g}_0 = \mathcal{O}\left(\bar{\theta}\frac{m_\pi^4}{M_{\rm QCD}^3},\ \tilde{\delta}_0\frac{m_\pi^4}{M_{\not{T}}^2}\frac{1}{M_{\rm QCD}}\right), \qquad \delta\bar{g}_1 = \mathcal{O}\left(\tilde{\delta}_1\frac{m_\pi^4}{M_{\not{T}}^2}\frac{1}{M_{\rm QCD}}\right). \tag{3.65}$$

For most practical purposes $\delta\bar{g}_0$ and $\delta\bar{g}_1$ can be absorbed into $\bar{g}_0$ and $\bar{g}_1$.

Finally, the second operator in (3.63) is the most interesting, as it is the first contribution of the qCEDM to the isospin-breaking πN interaction $\pi_3\bar{N}\tau_3 N$. At this order, all three possible nonderivative πN $\not{P}\not{T}$ interactions receive a contribution from the isovector qCEDM. It originates from $\varepsilon\bar{m}P_3\otimes\tilde{d}_3\tilde{W}_3$ and has the scaling

$$\bar{g}_2 = \mathcal{O}\left(\varepsilon\tilde{\delta}_3\frac{m_\pi^4}{M_{\not{T}}^2}\frac{1}{M_{\rm QCD}}\right). \tag{3.66}$$

The $\bar{\theta}$ term and isoscalar qCEDM generate $\bar{g}_2$ as well, but this requires a photon exchange such that $\bar{g}_2$ is suppressed by $\alpha_{\rm em}/4\pi$ and enters at $\Delta_6 = 2$ ($\Delta = 4$). We do not construct these operators here. This observation provides the second difference between $\not{P}\not{T}$ hadronic interactions originating from the $\bar{\theta}$ term and the qCEDM. However, for both sources $\bar{g}_2$ enters in the subleading Lagrangian and the difference is of little phenomenological interest.

Four-quark left-right operator

In case of the FQLR operator the πN operators start at $\Delta_6 = -3$. At this order there is only one operator,

$$\mathcal{L}^{(-3)}_{\mathrm{LR},f=2} = -\frac{\bar{g}_1}{F_\pi D}\pi_3\left(1-\frac{2\boldsymbol{\pi}^2}{F_\pi^2 D}\right)\bar{N}N, \tag{3.67}$$

with

$$\bar{g}_1 = \mathcal{O}\left(\xi\frac{M^3_{\mathrm{QCD}}}{M_T^2}\right). \tag{3.68}$$

It appears as if the FQLR only generates $\bar{g}_1$ at LO, in stark contrast with the $\bar{\theta}$ term and qCEDM which generate, respectively, $\bar{g}_0$ and $\bar{g}_{0,1}$ at LO. This would imply that the FQLR can relatively easily be separated from the other sources. However, as we will see in Sec. 3.4, the removal of the tadpole in Eq. (3.39) effectively causes the appearance of the $\bar{g}_0$ interaction at $\Delta_6 = -3$.

At $\Delta_6 = -2$ we find

$$\begin{aligned}\mathcal{L}^{(-2)}_{\mathrm{LR},f=2} &= +\frac{2\bar{\beta}_2}{F_\pi^2 D}\left(1-\frac{2\boldsymbol{\pi}^2}{F_\pi^2 D}\right)(\pi_3\mathcal{D}_\mu\boldsymbol{\pi})\cdot\bar{N}S^\mu\boldsymbol{\tau}N \\ &\quad+\frac{\bar{\beta}_3}{F_\pi}\left[\delta^{i3}\left(1-\frac{2\boldsymbol{\pi}^2}{F_\pi^2 D}\right)-\frac{2\pi_i\pi_3}{F_\pi^2 D}\left(3-\frac{4\boldsymbol{\pi}^2}{F_\pi^2 D}\right)\right]\bar{N}(\boldsymbol{\tau}\times v\cdot D\boldsymbol{\pi})_3 N \\ &\quad+\frac{2\bar{\beta}_4}{F_\pi^2 D}\left[(D_\mu\pi_3)\pi_i\ +(\boldsymbol{\pi}\cdot D_\mu\boldsymbol{\pi})\left(\delta_{i3}-\frac{4\pi_i\pi_3}{F_\pi^2 D}\right)\right]\bar{N}S^\mu\tau_i N,\end{aligned} \tag{3.69}$$

where

$$\bar{\beta}_i = \mathcal{O}\left(\xi\frac{M^2_{\mathrm{QCD}}}{M_T^2}\right). \tag{3.70}$$

The first two terms in Eq. (3.69) are similar to those arising from the isovector qCEDM in Eq. (3.56), but the pion structure is more complicated. The third operator does not appear for the qCEDM because the tensor structure of the FQLR allows for more complicated structures.

At $\Delta_6 = -1$ operators similar to Eq. (3.59) appear, but with the replacement

$$\begin{aligned}\left(\delta_{i3}-\frac{2\pi_3\pi_i}{F_\pi^2 D}\right) &\to \left[\delta_{i3}\left(1-\frac{2\boldsymbol{\pi}^2}{F_\pi^2 D}\right)-\frac{2\pi_i\pi_3}{F_\pi^2 D}\left(3-\frac{4\boldsymbol{\pi}^2}{F_\pi^2 D}\right)\right], \\ \frac{2\pi_3}{F_\pi D} &\to \frac{2\pi_3}{F_\pi D}\left(1-\frac{2\boldsymbol{\pi}^2}{F_\pi^2 D}\right).\end{aligned} \tag{3.71}$$

The RPI relations are the same as in Eq. (3.61). Apart from these interactions the FQLR generates

$$\begin{aligned}\mathcal{L}^{(-1)}_{\mathrm{LR},f=2} &= \frac{2\bar{\xi}_{12}}{F_\pi^3 D}\left[D^\mu\pi_3-\frac{2\pi_3(\boldsymbol{\pi}\cdot D_\mu\boldsymbol{\pi})}{F_\pi^2 D}\right](\boldsymbol{\pi}\cdot D_\mu\boldsymbol{\pi})\bar{N}N \\ &\quad+\frac{2\bar{\xi}_{13}}{F_\pi^3 D}\left[\delta_{i3}\pi_j+\delta_{j3}\pi_i-\frac{4\pi_3\pi_i\pi_j}{F_\pi^2 D}\right](D_\mu\boldsymbol{\pi}\times D_\mu\boldsymbol{\pi})_i\bar{N}i[S^\mu,S^\nu]\tau_j N \\ &\quad+\frac{2\bar{\xi}_{14}}{F_\pi^2 D}\left[\delta_{i3}\pi_j+\delta_{j3}\pi_i-\frac{4\pi_3\pi_i\pi_j}{F_\pi^2 D}\right](v\cdot D\pi_i)\bar{N}\tau_j S\cdot\mathcal{D}_- N,\end{aligned} \tag{3.72}$$

where

$$\bar{\xi}_i = \mathcal{O}\left(\xi\frac{M_{\mathrm{QCD}}}{M_T^2}\right), \tag{3.73}$$

and $\bar{\xi}_{14}$ is a recoil correction

$$\xi_{14} = -\frac{\bar{\beta}_4}{m_N}. \tag{3.74}$$

At the same order, operators appear due to an insertion of the quark mass (difference)

$$\begin{aligned}\mathcal{L}^{(-1)}_{\mathrm{LR},f=2} &= -\delta\bar{g}_0\bar{N}\boldsymbol{\tau}\cdot\boldsymbol{\pi}N - \frac{\pi_3}{F_\pi D}\left[\delta_1\bar{g}_1 + \delta_2\bar{g}_1\left(1-\frac{2\boldsymbol{\pi}^2}{F_\pi^2 D}\right)^2\right]\bar{N}N \\ &\quad -\frac{\bar{g}_2}{F_\pi D}\pi_3\left(1-\frac{2\boldsymbol{\pi}^2}{F_\pi^2 D}\right)\bar{N}\left(\tau_3 - \frac{2\pi_3}{F_\pi D}\boldsymbol{\tau}\cdot\boldsymbol{\pi}\right)N - \frac{\bar{g}_3}{F_\pi^3 D^3}\pi_3^2\bar{N}\boldsymbol{\tau}\cdot\boldsymbol{\pi}N. \end{aligned}\tag{3.75}$$

The LECs scale as

$$\delta_{1,2}\bar{g}_1 = \mathcal{O}\left(\xi\frac{m_\pi^2 M_{\mathrm{QCD}}}{M_{\not T}^2}\right),\ \ \delta\bar{g}_0 = \mathcal{O}\left(\xi\varepsilon\frac{m_\pi^2 M_{\mathrm{QCD}}}{M_{\not T}^2}\right),\ \ \bar{g}_{2,3} = \mathcal{O}\left(\xi\varepsilon\frac{m_\pi^2 M_{\mathrm{QCD}}}{M_{\not T}^2}\right). \tag{3.76}$$

Although the operators in Eq. (3.75) look very complicated, if we ignore operators with three or more pions the $\delta_{0,1}\bar{g}_1$ and $\delta\bar{g}_0$ terms are contributions to the standard nonderivative πN interactions. Just as for the isovector qCEDM, the third πN coupling $\bar{g}_2$ appears two orders higher than $\bar{g}_{0,1}$.

quark EDM

The πN interactions originating from the qEDM arise from the tensor product $(-d_0V_4+d_3W_3)\otimes e(I^\mu/6 + T^\mu_{34}/2)$ which generates

$$\begin{aligned}\mathcal{L}^{(2)}_{q,f=2} &= -\frac{\bar{g}_0}{F_\pi D}\bar{N}\boldsymbol{\tau}\cdot\boldsymbol{\pi}N - \frac{\bar{g}_1}{F_\pi D}\pi_3\bar{N}N \\ &\quad -\frac{\bar{g}_2}{F_\pi D}\pi_3\bar{N}\left[\tau_3 + \frac{2}{F_\pi^2 D}\left(\pi_3\boldsymbol{\tau}\cdot\boldsymbol{\pi} - \boldsymbol{\pi}^2\tau_3\right)\right]N. \end{aligned}\tag{3.77}$$

The scaling of the LECs is

$$\bar{g}_{0,1} = \mathcal{O}\left((\delta_0+\delta_3)\frac{\alpha_{\mathrm{em}}}{4\pi}\frac{m_\pi^2 M_{\mathrm{QCD}}}{M_{\not T}^2}\right), \qquad \bar{g}_2 = \mathcal{O}\left(\delta_3\frac{\alpha_{\mathrm{em}}}{4\pi}\frac{m_\pi^2 M_{\mathrm{QCD}}}{M_{\not T}^2}\right). \tag{3.78}$$

All possible nonderivative πN interactions appear at the same order (this only holds for the isovector qEDM, for the isoscalar qEDM $\bar{g}_2$ is suppressed). For all other $\not P\not T$ sources $\bar{g}_2$ is suppressed with respect to $\bar{g}_0$ and/or $\bar{g}_1$.

Chiral-invariant sources

In the πN sector no χI $\not P\not T$ operator can be constructed with zero or one covariant derivative. The first operators therefore start at $\Delta_6 = -1$ and have two covariant derivatives or one insertion of the quark mass (difference)

$$\begin{aligned}\mathcal{L}^{(-1)}_{w,f=2} &= -\frac{\bar{\imath}_0}{F_\pi^2}(v\cdot D\boldsymbol{\pi}\times D_\mu\boldsymbol{\pi})\cdot\bar{N}\boldsymbol{\tau}S^\mu N - \frac{\bar{\imath}_1}{F_\pi}(\mathcal{D}_{\perp\mu}D^\mu_\perp\boldsymbol{\pi})\cdot\bar{N}\boldsymbol{\tau}N \\ &\quad -\frac{\bar{g}_0}{F_\pi D}\bar{N}\boldsymbol{\tau}\cdot\boldsymbol{\pi}N - \frac{\bar{g}_1}{F_\pi D}\pi_3\bar{N}N, \end{aligned}\tag{3.79}$$

with the scaling

$$\bar{\iota}_i = \mathcal{O}\left(w\frac{M_{\rm QCD}}{M_{\not T}^2}\right), \qquad \bar{g}_0 = \mathcal{O}\left(w\frac{m_\pi^2 M_{\rm QCD}}{M_{\not T}^2}\right), \qquad \bar{g}_1 = \mathcal{O}\left(w\varepsilon\frac{m_\pi^2 M_{\rm QCD}}{M_{\not T}^2}\right). \tag{3.80}$$

It is interesting to notice that rotational invariance alone would allow a two-derivative operator of the form $\bar{\zeta}_1 D_\mu\boldsymbol{\pi}\cdot\bar{N}\boldsymbol{\tau}[S^\mu,S^\nu]\mathcal{D}_{\nu-}N$ in Eq. (3.79). However, this operator is not reparametrization-invariant by itself, and its variation cannot be absorbed by any other operator in the leading-order Lagrangian. RPI, therefore, forces $\bar{\zeta}_1$ to vanish in leading order (see App. A). The operator $\bar{\zeta}_1$ appears at NNLO and it is linked to $\bar{g}_0$ by RPI as in Eq. (3.61).

From Eq. (3.80) we see that the χI operators, just as the isovector qCEDM and in contrast to the $\bar{\theta}$ term and isoscalar qCEDM, induce $\bar{g}_1$ at the same order as $\bar{g}_0$. Differently from all the other sources, the χI operators also generate two-derivative operators of the same importance as $\bar{g}_0$ and $\bar{g}_1$.

One order higher we find χI operators with three covariant derivatives, one power of the quark mass and one covariant derivative, and electromagnetic operators coming from the tensor product $d_w\bar{I}\otimes e(I^\mu/6+T^\mu_{34}/2)\otimes e(I^\mu/6+T^\mu_{34}/2)$.

$$\begin{aligned}
\mathcal{L}^{(0)}_{w,f=2} \;=\;& \frac{i\,\bar{\iota}_0}{2m_N F_\pi^2}(D_\mu\boldsymbol{\pi}\times D_\nu\boldsymbol{\pi})\cdot\bar{N}\boldsymbol{\tau}S^\mu\mathcal{D}^\nu_{\perp-}N + \frac{i\,\bar{\iota}_1}{m_N F_\pi}\mathcal{D}_\mu(v\cdot D\boldsymbol{\pi})\cdot\bar{N}\boldsymbol{\tau}\mathcal{D}^\mu_{\perp-}N \\
&+\frac{\bar{\ell}_1}{F_\pi^2}\mathcal{D}_\mu(D\boldsymbol{\pi})^2\bar{N}S^\mu N + \frac{\bar{\ell}_2}{F_\pi^2}\mathcal{D}^\mu_\perp(D_\mu\boldsymbol{\pi}\cdot D_\nu\boldsymbol{\pi})\bar{N}S^\nu N \\
&+\frac{2\bar{\beta}_1}{F_\pi^2 D}(\boldsymbol{\pi}\cdot\mathcal{D}_\mu\boldsymbol{\pi})\bar{N}S^\mu N + \frac{2\bar{\beta}_2}{F_\pi^2 D}(\pi_3\mathcal{D}_\mu\boldsymbol{\pi})\cdot\bar{N}S^\mu\boldsymbol{\tau}N \\
&+\frac{\bar{\beta}_3}{F_\pi}\left(\delta_{i3}-\frac{2\pi_i\pi_3}{F_\pi^2 D}\right)\cdot\bar{N}(\boldsymbol{\tau}\times v\cdot D\boldsymbol{\pi})_i N \\
&-\frac{\bar{g}_2}{F_\pi D}\bar{N}\left[\pi_3\tau_3-\boldsymbol{\tau}\cdot\boldsymbol{\pi}\left(1-\frac{2}{F_\pi^2 D}(\boldsymbol{\pi}^2-\pi_3^2)\right)\right]N.
\end{aligned} \tag{3.81}$$

The operators in the first line are χI recoil corrections, the second line contains χI operators whose LECs are not determined by Lorentz invariance, the third and fourth lines contain operators that break chiral symmetry as the quark mass (difference), and the operator in the last line appears due to electromagnetic interactions. The LECs scale as

$$\bar{\ell}_i = \mathcal{O}\left(w\frac{1}{M_{\not T}^2}\right),\;\; \bar{\beta}_1 = \mathcal{O}\left(w\frac{m_\pi^2}{M_{\not T}^2}\right),\;\; \bar{\beta}_{(2,3)} = \mathcal{O}\left(w\varepsilon\frac{m_\pi^2}{M_{\not T}^2}\right),\;\; \bar{g}_2 = \mathcal{O}\left(w\frac{\alpha_{\rm em}}{4\pi}\frac{M_{\rm QCD}^3}{M_{\not T}^2}\right). \tag{3.82}$$

At this order the first contribution to $\bar{g}_2$ appears. With the usual assumption $\alpha_{\rm em}/4\pi \sim m_\pi^3/M_{\rm QCD}^3$, this interaction is suppressed by one power of $m_\pi/M_{\rm QCD}$ compared to $\bar{g}_0$ and $\bar{g}_1$.

3.3.3 Nucleon-nucleon sector

Apart from $\not P\not T$ πN couplings, chiral symmetry allows operators that connect nucleons directly. Such short-range interactions play a role in the $\not P\not T$ NN potential. These operators contain at least four nucleon fields and, in principle, have a higher chiral index than the $\not P\not T$ πN operators. One might think that these operators therefore play a marginal role compared to NN forces which are due to pion exchange. As we will demonstrate here, this reasoning is false for the gCEDM and χI four-quark operators.

$\bar{\theta}$ term, quark chromo-EDM, and four-quark left-right operator

We start with the interactions stemming from the $\bar{\theta}$ term, qCEDM and FQLR. As we saw in the mesonic and πN sectors, the $\bar{\theta}$ term and isoscalar qCEDM generate identical interactions. The isovector qCEDM and FQLR generate very similar interactions as well, even identical if one neglects operators with three or more pions. As we will see, πNN interactions play a marginal role in the $\not{P}\not{T}$ potential and we do not construct the detailed pion structure.

The $\bar{\theta}$ term, qCEDM, and FQLR generate

$$\begin{aligned}\mathcal{L}_{\bar{\theta},\tilde{q},\,\mathrm{LR},\,f=4} &= -\frac{1}{F_\pi D}\boldsymbol{\pi}\cdot\left(\bar{\gamma}_1\bar{N}\boldsymbol{\tau}N\,\bar{N}N+\bar{\gamma}_2\bar{N}\boldsymbol{\tau}S_\mu N\,\bar{N}S^\mu N\right)\\ &\quad -\frac{\pi_3}{F_\pi D}\left(\bar{\gamma}_3\bar{N}N\,\bar{N}N+\bar{\gamma}_4\bar{N}S_\mu N\,\bar{N}S^\mu N\right),\end{aligned}\tag{3.83}$$

where we left out some terms with three or more pions for the FQLR. The LECs scale as

$$\bar{\gamma}_{1,2}=\mathcal{O}\left(\bar{\theta}\frac{m_\pi^2}{F_\pi^2M_{\mathrm{QCD}}^2},\ \tilde{\delta}_0\frac{m_\pi^2}{F_\pi^2M_{\not{T}}^2}\right)\qquad \bar{\gamma}_{3,4}=\mathcal{O}\left(\tilde{\delta}_3\frac{m_\pi^2}{F_\pi^2M_{\not{T}}^2},\ \xi\frac{M_{\mathrm{QCD}}^2}{F_\pi^2M_{\not{T}}^2}\right).\tag{3.84}$$

One order down, we find the more interesting short-range interactions contributing directly to NN scattering. The isoscalar interactions for $\bar{\theta}$ and isoscalar qCEDM

$$\mathcal{L}_{\bar{\theta},\tilde{q},\,f=4} = \left(1-\frac{2\boldsymbol{\pi}^2}{F_\pi^2D}\right)\left[\bar{C}_1\bar{N}N\,\partial_\mu(\bar{N}S^\mu N)+\bar{C}_2\bar{N}\boldsymbol{\tau}N\cdot\mathcal{D}_\mu(\bar{N}S^\mu\boldsymbol{\tau}N)\right],\tag{3.85}$$

and the isovector ones for the isovector qCEDM and FQLR

$$\mathcal{L}_{\tilde{q},\,\mathrm{LR},\,f=4} = \left(\delta_{3i}-\frac{2\pi_3}{F_\pi^2D}\pi_i\right)\left[\bar{C}_3\bar{N}\tau_iN\,\partial_\mu\left(\bar{N}S^\mu N\right)+\bar{C}_4\bar{N}N\,\mathcal{D}_\mu\left(\bar{N}\tau_iS^\mu N\right)\right],\tag{3.86}$$

with the scalings

$$\bar{C}_{1,2}=\mathcal{O}\left(\bar{\theta}\frac{m_\pi^2}{F_\pi^2M_{\mathrm{QCD}}^3},\ \tilde{\delta}_0\frac{m_\pi^2}{F_\pi^2M_{\not{T}}^2M_{QCD}}\right),\qquad \bar{C}_{3,4}=\mathcal{O}\left(\tilde{\delta}_3\frac{m_\pi^2}{F_\pi^2M_{\not{T}}^2M_{QCD}},\ \xi\frac{M_{\mathrm{QCD}}}{F_\pi^2M_{\not{T}}^2}\right).\tag{3.87}$$

At this order, for all sources, there appear additional operators that start with one or more pions. The first contributions to $\bar{C}_{3,4}$ for the $\bar{\theta}$ term and isoscalar qCEDM appear, respectively, at $\Delta=5$ and $\Delta_6=3$ due to interference with the quark-mass difference.

A comparison between the πN and NN sector shows that, for the sources discussed here, the most important $\not{P}\not{T}$ πN interactions are larger by a factor M_{QCD}^2/Q^2 than the short-range $\not{P}\not{T}$ NN interactions, implying that for these sources the $\not{P}\not{T}$ NN potential is dominated by pion exchange. This observation justifies, *a posteriori*, the assumption often made in the literature that $\not{P}\not{T}$ nuclear observables can be calculated solely from the $\not{P}\not{T}$ πN interactions. However, for the other sources this assumption is not valid.

quark EDM

Just as for πN interactions, the NN interactions arising from qEDM originate from the tensor product $(-d_0V_4+d_3W_3)\otimes e(I^\mu/6+T_{34}^\mu/2)$. At $\Delta_6=3$ we find

$$\begin{aligned}\mathcal{L}_{q,f=4}^{(3)} &= -\frac{1}{F_\pi D}\boldsymbol{\pi}\cdot\left(\bar{\gamma}_1\bar{N}\boldsymbol{\tau}N\,\bar{N}N+\bar{\gamma}_2\bar{N}\boldsymbol{\tau}S_\mu N\,\bar{N}S^\mu N\right)\\ &\quad -\frac{\pi_3}{F_\pi D}\left(\bar{\gamma}_3\bar{N}N\,\bar{N}N+\bar{\gamma}_4\bar{N}S_\mu N\,\bar{N}S^\mu N\right)\\ &\quad -\frac{\pi_3}{F_\pi D}\left(\delta_{3i}+\frac{2}{F_\pi^2D}\left(\pi_3\pi_i-\boldsymbol{\pi}^2\delta_{3i}\right)\right)\left[\bar{\gamma}_5\bar{N}\tau_iN\bar{N}N+\bar{\gamma}_6\bar{N}\tau_iS_\mu N\bar{N}S^\mu N\right],\end{aligned}\tag{3.88}$$

with

$$\bar{\gamma}_{1,2,3,4} = \mathcal{O}\left((\delta_0+\delta_3)\frac{\alpha_{\rm em}}{4\pi}\frac{m_\pi^2}{F_\pi^2 M_{\not T}^2}\right), \qquad \bar{\gamma}_{5,6} = \mathcal{O}\left(\delta_3\frac{\alpha_{\rm em}}{4\pi}\frac{m_\pi^2}{F_\pi^2 M_{\not T}^2}\right). \tag{3.89}$$

One order higher we find

$$\begin{aligned}
\mathcal{L}^{(4)}_{q,f=4} &= \left(1-\frac{2\boldsymbol{\pi}^2}{F_\pi^2 D}\right)\left[\bar{C}_1\bar{N}N\,\partial_\mu(\bar{N}S^\mu N)+\bar{C}_2\bar{N}\boldsymbol{\tau}N\cdot\mathcal{D}_\mu(\bar{N}S^\mu\boldsymbol{\tau}N)\right] \\
&\quad+\left(\delta_{3i}-\frac{2\pi_3}{F_\pi^2 D}\pi_i\right)\left[\bar{C}_3\bar{N}\tau_i N\,\partial_\mu\left(\bar{N}S^\mu N\right)+\bar{C}_4\bar{N}N\,\mathcal{D}_\mu\left(\bar{N}\tau_i S^\mu N\right)\right] \\
&\quad+\Bigg\{\left(1-\frac{2\boldsymbol{\pi}^2}{F_\pi^2 D}\right)\left[\bar{C}_5\bar{N}\tau_l N\,\partial_\mu\left(\bar{N}S^\mu N\right)+\bar{C}_6\bar{N}N\,\mathcal{D}_\mu\left(\bar{N}\tau_l S^\mu N\right)\right] \\
&\quad+\bar{C}_7\left(\delta_{3k}-\frac{2\pi_3}{F_\pi^2 D}\pi_k\right)\bar{N}\tau_k N\,\mathcal{D}_\mu\left(\bar{N}S^\mu\tau_l N\right)\Bigg\}\left[\delta_{l3}+\frac{2}{F_\pi^2 D}\left(\pi_3\pi_l-\boldsymbol{\pi}^2\delta_{3l}\right)\right],
\end{aligned} \tag{3.90}$$

where we have ignored operators that start with one or more pions, and

$$\begin{aligned}
&\bar{C}_{1-4} = \mathcal{O}\left((\delta_0+\delta_3)\frac{\alpha_{\rm em}}{4\pi}\frac{m_\pi^2}{F_\pi^2 M_{\not T}^2 M_{\rm QCD}}\right), \qquad \bar{C}_{5,6} = \mathcal{O}\left(\delta_0\frac{\alpha_{\rm em}}{4\pi}\frac{m_\pi^2}{F_\pi^2 M_{\not T}^2 M_{\rm QCD}}\right), \\
&\bar{C}_7 = \mathcal{O}\left(\delta_3\frac{\alpha_{\rm em}}{4\pi}\frac{m_\pi^2}{F_\pi^2 M_{\not T}^2 M_{\rm QCD}}\right),
\end{aligned} \tag{3.91}$$

Since these operators are all suppressed by $\alpha_{\rm em}/4\pi$, their phenomenological impact is minimal, and we do not construct operators with higher chiral index.

Chiral-invariant sources

For the χI sources, one needs either two derivatives or an insertion of the quark mass to generate any operators in the πN sector. In the NN sector, however, one derivative is enough to construct χI interactions

$$\mathcal{L}^{(-1)}_{w,f=4} = \bar{C}_1\bar{N}N\,\mathcal{D}_\mu(\bar{N}S^\mu N)+\bar{C}_2\bar{N}\boldsymbol{\tau}N\cdot\mathcal{D}_\mu(\bar{N}S^\mu\boldsymbol{\tau}N), \tag{3.92}$$

with scalings

$$\bar{C}_{1,2} = \mathcal{O}\left(w\frac{M_{\rm QCD}}{F_\pi^2 M_{\not T}^2}\right). \tag{3.93}$$

For the χI sources, the chiral index of the LO $f=4$ LECs is the same as that of the LO $f=2$ LECs in Eq. (3.80), in contrast with the other $\not P\not T$ sources, where the $f=4$ LECs are suppressed by two powers of $Q/M_{\rm QCD}$ relative to the $f=2$ LECs. Whereas for $\bar{\theta}$, qCEDM, and FQLR the potential is dominated by pion exchange, the potential from the χI sources gets contributions of the same order from pion exchange and short-range NN interactions [78]. This only holds for the isospin-conserving part of the potential because the operators in Eq. (3.92) conserve isospin symmetry. The isospin-breaking part of the LO potential consists solely of pion-exchange contributions. The first $\not P\not T$ isospin-breaking NN interactions appear at NNLO with chiral index $\Delta_6 = 1$.

3.3.4 Electromagnetic interactions

Interactions with soft photons can be obtained using the $U(1)$ gauge-covariant derivatives (see Eq. (3.19)) in existing operators. More interesting are the interactions that arise through the field strength $F_{\mu\nu}$, which we describe here. Since the pion has spin 0, we cannot construct an EDM operator in the $f = 0$ sector. In contrast, there are plenty of $\not{P}\not{T}$ interactions in the $f = 2$ sector.

$\bar{\theta}$ term, quark chromo-EDM, and four-quark left-right operator

In the case of the $\bar{\theta}$ term, qCEDM, and FQLR, operators containing the electromagnetic field strength have the chiral properties of the tensor product of the $\not{P}\not{T}$ source and the electromagnetic interactions $(m_*\bar{\theta}P_4 - \tilde{d}_0\tilde{V}_4 + \tilde{d}_3\tilde{W}_3 + \mathrm{Im}[\Xi]X_{34}) \otimes e(I^\mu/6 + T^\mu_{34}/2)$.

As always, the isoscalar qCEDM generates the same interactions as the $\bar{\theta}$ term [48]. They start at $\Delta_6 = 1$ and transform as the fourth component of a vector, or as the product of a vector and an antisymmetric tensor

$$\begin{aligned}\mathcal{L}^{(1)}_{\tilde{d}_0,f=2\,\mathrm{em}} &= -2\bar{N}\left[\bar{d}_0\left(1-\frac{2\boldsymbol{\pi}^2}{F_\pi^2 D}\right)+\bar{d}_1\left(\tau_3-\frac{2\pi_3}{F_\pi^2 D}\boldsymbol{\tau}\cdot\boldsymbol{\pi}\right)\right]S^\mu\left(v^\nu+\frac{i\mathcal{D}^\nu_{\perp -}}{2m_N}\right)N\,F_{\mu\nu}\\ &\quad -2\bar{d}_1'\left(1-\frac{2\boldsymbol{\pi}^2}{F_\pi^2 D}\right)\bar{N}\left[\tau_3-\frac{2}{F_\pi^2 D}(\boldsymbol{\pi}^2\tau_3-\pi_3\boldsymbol{\pi}\cdot\boldsymbol{\tau})\right]S^\mu\left(v^\nu+\frac{i\mathcal{D}^\nu_{\perp -}}{2m_N}\right)N\,F_{\mu\nu}\\ &\quad +\frac{1}{F_\pi D}\varepsilon^{\mu\nu\alpha\beta}v_\alpha\bar{N}(\bar{c}_0\boldsymbol{\tau}\cdot\boldsymbol{\pi}+\bar{c}_1\pi_3)S_\beta N\,F_{\mu\nu}. \end{aligned} \tag{3.94}$$

The electromagnetic LECs scale as

$$(\bar{d}_{0,1},\,\bar{d}_1',\,\bar{c}_{0,1}) = \mathcal{O}\left(e\bar{\theta}\frac{m_\pi^2}{M_{\mathrm{QCD}}^3},\; e\tilde{\delta}_0\frac{m_\pi^2}{M_{\not{T}}^2 M_{\mathrm{QCD}}}\right). \tag{3.95}$$

The first term in Eq. (3.94) is a short-range contribution to the isoscalar nucleon EDM. The second and third term both contribute to the isovector nucleon EDM differing only by interactions involving two or more pions, such that separating them is practically impossible. For convenience, we added NLO recoil corrections to the EDM operators because these are needed for the NLO nucleon EDM calculation in the next chapter. The last two terms in Eq. (3.94) are $\pi N\gamma$ interactions. The $\bar{c}_0$ term will play a role in the calculation of the deuteron magnetic quadrupole moment. While in the LO pion, πN, and NN sectors, $\bar{\theta}$ and the isoscalar qCEDM generated only isoscalar interactions, here both isoscalar and isovector interactions appear due to breaking of isospin symmetry by the quark electric charge.

The isovector qCEDM generates very similar interactions,

$$\begin{aligned}\mathcal{L}^{(1)}_{\tilde{d}_3,f=2\,\mathrm{em}} &= -2\bar{N}\left[\bar{d}_0\left(1-\frac{2\boldsymbol{\pi}^2}{F_\pi^2 D}\right)+\bar{d}_1\left(\tau_3-\frac{2\pi_3}{F_\pi^2 D}\boldsymbol{\tau}\cdot\boldsymbol{\pi}\right)\right]S^\mu\left(v^\nu+\frac{i\mathcal{D}^\nu_{\perp -}}{2m_N}\right)N\,F_{\mu\nu}\\ &\quad +\frac{1}{F_\pi D}\varepsilon^{\mu\nu\alpha\beta}v_\alpha\bar{N}(\bar{c}_0\boldsymbol{\tau}\cdot\boldsymbol{\pi}+\bar{c}_1\pi_3)S_\beta N\,F_{\mu\nu},\\ &\quad +\bar{c}_1'\frac{\pi_3}{F_\pi D}\varepsilon^{\mu\nu\alpha\beta}v_\alpha\bar{N}\left(\tau_3-\frac{2}{F_\pi^2 D}(\boldsymbol{\pi}^2\tau_3-\pi_3\boldsymbol{\pi}\cdot\boldsymbol{\tau})\right)S_\beta N\,F_{\mu\nu} \end{aligned} \tag{3.96}$$

with

$$(\bar{d}_{0,1},\,\bar{c}_{0,1},\,\bar{c}_1') = \mathcal{O}\left(e\tilde{\delta}_3\frac{m_\pi^2}{M_{\not{T}}^2 M_{\mathrm{QCD}}}\right). \tag{3.97}$$

The FQLR generates operators with complicated pion structure due to the $X_{34} \otimes T_{34}$ tensor product. However, apart from terms with two or more pions which we do not construct for reasons given below, the Lagrangian is identical to Eqs. (3.94) and (3.96), but with the scaling

$$(\bar{d}_{0,1},\, \bar{d}'_1,\, \bar{c}_{0,1},\, \bar{c}'_1) = \mathcal{O}\left(e\xi \frac{M_{\rm QCD}}{M_T^2}\right). \tag{3.98}$$

The isoscalar qCEDM (and thus the $\bar{\theta}$ term), isovector qCEDM, and FQLR generate almost the same electromagnetic interactions. The main difference is the appearance of $\bar{c}'_1$ for the latter two sources, however, it is not clear for which observable this difference would play a role.

As will be discussed in upcoming chapters, for the sources discussed here, the nucleon Schiff moment and nuclear EDMs are dominated by $\not{P}\not{T}$ πN interactions. For these observables, the $\not{P}\not{T}$ $N\gamma$ operators have little impact and we do not construct operators with higher chiral index.

quark EDM

Because the qEDM contains an explicit soft photon, it yields $N\gamma$ operators that transform like itself, namely as the third and fourth components of, respectively, the vectors V and W in Eq. (2.64). At LO we find

$$\begin{aligned}\mathcal{L}^{(1)}_{d_{0,3},f=2\ \rm em} &= -2\bar{N}\left[\bar{d}_0\left(1-\frac{2\boldsymbol{\pi}^2}{F_\pi^2 D}\right)+\bar{d}_1\left(\tau_3-\frac{2\pi_3}{F_\pi^2 D}\boldsymbol{\tau}\cdot\boldsymbol{\pi}\right)\right] S^\mu\left(v^\nu+\frac{i\mathcal{D}^\nu_{\perp -}}{2m_N}\right) N\, F_{\mu\nu} \\ &\quad +\frac{1}{F_\pi D}\varepsilon^{\mu\nu\alpha\beta}\bar{N}(\bar{c}_0\boldsymbol{\tau}\cdot\boldsymbol{\pi}+\bar{c}_1\pi_3)S_\beta\left(v_\alpha+\frac{i\mathcal{D}_{\alpha -}}{2m_N}\right) N\, F_{\mu\nu},\end{aligned} \tag{3.99}$$

with

$$(\bar{d}_0, \bar{c}_0) = \mathcal{O}\left(e\delta_0 \frac{m_\pi^2}{M_T^2 M_{\rm QCD}}\right), \qquad (\bar{d}_1, \bar{c}_1) = \mathcal{O}\left(e\delta_3 \frac{m_\pi^2}{M_T^2 M_{\rm QCD}}\right). \tag{3.100}$$

In Eq. (3.99) we have incorporated the constraints imposed by Lorentz invariance at order $1/m_N$. In contrast to the qCEDM, we see that the isoscalar (isovector) qEDM generates isoscalar (isovector) $N\gamma$ interactions, since the symmetry properties of the qEDM are not mixed with isospin breaking from the quark charge.

In the case of the qEDM, long-range physics propagated by pions is suppressed by $\alpha_{\rm em}/4\pi$ and $\not{P}\not{T}$ observables are dominated by short-range $N\gamma$ interactions. Since the operators in (3.99) contribute only to the nucleon EDM and not to the momentum-dependent part of the nucleon EDFF, we need to construct electromagnetic operators with higher chiral index. It turns out that momentum dependence only arises at NNLO, such that we need to construct the Lagrangians with $\Delta_6 = 2$ and $\Delta_6 = 3$.

At $\Delta_6 = 2$, the $\not{P}\not{T}$ electromagnetic operators not constrained by Lorentz invariance contain

at least one pion,

$$\begin{aligned}\mathcal{L}^{(2)}_{d_{0,3},f=2\,\mathrm{em}} &= \frac{1}{F_\pi}\bar{N}\left[\bar{\wp}_1\left(1-\frac{2\boldsymbol{\pi}^2}{F_\pi^2 D}\right)(D^\mu\boldsymbol{\pi})\cdot\boldsymbol{\tau}+\bar{\rho}_1\left(D^\mu\pi_3-\frac{2\pi_3}{F_\pi^2 D}\boldsymbol{\pi}\cdot D^\mu\boldsymbol{\pi}\right)\right]N\,v^\nu F_{\mu\nu}\\ &+\frac{1}{F_\pi D}\bar{N}\left(\bar{\wp}_2\boldsymbol{\pi}\cdot\boldsymbol{\tau}+\bar{\rho}_2\pi_3\right)N\,v^\nu\partial^\mu F_{\mu\nu}\\ &+\frac{1}{F_\pi^2 D}\varepsilon^{\alpha\beta\mu\nu}v_\alpha\bar{N}\left(\bar{\wp}_3(\boldsymbol{\pi}\cdot D_\beta\boldsymbol{\pi})+\bar{\rho}_3\pi_3\,(D_\beta\boldsymbol{\pi})\cdot\boldsymbol{\tau}\right)N\,F_{\mu\nu}\\ &+\frac{1}{F_\pi^2 D}\bar{N}S^\mu\left[\bar{\wp}_4(\boldsymbol{\pi}\times D^\nu\boldsymbol{\pi})+\bar{\wp}_5(\boldsymbol{\pi}\times v\cdot D\boldsymbol{\pi})v^\nu\right]\cdot\boldsymbol{\tau}N\,F_{\mu\nu}\\ &+\frac{1}{F_\pi}\varepsilon^{\alpha\beta\mu\nu}\,\bar{N}\left[(\bar{\rho}_4 D_\alpha\boldsymbol{\pi}+\bar{\rho}_5 v_\alpha v\cdot D\boldsymbol{\pi})\times\boldsymbol{\tau}\right]_i S_\beta N\left(\delta_{i3}-\frac{2\pi_3\pi_i}{F_\pi^2 D}\right)F_{\mu\nu},\end{aligned}\tag{3.101}$$

where $\bar{\wp}_i$ ($\bar{\rho}_i$) originate in the isoscalar (isovector) qEDM and the LECs scale as

$$\bar{\wp}_i=\mathcal{O}\left(e\delta_0\frac{m_\pi^2}{M_{\not T}^2 M_{\rm QCD}^2}\right),\qquad \bar{\rho}_i=\mathcal{O}\left(e\delta_3\frac{m_\pi^2}{M_{\not T}^2 M_{\rm QCD}^2}\right).\tag{3.102}$$

At $\Delta_6=3$, we encounter operators with two covariant derivatives and operators due to insertions of the quark mass. Since it is unlikely that, at this order in the chiral series, operators containing pions are important for the calculation of observables, we focus on terms without pions

$$\begin{aligned}\mathcal{L}^{(3)}_{d_{0,3},f=2\,\mathrm{em}} &= -2\bar{N}\left(\delta\bar{d}_0+\delta\bar{d}_1\tau_3\right)S^\mu N\,v^\nu F_{\mu\nu}\\ &+\frac{1}{4m_N^2}\bar{N}\left(\bar{d}_0+\bar{d}_1\tau_3\right)S\cdot\mathcal{D}_{\perp-}\mathcal{D}^\mu_{\perp-}N\,v^\nu F_{\mu\nu}\\ &+\bar{N}\left(\bar{S}'_0+\bar{S}'_1\tau_3\right)\left(S\cdot\mathcal{D}_{\perp+}\mathcal{D}^\mu_{\perp+}+S^\mu\mathcal{D}^2_{\perp+}\right)N\,v^\nu F_{\mu\nu}+\ldots.\end{aligned}\tag{3.103}$$

The first two terms are corrections to the isoscalar and isovector nucleon EDM due the quark mass, the third and fourth terms are relativistic corrections, and the operators $\bar{S}_0^{\prime(3)}$ and $\bar{S}_1^{\prime(3)}$ are the first qEDM contributions to, respectively, the isoscalar and isovector Schiff moments. The dots denote multi-pion components of the listed operators and operators which start at one pion. The LECs scale as

$$\begin{aligned}\delta\bar{d}_0&=\mathcal{O}\left(e(\delta_0+\varepsilon\delta_3)\frac{m_\pi^4}{M_{\not T}^2 M_{\rm QCD}^3}\right),&\qquad \delta\bar{d}_1&=\mathcal{O}\left(e(\varepsilon\delta_0+\delta_3)\frac{m_\pi^4}{M_{\not T}^2 M_{\rm QCD}^3}\right),\\ \bar{S}'_0&=\mathcal{O}\left(e\delta_0\frac{m_\pi^2}{M_{\not T}^2 M_{\rm QCD}^3}\right),&\qquad \bar{S}'_1&=\mathcal{O}\left(e\delta_3\frac{m_\pi^2}{M_{\not T}^2 M_{\rm QCD}^3}\right).\end{aligned}\tag{3.104}$$

Chiral-invariant sources

The $\not P\not T$ χI sources generate electromagnetic interactions that transform as $\bar{I}\otimes(I^\mu/6+T^\mu_{34}/2)$. The LO operators have chiral index $\Delta_6=-1$,

$$\begin{aligned}\mathcal{L}^{(-1)}_{w,f=2\,\mathrm{em}} &= -2\left\{\bar{d}_0+\bar{d}_1\left[\tau_3+\frac{2}{F_\pi^2 D}\left(\pi_3\boldsymbol{\pi}\cdot\boldsymbol{\tau}-\boldsymbol{\pi}^{\,2}\tau_3\right)\right]\right\}\\ &\times\bar{N}S^\mu\left(v^\nu+\frac{i\mathcal{D}_{\nu-}}{m_N}\right)N\,F_{\mu\nu},\end{aligned}\tag{3.105}$$

where we included recoil corrections. The LECs scale as

$$\bar{d}_i = \mathcal{O}\left(ew\frac{M_{\rm QCD}}{M_{\not PT}^2}\right), \tag{3.106}$$

with again $w \in \{w, \sigma_1, \sigma_8\}$. Differently from the qCEDM and FQLR, for χI $\not P\not T$ sources the short-distance EDM operators have the same chiral index as the leading πN couplings in Eq. (3.79). The contributions of the latter to the nucleon EDM are due to one-loop diagrams which bring in an additional suppression. Therefore, for χI sources the nucleon EDM is dominated by the short-range $N\gamma$ interactions.

Furthermore, this enhancement of short-range over long-range physics causes the LO nucleon EDFF to be momentum independent. That is, at LO the nucleon EDFF is equal to the nucleon EDM. Similar as for the qEDM, momentum dependence enters only at NNLO in the $\Delta_6 = 1$ Lagrangian. We construct the complete $\Delta_6 = 0$ Lagrangian,

$$\begin{aligned}
\mathcal{L}^{(0)}_{w,f=2\rm em} \;=\;& \frac{\bar{\chi}_0}{F_\pi} D^\mu \boldsymbol{\pi}\cdot\bar{N}\boldsymbol{\tau}N\, v^\nu F_{\mu\nu} + \frac{1}{F_\pi^2 D}\left[\bar{\chi}_1(\boldsymbol{\pi}\times D^\mu\boldsymbol{\pi})_3 + \bar{\chi}_2(\boldsymbol{\pi}\times v\cdot D\boldsymbol{\pi})_3 v^\mu\right]\bar{N}S^\nu N\, F_{\mu\nu} \\
&+\frac{\bar{\chi}_3}{F_\pi^2 D}\varepsilon^{\alpha\beta\mu\nu}v_\alpha\bar{N}\left[(D_\beta\pi_3)\boldsymbol{\tau}\cdot\boldsymbol{\pi} - (\boldsymbol{\pi}\cdot D_\beta\boldsymbol{\pi})\tau_3\right]N\, F_{\mu\nu} \\
&+\left(\delta_{i3} + \frac{2}{F_\pi^2 D}[\pi_3\pi_i - \boldsymbol{\pi}^2\delta_{i3}]\right)\left\{\frac{\bar{\chi}_4}{F_\pi}(D^\mu\pi_i)\,\bar{N}N\, v^\nu F_{\mu\nu}\right. \\
&\left.+\varepsilon^{\alpha\beta\mu\nu}\bar{N}\left[\frac{\bar{\chi}_5}{F_\pi}(D_\alpha\boldsymbol{\pi}\times\boldsymbol{\tau})_i + \frac{\bar{\chi}_6}{F_\pi}(v\cdot D\boldsymbol{\pi}\times\boldsymbol{\tau})_i v_\alpha\right]S_\beta N\, F_{\mu\nu}\right\} \\
&+\frac{\bar{\chi}_7}{F_\pi}\varepsilon^{\alpha\beta\lambda\mu}v_\alpha\bar{N}(\boldsymbol{\tau}\times\boldsymbol{\pi})^3\mathcal{D}_{\beta,+}S_\lambda N\, v^\nu F_{\mu\nu},
\end{aligned} \tag{3.107}$$

with scalings

$$\bar{\chi}_i = \mathcal{O}\left(ew\frac{1}{M_{\not PT}^2}\right). \tag{3.108}$$

At $\Delta_6 = 1$ we only construct the operators that start without pions, since the operator with pions are of little phenomenological use. We find

$$\begin{aligned}
\mathcal{L}^{(1)}_{w,f=2\rm em} \;=\;& -2\bar{N}\left[\delta\bar{d}_0\left(1 - \frac{2\boldsymbol{\pi}^2}{F_\pi^2 D}\right) + \delta\bar{d}_1\left(\tau_3 - \frac{2\pi_3}{F_\pi^2 D}\boldsymbol{\pi}\cdot\boldsymbol{\tau}\right)\right]S^\mu N\, v^\nu F_{\mu\nu} \\
&-2\bar{\delta}d_1'\left(1 - \frac{2\boldsymbol{\pi}^2}{F_\pi^2 D}\right)\bar{N}\left[\tau_3 + \frac{2}{F_\pi^2 D}\left(\pi_3\boldsymbol{\pi}\cdot\boldsymbol{\tau} - \boldsymbol{\pi}^2\tau_3\right)\right]S^\mu N\, v^\nu F_{\mu\nu} \\
&+\frac{1}{4m_N^2}\bar{N}\left\{\bar{d}_0 + \bar{d}_1\left[\tau_3 + \frac{2}{F_\pi^2 D}\left(\pi_3\boldsymbol{\pi}\cdot\boldsymbol{\tau} - \boldsymbol{\pi}^2\tau_3\right)\right]\right\}S\cdot\mathcal{D}_{\perp-}\mathcal{D}^\mu_{\perp-}N\, v^\nu F_{\mu\nu} \\
&+\bar{N}\left(\bar{S}_0' + \bar{S}_1'\tau_3\right)\left(S\cdot\mathcal{D}_{\perp+}\mathcal{D}^\mu_{\perp+} + S^\mu\mathcal{D}^2_{\perp+}\right)N\, v^\nu F_{\mu\nu} + \dots\,.
\end{aligned} \tag{3.109}$$

The first three operators in Eq. (3.109) are proportional to the quark mass and are corrections to the isoscalar and isovector nucleon EDMs, while the fourth and fifth are relativistic corrections. The two operators in the last line are short-distance contributions to the first derivative of the nucleon EDFF; the Schiff moment. The scaling of the LECs is

$$\delta\bar{d}_i = \mathcal{O}\left(e(1+\varepsilon)w\frac{m_\pi^2}{M_{\not PT}^2 M_{\rm QCD}}\right),\ \delta\bar{d}_1' = \mathcal{O}\left(ew\frac{m_\pi^2}{M_{\not PT}^2 M_{\rm QCD}}\right),\ \bar{S}_i' = \mathcal{O}\left(ew\frac{1}{M_{\not PT}^2 M_{\rm QCD}}\right). \tag{3.110}$$

3.4 The role of tadpoles

We have seen in Sec. 3.3.1 that the transformation properties of the $\not{P}\not{T}$ dimension-six sources cause pion tadpoles to appear in the $\not{P}\not{T}$ mesonic Lagrangian in Eqs. (3.35), (3.37), (3.39), (3.41), (3.43), (3.45), and (3.47). Since the coupling constant of the neutral pion to the vacuum is small compared to the pion mass, these tadpoles can be dealt with in perturbation theory. This means that for any given $\not{P}\not{T}$ observable at a given accuracy, only a finite number of neutral pions disappearing into the vacuum need to be taken into account. For applications such as calculations of hadronic and nuclear EDMs, it is more convenient to eliminate the pion tadpoles from the mesonic Lagrangian, which can be achieved with field redefinitions of the form discussed in Ref. [48]. The main result of this section is to show that the vacuum misalignment signaled by the pion tadpoles causes the isoscalar operators, like $\bar{g}_0$ or $\bar{C}_{1,2}$, to receive additional contributions from isospin-breaking sources like the isovector qCEDM and the FQLR operator. These contributions can be schematically obtained by replacing $\tilde{\delta}_0$ with $\tilde{\delta}_0 + \varepsilon\tilde{\delta}_3 + \varepsilon\xi M_{QCD}^2/m_\pi^2$ in the power-counting estimates of isoscalar operators in the previous sections.

Let us now discuss the details. We define new fields $\zeta' = \pi'/F_\pi$ and N' for, respectively, the pion and nucleon through

$$\begin{aligned} \zeta_i &= \frac{1}{d'}\left\{\zeta_i' - \delta_{i3}[2C\zeta_3' + S(1-\boldsymbol{\zeta}'^2)]\right\}, \\ N &= U'N', \end{aligned} \tag{3.111}$$

in terms of the unitary matrix

$$U' = \frac{1}{\sqrt{d'}}\left[\sqrt{1-C} + \sqrt{C}(\zeta_3' + i\varepsilon_{3jk}\zeta_j'\tau_k)\right], \tag{3.112}$$

and

$$d' = 1 - C(1-\boldsymbol{\zeta}'^2) + 2S\zeta_3', \tag{3.113}$$

and

$$C = \frac{1}{2}(1-\cos\varphi), \qquad S = \frac{1}{2}\sin\varphi, \tag{3.114}$$

in terms of an angle φ. These transformations are complicated, but have the nice properties that the pion and nucleon covariant derivatives and nucleon bilinears transform simply as

$$\begin{aligned} &D_\mu\zeta_i = O'_{ij}D'_\mu\zeta_j, \qquad \mathcal{D}_\mu N = U'\mathcal{D}'_\mu N', \\ &\bar{N}N = \bar{N}'N', \qquad \bar{N}\tau_i N = O'_{ij}\bar{N}'\tau_j N', \end{aligned} \tag{3.115}$$

with an orthogonal matrix

$$O'_{ij} = \delta_{ij} - \frac{2}{d'}\left(C\left[(\boldsymbol{\zeta}'^2 - \zeta_3^2)\delta_{ij} - \varepsilon_{3ik}\varepsilon_{3jl}\zeta_k'\zeta_l'\right] + (C\zeta_3' + S)\left(\zeta_i'\delta_{3j} - \zeta_j'\delta_{3i}\right)\right). \tag{3.116}$$

The properties in Eq. (3.115) make sure that χI operators, built from nucleon fields and pion and nucleon covariant derivatives, are invariant under the field redefinitions in Eq. (3.111). This is not the case for operators that break chiral symmetry and involve the pion field directly.

Before performing any rotation, we summarize the chiral-breaking Lagrangian in the purely mesonic sector, including chiral-breaking PT operators with Δ up to 2 and $\not{P}\not{T}$ operators up to $\Delta_6 = 0$:

$$\begin{aligned}\mathcal{L}_{\rm tadpole} &= -\frac{m_\pi^2}{2D}\left(1+\frac{\Delta m_\pi^2}{m_\pi^2 D}\right)\boldsymbol{\pi}^2 + \frac{\delta m_\pi^2}{2D^2}\pi_3^2 + \left(\bar{\Delta}_1^{(-2)} + \tilde{\Delta}^{(-2)} + \bar{\Delta}_w^{(-2)}\right)\frac{F_\pi \pi_3}{2D} \\ &\quad + \left(\bar{\Delta}^{(-4)} + \tilde{\Delta}^{(0)} + \bar{\Delta}_w^{(0)}\right)\frac{F_\pi \pi_3}{2D}\left(1-\frac{2\boldsymbol{\pi}^2}{F_\pi^2 D}\right) + \bar{\Delta}_2^{(-2)}\frac{F_\pi \pi_3}{2D}\left(1-\frac{2\boldsymbol{\pi}^2}{F_\pi^2 D}\right)^2 . \end{aligned} \tag{3.117}$$

Here we ignored the $\not{P}\not{T}$ operators consisting of (at least) three pions and two covariant derivatives with LECs ϑ_i. These operators do not play any role in the upcoming chapters. The quark masses are responsible for the PT operators in the first line of Eq. (3.117). We have

$$\Delta m_\pi^2 = \mathcal{O}\left(\frac{m_\pi^4}{M_{\rm QCD}^2}\right), \qquad \delta m_\pi^2 = \mathcal{O}\left(\frac{\varepsilon^2 m_\pi^4}{M_{\rm QCD}^2}\right). \tag{3.118}$$

We omitted chiral-breaking operators generated by the electromagnetic interaction because these are not affected by the field redefinitions [48]. The scaling of the tadpoles in Eq. (3.117) is given in Sect. 3.3.1.

Our first goal is to remove for each source the dominant tadpole, that is the terms with index $\Delta_6 = -4$ for FQLR and $\Delta_6 = -2$ for qCEDM and χI sources. By performing the field redefinitions in Eq. (3.111) with angle

$$\begin{aligned}\tan\varphi &= -\frac{\bar{\Delta}^{(-4)} + \tilde{\Delta}^{(-2)} + \bar{\Delta}_w^{(-2)}}{m_\pi^2}, \\ &= \mathcal{O}\left(\xi\frac{M_{\rm QCD}^4}{m_\pi^2 M_{\not T}^2}\right) + \mathcal{O}\left(\tilde{\delta}_3\frac{M_{\rm QCD}^2}{M_{\not T}^2}\right) + \mathcal{O}\left(w\varepsilon\frac{M_{\rm QCD}^2}{M_{\not T}^2}\right), \end{aligned} \tag{3.119}$$

the dominant tadpoles are removed. Since the angle is small, $\tan\varphi \simeq \varphi$, we keep only terms linear in φ.

The effect of the field redefinition on the mesonic Lagrangian, apart from canceling the dominant tadpoles, is to modify the coefficients of the tensors,

$$\begin{aligned}\mathcal{L}_{\rm tadpole} &= -\frac{m_\pi^2}{2D}\left(1+\frac{\Delta m_\pi^2}{m_\pi^2 D}\right)\boldsymbol{\pi}^2 + \frac{\delta m_\pi^2}{2D^2}\pi_3^2 - \bar{\Delta}^{(-4)}\frac{\pi_3\boldsymbol{\pi}^2}{F_\pi D^2} + \bar{\Delta}_1^{(-2)}\frac{F_\pi\pi_3}{2D} \\ &\quad + \left(\bar{\Delta}^{(-2)\prime} + \tilde{\Delta}^{(0)\prime} + \bar{\Delta}_w^{(0)\prime}\right)\frac{F_\pi \pi_3}{2D}\left(1-\frac{2\boldsymbol{\pi}^2}{F_\pi^2 D}\right) + \bar{\Delta}_2^{(-2)}\frac{F_\pi \pi_3}{2D}\left(1-\frac{2\boldsymbol{\pi}^2}{F_\pi^2 D}\right)^2 , \end{aligned} \tag{3.120}$$

in terms of the shifted LECs

$$\begin{aligned}\bar{\Delta}^{(-2)\prime} &= -\bar{\Delta}^{(-4)}\frac{\Delta m_\pi^2 - \delta m_\pi^2}{m_\pi^2} = \mathcal{O}\left(\xi(1+\varepsilon^2)\frac{m_\pi^2 M_{\rm QCD}^2}{M_{\not T}^2}\right), \\ \tilde{\Delta}^{(0)\prime} &= \tilde{\Delta}^{(0)} - \tilde{\Delta}^{(-2)}\left(\frac{\Delta m_\pi^2 - \delta m_\pi^2}{m_\pi^2}\right) = \mathcal{O}\left(\left(\varepsilon\tilde{\delta}_0 + (1+\varepsilon^2)\tilde{\delta}_3\right)\frac{m_\pi^4}{M_{\not T}^2}\right), \\ \bar{\Delta}_w^{(0)\prime} &= \bar{\Delta}_w^{(0)} - \bar{\Delta}_w^{(-2)}\left(\frac{\Delta m_\pi^2 - \delta m_\pi^2}{m_\pi^2}\right) = \mathcal{O}\left(w\varepsilon(1+\varepsilon^2)\frac{m_\pi^4}{M_{\not T}^2}\right). \end{aligned}$$

We can thus rotate away the leading tadpole without introducing new interactions in the mesonic Lagrangian. The net effect of the rotation is only to change the dependence of the coefficients on the parameters $\tilde{\delta}_0$, $\tilde{\delta}_3$, and ε.

The remaining tadpoles in Eq. (3.120) can be eliminated by a second rotation, now with an even smaller angle

$$\varphi' = -\frac{1}{m_\pi^2}\left(\bar{\Delta}_1^{(-2)} + \bar{\Delta}_2^{(-2)} + \bar{\Delta}^{(-2)\prime} + \tilde{\Delta}^{(0)\prime} + \bar{\Delta}_w^{(0)\prime}\right), \tag{3.121}$$

which leaves us with

$$\begin{aligned}\mathcal{L}_{\text{tadpole}} &= -\frac{m_\pi^2}{2D}\left(1+\frac{\Delta m_\pi^2}{m_\pi^2 D}\right)\boldsymbol{\pi}^2 + \frac{\delta m_\pi^2}{2D^2}\pi_3^2 \\ &\quad -\frac{\pi_3\boldsymbol{\pi}^2}{F_\pi D^2}\left(\bar{\Delta}^{(-4)} + \bar{\Delta}^{(-2)\prime} + \frac{2\bar{\Delta}_2^{(-2)}}{D} + \tilde{\Delta}^{(0)\prime} + \bar{\Delta}_w^{(0)\prime}\right).\end{aligned} \tag{3.122}$$

Although the tadpoles are removed, residual $\not{P}\not{T}$ interactions involving an odd number of pions are left behind. In case of the qCEDM and χI sources these terms carry a higher chiral index than the LO $\not{P}\not{T}$ πN interactions and the $\not{P}\not{T}$ multi-pion vertices contribute to observables at high order. In case of the FQLR, due to its complicated $SO(4)$ properties, a three-pion vertex remains with a lower chiral index than the dominant $\not{P}\not{T}$ πN interactions. However, the most interesting $\not{P}\not{T}$ observables do not include pions in the initial or final state such that this interaction only enters in diagrams with multiple loops and its contributions are still suppressed with respect to the πN vertices.

The two rotations that allow to eliminate the tadpoles affect the other sectors of the Lagrangian as well. Most importantly, the nucleon σ term and nucleon-mass splitting

$$\mathcal{L}_{\chi,f\leq 2} = \Delta m_N\left(1-\frac{2\boldsymbol{\pi}^2}{F_\pi^2 D}\right)\bar{N}N + \frac{\delta m_N}{2}\bar{N}\left(\tau_3 - \frac{2\pi_3}{F_\pi^2 D}\boldsymbol{\tau}\cdot\boldsymbol{\pi}\right)N, \tag{3.123}$$

become after rotation Eq. (3.119)

$$\begin{aligned}\mathcal{L}_{\chi,f\leq 2} &= \Delta m_N\left[\left(1-\frac{2\boldsymbol{\pi}^2}{F_\pi^2 D}\right)\bar{N}N + \varphi\frac{2\pi_3}{F_\pi D}\bar{N}N\right] \\ &\quad +\frac{\delta m_N}{2}\left[\bar{N}\left(\tau_3 - \frac{2\pi_3}{F_\pi^2 D}\boldsymbol{\tau}\cdot\boldsymbol{\pi}\right)N + \varphi\frac{2}{F_\pi D}\bar{N}\boldsymbol{\tau}\cdot\boldsymbol{\pi}N\right],\end{aligned} \tag{3.124}$$

and the terms linear in φ contribute to $\not{P}\not{T}$ πN interactions. Comparing Eqs. (3.49) and (3.124) shows that $\bar{g}_0$ has been shifted,

$$\bar{g}_0 \;\to\; \bar{g}_0 + \delta m_N\frac{\tilde{\Delta}^{(-2)}}{m_\pi^2} = \mathcal{O}\left((\delta_0+\varepsilon\tilde{\delta}_3)\frac{m_\pi^2 M_{\text{QCD}}}{M_{\not{T}}^2}\right), \tag{3.125}$$

and now depends on the isovector qCEDM as well. Similarly, in the case of the FQLR where there was no direct $\bar{g}_0$ contribution at $\Delta_6 = -3$, after removal of the tadpole we find

$$\bar{g}_0 \;=\; \delta m_N\frac{\bar{\Delta}^{(-4)}}{m_\pi^2} = \mathcal{O}\left(\xi\varepsilon\frac{M_{\text{QCD}}^3}{M_{\not{T}}^2}\right), \tag{3.126}$$

of the same order as Eq. (3.67), although slightly smaller by a factor ε. In the case of χI sources

$$\bar{g}_0 \;\to\; \bar{g}_0 + \delta m_N\frac{\bar{\Delta}_w^{(-2)}}{m_\pi^2} = \mathcal{O}\left(w(1+\varepsilon^2)\frac{m_\pi^2 M_{\text{QCD}}}{M_{\not{T}}^2}\right), \tag{3.127}$$

and this shift is less interesting because the dependence on w has not been fundamentally changed. Eq. (3.124) shows that $\bar{g}_1$ gets shifted as well by terms proportional to Δm_N. However, these shifts are inconsequential in the sense that they do not change the dependence of the LECs on ξ, $\tilde{\delta}_{0,3}$, and w.

In the subleading πN Lagrangian, the effects of the rotation on operators that transform as $\tilde{W}_3$, like $\bar{\beta}_2$ and $\bar{\beta}_3$ in Eq. (3.56) and all the operators in Eq. (3.59), can be absorbed in a redefinition of the coefficients whose scaling is still determined by Eqs. (3.57) and (3.60). For operators that transform as P_4 or $\tilde{V}_4$, the scaling of the coefficients is modified and they get a contribution from the isospin-symmetry breaking Lagrangian at order $\Delta = 1, 2$ (listed, for example, in Ref. [48]). Schematically,

$$\bar{\beta}_1' = \mathcal{O}\left(\left(\tilde{\delta}_0 + \varepsilon\tilde{\delta}_3\right)\frac{m_\pi^2}{M_{\not T}^2}\right) \qquad \bar{\zeta}_i' = \mathcal{O}\left(\left(\tilde{\delta}_0 + \varepsilon\tilde{\delta}_3\right)\frac{m_\pi^2}{M_{\not T}^2 M_{\rm QCD}}\right). \tag{3.128}$$

Due to the tadpole removal, the FQLR induces the subleading isospin-conserving $\not P\not T$ operators $\bar{\beta}_1$ and all operators in Eq. (3.58), but with scalings

$$\bar{\beta}_1' = \mathcal{O}\left(\xi\varepsilon\frac{M_{\rm QCD}^2}{M_{\not T}^2}\right) \qquad \bar{\zeta}_i' = \mathcal{O}\left(\xi\varepsilon\frac{M_{\rm QCD}}{M_{\not T}^2}\right). \tag{3.129}$$

We have neglected so far the qEDM. The qEDM also generates tadpoles, as given in Eq. (3.43) which can be removed the same way as for the other sources. This removal alters the scalings of πN LECS in Eq. (3.77). Since, as Eq. (3.78) shows, $\bar{g}_0$ and $\bar{g}_1$ already receive a contribution from both the isoscalar and isovector qEDM, the change of the scaling of $\bar{g}_0$ is not particularly relevant.

The $\not P\not T$ NN sector is affected in a similar way as the πN sector by the tadpole rotations. The LECs of the operators in Sec. 3.3.3 induced by the isoscalar qCEDM get a contribution from the isovector qCEDM as well. This contribution is obtained by replacing $\tilde{\delta}_0$ by $\tilde{\delta}_0 + \varepsilon\tilde{\delta}_3$ in the scalings of the LECs. The contribution from the FQLR to isoscalar $\not P\not T$ NN interactions can be obtained by replacing $\tilde{\delta}_0 m_\pi^2$ by $\xi\varepsilon M_{\rm QCD}^2$. In case of χI sources, the NN sector is not affected by the tadpole removal because the operators are chiral invariant.

Finally, we discuss electromagnetic operators. In the case of the operators generated by qCEDM, the elimination of the leading tadpole modifies to coefficients in Eq. (3.94) in a way that can be schematically summarized by the replacement $\tilde{\delta}_0 \to \tilde{\delta}_0 + \varepsilon\tilde{\delta}_3$ in Eq. (3.95). Since most operators already receive contributions from both the isoscalar and isovector qCEDM these shifts are not particularly interesting. The same holds for the FQLR. For the χI sources, the leading $N\gamma$ interactions in Eq. (3.105) are χI or transform as the 3-4 component of an antisymmetric tensor. In both cases they are not affected by the field redefinition in Eq. (3.115). Only the NNLO operators $\delta\bar{d}_0$, $\delta\bar{d}_1$ and $\delta\bar{d}_1'$, which are proportional to the quark masses, are affected by the elimination of the tadpoles, in a way that corresponds to shifting $w \to w(1+\varepsilon^2)$. In case of the qEDM, tadpoles are much smaller than the $N\gamma$ interactions and their removal does not affect the operators in Sec. 3.3.4.

3.5 The P- and T-odd pion-nucleon form factor

An important element in the evaluation of hadronic and nuclear EDMs is the $\not P\not T$ πN coupling. In this section, we summarize the πN interactions for the different $\not P\not T$ sources we have considered, by calculating the $\not P\not T$ πN form factor (FF) with the Lagrangian derived above. For convenience,

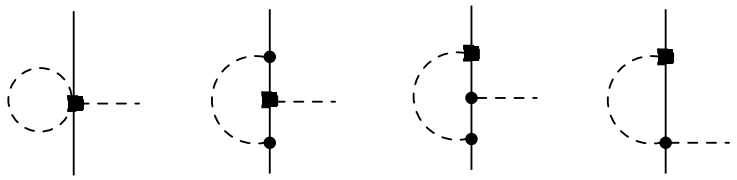

Figure 3.1: One-loop contributions of relative order $\mathcal{O}(m_\pi^2/(2\pi F_\pi)^2)$ to the pion-nucleon form factors $F_1(\vec{q},\vec{K})$ and $F_2(\vec{q},\vec{K})$. A nucleon (pion) is represented by a solid (dashed) line; the $\not{P}\not{T}$ vertices from Eqs. Eqs. (3.49) and (3.54) are indicated by a square. The other vertices represent LO PT interactions. For simplicity only one possible ordering is shown.

we consider the Lagrangian without pion tadpoles, as discussed in the previous section. The πN FF for the $\bar{\theta}$ term is given in Ref. [48] and is identical to that of the isoscalar qCEDM.

We consider the three-point Green's function for an incoming (outgoing) nucleon of momentum p^μ (p'^μ) and an outgoing pion of momentum $q^\mu = p^\mu - p'^\mu$ and isospin a. We take the incoming and outgoing nucleon to be nonrelativistic and on-shell, so

$$v\cdot p = \frac{\vec{p}^{\,2}}{2m_N} + \Delta m_N \mp \frac{\delta m_N}{2}, \quad v\cdot p' = \frac{\vec{p}^{\,\prime 2}}{2m_N} + \Delta m_N \mp \frac{\delta m_N}{2}, \tag{3.130}$$

where the $-(+)$ signs holds for protons (neutrons) and the arrow denotes vectors in three-dimensional Euclidean space, $p^\mu = (v\cdot p,\, \vec{p})$, $p_\mu = (v\cdot p,\, -\vec{p})$. The Green function for on-shell nucleons can be parameterized by three form factors, corresponding to three different isospin structures,

$$V_a(q,K) = -\frac{i}{F_\pi}\left[F_1(q,K)\tau_a + F_2(q,K)\delta_{a3} + F_3(q,K)\delta_{a3}\tau_3\right], \tag{3.131}$$

in terms of the functions $F_{1,2,3}$ of q^μ and $K^\mu = (p^\mu + p'^\mu)/2$. In what follows, we give F_1, F_2, and F_3 for each of the dimension-six $\not{P}\not{T}$ sources. We calculate the FFs up to the order where each of them gets a contribution. As derived in Sec. 3.3.2, this implies going to NNLO for the qCEDM and FQLR and to NLO for the χI sources. For the qEDM we need the LO contributions only.

Contributions from the quark chromo-EDM

The LO πN interactions stemming from the qCEDM are given in Eqs. (3.49) and (3.54). Apart from tree-level contributions to the πN FF, these interactions appear in the one-loop diagrams in Fig. 3.1. These loops give rise to divergences that are absorbed in the LECs of the operators in Eqs. (3.62) and (3.63). We use dimensional regularization in d spacetime dimensions, which introduces the renormalized scale μ and

$$L \;=\; \frac{2}{4-d} - \gamma_E + \ln 4\pi, \tag{3.132}$$

with $\gamma_E \approx 0.55721$, the Euler-Mascheroni constant. The loop diagrams yield contributions of the same order as the πN vertices with chiral index $\Delta_6 = 1$, and up this order in the loops we use $v\cdot q = 0$. The structure of the diagrams in Fig. 3.1 is such that the momentum of the external pion never flows into the loop and the only scale in the integral is the pion mass. As a consequence, the diagrams do not yield any nontrivial momentum dependence and they simply

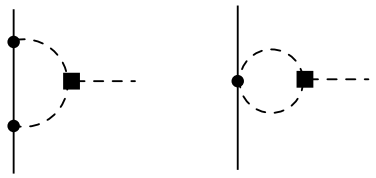

Figure 3.2: Contributions from purely mesonic $\not{P}\not{T}$ interactions to the pion-nucleon form factors. The square denotes the $\not{P}\not{T}$ vertex from Eq. (3.139). The notation is as in Fig. 3.1.

renormalize the LECs $\delta\bar{g}_{0,1}$. We define the renormalized LECs

$$\begin{aligned}\bar{\delta}\bar{g}_0 &= \delta\bar{g}_0 + \frac{\bar{g}_0}{4}\frac{m_\pi^2}{(2\pi F_\pi)^2}\left[(1+3g_A^2)\left(L+1-\log\frac{m_\pi^2}{\mu^2}\right)-2g_A^2\right],\\ \bar{\delta}\bar{g}_1 &= \delta\bar{g}_1 + \frac{3\bar{g}_1}{4}\frac{m_\pi^2}{(2\pi F_\pi)^2}\left[\left(\frac{5}{3}-3g_A^2\right)\left(L+1-\log\frac{m_\pi^2}{\mu^2}\right)+2g_A^2\right].\end{aligned} \tag{3.133}$$

Additionally, there are tree-level contributions from operators in Eqs. (3.56), (3.58), and (3.59). The operators $\bar{\beta}_3$ in Eq. (3.56) and its recoil correction contribute to the FF

$$V_a(\vec{q},\vec{K}) = \frac{\bar{\beta}_3}{F_\pi}\varepsilon^{3ab}\tau_b\left(v\cdot q-\frac{\vec{K}\cdot\vec{q}}{m_N}\right). \tag{3.134}$$

If we use the nucleon on-shell conditions (which we write in shorthand notation in terms of the nucleon isospin)

$$v\cdot q = \frac{\vec{K}\cdot\vec{q}}{m_N} + i\frac{\delta m_N}{2}\varepsilon^{3ab}\tau_b\,, \tag{3.135}$$

Eq. (3.134) becomes

$$V_a(\vec{q},\vec{K}) = -\frac{i}{F_\pi}(\tau_a-\delta_{a3}\tau_3)\delta m_N\bar{\beta}_3\,. \tag{3.136}$$

Combining everything, the πN FFs for on-shell nucleons read

$$\begin{aligned}F_1(\vec{q},\vec{K}) &= \bar{g}_0\left\{1-\frac{1}{2m_N^2}\left[\vec{K}^{\,2}+\vec{S}\cdot\left(\vec{K}\times\vec{q}\right)\right]\right\}+\bar{\delta}\bar{g}_0+\delta m_N\bar{\beta}_3-\bar{\zeta}_3\vec{q}^{\,2},\\ F_2(\vec{q},\vec{K}) &= \bar{g}_1\left\{1-\frac{1}{2m_N^2}\left[\vec{K}^{\,2}+\vec{S}\cdot\left(\vec{K}\times\vec{q}\right)\right]\right\}+\bar{\delta}\bar{g}_1-\bar{\xi}_3\vec{q}^{\,2},\\ F_3 &= \bar{g}_2-\delta m_N\bar{\beta}_3.\end{aligned} \tag{3.137}$$

We see that F_1 and F_2 receive contributions at the same order. Two orders down we find momentum dependence of these FFs and the first static contribution to F_3.

Contributions from the four-quark left-right operator

The main parts of the pion-nucleon FFs from the FQLR are very similar to those from the qCEDM. The different chiral structure of the isovector vertices $\bar{g}_1$ in Eq. (3.67) and the induced $\bar{g}_1'$ by the tadpole removal in Eq. (3.124) only affects the first diagram in Fig. 3.1, with the only consequence of modifying the counterterm $\bar{\delta}\bar{g}_1$ with respect to Eq. (3.133).

After replacing the scalings of the LECs, one sees that contributions to F_1 and F_2 start at LO ($\Delta_6=-3$), and contributions to F_3 at NNLO ($\Delta_6=-1$); at this order F_1 and F_2 obtain

analytic momentum dependence. The results in Eq. (3.137) give the dominant contributions to the three FFs, with the replacement $\bar{\delta}\bar{g}_1 \to \bar{\delta}\bar{g}_1 + \bar{\delta}\bar{g}_1'$, and

$$\begin{aligned}
\bar{\delta}\bar{g}_1 &= \delta\bar{g}_1 + \frac{3\bar{g}_1}{4}\frac{m_\pi^2}{(2\pi F_\pi)^2}\left[(5-3g_A^2)\left(L+1-\log\frac{m_\pi^2}{\mu^2}\right)+2g_A^2\right] \\
\bar{\delta}\bar{g}_1' &= \delta\bar{g}_1' + \frac{3\bar{g}_1}{4}\frac{m_\pi^2}{(2\pi F_\pi)^2}\left[\left(\frac{5}{3}-3g_A^2\right)\left(L+1-\log\frac{m_\pi^2}{\mu^2}\right)+2g_A^2\right].
\end{aligned} \tag{3.138}$$

However, this is not the whole story. As shown in Sec. 3.4, the elimination of the tadpoles in case of the FQLR leaves behind the mesonic $\not{P}\not{T}$ interaction

$$\mathcal{L}^{(-4)}_{\mathrm{FQ},f=0} = -\bar{\Delta}^{(-4)}\frac{\pi_3\boldsymbol{\pi}^2}{F_\pi D^2}, \tag{3.139}$$

with a lower chiral index than the dominant pion-nucleon interactions. The one-loop diagrams in Fig. 3.2 contribute to the pion-nucleon FFs at NLO ($\Delta_6 = -2$) and add to F_2 a non-analytic momentum dependence not present for the qCEDM. This FF becomes, instead of Eq. (3.137),

$$\begin{aligned}
F_2(\vec{q},\vec{K}) &= \bar{g}_1\left\{1-\frac{1}{2m_N^2}\left[\vec{K}^{\,2}+\vec{S}\cdot\left(\vec{K}\times\vec{q}\right)\right]\right\}+\bar{\delta}\bar{g}_1+\bar{\delta}\bar{g}_1'-\bar{\xi}_3\vec{q}^{\,2} \\
&\quad -\frac{5\pi g_A^2}{2}\frac{m_\pi\bar{\Delta}^{(-4)}}{(2\pi F_\pi)^2}\, f_2\left(\frac{|\vec{q}|}{2m_\pi}\right),
\end{aligned} \tag{3.140}$$

where

$$f_2(x) = 1+\frac{1+2x^2}{2x}\arctan x. \tag{3.141}$$

Precise measurements on the deuteron $\not{P}\not{T}$ electromagnetic form factors, which depend strongly on F_2 [80, 81], could, in principle, measure this momentum dependence and separate the FQLR from the qCEDM.

Contributions from the quark EDM

The FFs from the qEDM are very simple, since all three appear at the same order. From the Lagrangian in Eq. (3.77) we read off,

$$F_1 = \bar{g}_0, \qquad F_2 = \bar{g}_1, \qquad F_3 = \bar{g}_2. \tag{3.142}$$

Since these interactions are suppressed by $\alpha_{\mathrm{em}}/4\pi \sim \varepsilon m_\pi^3/M_{\mathrm{QCD}}^3$, they are not important for the calculations of nuclear EDMs, which will be dominated by short-range $N\gamma$ operators.

Contributions from the chiral-invariant sources

For the χI sources the relevant interactions at leading and subleading order are given in Eqs. (3.79) and (3.81). The contributions to the FFs can be read off easily

$$\begin{aligned}
F_1(\vec{q}) &= \bar{g}_0 - \bar{g}_2 + \vec{q}^{\,2}\,\bar{\imath}_1, \\
F_2 &= \bar{g}_1, \\
F_3 &= \bar{g}_2.
\end{aligned} \tag{3.143}$$

For the χI sources, F_1 and F_2 appear at the same order and F_3 appears one order down in the $Q/M_{\rm QCD}$ expansion. Apart from contributing to F_3, $\bar{g}_2$ also contributes to F_1, but this is of little interest since F_1 receives a larger contribution from $\bar{g}_0$. At LO F_1 depends on the pion momentum because of the presence of the χI operator $\bar{\imath}_1$. The consequences for the $\not{P}\not{T}$ NN potential have been worked out in Ref. [78], where it was showed that $\bar{\imath}_1$ generates a long-range $\not{P}\not{T}$ potential, which can be accounted for by redefining $\bar{g}_0$, and a short-range $\not{P}\not{T}$ potential, which can be absorbed in the $\bar{C}_2$ contribution.

3.6 Discussion

Before we proceed to detailed calculations of $\not{P}\not{T}$ hadronic observables, here we draw some qualitative conclusions by looking at the various constructed chiral Lagrangians. For the SM $\bar{\theta}$ term, we conclude that all LECs are proportional to negative powers of the scale $M_{\rm QCD}$ [48]. There are two reasons for this. First, the $\bar{\theta}$ term is proportional to the quark mass which scales as $m_\pi^2/M_{\rm QCD}$. Second, after vacuum alignment the $\bar{\theta}$ term conserves isospin symmetry. Therefore, it is not possible to construct a leading-order pion tadpole. The first tadpole appears from an insertion of the quark-mass difference, bringing in more inverse powers of $M_{\rm QCD}$. Time-reversal in QCD is therefore an accidental symmetry in the sense that it would be somewhat suppressed (by one power of $m_\pi/M_{\rm QCD}$) even if $\bar{\theta}$ were not small [48]. For the beyond-the-SM dimension-six sources, positive powers of $M_{\rm QCD}$ do appear, but they are overcompensated by two powers of the much larger $M_{\not{T}}$.

We can roughly divide the various $\not{P}\not{T}$ sources into three classes based on differences in chiral properties and field content. The first class consists of the $\bar{\theta}$ term, qCEDM, and the FQLR operator. These sources break chiral symmetry explicitly and do not contain photons. As a consequence, these sources induce chiral-breaking $\not{P}\not{T}$ interactions among pions and nucleons that do not contain a derivative on the pion field. These nonderivative πN interactions can be used in one-loop diagrams contributing to the nucleon EDM. Although the loops bring in a $m_\pi^2/(2\pi F_\pi)^2$ suppression (see the power-counting rules in Sec. 3.2), the loop diagrams appear at the same order as short-range contributions to the nucleon EDM [79]. More importantly, the nonderivative πN interactions induce long-range $\not{P}\not{T}$ NN interactions which dominate the $\not{P}\not{T}$ NN potential. Short-range NN interactions appear at subleading order. Hence, for the first class of sources, the $\not{P}\not{T}$ moments of bound nuclei, such as the deuteron [80, 81] and helion [82], are dominated by the one-pion-exchange potential (this is not true for the deuteron EDM coming from the $\bar{\theta}$ term, as will be explained in Chapters 5 and 6) and the observables depend only on a small number of LECs in the $f = 2$ $\not{P}\not{T}$ Lagrangian. Once these LECs are known from experiments, we can make predictions for other $\not{P}\not{T}$ observables.

The second class of $\not{P}\not{T}$ sources consists of the χI sources consisting of the gCEDM and two four-quark operators. As their name implies, these sources conserve chiral symmetry and they cannot directly induce nonderivative $\not{P}\not{T}$ πN interactions which do break chiral symmetry. The first contributions to the nonderivative πN interactions appear due to insertions of the quark mass (difference) and, as a result, the LECs are suppressed by $m_\pi^2/M_{\rm QCD}^2$. At this order, additional χI πN couplings appear with two derivatives (it is not possible to construct χI πN operators with zero or one derivative), which are also associated with two negative powers of $M_{\rm QCD}$. The consequence is that the nucleon EDM is dominated by short-range $N\gamma$ interactions, the pion-loop diagrams appearing at NNLO. Because $\not{P}\not{T}$ NN interactions that conserve chiral symmetry can be constructed with only one derivative, their short-range contributions to the $\not{P}\not{T}$ NN potential appear at the same order as the one-pion-exchange contributions. The EDMs of bound nuclei therefore depend on more unknown LECs, reducing our predictive power.

The third class of sources consists of the qEDM. This is the only source which contains an explicit photon. As a consequence, operators in the nonelectromagnetic sectors, *i.e.* the mesonic, πN, and NN sectors, are suppressed by powers of the fine-structure constant due to the need of integrating out a hard photon. As we will see in later chapters, the main conclusion is that the EDMs of bound nuclei are dominated by the EDMs of the constituent nucleons.

It is not only important if operators break chiral symmetry, but also how they break it. This is best illustrated by the three nonderivative $\not{P}\not{T}$ πN interactions

$$\mathcal{L}_{\not{T},\pi N} = -\frac{\bar{g}_0}{F_\pi}\bar{N}\boldsymbol{\tau}\cdot\boldsymbol{\pi}N - \frac{\bar{g}_1}{F_\pi}\pi_3\bar{N}N - \frac{\bar{g}_2}{F_\pi}\pi_3\bar{N}\tau_3 N. \tag{3.144}$$

In traditional approaches where the role of chiral symmetry is not emphasized, for example Refs. [80, 81, 82, 83], it is often assumed that these interactions are of the same size. When we consider the chiral properties of the fundamental $\not{P}\not{T}$ sources, this picture has to be adjusted. In the case of the chiral-symmetry breaking but isospin-conserving $\bar{\theta}$ term, at LO only $\bar{g}_0$ appears [31]. The $\bar{g}_1$ and $\bar{g}_2$ are respectively suppressed by two and three powers of $m_\pi/M_{\rm QCD}$ [48]. If one wants to study observables sensitive to $\bar{g}_1$ one needs to take into account the full NNLO Lagrangian, which includes, apart from $\bar{g}_1$, derivative πN and multi-πN interactions. An example of this is the $\not{P}\not{T}$ NN potential which, at the order where $\bar{g}_1$ appears, has a rich and nontrivial momentum dependence in the isoscalar channel [78].

For the qCEDM arguably the most natural case is the one where the isoscalar and isovector qCEDM are of similar size $|\tilde{\delta}_0| \simeq |\tilde{\delta}_3|$. In this scenario the $\bar{g}_0$ and $\bar{g}_1$ interactions appear at the same order. The third πN coupling $\bar{g}_2$ comes in two orders down in the chiral expansion. The case of a dominant isoscalar qCEDM $|\tilde{\delta}_0| \gg |\delta_3|$ generates an identical low-energy $\not{P}\not{T}$ Lagrangian as the $\bar{\theta}$ term, making it impossible to separate these two scenarios from low-energy $\not{P}\not{T}$ observables alone. However, due to link (see, for example, Eq. (3.53)) between $\not{P}\not{T}$ from the $\bar{\theta}$ term and isospin violation (a link not present for the qCEDM), precision experiments could, in principle, separate $\bar{\theta}$ from an isoscalar qCEDM. The appearance of a dominant isovector qCEDM $|\tilde{\delta}_3| \gg |\tilde{\delta}_0|$ implies, after tadpole removal, that $\bar{g}_0$ and $\bar{g}_1$ are of approximately the same order, although the former is expected to be somewhat smaller due to the extra factor ε.

The pattern of nonderivative πN interactions in the case of the chiral- and isospin-symmetry breaking four-quark operator FQLR is very similar to that of a dominant isovector qCEDM. The main differences are the appearance of interactions involving multiple pions and momentum dependence at NLO in the isovector πN FF. Separating the FQLR from an isovector qCEDM would require very precise EDM measurements and is therefore not very likely. Additional information could be obtained from measuring the $\not{T}$ correlation coefficient, D, in nuclear β-decay [40].

The χI operators, the gCEDM and two four-quark interactions, give rise to a similar hierarchy between the nonderivative πN couplings as an isovector qCEDM, although in this case it is $\bar{g}_1$ that is expected to be smaller than $\bar{g}_0$ by a factor ε and $\bar{g}_2$ is suppressed by only one power of $m_\pi/M_{\rm QCD}$. Also, at the same order as $\bar{g}_0$ and $\bar{g}_1$, derivative πN interactions appear. Within our framework, a separation of the different χI operators themselves is not possible. For that more advanced techniques than NDA, such as lattice QCD, are required to estimate the size of the LECs.

Only for the qEDM does the assumption of similar sized nonderivative πN interactions hold. However, for this source all πN interactions are suppressed by the electromagnetic fine-structure constant and, as mentioned, hadronic EDMs are dominated by short-range $N\gamma$ operators.

We conclude that for all sources where the $\not{P}\not{T}$ πN interactions play an important role, the $\bar{g}_2$ interaction is suppressed compared to $\bar{g}_0$ and $\bar{g}_1$. In this sense, Eq. (3.144) has too many degrees

Table 3.1: The LO scaling of important LECs for the different $\not{P}\not{T}$ sources. The $\bar{g}_i$ LECs are the nonderivative $\not{P}\not{T}$ πN interactions, $\bar{d}_0$ and $\bar{d}_1$ the isoscalar and isovector short-range nucleon EDMs, $\bar{c}_0$ and $\bar{c}_1$ the isoscalar and isovector $\not{P}\not{T}$ magnetic $\pi N\gamma$ interactions, and $\bar{C}_{1,2}$ and $\bar{C}_{3,4}$ isoscalar and isovector $\not{P}\not{T}$ NN interactions. The scaling of the LECs is determined by NDA.

Source	$\bar{\theta}$ term	quark CEDM	FQLR	quark EDM	χI
$\bar{g}_0$	$\bar{\theta}\frac{m_\pi^2}{M_{\rm QCD}}$	$(\tilde{\delta}_0+\varepsilon\tilde{\delta}_3)\frac{m_\pi^2 M_{\rm QCD}}{M_{\not{T}}^2}$	$\varepsilon\xi\frac{M_{\rm QCD}^3}{M_{\not{T}}^2}$	$(\delta_0+\delta_3)\frac{\alpha_{\rm em}}{4\pi}\frac{m_\pi^2 M_{\rm QCD}}{M_{\not{T}}^2}$	$w\frac{m_\pi^2 M_{\rm QCD}}{M_{\not{T}}^2}$
$\bar{g}_1/\bar{g}_0$	$\varepsilon\frac{m_\pi^2}{M_{\rm QCD}^2}$	$\tilde{\delta}_3/(\tilde{\delta}_0+\varepsilon\tilde{\delta}_3)$	$1/\varepsilon$	1	ε
$\bar{g}_2/\bar{g}_0$	$\frac{\alpha_{\rm em}}{4\pi}$	$\varepsilon\tilde{\delta}_3/(\tilde{\delta}_0+\varepsilon\tilde{\delta}_3)\frac{m_\pi^2}{M_{\rm QCD}^2}$	$\varepsilon\frac{m_\pi^2}{M_{\rm QCD}^2}$	$\delta_3/(\delta_0+\delta_3)$	$\frac{M_{\rm QCD}^2}{m_\pi^2}\frac{\alpha_{\rm em}}{4\pi}$
$\bar{d}_0$	$e\bar{\theta}\frac{m_\pi^2}{M_{\rm QCD}^3}$	$e(\tilde{\delta}_0+\tilde{\delta}_3)\frac{m_\pi^2}{M_{\not{T}}^2 M_{\rm QCD}}$	$e\xi\frac{M_{\rm QCD}}{M_{\not{T}}^2}$	$e\delta_0\frac{m_\pi^2}{M_{\not{T}}^2 M_{\rm QCD}}$	$ew\frac{M_{\rm QCD}}{M_{\not{T}}^2}$
$\bar{d}_1/\bar{d}_0$	1	1	1	δ_3/δ_1	1
$\bar{c}_0/\bar{d}_0$	1	1	1	1	$\frac{m_\pi^2}{M_{\rm QCD}^2}$
$\bar{c}_1/\bar{d}_0$	1	1	1	δ_3/δ_1	$\frac{m_\pi^2}{M_{\rm QCD}^2}$
$\bar{C}_{1,2}$	$\bar{\theta}\frac{m_\pi^2}{F_\pi^2 M_{\rm QCD}^3}$	$(\tilde{\delta}_0+\varepsilon\tilde{\delta}_3)\frac{m_\pi^2}{F_\pi^2 M_{\not{T}}^2 M_{\rm QCD}}$	$\xi\frac{M_{\rm QCD}}{F_\pi^2 M_{\not{T}}^2}$	$(\delta_0+\tilde{\delta}_3)\frac{\alpha_{\rm em}}{4\pi}\frac{m_\pi^2}{F_\pi^2 M_{\not{T}}^2 M_{\rm QCD}}$	$w\frac{M_{\rm QCD}}{F_\pi^2 M_{\not{T}}^2}$
$\bar{C}_{3,4}/\bar{C}_{1,2}$	$\varepsilon\frac{m_\pi^2}{M_{\rm QCD}^2}$	$\tilde{\delta}_3/(\tilde{\delta}_0+\varepsilon\tilde{\delta}_3)$	$1/\varepsilon$	1	$\varepsilon\frac{m_\pi^2}{M_{\rm QCD}^2}$

of freedom and can be simplified, reducing the number of LECs that needs to be determined by experiments.

The second assumption often made in the literature is that the πN interactions in Eq. (3.144) give the dominant contribution to the $\not{P}\not{T}$ NN potential. Our analysis shows that this is a valid assumption for the $\bar{\theta}$ term, qCEDM, and FQLR (if the hierarchy among $\bar{g}_{0,1,2}$ is taken into account), but not for the qEDM and χI sources. For the qEDM, due to the suppression of πN interactions, one-pion-exchange contributions to the $\not{P}\not{T}$ NN potential appear at the same order as one-photon-exchange contributions where one vertex originates in the nucleon EDM. We will come back to this in Chapter 6. For χI sources, short-range NN interactions need to be taken into account.

Furthermore, in the calculations of observables, there is no reason to not consider other types of $\not{P}\not{T}$ operators such as $N\gamma$ and $\pi N\gamma$ interactions. The results in Chapter 6 will show that the EDMs of light nuclei depend in general on six different LECs. They consist of two $\not{P}\not{T}$ πN interactions $\bar{g}_0$ and $\bar{g}_1$, the short-range isoscalar and isovector nucleon EDMs $\bar{d}_0$ and $\bar{d}_1$, and the short-range isoscalar $\not{P}\not{T}$ NN interactions $\bar{C}_0$ and $\bar{C}_1$. Higher electromagnetic moments can depend on additional interactions such as the isoscalar and isovector $\not{P}\not{T}$ $\pi N\gamma$ vertices $\bar{c}_0$ and $\bar{c}_1$. We summarize the size of these important LECs (extended with some others) for all sources, in Table 3.1.

The fact that different $\not{P}\not{T}$ sources are responsible for different hierarchies between the nonderivative $\not{P}\not{T}$ πN couplings and between the πN, $N\gamma$, and NN sectors has important implications for the $\not{P}\not{T}$ electromagnetic moments of nucleons and nuclei. The next chapters are devoted to such observables, which, when measured, give us a handle on identifying the fundamental mechanism of time-reversal violation.

Chapter 4

The Nucleon Electric Dipole Form Factor

4.1 Introduction[1]

The most important observable to calculate when studying hadronic P and T violation is the nucleon electric dipole moment. Experimentally the neutron EDM is one of the best studied $\not{P}\not{T}$ observables with the current upper limit being $|d_n| < 2.9 \cdot 10^{-13}\, e\,\text{fm}$ [8]. Ongoing experiments aim to improve this bound by one or two orders of magnitude [15]. On the other hand, there are plans to measure the EDM of the proton, for which there only exists an indirect bound $|d_p| < 7.9 \cdot 10^{-12}\, e\,\text{fm}$ from the atomic mercury EDM [16], in a storage ring [22]. The indirect bound, of course, depends on theoretical atomic and nuclear structure calculations of the dependence of the mercury EDM on the proton EDM. A storage ring experiment would provide a cleaner probe of the proton EDM. On the theoretical side the nucleon EDM is attractive since the system is relatively simple and the nucleon EDM is an important building block for the calculation of nuclear and atomic EDMs. Apart from the static moment, the complete electric dipole form factor (EDFF) could be of interest as well. The first momentum dependent correction to the EDM, the nucleon Schiff Moment, gives rise to a short-range $\not{P}\not{T}$ nucleon-electron interaction in an atomic system. Furthermore, the EDFF can be used in lattice simulations to extract the EDM by extrapolation from a finite-momentum calculation.

In this chapter the nucleon EDFF is calculated up to NLO in the χPT power counting, for each of the fundamental $\not{P}\not{T}$ sources discussed in Sect. 2.5: the QCD $\bar{\theta}$ term and the beyond-the-SM sources consisting of the qCEDM, qEDM, FQLR, and the chiral-invariant sources consisting of gCEDM and $\not{P}\not{T}$ four-quark interactions. These calculations in combination with the experimental upper bounds put strong limits on the size of $\bar{\theta}$ and the scale of beyond-the-SM physics. Model builders should keep the latter limits in mind when constructing models of new physics that solve, for example, fine-tuning problems within the SM. The hope is, of course, that a finite EDM signal is measured in any of the upcoming EDM experiments. An important question is what such a measurement would imply. Has an extremely small, but finite, value for $\bar{\theta}$ been found or is there fundamentally new physics at play? The results in this chapter can partially answer this question.

[1] This chapter is based on J. de Vries, E. Mereghetti, R. G. E. Timmermans, and U. van Kolck, Phys. Lett. B **695**, 268 (2011) and E. Mereghetti, J. de Vries, W.H. Hockings, C.M. Maekawa, and U. van Kolck, Phys. Lett. B **696**, 97 (2011).

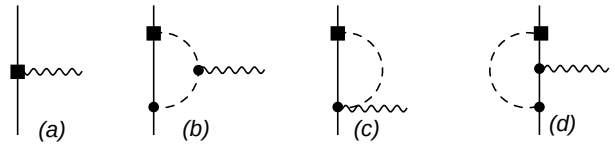

Figure 4.1: Tree-level and one-loop diagrams contributing to the nucleon EDFF for the $\bar{\theta}$ term, qCEDM, and FQLR. Solid, dashed and wavy lines represent the propagation of nucleons, pions and photons, respectively. A square marks a LO $\not{P}\not{T}$ interaction from Eqs. (3.49, 3.54, 3.67, 3.124), other vertices representing PT interactions from Eq. (3.24). For simplicity only one possible ordering is shown here.

4.2 The nucleon electric dipole form factor

Together with the PT electric and magnetic form factors and the $\not{P}T$ anapole form factor, the $\not{P}\not{T}$ EDFF completely specifies the Lorentz-invariant electromagnetic current of a particle with spin 1/2. We consider a nucleon of initial (final) momentum p (p') and a (space-like) photon of momentum $q = p - p'$ ($q^2 = -Q^2 < 0$). It is convenient to take q and $K = (p + p')/2$ as the independent momenta. The isoscalar (F_0) and isovector (F_1) EDFFs are defined from the nucleon electromagnetic current $J^\mu_{\rm em}(q, K)$ via

$$\begin{aligned} J^\mu_{\rm em}(q,K) &= 2\left(F_0(Q^2) + F_1(Q^2)\tau_3\right)\{S\cdot q v^\mu - S^\mu v\cdot q \\ &\quad + \frac{1}{m_N}\left[S\cdot q K^\mu - q\cdot K S^\mu\right] + \frac{1}{2m_N^2} S\cdot K\left[K\cdot q v^\mu - K^\mu v\cdot q\right] + \ldots\Big\}. \end{aligned} \tag{4.1}$$

The first term corresponds to the definition in Ref. [79], while the second is a recoil correction [48] and the remaining are consequences of Lorentz covariance. The form factors are decomposed

$$F_i(Q^2) = d_i - S_i' Q^2 + H_i(Q^2), \tag{4.2}$$

where d_i is the isospin i component of the EDM, S_i' the Schiff moment, and $H_i(Q^2)$ accounts for the remaining Q^2 dependence. The EDFF of the proton (neutron) is $F_0 + F_1$ ($F_0 - F_1$).

As will be seen the calculation of the nucleon EDFF from $\bar{\theta}$ term, qCEDM, and FQLR is very similar and we will consider these sources first. The LO calculation of the nucleon EDM from the $\bar{\theta}$ term has been done a long time ago [31] and later extended to the Schiff moment [76] and finally to the full momentum dependence [79]. The EDM calculation for $\bar{\theta}$ term up to NLO has been performed as well [84]. In this section we reproduce these results and calculate the nucleon EDFF for the other sources.

From the χPT power-counting rules in Sect. 3.2 we see that an additional loop in a diagram causes the chiral index of the diagram to increase by two or, equivalently, it suppresses the diagram by $Q^2/M_{\rm QCD}^2$ where $Q \sim m_\pi$ is the typical energy scale of the process. Simply put, the nucleon EDM is dominated by diagrams with the smallest number of loops. This means tree-level diagrams for $\not{P}\not{T}$ $N\gamma$ interactions and one-loop diagrams for $\not{P}\not{T}$ πN interactions. The LO short-range $\not{P}\not{T}$ $N\gamma$ and πN interactions for the various sources are given in, respectively, Eqs. (3.94, 3.96) and Eqs. (3.49, 3.54, 3.67, 3.124). Equivalently, the LO $\not{P}\not{T}$ πN form factor can be read off from the results in Sec. 3.5. The diagrams that contribute to the LO EDFF are shown in Fig. 4.1. The tree-level diagrams contribute to the current at order $\mathcal{O}(\bar{d}_{0,1})$ and the one-loop diagrams at order $\mathcal{O}(e\bar{g}_i Q/(2\pi F_\pi)^2)$. Plugging in the scaling of the LECs shows that the tree-level and one-loop diagrams contribute at the same order.

As discussed in the previous section, the main difference between the $\bar{\theta}$ term on the one hand and the qCEDM and FQLR on the other is the hierarchy between the nonderivative $\not{P}\not{T}$ πN couplings $\bar{g}_0$ and $\bar{g}_1$. For the latter sources $\bar{g}_1$ and $\bar{g}_0$ appear at the same order whereas for $\bar{\theta}$, $\bar{g}_1$ is suppressed with respect to $\bar{g}_0$. A calculation shows that of the three loop diagrams in Fig. 4.1 only diagram 4.1(b), where the photon couples to a charged pion, gives a nonvanishing result. This means that the LO EDFF does not depend on the isospin-breaking $\bar{g}_1$ interaction, which couples nucleons to neutral pions, such that the LO EDFF originating from $\bar{\theta}$, qCEDM, and FQLR is identical.

The explicit calculation of the LO diagrams in Fig. 4.1 is fairly straightforward (for some details regarding the evaluation of the integrals, see App. C). Since at this order the nucleon is static, in one-loop diagrams we take $v \cdot q = v \cdot K = 0$. We use dimensional regularization in d dimensions and encode divergences in the factor

$$L \equiv \frac{2}{4-d} - \gamma_E + \ln 4\pi \ . \tag{4.3}$$

The loops bring in also a renormalization scale μ, which is eliminated through the accompanying LECs.

The LO loop diagrams do not generate an isoscalar EDFF and therefore the LO isoscalar EDFF is purely tree level and static

$$d_0 = \bar{d}_0, \tag{4.4}$$
$$S_0' = 0, \tag{4.5}$$
$$H_0(Q^2) = 0. \tag{4.6}$$

In contrast, the loop diagrams not only renormalize the contributions of short-distance operators to the isovector EDM, but also generate a nontrivial momentum dependence in the isovector EDFF. The μ-independent isovector EDM is found to be

$$d_1 = \bar{d}_1 + \vec{d}_1' + \frac{e g_A \bar{g}_0}{(2\pi F_\pi)^2}\left(L - \ln\frac{m_\pi^2}{\mu^2}\right), \tag{4.7}$$

while the momentum dependence is encoded in

$$S_1' = \frac{e g_A \bar{g}_0}{6 m_\pi^2 (2\pi F_\pi)^2}, \tag{4.8}$$
$$H_1(Q^2) = \frac{4 e g_A \bar{g}_0}{15(2\pi F_\pi)^2}\, h_1^{(0)}\left(\frac{Q^2}{4m_\pi^2}\right), \tag{4.9}$$

where the function $f(Q^2/4m_\pi^2)$ is defined as

$$h_1^{(0)}(x) \equiv -\frac{15}{4}\left[\sqrt{1+\frac{1}{x}}\ln\left(\frac{\sqrt{1+\frac{1}{x}}+1}{\sqrt{1+\frac{1}{x}}-1}\right) - 2\left(1+\frac{x}{3}\right)\right]. \tag{4.10}$$

Note that $h_1^{(0)}(x \ll 1) = x^2 + \mathcal{O}(x^3)$.

As mentioned before there is no $\bar{g}_1$ dependence at this order, such that the results for $\bar{\theta}$, qCEDM, and FQLR are equal. The results for the nucleon EDM, Schiff moment, and residual momentum dependence in Eqs. (4.7, 4.8, 4.9) match the results in Refs. [31, 76, 79]. The short-range isovector LECs $\bar{d}_1 + \vec{d}_1'$ absorb the μ-dependence coming from the loops. The short-range

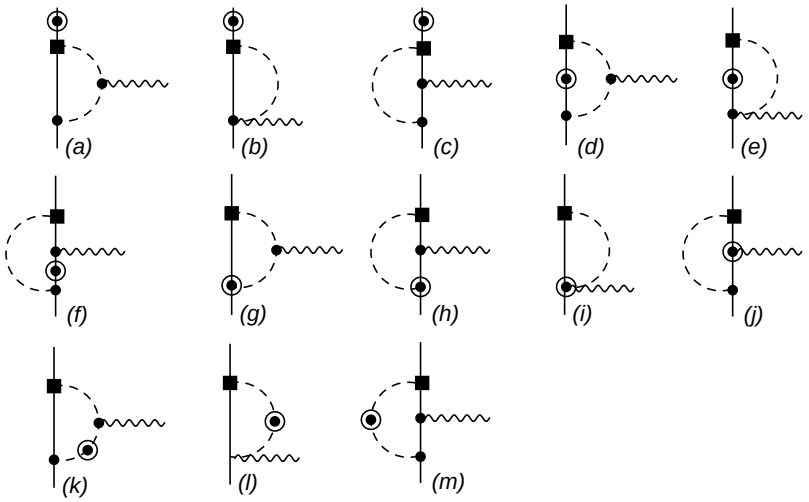

Figure 4.2: One-loop diagrams contributing to the nucleon EDFF in subleading order for the $\bar{\theta}$ term, qCEDM, and FQLR. Circled circles denote NLO PT interactions from the Lagrangian in Eqs. (3.25, 3.27, 3.30). Other notation as in Fig. 4.1. For simplicity only one possible ordering is shown here.

part is expected to be of the same order as the part, which is nonanalytic in m_π^2, coming from the loop. Even though the contributions are of similar size, a cancellation between the two is unlikely due to the different m_π dependence of the nonanalytic part. The isoscalar short-range contribution $\bar{d}_0$ is not needed to absorb any μ-dependence, but there is no reason to think that it should be smaller then the isovector short-range part. A deuteron EDM experiment will probe the isoscalar combination of neutron and proton EDMs (in addition to $\not{P}\not{T}$ two-nucleon effects). Because the isoscalar nucleon EDM at this order is a purely short-range effect, it is interesting to study the nucleon EDFF at NLO where longer-range effects, mediated by pions, do come into play.

The NLO short-range EDM operators do not bring in any new $\not{P}\not{T}$ LECs, since they are fixed by Lorentz invariance. They simply ensure the form of Eq. (4.1). The NLO diagrams of Fig. 4.2 are built from the leading $\not{P}\not{T}$ interactions ($\bar{g}_0$ for $\bar{\theta}$, qCEDM, and FQLR and $\bar{g}_1$ for qCEDM and FQLR) and one insertion of an operator from Eqs. (3.25, 3.27, 3.30). The other PT vertices are from Eq. (3.24). Diagrams 4.2(a,b,c) represent a correction to the external energies,

$$v \cdot q = -\frac{q \cdot K}{m_N}, \tag{4.11}$$

$$v \cdot K = -\frac{1}{2m_N}\left(K^2 + \frac{q^2}{4}\right) \mp \frac{\delta m_N}{2}, \tag{4.12}$$

of a proton ($-$ sign) or neutron ($+$ sign) in LO diagrams. (In the remaining NLO diagrams, we set the right-hand side of these equations to zero.) Analogous insertions in the nucleon propagator are represented by Diagrams 4.2(d,e,f). Diagrams 4.2(g,h,i) originate in the recoil correction in pion emission/absorption, while diagram (j) arises from the magnetic photon-nucleon interaction. Diagrams 4.2(k,l,m) represent an insertion of the pion-mass splitting in pion propagation. These one-loop diagrams contribute to the current at order $\mathcal{O}(e\bar{g}_i Q^2/(2\pi F_\pi)^2 m_N)$.

The NLO diagrams in Fig. 4.3 are built from the leading interactions in Eq. (3.24) with one insertion of a NLO $\not{P}\not{T}$ interaction from Eqs. (3.56) and (3.69). Diagrams 4.3(a,b) stem from the subleading $\pi\pi N$ couplings, and Diagrams 4.3(c,d,e,f) from the subleading πN couplings,

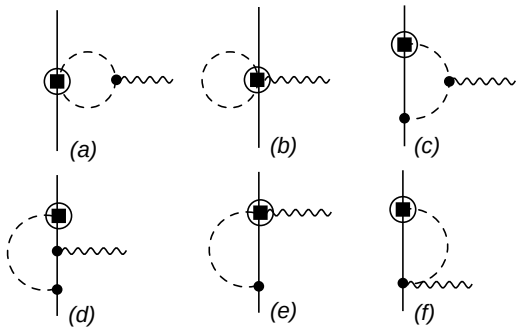

Figure 4.3: One-loop diagrams contributing to the nucleon EDFF in subleading order for the $\bar{\theta}$ term, qCEDM, and FQLR. Circled squares denote NLO $\not{P}\not{T}$ interactions from Eqs. (3.56, 3.69). Other notation as in Fig. 4.1. For simplicity only one possible ordering is shown here.

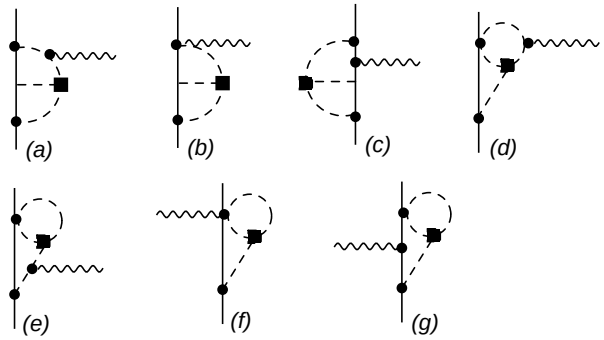

Figure 4.4: Two-loop diagrams contributing to the nucleon EDFF in subleading order for the FQLR. A square denotes the $\not{P}\not{T}$ three-pion vertex in Eq. (3.122). Other notation as in Fig. 4.1. For simplicity only one possible ordering is shown here.

present only for qCEDM and FQLR. These one-loop diagrams contribute to the current at order $\mathcal{O}(e\bar{\beta}_i Q^2/(2\pi F_\pi)^2)$, which is precisely the same order as the diagrams in Fig. 4.2.

Finally, in case of the FQLR there are two-loop diagrams in Fig. 4.4 built from leading PT interactions in Eq. (3.24) and an insertion of the $\not{P}\not{T}$ three-pion vertex in Eq. (3.122). These diagrams come in at $\mathcal{O}(e\bar{\Delta}^{(-4)}Q^2/(2\pi F_\pi)^4)$ which again is of the same order as the diagrams in Figs. 4.2 and 4.3.

Although there are a lot of diagrams to evaluate, most of them vanish when the on-shell conditions are consistently enforced. All diagrams in Fig. 4.4 and Diagrams 4.3(a,b) vanish due to isospin. Consequently, at NLO there is no difference between the qCEDM and FQLR. Since Diagrams 4.3(c,d,e,f) vanish too, the EDFF to this order depends only on the leading $\not{P}\not{T}$ parameters $\bar{g}_{0,1}$ through Fig. 4.2. Diagram 4.2(j) vanishes due to its spin structure and therefore the EDFF does not depend on the anomalous magnetic moments, either. Diagram 4.2(h) gives both isoscalar and isovector contributions. The remaining nonvanishing diagrams are 4.2(a,d,k). Neglecting PT isospin violation, these diagrams give purely isovector results. In the case of $\bar{\theta}$, the results are proportional to $eg_A\bar{g}_0/(2\pi F_\pi)^2$, as in LO, times the recoil suppression factor m_π/m_N. For qCEDM and FQLR, there is an additional momentum-independent contribution proportional to $\bar{g}_1$.

The diagrams in Fig. 4.2 contribute to both isoscalar and isovector EDMs. Taking the NLO

contributions together with the LO from Eqs. (4.4-4.8), we have

$$d_0 = \bar{d}_0 + \frac{eg_A\bar{g}_0}{(2\pi F_\pi)^2}\,\pi\left[\frac{3m_\pi}{4m_N}\left(1+\frac{\bar{g}_1}{3\bar{g}_0}\right)-\frac{\delta m_N}{m_\pi}\right], \tag{4.13}$$

$$d_1 = \bar{d}_1 + \vec{d}_1 + \frac{eg_A\bar{g}_0}{(2\pi F_\pi)^2}\left[L-\ln\frac{m_\pi^2}{\mu^2}+\frac{5\pi}{4}\frac{m_\pi}{m_N}\left(1+\frac{\bar{g}_1}{5\bar{g}_0}\right)-\frac{\breve{\delta}m_\pi^2}{m_\pi^2}\right]. \tag{4.14}$$

At NLO, both the isoscalar and isovecter EDM receive finite (within dimensional regularization) nonanalytic corrections, which depend also on $\bar{g}_1$ for qCEDM and FQLR. From Eqs. (4.13) and (4.14) we see that, as usual in baryon χPT, the NLO contributions are enhanced by π over NDA. These anomalous factors of π are hard to incorporate in the power counting, since they depend on the topological structure of the loops. Despite this enhancement by π, the dimensionless factors are not large enough to overcome the m_π/m_N suppression. Setting μ to m_N as a representative value for the size of d_1 [31], the NLO term in Eq. (4.14) (Eq. (4.13)) is about 15% (10%) of the leading nonanalytic term in Eq. (4.14), indicating good convergence of the chiral expansion. The isovector character of the LO nonanalytic terms is approximately preserved at NLO. Isospin-breaking contributions, although formally NLO, are pretty small, amounting to 15-20% of the total NLO contribution. This additional suppression can be understood by noticing that $\varepsilon \simeq 1/3$.

In the case of $\bar{\theta}$ we can use the link between isospin-breaking PT and isospin-conserving $\not{P}\not{T}$ interactions in Eq. (3.53) and expect

$$\begin{aligned}|d_n| = |d_0 - d_1| &\gtrsim \frac{eg_A}{(2\pi F_\pi)^2}\frac{\delta m_N}{2\varepsilon}\left[\ln\frac{m_N^2}{m_\pi^2}+\frac{\pi}{2}\frac{m_\pi}{m_N}-\frac{\breve{\delta}m_\pi^2}{m_\pi^2}+\pi\frac{\delta m_N}{m_\pi}\right]\bar{\theta}\\ &\simeq (1.99+0.12-0.04+0.03)\cdot 10^{-3}\,\bar{\theta}\,e\,\mathrm{fm}\end{aligned} \tag{4.15}$$

for the neutron EDM and

$$\begin{aligned}|d_p| = |d_0 + d_1| &\gtrsim \frac{eg_A}{(2\pi F_\pi)^2}\frac{\delta m_N}{2\varepsilon}\left[\ln\frac{m_N^2}{m_\pi^2}+2\pi\frac{m_\pi}{m_N}-\frac{\breve{\delta}m_\pi^2}{m_\pi^2}-\pi\frac{\delta m_N}{m_\pi}\right]\bar{\theta}\\ &\simeq (1.99+0.46-0.04-0.03)\cdot 10^{-3}\,\bar{\theta}\,e\,\mathrm{fm}\end{aligned} \tag{4.16}$$

for the proton EDM, using the lattice-QCD value $\delta m_N/2\varepsilon = 2.8$ MeV [71]. Nonanalytic NLO corrections are therefore somewhat larger for the proton EDM, but this difference is unlikely to be significant in light of our ignorance about the size of short-range contributions.

The main motivation for going to NLO is the appearance of the nonanalytic contribution to the isoscalar EDM. These terms in Eq. (4.13), represent a lower bound, since the short-range contribution $\bar{d}_0$ is formally of higher order. This expected lower bound on the nucleon isoscalar EDM has implications for proposed experiments on EDMs of light nuclei. In these cases, there will be additional many-nucleon contributions, but the average of the one-nucleon contributions still provides an estimate of the order of magnitude of the expected nuclear EDM. In the case of the deuteron, the one-nucleon contribution is $d_n + d_p = 2d_0$, because the nucleon spins are aligned. Therefore, if there are no unlikely cancellations between one- and two-body contributions, in the case of $\bar{\theta}$ we expect for the deuteron EDM

$$|d_d| \gtrsim \frac{2eg_A}{(2\pi F_\pi)^2}\frac{\delta m_N}{2\varepsilon}\,\pi\left[\frac{3m_\pi}{4m_N}-\frac{\delta m_N}{m_\pi}\right]\bar{\theta} \simeq (3.4-0.6)\cdot 10^{-4}\,\bar{\theta}\,e\,\mathrm{fm}. \tag{4.17}$$

We see that a deuteron EDM signal from $\bar{\theta}$ is expected to be larger than about 10% of the neutron EDM signal. A similar lower bound, of course, appears for the qCEDM and FQLR but in these cases we cannot do better than NDA.

Short- and long-range physics cannot be separated with a measurement of the neutron and proton EDMs alone. On the other hand, the momentum dependence of the EDFF is completely determined, to the order we are working, by long-range contributions generated by $\bar{g}_0$. It is therefore the same for $\bar{\theta}$, qCEDM, and FQLR. It turns out that the isoscalar form factor receives momentum dependence only from isospin-breaking terms, while there is a nonvanishing correction to the isovector momentum dependence also from isospin-conserving terms.

The variation of the form factor with Q^2 can be characterized at very small momenta by the electromagnetic contribution to the nucleon Schiff moment, the leading and subleading contributions of which we find to be

$$S_0' = -\frac{eg_A\bar{g}_0}{6(2\pi F_\pi)^2 m_\pi^2}\frac{\pi}{2}\frac{\delta m_N}{m_\pi}, \tag{4.18}$$

$$S_1' = \frac{eg_A\bar{g}_0}{6(2\pi F_\pi)^2 m_\pi^2}\left[1-\frac{5\pi}{4}\frac{m_\pi}{m_N}-\frac{\breve{\delta}m_\pi^2}{m_\pi^2}\right]. \tag{4.19}$$

The NLO correction, which agrees with the $\bar{\theta}$ result of Ref. [84] when T-conserving isospin violation is neglected, vanishes in the chiral limit but gives a relatively large correction to the isovector Schiff moment of about 60%, due to the numerical factor $5\pi/4$. Again, the isospin-breaking corrections are relatively small, and, as a consequence, at NLO the Schiff moment remains mostly isovector.

To this order, the Schiff moment is entirely given, apart for $\bar{g}_0$, by quantities that can be determined from other processes. In the case of $\bar{\theta}$, we can again use Eq. (3.53) to estimate

$$S_0' = -\frac{eg_A}{12(2\pi F_\pi)^2}\frac{\pi(\delta m_N)^2}{2\varepsilon m_\pi^3}\,\bar{\theta} \simeq -5.0\cdot 10^{-6}\,\bar{\theta}\,e\,\mathrm{fm}^3, \tag{4.20}$$

$$S_1' = \frac{eg_A}{12(2\pi F_\pi)^2}\frac{\delta m_N}{\varepsilon m_\pi^2}\left[1-\frac{5\pi}{4}\frac{m_\pi}{m_N}-\frac{\breve{\delta}m_\pi^2}{m_\pi^2}\right]\bar{\theta} \simeq 6.8\cdot 10^{-5}\,\bar{\theta}\,e\,\mathrm{fm}^3, \tag{4.21}$$

where again we used the lattice-QCD value [71] for $\delta m_N/2\varepsilon$. From these results we can straightforwardly obtain the Schiff moment for the proton and the neutron. Although we could again use the isoscalar component as an estimate for a lower bound on the deuteron Schiff moment, there could be potentially significant contributions from the deuteron binding momentum.

The full momentum dependence of the EDFF is given in addition by the functions $H_i(Q^2)$ introduced in Eq. (4.2),

$$H_0(Q^2) = -\frac{4eg_A\bar{g}_0}{15(2\pi F_\pi)^2}\frac{3\pi}{4}\frac{\delta m_N}{m_\pi}\,h_0^{(1)}\left(\frac{Q^2}{4m_\pi^2}\right), \tag{4.22}$$

$$H_1(Q^2) = \frac{4eg_A\bar{g}_0}{15(2\pi F_\pi)^2}\left[h_1^{(0)}\left(\frac{Q^2}{4m_\pi^2}\right)-\frac{7\pi}{8}\frac{m_\pi}{m_N}\,h_1^{(1)}\left(\frac{Q^2}{4m_\pi^2}\right)-\frac{2\breve{\delta}m_\pi^2}{m_\pi^2}\,\breve{h}_1^{(1)}\left(\frac{Q^2}{4m_\pi^2}\right)\right] \tag{4.23}$$

Here $h_1^{(0)}$ was defined in Eq. (4.2), while we now obtain the NLO isovector functions

$$h_1^{(1)}(x) = -\frac{1}{7}\left[3(1+2x)\,h_0^{(1)}(x)-10x^2\right], \tag{4.24}$$

and

$$\breve{h}_1^{(1)}(x) = -\frac{1}{4(1+x)}\left(h_1^{(0)}(x)-5x^2\right), \tag{4.25}$$

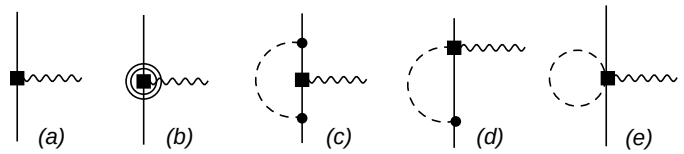

Figure 4.5: Tree-level and one-loop diagrams contributing to the nucleon EDFF up to NNLO for the qEDM. Squares denote LO $\not{P}\not{T}$ interactions from Eq. (3.99), double circled squares from Eq. (3.103). Other notation as in Fig. 4.1. For simplicity only one possible ordering is shown here.

and the NLO isoscalar function

$$h_0^{(1)}(x) = 5\left(\frac{1}{\sqrt{x}}\arctan\sqrt{x} - 1 + \frac{x}{3}\right). \tag{4.26}$$

In compliance with the definition of H_i, all functions behave as $h_i^{(n)}(x) = x^2 + \mathcal{O}(x^3)$ for $x \ll 1$.

As in lowest order, the momentum dependence is fixed by the pion cloud. Thus the scale for momentum variation is determined by $2m_\pi$. As for the Schiff moment, NLO corrections can be significant, but the isospin-breaking contributions are small. Both the Schiff moment and the functions $H_{0,1}(Q^2)$ are testable predictions of χPT. Unfortunately, since the full momentum dependence of the EDFF will not be measured anytime soon this observation carries no practical implications for the next generation of EDM experiments.

Before discussing other implications of the above results, we first consider the other dimension-six sources: the qEDM and the χI sources. The tree-level and one-loop diagrams relevant for the qEDM are shown in Fig. 4.5. At LO the EDFF originating from the qEDM is purely short-range and therefore the EDFF is momentum independent and equal to the EDM. At NLO, there is only a recoil correction to the EDM. At NNLO we find the first contributions to the momentum-dependent part of the EDFF. They originate from short-range contributions to the nucleon Schiff moment in Eq. (3.103). At this order we also need to take the one-loop diagrams in Fig. 4.5 into account. These loops do not enrich the EDFF with additional momentum dependence, but only renormalize the short-range EDM contributions. To $\mathcal{O}(e\delta m_\pi^4/M_{\not{T}}^2 M_{\rm QCD}^3)$, we find the EDMs

$$d_{0,\rm qEDM} = \bar{d}_0 + \delta\bar{d}_0 + \frac{3}{4}\bar{d}_0\frac{m_\pi^2}{(2\pi F_\pi)^2}\left[(2+4g_A^2)\left(L - \ln\frac{m_\pi^2}{\mu^2}\right) + 2 + g_A^2\right], \tag{4.27}$$

$$d_{1,\rm qEDM} = \bar{d}_1 + \delta\bar{d}_1 + \frac{1}{4}\bar{d}_1\frac{m_\pi^2}{(2\pi F_\pi)^2}\left[(2+8g_A^2)\left(L - \ln\frac{m_\pi^2}{\mu^2}\right) + 2 + 3g_A^2\right], \tag{4.28}$$

and the momentum dependence given entirely by the Schiff moments,

$$\begin{aligned} S'_{i,\rm qEDM} &= \bar{S}'_i, \\ H_{i,\rm qEDM}(Q^2) &= 0. \end{aligned} \tag{4.29}$$

The contributions from one-loop diagrams with $\not{P}\not{T}$ πN interactions are suppressed by $\alpha_{\rm em}/\pi \sim \mathcal{O}(m_\pi^3/M_{\rm QCD}^3)$ relative to the LO contributions, and come in at N^{3}LO.

The relevant diagrams in case of χI sources are shown in Fig. 4.6. The LO+NLO nucleon EDFF coming from the χI sources is, just as for the qEDM, purely short range and static. At NNLO, apart from short-range contributions to the nucleon EDM and Schiff moment, there are

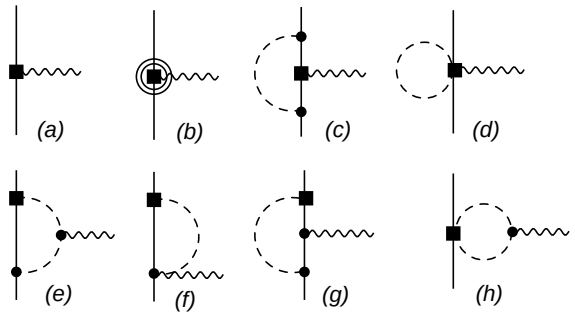

Figure 4.6: Tree-level and one-loop diagrams contributing to the nucleon EDFF up to NNLO for the gCEDM and two chiral-invariant $\not{P}\not{T}$ FQ operators. Squares denote LO $\not{P}\not{T}$ interactions from Eq. (3.79, 3.105), double circled squares from Eq. (3.109). Other notation as in Fig. 4.1 For simplicity only one possible ordering is shown here.

the one-loop diagrams 4.6(c-h). They depend on $\not{P}\not{T}$ $N\gamma$ and πN interactions in Eqs (3.105, 3.79). Thus, to $\mathcal{O}(ewm_\pi^2/M_{\not{T}}^2 M_{\rm QCD})$ we find the μ-independent EDMs

$$d_{0,\chi\rm I} = \bar{d}_0 + \delta\bar{d}_0 + 3g_A^2\bar{d}_0\frac{m_\pi^2}{(2\pi F_\pi)^2}\left(L - \ln\frac{m_\pi^2}{\mu^2}\right) , \tag{4.30}$$

$$\begin{aligned} d_{1,\chi\rm I} &= \bar{d}_1 + \delta\bar{d}_1 + \delta\vec{d}_1 + \frac{m_\pi^2}{(2\pi F_\pi)^2}\left\{\left(1+g_A^2\right)\bar{d}_1 + \frac{e\bar{\imath}_0}{8}\right. \\ &\quad \left. + \left[\left(1+2g_A^2\right)\bar{d}_1 + e\left(\frac{\bar{g}_0 g_A}{m_\pi^2} + \frac{\bar{\imath}_0}{8}\right)\right]\left(L - \ln\frac{m_\pi^2}{\mu^2}\right)\right\} . \end{aligned} \tag{4.31}$$

The isoscalar momentum dependence is entirely due to short-range operators in Eq. (3.109),

$$S'_{0,\chi\rm I} = \bar{S}'_0 . \tag{4.32}$$

$$H_{0,\chi\rm I}(Q^2) = 0. \tag{4.33}$$

The isovector part, on the other hand, receives also nonanalytic contributions:

$$S'_{1,\chi\rm I} = \bar{S}'_1 + \frac{e}{6(2\pi F_\pi)^2}\left[-\frac{\bar{\imath}_0}{8}\left(L - \ln\frac{m_\pi^2}{\mu^2}\right) + \frac{g_A\bar{g}_0}{m_\pi^2}\right] , \tag{4.34}$$

$$\begin{aligned} H_{1,\chi\rm I}(Q^2) &= \frac{4em_\pi^2}{15(2\pi F_\pi)^2}\left\{\left(\frac{g_A\bar{g}_0}{m_\pi^2} + \frac{\bar{\imath}_0}{12}\right) f\left(\frac{Q^2}{4m_\pi^2}\right)\right. \\ &\quad \left. + \frac{\bar{\imath}_0}{12}\frac{Q^2}{4m_\pi^2}\left[-\frac{5}{2}\frac{Q^2}{4m_\pi^2} + f\left(\frac{Q^2}{4m_\pi^2}\right)\right]\right\} . \end{aligned} \tag{4.35}$$

4.3 Discussion

We are now in position to discuss the implications of the various dimension-six $\not{P}\not{T}$ sources to the nucleon EDFF. First, we notice that up to NLO the nucleon EDFF stemming from $\bar{\theta}$, qCEDM, and FQLR have identical forms. At LO they coincide exactly and at NLO the only difference is a $\bar{g}_1$ dependence of d_i for qCEDM and FQLR, which is experimentally hard to disentangle from the larger short-range contributions. Although $\bar{g}_1$ plays a minor role in the nucleon EDFF calculation it is very important for nuclear $\not{P}\not{T}$ observables, in particular for the deuteron EDM.

We will discuss this in detail in later chapters. Up to NLO there are no differences between the qCEDM and FQLR.

For $\bar{\theta}$, qCEDM, and FQLR the momentum dependence (and thus the Schiff Moment) is mostly isovector, has a scale (relative to the EDM) set by $2m_\pi$, and is determined by the lowest-order pion-nucleon coupling $\bar{g}_0$. The isoscalar momentum dependence of the EDFF originates entirely from the nucleon-mass splitting, and is only about 10% of the isovector EDFF. The EDFF depends on just three (not counting $\bar{g}_1$) independent combinations of LECs, $\bar{g}_0$ and the short-range EDM contributions $\bar{d}_0$ and $\bar{d}_1 + \bar{d}_1'$, which contain nucleon matrix elements of $\tilde{V}_4$ and $\tilde{W}_3$ for qCEDM, X_{34} for FQLR, and P_4 for the $\bar{\theta}$ term. The numerical factors relating these couplings to either $\tilde{\delta}$, ξ, and $\bar{\theta}$ will thus be different. In the case of $\bar{\theta}$, the matrix element in $\bar{g}_0$ can be determined from PT observables, because it is related [48] to the matrix element of P_3 that generates the quark-mass contribution to the nucleon-mass splitting: $\bar{g}_0/\bar{\theta} \simeq 3$ MeV. For the qCEDM and FQLR, an argument identical to that in Ref. [31] serves to estimate d_1 in terms of $\bar{g}_0$, but no analogous constraint exists for $\bar{g}_0$ in this case and without a lattice calculation or a model we cannot do better than dimensional analysis. (For an estimate with QCD sum rules, see Ref. [85].) In any case, to the order we consider here, any EDFF measurement alone will be equally well reproduced by a certain value of $\bar{\theta}$, $\tilde{\delta}$, or ξ.

It is encouraging to see the good convergence of the chiral expansion even though some of the NLO contributions are enhanced by π. Under the assumption that higher-order results are not afflicted by anomalously-large dimensionless factors (which are not incorporated into the power counting), the relative error of our results at momentum Q should be $\sim (Q/M_{QCD})^2$.

Second, the πN sector of the qEDM is suppressed compared to that of the qCEDM because of the smallness of $\alpha_{\rm em}$ compared to $g_s^2/4\pi$ at low energies. The consequence is that, up to the lowest order where momentum dependence appears, both the EDM and the Schiff moment from the qEDM are determined by four combinations of six independent LECs, which at this point can only be estimated by dimensional analysis. The momentum dependence is expected to be governed by the QCD scale M_{QCD}, small relative to the EDM, and nearly linear in Q^2.

Finally, in the case of the χI sources loops are also suppressed, but do bring in nonanalytic terms not only to isoscalar and isovector EDMs, but also to the isovector momentum dependence (and thus Schiff moment). Again the momentum dependence is governed by $M_{\rm QCD}$. In addition to seven short-range contributions to the EDMs and Schiff moments, also two independent πN LECs appear ($\bar{g}_0$ and $\bar{\imath}_0$) which endow the isovector EDFF with a richer momentum dependence than in other cases. The isoscalar momentum dependence is identical to qEDM. For the χI sources, using the pion loop together with an estimate of $\bar{g}_0$ [86] is likely to be an underestimate of the EDM, because chiral symmetry allows a short-range contribution that is larger by a factor M_{QCD}^2/m_π^2. Again, under the assumption that higher-order results are not afflicted by anomalously-large dimensionless factors the relative error of our results for qEDM and χI sources at momentum Q should be $\sim (Q/M_{QCD})^3$.

As it is clear from Eqs. (4.22), (4.23), (4.29), (4.33), and (4.35), the full EDFF momentum dependences (for example, the second derivatives of F_i with respect to Q^2) are different for qCEDM (and $\bar{\theta}$ and FQLR), qEDM, and χI sources. Although the isoscalar components all have linear dependences in Q^2 (with different slopes) to the order considered here, the isovector components show an increasingly complex structure as one goes from qEDM to $\bar{\theta}$, qCEDM, and FQLR to χI sources. Determination of nucleon EDMs and Schiff moments alone would not be enough to separate the sources, yet they would yield clues. Expectations about the orders of magnitude of various dimensionless quantities are summarized in Table 6.1.

In the first line of Table 6.1 one finds the expected NDA size of the neutron EDM. As it is well known [9], this is consistent with many other estimates, such as $d_n = \mathcal{O}(d_i)$ in the constituent

Table 4.1: Expected orders of magnitude for the neutron EDM (in units of $e/M_{\rm QCD}$), the ratio of proton-to-neutron EDMs, and the ratios of the proton and isoscalar Schiff moments (in units of $1/m_\pi^2$) to the neutron EDM, for the $\bar\theta$ term [79, 84] and for the dimension-six $\not{P}\not{T}$ sources discussed in the text.

Source	$\bar\theta$	qCEDM	FQLR	qEDM	χI
$M_{\rm QCD}\, d_n/e$	$\mathcal{O}\left(\bar\theta \frac{m_\pi^2}{M_{\rm QCD}^2}\right)$	$\mathcal{O}\left(\tilde\delta \frac{m_\pi^2}{M_{\not{T}}^2}\right)$	$\mathcal{O}\left(\xi \frac{M_{\rm QCD}^2}{M_{\not{T}}^2}\right)$	$\mathcal{O}\left(\delta \frac{m_\pi^2}{M_{\not{T}}^2}\right)$	$\mathcal{O}\left(w \frac{M_{\rm QCD}^2}{M_{\not{T}}^2}\right)$
d_p/d_n	$\mathcal{O}(1)$	$\mathcal{O}(1)$	$\mathcal{O}(1)$	$\mathcal{O}(1)$	$\mathcal{O}(1)$
$m_\pi^2 S'_p/d_n$	$\mathcal{O}(1)$	$\mathcal{O}(1)$	$\mathcal{O}(1)$	$\mathcal{O}\left(\frac{m_\pi^2}{M_{\rm QCD}^2}\right)$	$\mathcal{O}\left(\frac{m_\pi^2}{M_{\rm QCD}^2}\right)$
$m_\pi^2 S'_0/d_n$	$\mathcal{O}\left(\frac{m_\pi}{M_{\rm QCD}}\right)$	$\mathcal{O}\left(\frac{m_\pi}{M_{\rm QCD}}\right)$	$\mathcal{O}\left(\frac{m_\pi}{M_{\rm QCD}}\right)$	$\mathcal{O}\left(\frac{m_\pi^2}{M_{\rm QCD}^2}\right)$	$\mathcal{O}\left(\frac{m_\pi^2}{M_{\rm QCD}^2}\right)$

quark model, and $d_n = \mathcal{O}(e\tilde d_i/4\pi, e d_W M_{\rm QCD}/4\pi)$ from QCD sum rules. If $\tilde\delta \sim \delta \sim \xi \sim w = \mathcal{O}(1)$ (as would be the case for $g_s \sim 4\pi$ and no small phases), then the FQLR and χI sources give the biggest dimension-six contribution to the EDFF because of the chiral-symmetry-breaking suppression $\mathcal{O}(m_\pi^2/M_{\rm QCD}^2)$ for the qCEDM and qEDM. However, models exist (for example, Ref. [87]) where δ and $\tilde\delta$ are enhanced relative to w, and all three sources produce EDFF contributions of the same overall magnitude. Even so, there is no *a priori* reason to expect cancellations among the various sources. A measurement of the neutron EDM d_n could be fitted by any one source. Conversely, barring unlikely cancellations, the current bound yields order-of-magnitude bounds on the various parameters at the scale where NDA applies: using $2\pi F_\pi \simeq 1.2$ GeV for $M_{\rm QCD}$,

$$\bar\theta \lesssim 10^{-10}, \tag{4.36}$$

$$\frac{\tilde\delta}{M_{\not{T}}^2}, \frac{\delta}{M_{\not{T}}^2} \lesssim \left(10^5\ \text{GeV}\right)^{-2}, \tag{4.37}$$

$$\frac{w}{M_{\not{T}}^2}, \frac{\xi}{M_{\not{T}}^2} \lesssim \left(10^6\ \text{GeV}\right)^{-2}. \tag{4.38}$$

(For comparison, Eq. (4.36) is consistent within a factor of a few with bounds obtained by taking representative values of μ in the nonanalytic terms to estimate [31] the size of the renormalized LECs for the EDM, and using either $SU(2)$ [48] or $SU(3)$ [84] symmetry to constrain $\bar g_0$.) In all four cases we expect the proton and neutron EDMs to be comparable, $|d_p| \sim |d_n|$, but the presence of undetermined LECs does not allow further model-independent statements.

Even though the measurement of d_n and d_p is not sufficient to disentangle the fundamental sources this does not imply that measuring both nucleon EDMs, is of no more interest than measuring one of them. Although, for all sources, we expect d_p to be of the same order as d_n, the sign and precise magnitude of both d_n and d_p are important for calculating nuclear EDMs. For example, if the qEDM is the dominant $\not{P}\not{T}$ source, measuring d_n and d_p is enough to predict the EDMs of other light nuclei such as the deuteron or the helion (the nucleus of ^{3}He). We will come back to this in detail in Chapters 5 and 6.

It is in the pattern of the S'_i that we see some texture. (This pattern is not evident in Ref. [88], possibly because of the way chiral symmetry is broken explicitly in the model used, both in the form of the PT πN Lagrangian and in the magnitude of the $\not{P}\not{T}$ πN coupling for the gCEDM.) While in all cases one expects $|S'_p| \sim |S'_n|$, the relative size to the EDMs, in particular

of the isovector component, allows one in principle to separate qEDM and χI sources from $\bar{\theta}$, qCEDM and FQLR. Since all these sources generate different πN interactions thanks to their different chiral-symmetry-breaking properties, nuclear EDMs might provide further probes of the hadronic source of $\not{P}\not{T}$.

More could be said with input from lattice QCD. For each source the pion-mass dependence is different. A fit to lattice data on the Q^2 *and* m_π^2 dependences of the nucleon EDFF with the expressions of this paper would allow in principle the separate determination of LECs. In this case a measurement of the neutron and proton alone would suffice to pinpoint a dominant source if it exists, but in the more general case of two or more comparable sources further observables are needed.

One should keep in mind that our approach is limited to low energies. The contributions associated with quarks heavier than up and down are buried in the LECs, as done, for example, in other calculations of nucleon form factors: electric and magnetic [89], anapole [90], and electric dipole from $\bar{\theta}$ [79]. Heavy-quark EDMs and CEDMs are also singlets under $SU(2)_L \times SU(2)_R$, so they generate in two-flavor χPT interactions with the same structure as those from the gCEDM and four-quark operators, and therefore cannot be separated explicitly. (This is clear already in the one-loop running of d_W, which gets a contribution of the heavy-quark CEDMs [43].) The parameter w here should be interpreted as subsuming heavier-quark EDMs and CEDMs. With the additional assumption that m_s makes a good expansion parameter, effects of the s quark could be included explicitly. The larger $SU(3)_L \times SU(3)_R$ symmetry would yield further relations among observables (for example, between the EDFFs of the nucleon and of the Λ), and we could, in principle, isolate the contributions of the strange quark. Since our nucleon results, which can be used as input in nuclear calculations in two-flavor nuclear EFT, would be recovered in the low-energy limit anyway —as was explicitly verified in Ref. [84] for the $\bar{\theta}$ results of Ref. [79]— we leave a study of the identification of explicit s-quark effects to future work.

In summary, we have investigated the low-energy electric dipole form factor that emerges as a consequence of effectively $\not{P}\not{T}$ dimension-four to -six sources at the quark-gluon level: the QCD $\bar{\theta}$ term, the quark electric and color-electric dipole moments, the gluon color-electric dipole moment, and four-quark operators. Only the full momentum dependence could in principle separate these sources, although the Schiff moments, if they were isolated, would exhibit some texture, allowing a partial separation. For $\bar{\theta}$ term, qCEDM and FQLR we have provided a lower-bound estimate for the isoscalar nucleon EDM, expected to set also the minimum size of the deuteron EDM.

Chapter 5

The Deuteron P- and T-odd Form Factors with Perturbative Pions

5.1 Introduction[1]

In the previous chapter we calculated the electric dipole form factors of the neutron and proton which arise as a low-energy manifestation of parity and time-reversal violation in quark-gluon interactions. We showed that nonzero measurements of the neutron and proton EDM can be explained by a small, but finite, value of $\bar{\theta}$, or by any of the $\not{P}\not{T}$ dimension-six sources. With measurements of the nucleon Schiff Moments it becomes possible to separate some of the sources. However, it is unlikely that they, let alone the full momentum dependence of the EDFF, can be probed experimentally. We concluded that apart from the nucleon EDMs additional experimentally accessible observables are required to learn more about the fundamental physics responsible for low-energy $\not{P}\not{T}$ form factors.

Historically it has only been possible to measure the EDMs of neutral particles directly, because EDM experiments apply a static electric field such that any charged particle would immediately escape the experimental setup. EDMs of charges particles such as the proton and the electron are inferred from neutral systems containing these particles. In the last decade or so, new techniques have been proposed to directly measure the EDMs of charged particles in electric and magnetic storage rings [20]. This has already been done for the muon [21]. An experiment to measure the proton EDM directly is planned at Brookhaven Nation Laboratory [22], while an experiment for measuring the EDMs of several light nuclei, deuteron and helion in particular, is being pursued at Jülich Forschungszentrum. These experiments have a claimed accuracy of around d_p, d_d, $d_{^3\mathrm{He}} \sim 10^{-16}\, e\,\mathrm{fm}$ which is three orders of magnitude better than the current neutron EDM limit [8]. Whether this precision can actually be achieved remains to be seen, but it is clear that these storage ring experiments are very promising and of great interest.

Theoretically the deuteron EDM is interesting since it is the simplest bound nucleus and it can be treated with firm theoretical tools. The main problem, not appearing for single nucleons, is the appearance of the nucleon-nucleon (NN) interactions. The NN scattering lengths in the S-wave channels are unnaturally large and similarly the deuteron binding momentum is unnaturally small (smaller than the pion mass by a factor 3), implying a cancellation between different effects and suggesting a fine-tuning in the QCD parameters. Lattice-QCD calculations find scattering lengths of natural value $\sim 1/m_\pi$ at a pion mass around 350 MeV [91] which

[1] This chapter is based on J. de Vries, E. Mereghetti, R. G. E. Timmermans, U. van Kolck, Phys. Rev. Lett. **107**, 091804 (2011).

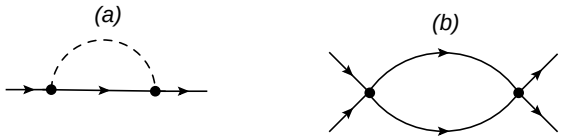

Figure 5.1: Two one-loop diagrams contributing to, respectively, the nucleon self-energy and NN scattering. Solid lines denote nucleons and dashed lines denote pions. The second diagram obtains an infrared singularity if the power-counting rules in Sect. 3.2 are consistently enforced.

suggests that the fine-tuning is related to the light-quark masses.

In this chapter we use a framework developed by Kaplan, Savage, and Wise (KSW) [92], which assumes the leading S-wave NN interactions to be enhanced compared to standard χPT estimates [64]. The enhancement causes these interactions to become nonperturbative and the deuteron binding momentum arises from the summation of the enhanced interactions to all orders. All other effects, such as pion exchange, are treated as perturbations, explaining the name "perturbative pions". A major advantage of the KSW framework is that calculations can be done analytically.

We start this chapter with a brief discussion in Sec. 5.2 how to extend χPT to few-nucleon systems. In particular we discuss the KSW framework and how to implement time-reversal violation. In Sec. 5.3 we calculate the leading-order (LO) $\not{P}\not{T}$ deuteron form factors and discuss the results in Sec. 5.4. We calculate a subset of the next-to-leading order (NLO) corrections in Sec. 5.5.

5.2 Perturbative pions

In the one-nucleon sector the power-counting rules given in Sect. 3.2 generate an expansion in $Q/M_{\rm QCD}$, where $Q \sim m_\pi$ is the typical external momentum in the problem. Applying the heavy-baryon formalism, the nucleon propagator is given by $i/(v\cdot q + i\epsilon)$ where q is the nucleon four-momentum. The nucleon kinetic energy comes in at NLO and is treated as a perturbation (as we did in the calculation of the NLO nucleon EDFF). A typical loop diagram where these power-counting rules apply is Diagram 5.1(a). Neglecting the πN vertices which are not relevant for the discussion, the intermediate part of the diagram is given by

$$\int \frac{{\rm d}^4k}{(2\pi)^4}\,\frac{i}{[v\cdot(p-k)+i\epsilon]}\,\frac{i}{[k^2-m_\pi^2+i\epsilon]} + \mathcal{O}(\frac{p}{m_N}),$$

where p is the four-momentum of the on-shell nucleon and k the loop momentum. Since $v\cdot p = \mathcal{O}(p^2/m_N)$ we can neglect this term in the numerator and write

$$\int \frac{{\rm d}^4k}{(2\pi)^4}\,\frac{i}{[-k_0+i\epsilon]}\,\frac{i}{[k_0^2-(\vec{k}^2+m_\pi^2)+i\epsilon]} + \mathcal{O}(\frac{p}{m_N}).$$

Because there is at most one intermediate nucleon propagator, the contour integration over the zeroth component of the loop momentum can always be performed in such a way that the nucleon pole is avoided and we find $k_0 = \sqrt{\vec{k}^2+m_\pi^2} = \mathcal{O}(Q)$. This justifies the counting of a nucleon propagator as $1/Q$ in Sect. 3.2. On the other hand, consider Diagram 5.1(b) contributing to NN scattering. In the center-of-mass frame the ingoing on-shell nucleons have momentum $p_1 = (v\cdot p, \vec{p})$ and $p_2 = (v\cdot p, -\vec{p})$ and we find for the intermediate part of the diagram

$$\int \frac{{\rm d}^4k}{(2\pi)^4}\,\frac{i}{[v\cdot k+i\epsilon]}\,\frac{i}{[v\cdot(-k)+i\epsilon]} + \mathcal{O}(\frac{p}{m_N}).$$

Closing the pole in either plane gives rise to an infrared divergence [64]. This divergence, of course, is not physical but arises from neglecting the nucleon kinetic energy. Taking the kinetic term into account gives

$$\int \frac{\mathrm{d}^4k}{(2\pi)^4} \frac{i}{[v\cdot(p+k)-\frac{1}{2m_N}(\vec{p}+\vec{k})^2+i\epsilon]} \frac{i}{[v\cdot(p-k)-\frac{1}{2m_N}(\vec{p}-\vec{k})^2+i\epsilon]} \sim \int \frac{\mathrm{d}^3k}{(2\pi)^3} \frac{i}{\vec{k}^2/m_N}.$$

The conclusion is that in diagrams where the nucleon pole cannot be avoided, the energy of the intermediate nucleons is $\mathcal{O}(Q^2/m_N)$ instead of $\mathcal{O}(Q)$. These diagrams are additionally enhanced by a factor 4π. Due to these enhancements certain diagrams with the topology of Diagram 5.1(b) (bubble diagrams) become nonperturbative and need to be resummed leading to bound states [64]. This need for resummation led Weinberg to propose an approach consisting of two steps. First one derives an effective potential which contains only contributions from diagrams without pure-nucleon intermediate states. Such a potential not suffering from enhanced nucleon propagators can be expanded in Q/M_{QCD} with the use of the power counting in Sect. 3.2. Amplitudes are then calculated by iterating the potential to all orders which is done by solving the the Lippman-Schwinger equation (or, equivalently, the Schrödinger equation). We apply this approach to the EDMs of light nuclei in Chapter 6 although we use a slightly different power counting than the original one in Ref. [64].

Weinberg's approach uses naive dimensional analysis (NDA) [63] for the LECs which gives for LO NN S-wave interactions an expected scaling $C_{0s,t} = \mathcal{O}(4\pi/M_{\mathrm{QCD}}M_{NN})$, where M_{NN} is the scale where the EFT breaks down. With this scaling S-wave NN interactions appear at the same order as LO one-pion exchange (OPE). However, since the ${}^1S_0$ and ${}^3S_1$ scattering lengths are unnaturally large (respectively, $a_t = -23.7\,\mathrm{fm}$ and $a_s = 5.4\,\mathrm{fm}$, both significantly larger than the natural range $1/m_\pi = 1.4\,\mathrm{fm}$) the LECs $C_{0s,t}$ have to be larger than expected from NDA.

Kaplan, Savage, and Wise proposed a new power-counting scheme to account for the large scattering lengths by modifying the power counting of S-wave NN interactions. Instead of the NDA estimates above the LECs scale as $C_{0s,t} = \mathcal{O}(4\pi/M_{\mathrm{QCD}}Q)$, with Q the typical momentum of the external particles. Thus, the S-wave NN interactions are enhanced by a factor M_{NN}/Q with respect to Weinberg counting. Since in Weinberg counting pion exchange and the S-wave NN interaction appear both at LO, in KSW counting pion exchange can be regarded as a perturbation as long as $Q \ll M_{NN}$. The enhancement of the S-wave LECs can be understood by solving a renormalization group equation in the Power-Divergent Subtraction (PDS) scheme. In this scheme not only the poles in $d = 4$ dimensions are subtracted, but also poles in $d = 3$ dimensions which correspond to linear divergences if a cut-off had been used. Solving the renormalization group equation gives

$$C_{0s,t}(\mu) = \frac{4\pi}{m_N} \frac{1}{1/a_{s,t} - \mu}, \tag{5.1}$$

and the KSW scaling is obtained if we choose $\mu \sim Q$ and use that the scattering lengths are large. A more detailed description of the PDS scheme can be found in, for example, Ref. [93]. Other NN interactions that connect S waves are enhanced because they are renormalized by insertions of $C_{0,st}$. In the KSW counting the most important operators, decomposed in partial waves, are given by

$$\begin{aligned} \mathcal{L}_{f=4,\,PT} &= -\sum_{i=s,t} \left(C_{0i} + D_{2i}m_\pi^2\right) (N^T P_i N)^\dagger N^T P_i N \\ &\quad -\sum_{i=s,t} \frac{C_{2i}}{8} \left[(N^T P_i N)^\dagger N^T P_i \mathcal{D}_{\perp,-}^2 N\right] + \mathrm{h.c}, \end{aligned} \tag{5.2}$$

where P_i are the isospin triplet and singlet projectors

$$P_t^a = \frac{1}{\sqrt{8}}\tau_2\tau_a\sigma_2, \qquad P_s^i = \frac{1}{\sqrt{8}}\tau_2\sigma_2\sigma^i. \tag{5.3}$$

The interactions that connect S to S waves with two additional derivatives scale as $C_{2i} \eqsim 4\pi/m_N M_{NN} Q^2$ (compared with $4\pi/m_N M_{NN}^3$ in Weinberg counting). Similarly, the chiral-breaking operator with LEC $m_\pi^2 D_{2s,t}$ connects two S waves and scales as $4\pi/m_N M_{NN} Q^2$. Other operators with two derivatives that connect S to D waves are only renormalized on one side and scale as $4\pi/m_N M_{NN}^2 Q$, while operators that do not connect S waves (for example, P to P transitions) scale as in Weinberg counting.

Within this framework KSW calculated the PT electromagnetic form factors of the deuteron [94]. The deuteron charge radius was calculated up to NLO and agreed within 10% with the experimental value. NLO corrections are about 25% of the LO results indicating good convergence. The deuteron magnetic moment at LO was remarkably close to the experimental value. At NLO only one new counterterm appears that can be fitted to the data. The electric quadrupole moment comes in at NLO and was found to be off by $\sim 40\%$ from the experimental value. Furthermore, the momentum dependence of the charge and magnetic FFs agreed well with experimental data up to momenta $\sim 300\,\mathrm{MeV}$. Less successful has been the calculation of the phase shifts in NN scattering. In Ref. [95] the S, D, and P phase shifts were calculated up to NNLO. In the spin-singlet channels ${}^1S_0$, ${}^1P_1$, and ${}^1D_2$ the series converges (albeit slowly) up to momenta of order $300\,\mathrm{MeV}$. However, in the ${}^3S_1$, ${}^3P_0$, and ${}^3D_1$ channels the NNLO effects already at momenta of order m_π are much larger than the NLO effects and the agreement with data is ruined. Apparently the breakdown scale of the perturbative expansion in the triplet channels is of the order of the pion mass and pions should be treated nonperturbatively for such, and higher, energies. Because the electromagnetic properties of the deuteron, which is mostly in a ${}^3S_1$ state, are well described with perturbative pions, this suggests that the typical momenta in the deuteron is small enough ($Q < m_\pi$) such that Q/M_{NN} can be treated as a perturbation. We will come back to this in Chapter 6 when we compare the results for the deuteron EDM from a perturbative and a nonperturbative calculation.

Here we will use the KSW framework to calculate the $\not{P}\not{T}$ form factors of the deuteron. Similar as the PT NN interactions, the $\not{P}\not{T}$ NN interactions that involve S waves acquire a different scaling than the one given in Sec. 3.3.3. The Q dependence of these LECs can be understood from the PDS scheme, but it is not completely obvious how the LECs depend on the high scale, since there are two of them, M_{QCD} and M_{NN}. To overcome this problem we again use NDA, but where before we matched high-energy QCD to low-energy χPT we now match the nonperturbative χPT to the lower-energy perturbative χPT. Details are given in App. B. In the present chapter it is understood that the scalings of NN interactions are those given here and not those in Sec. 3.3.3. For the LO calculation we require the following $\not{P}\not{T}$ NN interactions

$$\begin{aligned}\mathcal{L}_{f=4,\not{P}\not{T}} &= \bar{C}_1 \bar{N} N\, \partial_\mu(\bar{N} S^\mu N) + \bar{C}_2 \bar{N} \boldsymbol{\tau} N \cdot \partial_\mu(\bar{N} S^\mu \boldsymbol{\tau} N) \\ &\quad + \bar{C}_3 \bar{N} \tau_3 N\, \partial_\mu(\bar{N} S^\mu N) + \bar{C}_4 \bar{N} N\, \partial_\mu(\bar{N} \tau_3 S^\mu N) + \ldots,\end{aligned} \tag{5.4}$$

where we neglected the detailed chiral structure since the terms with additional pions are not necessary for the calculation. As we saw in Sec. 3.3.3, at LO the $\bar{\theta}$ term only contributes to the isospin-conserving operators $\bar{C}_{1,2}$, while the dimension-six sources generate the isospin-breaking operators $\bar{C}_{3,4}$ at the same order. The $\bar{C}_{1,2}$ interactions cause a transition of two nucleons in a ${}^3S_1$ state into a ${}^1P_1$ state. The $\bar{C}_{3,4}$ operators turn the ${}^3S_1$ state into a ${}^3P_1$ state. Since these operators connect to S waves on one side, we expect them to scale as $1/Q$. The NDA rules in

App. B then assign the following scalings to the LECs: For the $\bar{\theta}$ term

$$\bar{C}_{1,2} = \mathcal{O}\left(\bar{\theta}\frac{4\pi}{m_N Q}\frac{m_\pi^2}{M_{\rm QCD}M_{NN}^2}\right), \qquad \bar{C}_{3,4} = \mathcal{O}\left(\bar{\theta}\frac{4\pi}{m_N Q}\frac{\varepsilon m_\pi^4}{M_{\rm QCD}^3 M_{NN}^2}\right), \tag{5.5}$$

for the χI sources

$$\bar{C}_{1,2} = \mathcal{O}\left(w\frac{4\pi}{m_N Q}\frac{M_{\rm QCD}}{M_{\not T}^2}\right), \qquad \bar{C}_{3,4} = \mathcal{O}\left(w\frac{4\pi}{m_N Q}\frac{\varepsilon m_\pi^2 M_{\rm QCD}}{M_{NN}^2 M_{\not T}^2}\right), \tag{5.6}$$

and for the other dimension-six sources

$$\bar{C}_{1,2,3,4} = \mathcal{O}\left(\frac{4\pi}{m_N Q}\left\{\tilde{\delta}\frac{m_\pi^2 M_{\rm QCD}}{M_{NN}^2 M_{\not T}^2}, \xi\frac{M_{\rm QCD}^3}{M_{NN}^2 M_{\not T}^2}, \delta\frac{\alpha_{\rm em}}{4\pi}\frac{m_\pi^2 M_{\rm QCD}}{M_{NN}^2 M_{\not T}^2}\right\}\right), \tag{5.7}$$

where for simplicity of notation we have combined $\delta_{0,3}$ and $\tilde{\delta}_{0,3}$ into δ and $\tilde{\delta}$. The detailed dependence on the isoscalar and isovector q(C)EDMs can be found in Chapter 3.

We also require the following $NN\gamma$ interactions

$$\mathcal{L}_{f=4,\not P\not T,\rm em} = -\bar{D}\bar{N}S^\mu v^\nu N\,\bar{N}N\,F_{\mu\nu} - \bar{M}\varepsilon^{\alpha\beta\mu\nu}v_\alpha \bar{N}S_\beta N\,\bar{N}S^\lambda N\,\partial_\lambda F_{\mu\nu}, \tag{5.8}$$

which are short-range contributions to the deuteron EDM and MQM. These operators connect S waves and scale as

$$\bar{D} = \mathcal{O}\left(\bar{\theta}\frac{4\pi}{m_N Q^2}\frac{m_\pi^2}{M_{\rm QCD}^2 M_{NN}}\right), \qquad \bar{M} = \mathcal{O}\left(\bar{\theta}\frac{4\pi}{m_N Q^2}\frac{m_\pi^2}{M_{\rm QCD}^2 M_{NN}^2}\right) \tag{5.9}$$

for the $\bar{\theta}$ term, and as

$$\bar{D} = \mathcal{O}\left(e\frac{4\pi}{m_N Q^2}\left\{\tilde{\delta}\frac{m_\pi^2 M_{\rm QCD}}{M_{NN}^2 M_{\not T}^2}, \xi\frac{M_{\rm QCD}^3}{M_{NN}^2 M_{\not T}^2}, \delta\frac{m_\pi^2}{M_{\rm QCD}M_{\not T}^2}, w\frac{M_{\rm QCD}}{M_{\not T}^2}\right\}\right), \tag{5.10}$$

$$\bar{M} = \mathcal{O}\left(e\frac{4\pi}{m_N Q^2}\left\{\tilde{\delta}\frac{m_\pi^2}{M_{NN}^2 M_{\not T}^2}, \xi\frac{M_{\rm QCD}^2}{M_{NN}^2 M_{\not T}^2}, \delta\frac{m_\pi^2}{M_{\rm QCD}M_{NN}M_{\not T}^2}, w\frac{1}{M_{\not T}^2}\right\}\right), \tag{5.11}$$

for the dimension-six sources. The scalings of these counterterms is such that they have the exact size necessary to absorb certain divergences in pion-loop diagrams calculated below.

Combining all of the above, the scaling of a diagram can be obtained by the following rules

- a factor $Q^5/(4\pi m_N)$ for each loop integral,
- a factor of m_N/Q^2 for each nucleon propagator,
- a factor of $1/Q^2$ for each pion propagator,
- the NDA estimate for the LECs (KSW scaling for NN operators) corresponding to the interactions in the diagram.

An insertion of $C_{0s,t}$ costs one extra loop $\sim Q^5/4\pi m_N$, two nucleon propagators $\sim m_N^2/Q^4$, an insertion of the LEC $C_{0s,t} \sim 4\pi/m_N Q$, which combine to a factor of $\mathcal{O}(1)$, confirming that the leading NN interactions need to be summed to all orders. On the other hand, a LO pion exchange costs one additional loop $\sim Q^5/(4\pi m_N)$, two nucleon propagators $\sim m_N^2/Q^4$, a pion propagator $\sim 1/Q^2$, and two insertions of the strong πN vertex $\sim (Q/F_\pi)^2$. Combining these factors, the extra one-pion exchange amounts to Q/M_{NN}, where $M_{NN} = 4\pi F_\pi^2/m_N \sim 450\,\text{MeV}$. In this chapter we assume that Q/M_{NN} is a good expansion parameter.

5.3 The deuteron P- and T-odd form factors at leading order

The deuteron has two $\not{P}\not{T}$ electromagnetic FFs which, part from small relativistic corrections, are defined from the $\not{P}\not{T}$ part of the electromagnetic current, $J^\mu_{\not{P}\not{T}}$, by

$$\langle \vec{p}', j|J^0_{\not{P}\not{T}}|\vec{p}, i\rangle = \varepsilon^{ijl} q^l F_D(\vec{q}^2) + \varepsilon^{lmn} K^l q^m (\delta^{ni} q^j + \delta^{nj} q^i) \frac{F_M(\vec{q}^2)}{4m_d}, \tag{5.12}$$

$$\langle \vec{p}', j|J^k_{\not{P}\not{T}}|\vec{p}, i\rangle = \varepsilon^{mnl} q^l \left[\delta^{mi}\delta^{nj} K^k \frac{F_D(\vec{q}^2)}{m_d} - \frac{1}{4}\delta^{mk}(\delta^{ni} q^j + \delta^{nj} q^i) F_M(\vec{q}^2) \right], \tag{5.13}$$

where $|\vec{p}, i\rangle$ denotes a deuteron state of momentum $\vec{p}$ and polarization δ^μ_i in the rest frame, normalized so that $\langle \vec{p}', j|\vec{p}, i\rangle = \sqrt{1+\vec{p}^2/m_d^2}(2\pi)^3\delta^{(3)}(\vec{q})\delta_{ij}$, $\vec{q} = \vec{p} - \vec{p}'$ is the outgoing photon momentum, $\vec{K} = (\vec{p}' + \vec{p})/2$, and $m_d = 2m_N - \gamma^2/m_N + \ldots$ is the deuteron mass in terms of the nucleon mass m_N and the binding momentum $\gamma \sim 45\,\text{MeV}$. The EDFFs at zero momentum transfer define the deuteron EDM $d_d = F_D(0)$ and MQM $\mathcal{M}_d = F_M(0)$.

To calculate the matrix element of the $\not{P}\not{T}$ electromagnetic current we use

$$\langle \vec{p}', j|J^\mu_{\not{P}\not{T}}|\vec{p}, i\rangle = i \left[\frac{\Gamma^\mu_{ij}(\bar{E}, \bar{E}', \vec{q})}{d\Sigma(\bar{E})/dE} \right]_{\bar{E}, \bar{E}' \to -B}, \tag{5.14}$$

which is derived via the LSZ formula in Ref. [94]. In this expression Γ^μ_{ij} and Σ are, respectively, the irreducible three- and two-point functions of the deuteron interpolating field $\mathcal{D}_i$. Irreducible diagrams are defined as diagrams which do not fall apart when the graph is cut at a LO NN vertex $C_{0s,t}$. For the interpolating field we choose $\mathcal{D}_i(x) = N(x)P^j_s N(x)$, where P^j_s is the projector on the quantum numbers of the deuteron (spin 1 and isospin 0). The energy $\bar{E} = E - \vec{p}^2/4m_N$ ($\bar{E}' = E' - \vec{p}\,'^2/4m_N$) is the energy of the two incoming (outgoing) nucleons in the center-of-mass frame. In the end we have to set the nucleons on-shell, $\bar{E}, \bar{E}' \to -B$, with $B = \gamma^2/m_N$ the deuteron binding energy.

The two- and three-point functions can be expanded in Q/M_{NN} and, if subleading terms in the PT and $\not{P}\not{T}$ Langrangian are used, in $Q/M_{\rm QCD}$. Expanding Eq. (5.14) up to NLO gives

$$\langle \vec{p}', j|J^\mu_{\not{P}\not{T}}|\vec{p}, i\rangle = i \left[\frac{\Gamma^{(0)}}{d\Sigma^{(0)}/dE} + \frac{\Gamma^{(1)}}{d\Sigma^{(0)}/dE} - \frac{\Gamma^{(0)}}{[d\Sigma^{(0)}/dE]^2}\frac{d\Sigma^{(1)}}{dE} \right]_{\bar{E}, \bar{E}' \to -B}. \tag{5.15}$$

In this chapter, we will first calculate the LO term in Eq. (5.15), which is sufficient for the LO deuteron EDFF and MQFF. This calculation already gives a lot of insight and provides valuable results. After discussing these results we return to the calculation of the subleading terms in Eq. (5.15). This is computationally a formidable task, but provides an important check of the convergence of the expansion.

5.3.1 The two- and three-point functions

We start with the two-point function. At LO it is the trivial diagram in Fig. 5.2 which gives

$$\left[\frac{d\Sigma^{(0)}(\bar{E})}{dE} \right]_{\bar{E} \to -B} = \frac{-im_N^2}{8\pi\gamma}. \tag{5.16}$$

It turns out that at this order one insertion of a $\not{P}\not{T}$ vertex into the two-point function causes it to vanish, such that in Eq. (5.14) all $\not{P}\not{T}$ physics needs to occur in the three-point function.

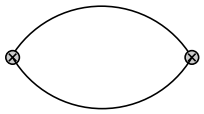

Figure 5.2: The irreducible two-point function $\Sigma(\bar{E})$ at LO. Solid lines represent nucleons. The crossed vertex represents an insertion of the interpolating field $D_i(x)$.

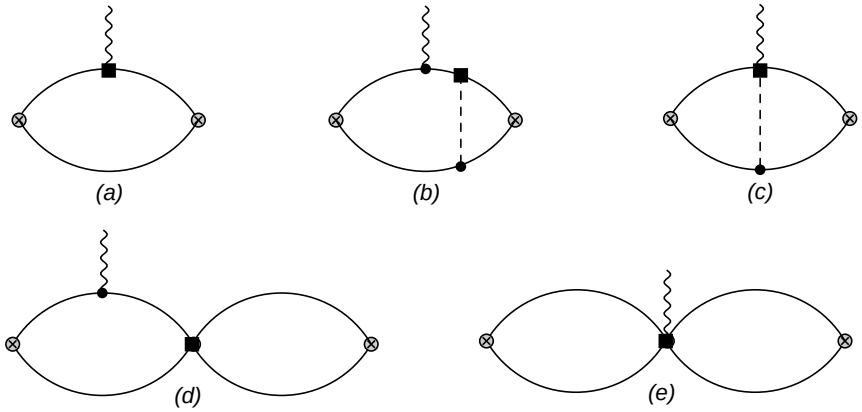

Figure 5.3: Different classes of irreducible diagrams contributing to the three-point function $\Gamma^0_{ij}(\bar{E}, \bar{E}', \vec{q})$. Solid, dashed, and wavy lines represent nucleons, pions, and photons, respectively. A square marks a LO $\not{P}\not{T}$ interaction, other vertices representing PT interactions from Eq. (3.24). The crossed vertex represents an insertion of the interpolating field $D_i(x)$. For simplicity only one possible ordering is shown here.

Before going into a detailed calculation of the three-point function, it is important to identify the dominant contributions to the EDFF and MQFF for each separate $\not{P}\not{T}$ source. To do that we first identify the dominant diagrams for generic $\not{P}\not{T}$ hadronic interactions. We take the LO $\not{P}\not{T}$ $N\gamma$, πN, and $\pi N\gamma$ vertices from Sec. 3.3 and the $\not{P}\not{T}$ NN and $NN\gamma$ vertices from Eqs. (5.4) and (5.8). Vertices with additional pions will always give smaller contributions since they require additional loops. The dominant diagrams for the deuteron EDFF for each of these interactions are shown in Fig. 5.3. The PT πN vertex is the standard axial-vector coupling, $g_A = 1.27$, and the photon vertex denoted by a filled circle is the coupling to the charge e. The crossed circles denote the deuteron interpolating field $\mathcal{D}_i$. The black squares denote $\not{P}\not{T}$ vertices.

The power-counting rules given above assign a scaling to each of the diagrams in Fig. 5.3. After taking into account the normalization by the two-point function, we find

$$D_a = \mathcal{O}\left(Q\bar{d}_{0,1}\right), \qquad D_b = \mathcal{O}\left(\frac{1}{M_{NN}} e\bar{g}_i\right), \qquad D_c = \mathcal{O}\left(\frac{Q^4}{M_{\rm QCD} M_{NN}} \bar{d}_{\pi,i}\right),$$
$$D_d = \mathcal{O}\left(\frac{Q^4}{M_{NN}} e\bar{C}_i\right), \qquad D_e = \mathcal{O}\left(\frac{Q^6}{M_{\rm QCD} M_{NN}} \bar{D}_i\right), \tag{5.17}$$

in terms of the different types of hadronic $\not{P}\not{T}$ interactions. The $\not{P}\not{T}$ $\pi N\gamma$ vertex is from Eqs. (3.101) and (3.107) where we relabeled the LECs as $\bar{d}_\pi$. In these estimates we used $Q \sim F_\pi \sim m_\pi \sim \gamma$, $g_A \sim 1$, and $4\pi F_\pi^2 \sim M_{\rm QCD} M_{NN}$.

The ground state of the deuteron is mainly a ${}^3S_1$ state. The deuteron obtains a ${}^1P_1$ component after a pion exchange with $\bar{g}_0$ as the $\not{P}\not{T}$ πN vertex in Diagram 5.3(b) or after an insertion of $\bar{C}_{1,2}$ in Diagram 5.3(d). Since the LO PT one-nucleon current, *i.e.* the proton charge, is spin

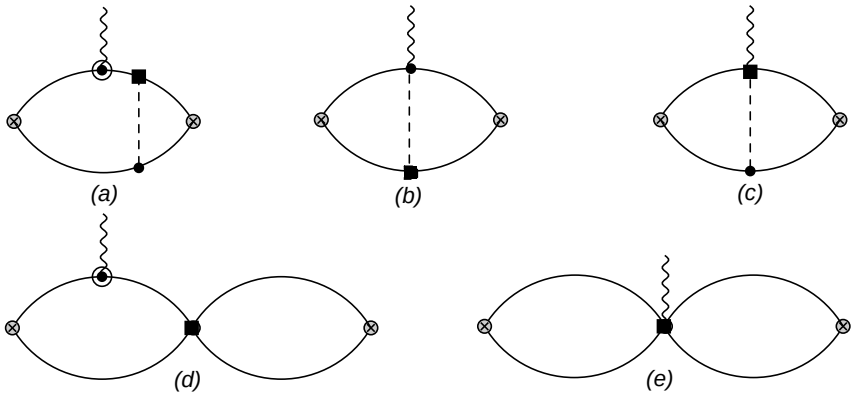

Figure 5.4: Different classes of irreducible diagrams contributing to the three-point function $\Gamma^k_{ij}(\bar{E}, \bar{E}', \vec{q})$. The circled dots are taken from Eqs. (3.25) and (3.30). The other notation is as in Fig. 5.3. For simplicity only one possible ordering is shown here.

independent, it cannot bring the deuteron wave function from ${}^1P_1$ to ${}^3S_1$ and therefore these contributions vanish for the deuteron. This implies that the $\not{P}\not{T}$ πN vertex in Diagram 5.3(b) needs to be $\bar{g}_1$ and the $\not{P}\not{T}$ NN vertex in Diagram 5.3(d) either $\bar{C}_3$ or $\bar{C}_4$. Similarly, the $\not{P}\not{T}$ currents in Diagrams 5.3(a,c,e) need to be isoscalar. By combining Eq. (5.17) with the scaling of the LECs for the different sources, we draw the following conclusions:

- The $\bar{\theta}$ term conserves isospin and therefore $\bar{g}_1$ is suppressed by $\varepsilon m_\pi^2/M_{\rm QCD}^2$ compared to $\bar{g}_0$ and the dominant contribution to the deuteron EDFF comes from Diagram 5.3(a). At NLO in the Q/M_{NN} expansion Diagrams 5.3(b,e) need to be considered. At this order other NLO corrections must be included as well. We discuss these corrections in Sec. 5.5.

- In case of the qCEDM and FQLR, there is no suppression for $\bar{g}_1$ and Diagram 5.3(b) provides the dominant contribution to deuteron EDFF.

- In case of the qEDM, $\not{P}\not{T}$ πN interactions are suppressed and it is not surprising that the deuteron EDFF is dominated by the nucleon EDM.

- Finally, for χI sources πN interactions are suppressed as well and the nucleon EDM gives the main contribution. At NLO Diagram 5.3(b) needs to be considered.

The conclusion is that at LO only Diagrams 5.3(a,b) need to be taken into account.

For the deuteron MQFF, the possible diagrams are shown in Fig. 5.4. The photon vertex denoted by the circled dot is the nucleon magnetic moment in Eq. (3.30) or the $N\gamma$ interaction obtained from gauging the nucleon kinetic term in Eq. (3.25). The power-counting rules assign the following scaling to each of the diagrams

$$D_a = \mathcal{O}\left(\frac{Q}{M_{\rm QCD}M_{NN}} e\bar{g}_i\right), \qquad D_b = \mathcal{O}\left(\frac{Q}{M_{\rm QCD}M_{NN}} e\bar{g}_i\right), \qquad D_c = \mathcal{O}\left(\frac{Q^3}{M_{\rm QCD}M_{NN}} \bar{c}_i\right),$$
$$D_d = \mathcal{O}\left(\frac{Q^5}{M_{\rm QCD}M_{NN}} e\bar{C}_i\right), \qquad D_e = \mathcal{O}\left(\frac{Q^7}{M_{\rm QCD}M_{NN}} \bar{M}_i\right). \tag{5.18}$$

This time the $\not{P}\not{T}$ $\pi N\gamma$ vertex is taken from Eqs. (3.94), (3.96), and (3.99). Since the nucleon magnetic moment is spin dependent the $\not{P}\not{T}$ πN and NN interactions in Diagrams 5.4(a,d) can be isoscalar or isovector. However, the $\not{P}\not{T}$ currents in the remaining diagrams have to be

isoscalar in order for the diagrams to be nonvanishing. We plug in the scalings of the LECs for the different sources and find:

- For $\bar{\theta}$ term, the deuteron MQFF is dominated by Diagram 5.4(a) where the $\not{P}\not{T}$ πN vertex is $\bar{g}_0$. In principle Diagram 5.4(b) contributes at the same order, but the $\not{P}\not{T}$ current is isovector and vanishes on the deuteron.
- For qCEDM and FQLR, the MQFF is dominated by the same effect as the $\bar{\theta}$ term. However, the $\not{P}\not{T}$ vertex can be either $\bar{g}_0$ or $\bar{g}_1$.
- In case of the qEDM, $\not{P}\not{T}$ πN and NN interactions are suppressed. The dominant effect comes from $\not{P}\not{T}$ $\pi N\gamma$ interactions (see Eq. (3.99)) in Diagram 5.4(c) and the counterterm in Diagram 5.4(e).
- For χI sources, even though $\not{P}\not{T}$ πN and NN interactions appear with the same chiral index in Secs. 3.3.2 and 3.3.3, the KSW scaling enhances the latter over the former, see Eq. (5.6). Therefore, the dominant contribution comes from Diagram 5.4(d).

The actual LO calculation is rather straightforward (for some details regarding the integrals, see App. C). We use dimensional regularization with power-divergence subtraction [92] at a renormalization scale μ. Our results depend on the ratio $\xi = \gamma/m_\pi$ and on three functions of the momentum in the ratio $x = |\vec{q}|/4\gamma$:

$$F_1(x) = \arctan(x)/x, \tag{5.19}$$

which originates in a bubble with only a $N\gamma$ coupling and appears also in the charge FF [94], and two complicated functions that result from two-loop diagrams with a pion propagator, which can be expanded as

$$F_2(x) = 1 - x^2 \frac{10 + 65\xi + 144\xi^2 + 72\xi^3}{30(1+\xi)(1+2\xi)^2} + \mathcal{O}(x^4), \tag{5.20}$$

$$F_3(x) = 1 - x^2 \frac{\xi^2(12+8\xi)}{5(1-2\xi)(1+2\xi)^2} + \mathcal{O}(x^4). \tag{5.21}$$

The scale of momentum variation is set by 4γ.

The LO deuteron EDFF is due to Diagrams 5.3(a,b),

$$F_D(\vec{q}^{\,2}) = 2\bar{d}_0 F_1(x) - \frac{e g_A \bar{g}_1 m_N}{6\pi F_\pi^2 m_\pi} \frac{1+\xi}{(1+2\xi)^2} F_2(x), \tag{5.22}$$

where the first term is dominant for $\bar{\theta}$, qEDM, and χI sources, and the second one for qCEDM and FQLR. The LO MQFF comes from Diagrams 5.4(a,c,d,e),

$$\begin{aligned} F_M(\vec{q}^{\,2}) \;=\; & \frac{e(1+\kappa_0)}{8\pi}(\mu-\gamma)(\bar{C}_1 - 3\bar{C}_2) F_1(x) \\ & + \frac{e g_A}{2\pi F_\pi^2 m_\pi}\left[\bar{g}_0(1+\kappa_0) + \frac{\bar{g}_1}{3}(1+\kappa_1)\right] \frac{1+\xi}{(1+2\xi)^2} F_2(x) \\ & + \frac{2\gamma}{\pi}(\mu-\gamma)^2 \bar{M} + \frac{g_A \bar{c}_0 \gamma}{\pi F_\pi^2}\left(\frac{1-2\xi}{1+2\xi} F_3(x) + 2\ln\frac{\mu/m_\pi}{1+2\xi}\right), \end{aligned} \tag{5.23}$$

where at this order $\bar{g}_0$ originates from $\bar{\theta}$, qCEDM, and FQLR, $\bar{g}_1$ from qCEDM and FQLR, $\bar{C}_{1,2}$ from χI sources, and $\bar{M}$ and $\bar{c}_0$ from qEDM. For the qEDM the $\bar{M}$ counterterm is required to absorb the divergence caused by the diagram involving $\bar{c}_0$.

5.4 Discussion

We can now discuss the implications of the various $\not{P}\not{T}$ sources for the deuteron EDFF and MQFF. In Table 6.1 we list the orders of magnitude for the deuteron EDM, d_d, the ratio of deuteron-to-neutron EDMs, d_d/d_n, and the ratio of the deuteron MQM and EDM, $\mathcal{M}_d/d_d$, for the different $\not{P}\not{T}$ sources. Just as for d_n, a d_d signal by itself could be attributed to any source with a parameter of appropriate size. For $\bar{\theta}$, qEDM, and χI sources the deuteron EDFF is determined by the LO isoscalar nucleon EDM, and thus well approximated by the sum of neutron and proton EDM. For $\bar{\theta}$ in particular, using the most important long-range contributions in Eq. (4.17), which appear at NLO, as a lower bound for $\bar{d}_0$, one finds $|d_d| \gtrsim 2.8 \cdot 10^{-4}\,\bar{\theta}\ e\,\text{fm}$. If, however, the dominant $\not{P}\not{T}$ source is the qCEDM or FQLR, d_d comes mainly from neutral-pion exchange and is given by

$$d_d(\text{qCEDM, FQLR}) = -\frac{e g_A \bar{g}_1 m_N}{6\pi F_\pi^2 m_\pi} \frac{1+\gamma/m_\pi}{(1+2\gamma/m_\pi)^2} = -0.23\,\frac{\bar{g}_1}{F_\pi}\ e\,\text{fm}\ . \tag{5.24}$$

By power counting the contribution from $2\bar{d}_0$ is expected to be suppressed by $m_\pi M_{NN}/M_{\rm QCD}^2$ compared to Eq. (5.24). From Eqs. (3.55, 3.73, 3.97, 3.98) we infer $\bar{d}_0 F_\pi/\bar{g}_1 = \mathcal{O}(eF_\pi/M_{\rm QCD}^2) \sim 0.03\ e\,\text{fm}$, implying that, in the case of qCEDM or FQLR, the nucleon EDMs contribute at the 25% level to the deuteron EDM. This suppression is somewhat less than formally expected, but still significant. If we assume the isoscalar nucleon EDM is saturated by its long-range part, Eq. (4.13), the contribution is at the 10% level. We conclude that a measurement of d_d significantly larger than $d_n + d_p$ would be indicative of a qCEDM or FQLR.

A null-measurement of the deuteron EDM at the $10^{-16}\ e\,\text{fm}$ level [20] would strengthen the bounds from the neutron EDM in Eq. (4.36) on $\bar{\theta}$ to

$$\bar{\theta} \quad \lesssim \quad 3 \cdot 10^{-13}, \tag{5.25}$$

and the bounds on the dimension-six sources in Eq. (4.38) to

$$\begin{aligned} \frac{\tilde{\delta}}{M_{\not{T}}^2} &\lesssim \left(2 \cdot 10^7\ \text{GeV}\right)^{-2}, \qquad \frac{\delta}{M_{\not{T}}^2} \lesssim \left(5 \cdot 10^6\ \text{GeV}\right)^{-2}, \\ \frac{\xi}{M_{\not{T}}^2} &\lesssim \left(10^8\ \text{GeV}\right)^{-2}, \qquad \frac{w}{M_{\not{T}}^2} \lesssim \left(5 \cdot 10^7\ \text{GeV}\right)^{-2}. \end{aligned} \tag{5.26}$$

More quantitative statements could be made with lattice-QCD calculations of the EFT LECs.

Additional information comes from the ratio $\mathcal{M}_d/d_d$. For $\bar{\theta}$, $m_d|\mathcal{M}_d|$ is expected to be larger than $|d_d|$, whereas for the dimension-six sources we expect $m_d|\mathcal{M}_d|$ to be of similar size or somewhat smaller than $|d_d|$. For $\bar{\theta}$, $\mathcal{M}_d$ is determined by pion exchange, and we can again use the link with isospin violation in Eq. (3.53) to find $\mathcal{M}_d \simeq 2.0 \cdot 10^{-3}\,\bar{\theta}\ e\ \text{fm}^2$. An upper bound on $\mathcal{M}_d$ can therefore constrain $\bar{\theta}$ without relying on an estimate of short-range physics via the size of the chiral log, which is necessary when using d_n [31]. Moreover, if $m_d|\mathcal{M}_d|$ is found to be much smaller than $|d_d|$, the source would likely be qEDM. This shows that a measurement of $\mathcal{M}_d$, in addition to d_n and d_d, would be very valuable.

The deuteron EDM and MQM were calculated previously in Refs. [80, 81]. Since these calculations did not use the chiral properties of the fundamental $\not{P}\not{T}$ sources, the $\not{P}\not{T}$ πN interactions were assumed to be all of the same size. When the dominant source is the qCEDM or FQLR, their results agree with ours. The advantage of our EFT framework is that it has a direct link to QCD by exploiting the chiral properties of the $\not{P}\not{T}$ dimension-four and -six operators. This

Table 5.1: Orders of magnitude for the deuteron EDM (in units of e/m_d), the ratio of deuteron-to-neutron EDMs, and the ratio of the deuteron MQM and EDM (in units of $1/m_d$), for $\not{P}\not{T}$ sources of effective dimension up to six.

Source	$\bar{\theta}$	qCEDM	FQLR	qEDM	χI
$m_d\, d_d/e$	$\mathcal{O}\left(\bar{\theta}\frac{m_\pi^2}{M_{\rm QCD}^2}\right)$	$\mathcal{O}\left(\tilde{\delta}\frac{m_\pi M_{\rm QCD}^2}{M_{NN}M_{\not{T}}^2}\right)$	$\mathcal{O}\left(\xi\frac{M_{\rm QCD}^4}{m_\pi M_{NN}M_{\not{T}}^2}\right)$	$\mathcal{O}\left(\delta\frac{m_\pi^2}{M_{\not{T}}^2}\right)$	$\mathcal{O}\left(w\frac{M_{\rm QCD}^2}{M_{\not{T}}^2}\right)$
d_d/d_n	$\mathcal{O}(1)$	$\mathcal{O}\left(\frac{M_{\rm QCD}^2}{m_\pi M_{NN}}\right)$	$\mathcal{O}\left(\frac{M_{\rm QCD}^2}{m_\pi M_{NN}}\right)$	$\mathcal{O}(1)$	$\mathcal{O}(1)$
$m_d\, \mathcal{M}_d/d_d$	$\mathcal{O}\left(\frac{M_{\rm QCD}^2}{m_\pi M_{NN}}\right)$	$\mathcal{O}(1)$	$\mathcal{O}(1)$	$\mathcal{O}\left(\frac{\gamma}{M_{NN}}\right)$	$\mathcal{O}(1)$

is demonstrated by the $\bar{g}_2\bar{N}\pi_3\tau_3 N$ interaction used in many previous calculations, which due to its chiral properties only comes in at higher order for all $\not{P}\not{T}$ sources. Consequently, for the qCEDM and FQLR, the ratio of d_d to $\mathcal{M}_d$ depends at LO only on the ratio $\bar{g}_1/\bar{g}_0$,

$$\left|\frac{m_d\mathcal{M}_d}{2d_d}\right| = 1 + \kappa_1 + \frac{3\bar{g}_0}{\bar{g}_1}(1+\kappa_0). \tag{5.27}$$

The ratio can be measured independently: $\bar{g}_1$ could be inferred from d_d, and $\bar{g}_0$ in principle from another observable, such as the proton Schiff moment (Eq. (4.8)) or the ^{3}He EDM [82]. In addition, the power-counting scheme allows a perturbative framework with analytical results that can be improved systematically. Under the assumption that higher-order results are not afflicted by anomalously-large dimensionless factors, the relative error of our results should be $Q/M_{NN} \sim 30\%$, as was explicitly verified for the charge FF [94]. We will check these errors in the next section by calculating NLO corrections. Our estimates for d_d are consistent with those from QCD sum rules [96].

In summary, we have investigated the leading-order, low-energy electric-dipole and magnetic-quadrupole form factors of the deuteron that result from the $\bar{\theta}$ angle, the quark electric and chromo-electric dipole moments, the gluon chromo-electric dipole moment, and $\not{P}\not{T}$ four-quark operators. While for qCEDM and FQLR we expect $|d_d|$ to be larger than $|d_n|$ by a factor $\mathcal{O}(M_{\rm QCD}^2/m_\pi M_{NN})$, for the other $\not{P}\not{T}$ sources we have shown that d_d is given by the sum of d_n and d_p. Furthermore, the SM predicts $m_d|\mathcal{M}_d|$ to be larger than $|d_d|$, whereas beyond-the-SM physics prefers $m_d|\mathcal{M}_d|$ smaller than, or of similar size as $|d_d|$. EDM and MQM measurements are therefore complementary.

5.5 A check of convergence: next-to-leading order corrections[2]

In order to investigate the reliability of the results in the previous section we calculate some NLO, *i.e.* $\mathcal{O}(Q/M_{NN})$, corrections to the deuteron $\not{P}\not{T}$ moments. For simplicity we do not calculate the momentum-dependent part of the form factors. This calculation provides a check of the power counting in two ways:

- The size of certain counterterms in Eqs. (5.4) and (5.8) can be compared with the size of divergences appearing in NLO pion-exchange diagrams. There should be enough counterterms to absorb all divergences.

[2]This section is based on J. de Vries, E. Mereghetti, R. G. E. Timmermans, and U. van Kolck, in preparation.

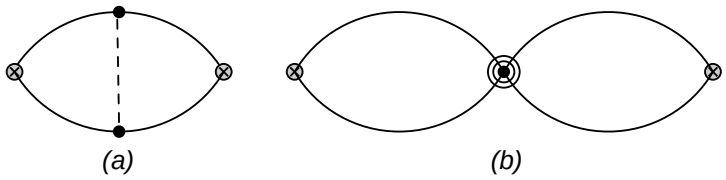

Figure 5.5: Diagrams contributing to the deuteron NLO two-point function. The double circled NN vertex denotes an insertion of the subleading NN operators C_{2s} and D_{2s}. The other notation is as in Fig. 5.3.

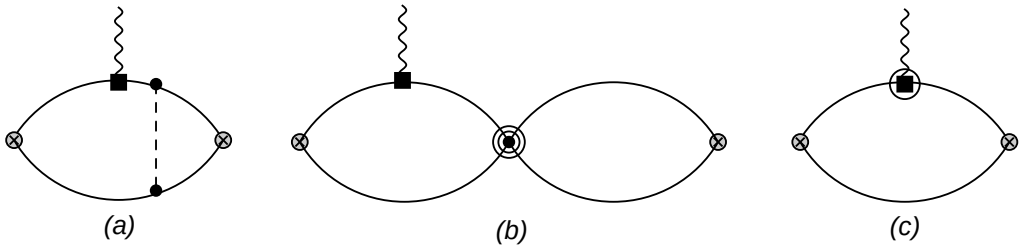

Figure 5.6: NLO one-body corrections to the deuteron EDM. The square and circled square denote, respectively, the LO and NLO isoscalar nucleon EDM. The other notation is as in Figs. (5.3) and (5.5). For each diagram, only one possible ordering is shown.

- The calculation of two-pion-exchange (TPE) diagrams checks the convergence of the expansion in Q/M_{NN}.

At this moment a full NLO calculation of the deuteron EDM and MQM for all sources has not been completed, and we can only give a partial result.

First of all it is necessary to include Q/M_{NN} corrections to the two-point function. These are shown in Fig. 5.5. These corrections are independent of the $\not{P}\not{T}$ source. Diagram 5.5(a) is an OPE correction and Diagram 5.5(b) a correction due to an insertion of the subleading S-wave NN interactions C_{2s} and D_{2s} given in Eq. (5.2). The subleading two-point function obtained from these diagrams is

$$\frac{d\Sigma^{(1)}(\bar{E})}{dE}_{\bar{E}\to -B} = \frac{im_N^2}{8\pi\gamma}\frac{m_N}{2\pi}\left[\frac{g_A^2}{F_\pi^2}\left(\mu-\gamma-\frac{m_\pi^2}{2\gamma+m_\pi}\right) + C_{2s}\gamma(\mu-\gamma)(\mu-2\gamma) + D_{2s}m_\pi^2(\mu-\gamma)\right], \tag{5.28}$$

in agreement with Ref. [94].

More interesting are the corrections to the three-point function because these do depend on the $\not{P}\not{T}$ source. We focus first on some of the NLO corrections to the deuteron EDM in case of the QCD $\bar{\theta}$ term (the isoscalar qCEDM case is identical). The LO contribution is the one-body contribution in Diagram 5.3(a). The corrections to the one-body term are shown in Fig. 5.6. Diagrams 5.6(a,b) are corrections to the deuteron wave function due to OPE or an insertion of the subleading S-wave NN interactions C_{2s} and D_{2s}. Diagram 5.6(c) represents the correction to the isoscalar nucleon EDFF calculated in Chapter 4. The latter correction can be implemented easily by using the NLO isoscalar nucleon EDM d_0 given in Eqs. (4.13). The NLO three-point

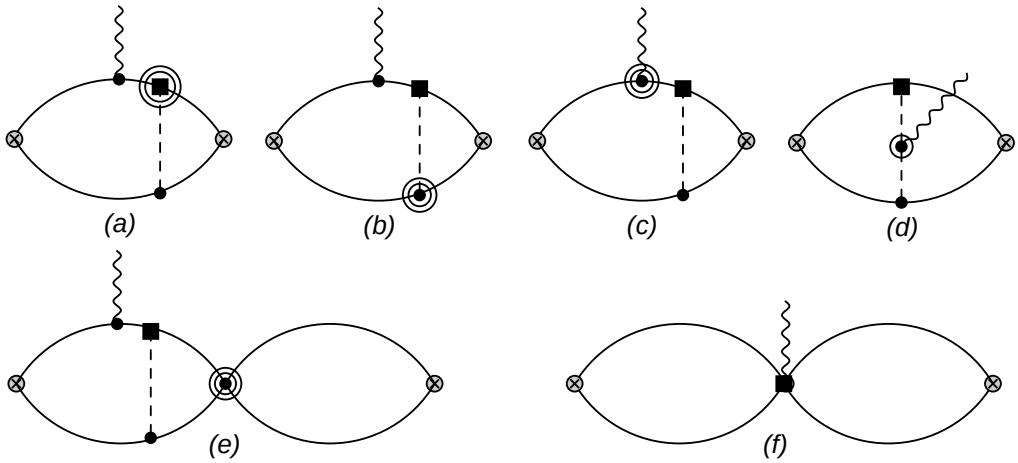

Figure 5.7: NLO diagrams for the deuteron EDM in case of the $\bar{\theta}$ term. A square marks the $\not{P}\not{T}$ vertex $\bar{g}_0$ or the $\not{P}\not{T}$ four-nucleon current $\bar{D}$, while a double-circled square is taken from the subleading Lagrangian in Eqs. (3.58) and (3.62). Circles denote LO PT interactions, while circled and double circled circles are taken from Eqs. (3.26, 3.29, 3.31). The double circled NN vertex denotes a relativistic correction to the S-wave NN interactions. The other notation is as in Fig. 5.3. For each diagram, only one possible ordering is shown.

function becomes

$$\begin{aligned}\Gamma^{(1)}(\bar{E},\bar{E}',\vec{q})_{\bar{E},\bar{E}'\to -B} &= (d_0\varepsilon^{ijk}q^k v^\mu)\frac{m_N^2}{8\pi\gamma}\frac{m_N}{\pi}\left[\frac{g_A^2}{F_\pi^2}\left(\mu-\gamma-\frac{m_\pi^2}{2\gamma+m_\pi}\right)\right.\\ &\left.+C_{2s}\gamma(\mu-\gamma)(\mu-2\gamma)+D_{2s}m_\pi^2(\mu-\gamma)\right]+\mathcal{O}(\vec{q}^{\,2}),\end{aligned} \tag{5.29}$$

which has exactly the same form as NLO two-point function in Eq. (5.28). In fact, by inserting these NLO corrections into Eq. (5.15), the corrections to the two-point function cancel most of the corrections to the three-point function. The only one remaining is the correction to the isoscalar nucleon EDM itself

$$d_d^{\rm one-body}(\bar{\theta}) = 2\bar{d}_0+\frac{2eg_A\bar{g}_0}{(2\pi F_\pi)^2}\,\pi\left[\frac{3m_\pi}{4m_N}-\frac{\delta m_N}{m_\pi}\right]. \tag{5.30}$$

This correction does not change the conclusion that for $\bar{\theta}$ the deuteron EDM is dominated by the sum of d_n and d_p.

In case of the $\bar{\theta}$ term, apart from one-body corrections, there are additional NLO contributions to the deuteron EDM. These contributions consist mostly of diagrams with the same topology as Diagram 5.3(b), but one of the PT or $\not{P}\not{T}$ interactions is suppressed by two powers of $Q/M_{\rm QCD}$. These diagrams are shown in Fig. 5.7(a,b,c). By the power-counting rules of the previous section, they enter at NLO in the Q/M_{NN} expansion. The first diagrams we consider arise due to isospin breaking in one of the vertices. Diagram 5.7(a) reflects isospin breaking in the $\not{P}\not{T}$ vertex $\bar{g}_1$, suppressed in case of the $\bar{\theta}$ term. Diagrams 5.7(b,d) consists of the LO $\not{P}\not{T}$ vertex $\bar{g}_0$ and an isospin-breaking PT interaction taken from Eq. (3.29). Together their contribution to the deuteron EDM is

$$d_d^I(\bar{\theta}) = -\frac{eg_A\bar{g}_0 m_N}{6\pi F_\pi^2 m_\pi}\left[\left(\frac{\bar{g}_1}{\bar{g}_0}+\frac{\beta_1}{2g_A}\right)\frac{1+\xi}{(1+2\xi)^2}+\frac{\delta m_N}{m_N}\frac{2-3\xi}{1+2\xi}\right], \tag{5.31}$$

in terms of $\xi = \gamma/m_\pi$. The isospin-breaking corrections can be compared to the correction to the isoscalar nucleon EDM in Eq. (5.30). By NDA, we estimate $\bar{g}_1/\bar{g}_0 \sim \beta_1/2g_A = \mathcal{O}(\varepsilon m_\pi^2/M_{\rm QCD}^2) = 10^{-2}$. At present there exists only an upper bound on β_1 from NN phase-shift analysis [70, 74], which is consistent with NDA. Plugging these estimates in Eq. (5.32) and using the lattice value $\delta m_N = 2.26\,\text{MeV}$, we find that the isospin-breaking corrections are approximately 20% of the correction to the isoscalar nucleon EDM. The conclusion is that the LO result from the previous section is not significantly affected by isospin-breaking corrections.

Additional NLO corrections arise from Diagrams 5.7(a,b,c,e), where one of the vertices is a relativistic, $1/m_N^2$, correction. Diagram 5.7(a) contains a relativistic correction to $\bar{g}_0$ taken from Eq. (3.58), while Diagrams 5.7(b,c,e) contain a relativistic correction to, respectively, the PT πN, $N\gamma$, and S-wave NN interactions. The calculation of the deuteron moments due to corrections to the S-wave NN interactions has not been completed yet. Since only a full calculation gives rise to physical meaningful results, *i.e.* results that are gauge and Galilean invariant and renormalizable, we do not give the partial results we have so far. We make an exception for Diagram 5.7(c) which does have physical meaning by itself. The $N\gamma$ vertex is taken from Eq. (3.31) and depends on the isoscalar anomalous magnetic moment κ_0. At this order, this is the only contribution to the deuteron EDM depending on κ_0 and other corrections, we have not fully calculated yet, cannot affect this result. The diagram gives the logarithmically divergent contribution

$$d_d^{\kappa_0}(\bar{\theta}) \;=\; -\frac{e g_A \bar{g}_0 \gamma}{8\pi F_\pi^2 m_N}(1+2\kappa_0)\left(\frac{1-2\xi}{1+2\xi} + 2\log\frac{\mu/m_\pi}{1+2\xi}\right). \tag{5.32}$$

Evaluating the log at $\mu = m_\pi$, Eq. (5.32) is approximately 5% of the correction to the isoscalar nucleon EDM in Eq. (5.30). Numerically the contribution can be neglected, but in order to absorb the divergence a counterterm is required. This counterterm is provided by the short-range four-nucleon current $\bar{D}$ in Eq. (5.8) and shown in Diagram 5.7(f). It adds to the deuteron EDM

$$d_d^{\bar{\rm D}}(\bar{\theta}) \;=\; \gamma \bar{D}(\mu)\frac{(\mu-\gamma)^2}{\pi}, \tag{5.33}$$

which, with the scaling of $\bar{D}$ in Eq. (5.9), is of exactly the right size to absorb the logarithmic divergence. This adds credibility to the NDA estimates of the LECs.

As mentioned, the contribution from other relativistic corrections has not been fully calculated and we cannot say much about their size. However, typically in χPT relativistic corrections (Q^2/m_N^2) are smaller than corrections in the chiral expansion $(Q^2/M_{\rm QCD}^2)$ and we do not expect the remaining corrections to alter the LO result any more than the terms we calculated so far. A complete calculation is necessary to verify this claim.

For the other sources the situation is radically different. In case of a qEDM, $\not{P}\not{T}$ πN interactions are suppressed and the only NLO corrections are those in Fig. 5.6. As we found above, these corrections mostly cancel against the corrections to the two-point function. In Chapter 4 we concluded that for the qEDM there are no NLO corrections to the isoscalar EDM implying that the result for the deuteron EDM

$$d_d(\text{qEDM}) \;=\; 2\bar{d}_0, \tag{5.34}$$

holds at NLO.

For the χI sources, the situation lies in between those of the $\bar{\theta}$ term and qEDM. Again at LO the deuteron EDM is given by one-body contributions. Just as for the qEDM there are no

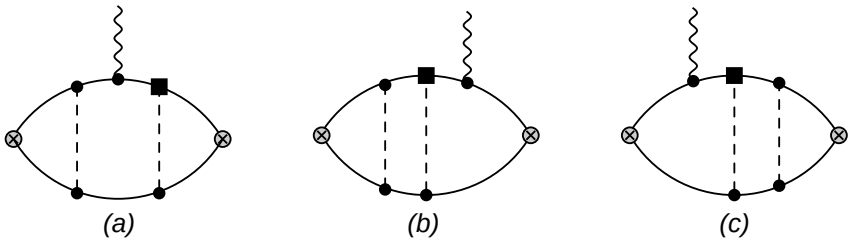

Figure 5.8: TPE diagrams contributing to the deuteron EDM. The notation is as in Fig. 5.3. For each diagram, only one possible ordering is shown.

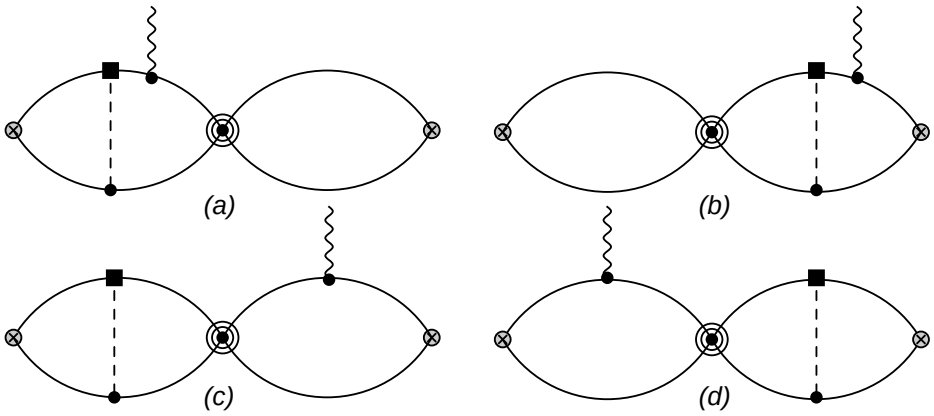

Figure 5.9: NLO corrections to the deuteron EDM arising from subleading NN operators C_{2s} and D_{2s}. The notation is as in Figs. 5.3 and 5.5. For each diagram, only one possible ordering is shown.

NLO corrections to the isoscalar nucleon EDM. At NLO we do find contributions from Diagram 5.3(b). This diagram is built from the $\not{P}T$ πN vertex $\bar{g}_1$ and LO PT vertices from Eq. (3.24). The complications occurring for $\bar{\theta}$ term, such as relativistic corrections and counterterms, do not appear for the χI sources. The reason is, as discussed in detail in Chapter 3, that both $\bar{g}_0$ and $\bar{g}_1$ are suppressed with respect to the short-range isoscalar nucleon EDM. For $\bar{\theta}$ this only holds for $\bar{g}_1$ and corrections to $\bar{g}_0$ need to be taken into account. Diagram 5.3(b) has already been calculated in the previous section and together with the one-body contribution, the NLO deuteron EDM becomes

$$\begin{aligned} d_d(\chi\mathrm{I}) &= 2\bar{d}_0 - \frac{e g_A \bar{g}_1 m_N}{6\pi F_\pi^2 m_\pi} \frac{1+\xi}{(1+2\xi)^2} \\ &= 2\bar{d}_0 - 0.23\,\frac{\bar{g}_1}{F_\pi}\, e\,\mathrm{fm}. \end{aligned} \tag{5.35}$$

From the scaling of the LECs in Eqs. (3.80, 3.106) we estimate $F_\pi \bar{d}_0/\bar{g}_1 = \mathcal{O}(eF_\pi/\varepsilon m_\pi^2) \sim 5\, e\,\mathrm{fm}$. We conclude that for χI sources the NLO correction from $\bar{g}_1$ OPE affects the deuteron EDM by only a few percent.

Finally we focus on the isovector qCEDM and FQLR. These are the most interesting cases since for these sources the deuteron EDM is dominated by pion exchange. The NLO corrections consist of the TPE diagrams in Fig. 5.8. The calculation of TPE contributions tests whether pions can be treated perturbatively which is one of the assumptions on which the KSW framework is built. The diagrams in Fig. 5.8 can be calculated analytically, although this is a difficult

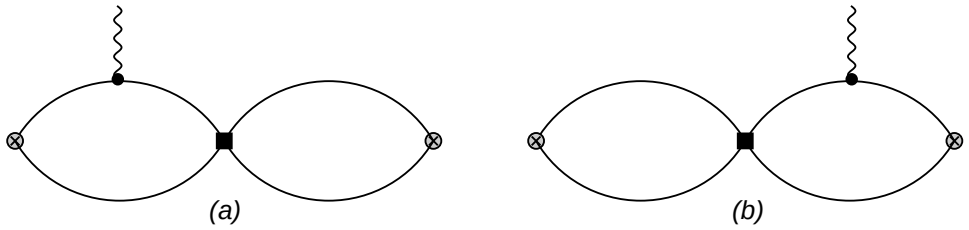

Figure 5.10: NLO corrections to the deuteron EDM arising from $\not{P}\not{T}$ NN operators. The notation is as in Fig. 5.3.

task because it is a three-loop computation. Here we only give the final result and refer to App. C for some computational details. Apart from the TPE diagrams there are the diagrams in Fig. 5.9 which reflect the subleading S-wave NN interactions C_{2s} and D_{2s} defined in Eq. (5.2). Finally, Diagrams 5.8(b,c) are divergent and the associated counterterm is provided by the $\not{P}\not{T}$ NN interactions $\bar{C}_{3,4}$ in Eq. (5.4). The diagrams involving these counterterms are depicted in Fig. 5.10.

Combining all these corrections with the corrections to the two-point function and the LO result, gives the following expression for the deuteron EDM up to NLO

$$\begin{aligned} d_d &= -\frac{e g_A \bar{g}_1 m_N}{6\pi F_\pi^2 m_\pi}\left\{\frac{1+\xi}{(1+2\xi)^2}\left[1+\frac{\gamma m_N}{2\pi}C_{2s}(\mu-\gamma)^2\right]-\frac{g_A^2 m_N m_\pi}{4\pi F_\pi^2}g(\xi,\mu/m_\pi)\right\} \\ &\quad -e\frac{m_N(\bar{C}_3-\bar{C}_4)(\mu-\gamma)}{2\pi}, \end{aligned} \tag{5.36}$$

where $g(\xi,\mu/m_\pi)$ is a three-loop function depending only on ξ and μ/m_π

$$\begin{aligned} g(\xi,\mu/m_\pi) &= \frac{1}{4}\Bigg[-\frac{45+195\xi+135\xi^2-369\xi^3-512\xi^4-162\xi^5-84\xi^6-24\xi^7+48\xi^8}{4\xi^4(1+\xi)(1+2\xi)^3} \\ &\quad -\frac{45+135\xi-30\xi^2-300\xi^3-104\xi^4+38\xi^5+24\xi^6+88\xi^7}{2\xi^5(1+2\xi)^2}\log\left(\frac{2(1+\xi)}{1+2\xi}\right) \\ &\quad -\frac{45-90\xi^2-8\xi^4}{4\xi^6}\left[\mathrm{Li}_2\left(\frac{-1}{1+2\xi}\right)+\frac{\pi^2}{12}\right]+\log\left(\frac{2(1+\xi)}{\mu/m_\pi}\right)\Bigg], \end{aligned} \tag{5.37}$$

where $\mathrm{Li}_2(x)$ is the dilogarithm of x. The μ dependence of $g(\xi,\mu/m_\pi)$ is absorbed by the counterterm $(\bar{C}_3-\bar{C}_4)$. Although it is not obvious at first sight, the function $g(\xi,\mu/m_\pi)$ is finite in the limit of zero binding momentum ($\xi\to 0$). The first term in Eq. (5.36) is the LO result calculated in the previous section, the second term the correction from the subleading PT NN interactions, the third term arises from TPE corrections, and the fourth term is the counterterm contribution. Following Ref. [94], we use for the renormalization scale $\mu=m_\pi$ and $C_{2s}(m_\pi)=9.91\,\mathrm{fm}^4$ and find

$$d_d = -\frac{\bar{g}_1}{F_\pi}(0.23+0.097)\,e\,\mathrm{fm}-e\frac{m_N(\bar{C}_3-\bar{C}_4)(\mu-\gamma)}{2\pi}, \tag{5.38}$$

where the first term is the LO result and the second term the NLO result apart from the counterterm which is kept explicit. Neglecting the counterterm, whose size we cannot estimate beyond NDA, the NLO correction is approximately 40% of the LO term, which is of the expected size. Corrections of similar size were found in the calculation of the deuteron charge FF [94].

The main point we make in this section is that the conclusions on the deuteron EDM, drawn in the previous section, are not significantly affected by NLO corrections. That is, for all sources but the qCEDM and FQLR the deuteron EDM is dominated by the sum of d_n and d_p, whereas for the qCEDM and FQLR the deuteron EDM is expected to be significantly larger than that sum. A deuteron EDM measurement is therefore complementary to a nucleon EDM measurement.

At this point it is tempting to argue that for the calculation of the deuteron MQM it is also safe to treat pions perturbatively. However, as can be seen from Eq. (5.23), for several sources the LO deuteron MQM depends on pion exchange involving $\bar{g}_0$. There is no such dependence for the EDM. The deuteron wave function obtains a different partial wave admixture after a $\bar{g}_0$ OPE than after a $\bar{g}_1$ OPE, and it is not necessarily the case that the Q/M_{NN} expansion behaves similarly in both channels. In fact, in Ref. [95] it is found for NN scattering that in certain channels the perturbative-pion expansion works well up to a certain energy, while in other channels the series does not converge at that same energy. In order to be sure, we should calculate the NLO corrections to the deuteron MQM and compare their size with the LO results. Unfortunately, this calculation is even more difficult than the NLO deuteron EDM calculation and presently it is not finished. We do have some preliminary results for the TPE diagrams analogous to Fig. 5.8, but with the $N\gamma$ coupling originating in the nucleon magnetic moment. As mentioned, the $\not{P}\not{T}$ πN vertex in these diagrams can be both $\bar{g}_0$ and $\bar{g}_1$. For the $\bar{g}_1$ diagrams our preliminary results indicate that, just as for the deuteron EDM, the NLO contributions are of $\mathcal{O}(40\%)$ suggesting good convergence. However, for the $\bar{g}_0$ diagrams we find that the NLO corrections are as large as the LO contributions, indicating a failure of the expansion. These findings should be verified by a complete calculation which is in progress.

In the next chapter, we work around the problem of the questionable Q/M_{NN} expansion, by studying the $\not{P}\not{T}$ moments of the deuteron (and other light nuclei) in an EFT that treats pions nonperturbatively. The disadvantages of this approach are that we have to resort to numerical calculations and, at present, to a phenomenological model for the PT NN interaction.

Chapter 6

The Electric Dipole Moments of Light Nuclei from Chiral Effective Theory

6.1 Introduction[1]

In the previous chapters it was argued that a measurement of the deuteron EDM in combination with the neutron or proton EDM could partially separate the fundamental $\not{P}\not{T}$ sources. A measurement of the deuteron EDM significantly larger than the nucleon EDM would point toward new physics in the form of a quark chromo-EDM or the FQLR operator. The calculation was based on a perturbative-pion approach [56, 92] to nuclear EFT, which assumes that iterations of the leading-order (LO) one-pion-exchange (OPE) interaction can be treated within perturbation theory. A major advantage of this approach is that analytical results can be obtained. On the other hand, such a framework is applicable only below the scale ($\sim$ 300 MeV) at which OPE becomes significant. This is the case for nuclei where the binding momentum per nucleon is small compared to the pion mass, but even then the size of uncertainties is set by the inverse of the relatively low energy scale. It was found that the NLO corrections in most cases were of the expected size, but certain diagrams contributing to the NLO MQM were larger than expected, possibly spoiling the LO conclusions.

Our goal in this chapter is to provide a framework for the calculation of the EDMs of light nuclei using chiral EFT with nonperturbative OPE [56, 62, 64, 66]. By treating OPE nonperturbatively, the EFT gets extended to higher momenta and thus denser nuclei, and convergence improves. The fact that nuclear binding momenta are small in the typical scale of QCD ($\sim$ 1 GeV) is sufficient for a general power counting that is able to estimate which hadronic interactions are dominant for each fundamental $\not{P}\not{T}$ source. To perform the nonperturbative calculation we need to derive the $\not{P}\not{T}$ nucleon-nucleon (NN) potential and currents. As explicit examples we consider the EDM and MQM of the deuteron (^{2}H), and the EDMs of the triton (^{3}H), and the helion (^{3}He).

The EDMs of the deuteron [80, 81, 97, 98, 99] and helion [82, 100] have been investigated previously within traditional meson-exchange frameworks. In the most comprehensive studies [81, 82] one started from "realistic" nuclear-force models and a general $\not{P}\not{T}$ NN interaction

[1]This chapter is based on J. de Vries, R. Higa, C.-P. Liu, E. Mereghetti, I. Stetcu, R. G. E. Timmermans, and U. van Kolck, Phys. Rev. C **84**, 065501 (2011). The $\not{P}\not{T}$ potential is taken from C. M. Maekawa, E. Mereghetti, J. de Vries, and U. van Kolck, Nucl. Phys. A **872**, 117 (2011).

[81, 101]. The EDMs were expressed in terms of three $\not{P}\not{T}$ nonderivative πN interactions, which are often assumed to be of similar size and dominate the EDMs, and in addition short-range $\not{P}\not{T}$ interactions due to the exchange of heavier mesons were included. The major advantage of a chiral EFT framework is that it has a direct link to QCD and exploits the chiral properties of the fundamental $\not{P}\not{T}$ sources. Moreover, the power-counting scheme allows a perturbative framework such that the theoretical uncertainties can be estimated and the results can be improved systematically.

When the chiral-symmetry properties of the dimension-four and dimension-six operators are considered new insights are in fact obtained as discussed in detail in Chapter 3. At leading order, only two of the three $\not{P}\not{T}$ πN interactions contribute. Moreover, there are in general at the same order more contributions, *viz.* short-range contributions to the neutron and proton EDMs and two $\not{P}\not{T}$ NN contact interactions. As we will demonstrate below, the EDMs of light nuclei can be expressed in terms of these six $\not{P}\not{T}$ parameters, or low-energy constants (LECs). (Other $\not{P}\not{T}$ moments, such as the deuteron MQM, depend in addition on $\not{P}\not{T}$ $\pi N\gamma$ interactions). For three of the four $\not{P}\not{T}$ sources, only a subset of these six LECs is in fact needed. Each LEC can in principle be calculated from the underlying $\not{P}\not{T}$ source using an explicit solution of QCD at low energies, for example through lattice simulations. Compared to nucleons, the EDMs of light nuclei can give crucial complementary information about the fundamental $\not{P}\not{T}$ source. However, the conventional assumption that the three $\not{P}\not{T}$ πN interactions can cover the whole range of nuclear EDMs is oversimplified.

For the PT potential we use here realistic phenomenological potentials [102, 103, 104]. This "hybrid" approach [64, 105] is justified whenever there is little sensitivity to the details of short-range physics, since such realistic potentials all include the long-range pion exchange that appears in chiral EFT at LO. Such an approach has been tested successfully for other observables [56], such as the PT form factors of the deuteron [106] and $\not{P}T$ NN observables [107]. The results in Refs. [81, 82] suggest that the same is true for EDMs, and we partially confirm this below. We use the codes from Refs. [81, 82], but we recast and extend the results in the framework of chiral EFT with nonperturbative OPE. In particular, we apply power counting in order to make more model-independent statements. The cases of the helion and the triton are typical of a generic nucleus. However, in the deuteron, because of its isoscalar character, the formally LO contribution from the $\bar{\theta}$ term vanishes [80, 81], a property expected [108] for nuclei with equal number of protons and neutrons, $N = Z$ and verified in the previous chapter. We exploit the systematic character of EFT to extend the deuteron calculation for the $\bar{\theta}$ term to the first nonvanishing order. We compare the results with the perturbative-pion calculation.

This chapter is organized as follows. In Sect. 6.2, we briefly repeat the $\not{P}\not{T}$ interactions relevant for the calculation of light nuclear EDMs. In Sect. 6.3 we discuss in general the power counting of the various contributions, and present the leading $\not{P}\not{T}$ potentials and currents, while in Sect. 6.4 we specifically address nuclei with $N = Z$. Next, we evaluate the EDM of the deuteron in Sect. 6.5 and the EDMs of the helion and the triton in Sect. 6.6. In Sect. 6.7 we discuss our results and their implications. Finally, we revisit the deuteron magnetic quadrupole moment in Sect. 6.8.

6.2 Review of the P- and T-odd Lagrangian

We now present a subset of the complete $\not{P}\not{T}$ chiral Lagrangian originating from the fundamental sources above. We only give the operators that play a role in the LO calculation of light-nuclei EDMs, the more general Lagrangian being found in Chapter 3. In general, a LO calculation of

the EDM of a light nucleus requires *six* $\not{P}\not{T}$ interactions:

$$\begin{aligned}\mathcal{L}_{\not{P}\not{T}} &= -2\,\bar{N}\left(\bar{d}_0+\bar{d}_1\tau_3\right)S^\mu N\,v^\nu F_{\mu\nu}-\frac{1}{F_\pi}\bar{N}\left(\bar{g}_0\,\boldsymbol{\tau}\cdot\boldsymbol{\pi}+\bar{g}_1\pi_3\right)N\\ &\quad+\bar{C}_1\bar{N}N\,\partial_\mu(\bar{N}S^\mu N)+\bar{C}_2\bar{N}\boldsymbol{\tau}N\cdot\partial_\mu(\bar{N}S^\mu\boldsymbol{\tau}N)+\dots\,,\end{aligned}\tag{6.1}$$

which represent short-range isoscalar ($\bar{d}_0$) and isovector ($\bar{d}_1$) contributions to the nucleon EDM, isoscalar ($\bar{g}_0$) and isovector ($\bar{g}_1$) nonderivative πN couplings, and two short-range $\not{P}\not{T}$ NN interactions ($\bar{C}_1$, $\bar{C}_2$). Here we relegate to the "..." terms related to the above by chiral symmetry. The explicit forms of these terms depend on the $\not{P}\not{T}$ source but, because they involve more pion fields, they do not appear in the LO EDMs we are interested in. Note that Eq. (6.1) is the form of $\mathcal{L}_{\not{P}\not{T}}$ after a field redefinition is performed to eliminate pion tadpoles and guarantee vacuum alignment; the parameters thus absorb contributions generated by this field redefinition. For details see Sect. 3.4. In this chapter the isoscalar and isovector nucleon EDM should be interpreted as the full result calculated in Chapter 4. That is, there is an implicit dependence of $\bar{d}_{0,1}$ on $\bar{g}_{0,1}$, but the loop contributions cannot be separated from the short-range pieces in a model-independent way.

Which of these six interactions is relevant depends on the system we are studying and on the fundamental $\not{P}\not{T}$ source. As will be seen, the spin and isospin of the deuteron cause the deuteron EDM to be sensitive to only three of the above operators. In more general cases, the EDMs of light nuclei are sensitive to all six interactions. The EDMs of heavy nuclei could involve more operators than the set above. Generically one might expect a dominance by effects from (i) a single nucleon, since multi-nucleon contributions tend to be suppressed at low energies by phase space; and (ii) pions, thanks to their small mass and related long range. However, significant deviation from this expectation comes from the relative sizes of the various LECs, which depends on the $\not{P}\not{T}$ source. NDA leads to the following estimates for the dimension-four and -six $\not{P}\not{T}$ sources:

- For the $\bar{\theta}$ term, four operators play a role at LO, the other two appearing only at subleading orders. In order to generate $\bar{g}_1$, which is relevant for the deuteron EDM, the $\bar{\theta}$ term requires an insertion of the quark-mass difference, which causes a relative suppression of $\bar{g}_1$ relative to $\bar{g}_0$ by a factor $\varepsilon m_\pi^2/M_{\rm QCD}^2$ [48]. (At the same order, there exists also a two-derivative πN coupling, but for our purpose here it can be absorbed by a small change in $\bar{g}_0$ [78].) The LECs scale as

$$\bar{g}_0=\mathcal{O}\left(\bar{\theta}\frac{m_\pi^2}{M_{\rm QCD}}\right),\qquad \bar{g}_1=\mathcal{O}\left(\varepsilon\bar{\theta}\frac{m_\pi^4}{M_{\rm QCD}^3}\right),\qquad \bar{d}_{0,1}=\mathcal{O}\left(e\bar{\theta}\frac{m_\pi^2}{M_{\rm QCD}^3}\right).\tag{6.2}$$

- For the qCEDM and FQLR, the same four operators are needed. In this case, there is no *a priori* relative suppression of $\bar{g}_1$ and the LECs scale as

$$\begin{aligned}\bar{g}_0 &= \mathcal{O}\left((\tilde{\delta}_0+\varepsilon\tilde{\delta}_3)\frac{m_\pi^2 M_{\rm QCD}}{M_{\not{T}}^2},\,\xi\varepsilon\frac{M_{\rm QCD}^3}{M_{\not{T}}^2}\right),\ \bar{g}_1=\mathcal{O}\left(\tilde{\delta}_3\frac{m_\pi^2 M_{\rm QCD}}{M_{\not{T}}^2},\,\xi\frac{M_{\rm QCD}^3}{M_{\not{T}}^2}\right),\\ \bar{d}_{0,1} &= \mathcal{O}\left(e(\tilde{\delta}_0+\tilde{\delta}_3)\frac{m_\pi^2}{M_{\rm QCD}M_{\not{T}}^2},\,e\xi\frac{M_{\rm QCD}}{M_{\not{T}}^2}\right).\end{aligned}\tag{6.3}$$

  (Here the "+" signs are not to be taken literally; they are only meant to signify two independent contributions to a LEC.)

- For the qEDM, only the short-range EDM contributions are important, and they scale as

$$\bar{d}_{0,1} = \mathcal{O}\left(e\delta_{0,3}\frac{m_\pi^2}{M_{\rm QCD}M_{\not P\not T}^2}\right). \tag{6.4}$$

- For the χI (gCEDM and FQ) $\not P\not T$ sources, the nonderivative πN interactions, which break chiral symmetry, are suppressed by a factor $m_\pi^2/M_{\rm QCD}^2$ compared to short-range nucleon EDM contributions and $\not P\not T$ NN interactions, which conserve chiral symmetry. (Again, a two-derivative πN interaction exists at the same order but can be absorbed in $\bar{g}_0$ and $\bar{C}_2$ [78].) All six operators thus become relevant, and the LECs scale as

$$\begin{aligned}
\bar{g}_0 &= \mathcal{O}\left(w\frac{m_\pi^2 M_{\rm QCD}}{M_{\not P\not T}^2}\right), \qquad \bar{g}_1 = \mathcal{O}\left(\varepsilon w\frac{m_\pi^2 M_{\rm QCD}}{M_{\not P\not T}^2}\right), \\
\bar{d}_{0,1} &= \mathcal{O}\left(ew\frac{M_{\rm QCD}}{M_{\not P\not T}^2}\right), \qquad \bar{C}_{1,2} = \mathcal{O}\left(w\frac{M_{\rm QCD}}{F_\pi^2 M_{\not P\not T}^2}\right).
\end{aligned} \tag{6.5}$$

6.3 Ingredients: the generic case

The EDM of a nucleus with $A \geq 2$ nucleons can be separated into two contributions. The first contribution comes from an insertion of the $\not P\not T$ electromagnetic current $J^0_{\not P\not T}$. The second stems from the PT charge density J^0_{PT} upon perturbing the wave function of the nucleus with the $\not P\not T$ potential $V_{\not P\not T}$, such that the wave function obtains a $\not P\not T$ component. To first order in the $\not P\not T$ sources, the EDM is thus a sum of two reduced matrix elements

$$d_A = \frac{1}{\sqrt{6}}\left(\left\langle \Psi_A \left|\left| \vec{D}_{\not P\not T} \right|\right| \Psi_A \right\rangle + 2\left\langle \Psi_A \left|\left| \vec{D}_{PT} \right|\right| \widetilde{\Psi}_A \right\rangle\right). \tag{6.6}$$

The nuclear ground state $|\Psi_A\rangle$ and its parity admixture $|\widetilde{\Psi}_A\rangle$ are the solutions of homogeneous and inhomogeneous Schrödinger equations,

$$\begin{aligned}
(E - H_{PT})|\Psi_A\rangle &= 0\,, \\
(E - H_{PT})|\widetilde{\Psi}_A\rangle &= V_{\not P\not T}|\Psi_A\rangle\,,
\end{aligned} \tag{6.7}$$

respectively, where H_{PT} is the PT Hamiltonian. The $\not P\not T$ potential $V_{\not P\not T}$ is shown in coordinate space in App. D. The EDM operators $\vec{D}_{PT}$ and $\vec{D}_{\not P\not T}$ are obtained from the corresponding charge densities J^0_{PT} and $J^0_{\not P\not T}$, respectively, as discussed in App. D. The factor of 2 in front of the second matrix element corresponds to the number of time-ordered diagrams, and the phases of wave functions are chosen so that these matrix elements are purely real.

In this section we identify the ingredients needed for the LO calculation of d_A, assuming no particular cancellations or suppressions due to spin/isospin factors.

6.3.1 Power counting

Both the potential $V_{\not P\not T}$ and the current $J^0_{\not P\not T}$ can be obtained from the Lagrangians in Eq. (6.1) and (3.24). The potential $V_{\not P\not T}$ for the various $\not P\not T$ sources is derived below. To the order we are concerned with here, the potential can be taken as two-body. The $\not P\not T$ and PT currents can also be divided into one-body and more-body currents. As we will see, the latter are dominated by two-body effects as well. There are thus four classes of contributions to a nuclear EDM,

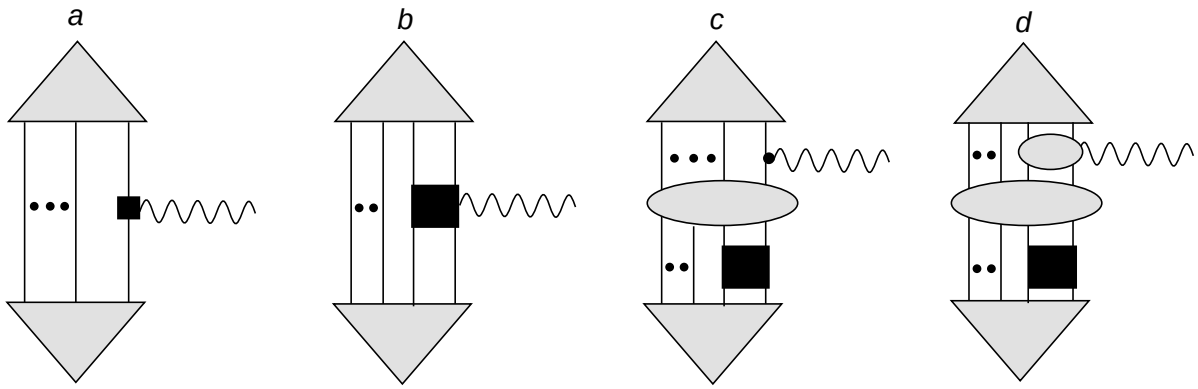

Figure 6.1: The four general classes of diagrams contributing to a nuclear EDM described in the text. Solid and wavy lines represent nucleons and photons. The three (two) dots stand for $A-3$ ($A-4$) nucleon propagators. The large triangle denotes the nuclear wave function; the oval, iterations of the PT potential; the dot with an attached photon, the PT one-body current; the oval with an attached photon, the PT two-body current; the black square, the $\not{P}\not{T}$ potential; and the black square with an attached photon, the $\not{P}\not{T}$ current.

schematically drawn in Fig. 6.1. In order to determine which diagram(s) give(s) the most important contribution(s) we need to estimate their sizes by applying power counting.

We need to count powers of the generic momentum Q in the process, in order to get an expansion in $Q/M_{\rm QCD}$. Here Q is given by the nuclear binding momentum, which for a typical nucleus can be taken as $Q \sim m_\pi \sim F_\pi$, as standard in χPT. However, as pointed out by Weinberg [64] and explained in Sect. 5.2, the power counting of χPT needs to be adapted to the existence for $A \geq 2$ of intermediate states consisting purely of propagating nucleons. A generic diagram can be split into "reducible" parts, that contain such states, and "irreducible" subdiagrams, which do not. Within an irreducible subloop, the contour integration over the 0th component of the loop momentum can always be performed in such a way as to avoid the nucleon pole. In these diagrams the nucleon energy is of order Q, as assumed in χPT power counting. On the other hand, in diagrams where the intermediate state consists purely of propagating nucleons, *i.e.* reducible diagrams, one cannot avoid the poles of nucleon propagators, thus picking up energies $\sim Q^2/m_N$ [64] rather than $\sim Q$. Moreover, such loops also obtain an additional enhancement of 4π. The contribution of such a reducible diagram can be counted by applying the modified rules [56]:

- a factor $Q^5/(4\pi m_N)$ for each loop integral;
- a factor m_N/Q^2 for each nucleon propagator;
- a factor $1/Q^2$ for each pion propagator;
- the NDA estimate for the LECs corresponding to the interactions in the diagram.

As an example, consider an insertion of a LO, PT pion exchange in a diagram. It gives rise to one additional loop $\sim Q^5/(4\pi m_N)$, two nucleon propagators $\sim m_N^2/Q^4$, a pion propagator $\sim 1/Q^2$, and two insertions of the strong πN vertex $\sim (Q/F_\pi)^2$. Combining these factors, the extra one-pion exchange amounts to Q/M_{NN}, where $M_{NN} = 4\pi F_\pi^2/m_N \sim F_\pi$. A similar power counting holds for short-range PT interactions, although the situation for them is more complicated [66]. For very light nuclei, $Q < M_{NN}$ and pion exchange can be treated perturbatively [56, 92] as

we did for the deuteron in the previous chapter. For less dilute nuclei, however, one expects $Q \sim M_{NN}$ and pion exchange needs to be summed to all orders [56, 66].

We can now estimate the size of each of the classes of diagrams in Fig. 6.1. For each class we take the PT and $\not{P}\not{T}$ LO interactions in Eqs. (3.24) and (6.1), respectively. The iteration of the LO PT potential costs no factors, and is necessary among nucleons in reducible intermediate states, as indicated in diagrams (c) and (d) of Fig. 6.1. Such iteration among nucleons before and after all $\not{P}\not{T}$ and electromagnetic insertions builds up the PT wave function, represented in Fig. 6.1 as well, which introduces an overall normalization of the diagrams. This normalization can be read off from the diagram analogous to (a), where the one-body current is given instead by the electromagnetic charge. In the following we account for this normalization by omitting the $A-1$ loops and $A+1$ nucleon propagators that are common to all diagrams. Thus, diagram (a) is simply

$$D_a = \mathcal{O}\left(d_{p,n} Q\right). \tag{6.8}$$

In contrast, diagram (b) has one additional irreducible loop $\sim Q^5/(4\pi m_N)$, one additional nucleon propagator $\sim m_N/Q^2$, and the leading $\not{P}\not{T}$ two-body current. For both qEDM and χI sources the latter brings a suppression of a factor $Q^2/M_{\rm QCD}^2$, whereas for the other sources the contribution is comparable to the one-body term. One can continue in this fashion to find that for diagram (c),

$$D_c = \mathcal{O}\left(e\,\frac{\bar{g}_{0,1}}{F_\pi^2} Q\right) + \mathcal{O}\left(e\,\bar{C}_{1,2} F_\pi^2 Q\right), \tag{6.9}$$

while for diagram (d) there is always a suppression by a factor $Q^2/M_{\rm QCD}^2$. Analogously, more-body potentials and currents bring further suppression.

Plugging in the scaling of the LECs for the different sources, Eqs. (6.2), (6.3), (6.4), and (6.5), we can draw the following general expectations for the EDMs of light nuclei:

- For the $\bar{\theta}$ term, the nuclear EDM is dominated by diagram (c): the nuclear wave function acquires a $\not{P}\not{T}$ admixture after a one-pion exchange involving the isoscalar $\bar{g}_0$ vertex; the admixed wave function then couples to the proton charge.

- For the qCEDM and FQLR, the nuclear EDM is dominated by the same effect as the $\bar{\theta}$ term. However, for the qCEDM the $\not{P}\not{T}$ πN vertex can be either $\bar{g}_0$ or $\bar{g}_1$.

- For the qEDM, the nuclear EDM is dominated by the sum of the EDMs of the constituent nucleons, diagram (a).

- For χI sources, the nuclear EDM is more complicated than for the other sources. Due to the chiral suppression of the πN interactions, diagrams (a) and (c) are equally important, and in the latter the short-range $\not{P}\not{T}$ interactions $\bar{C}_{1,2}$ need to be included besides the one-pion exchange from both $\bar{g}_0$ and $\bar{g}_1$ couplings.

6.3.2 The P- and T-odd nucleon-nucleon potential

The calculation of nuclear EDMs requires the use of the $\not{P}\not{T}$ NN potential in order to calculate the parity admixture in the wave function in Eq. (6.7). This potential can be derived from the chiral Lagrangian in Chapter 3. The power counting used throughout this thesis allows us to identify for each source the most important contributions to the $\not{P}\not{T}$ potential, which we derive here up to LO.

In case of the $\bar{\theta}$ term, qCEDM, and FQLR the scalings of the LO $\not{P}\not{T}$ πN and NN interactions, indicate that the latter appears two orders higher than the former. For these sources, the $\not{P}\not{T}$

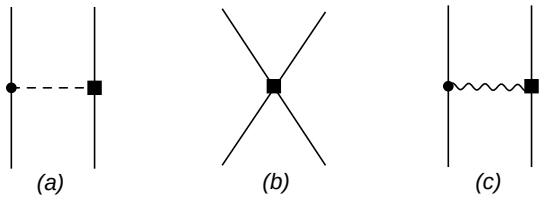

Figure 6.2: Diagrams contributing to the PT two-nucleon potential. Solid, dashed, and wavy lines represent nucleons, pions, and photons. A square marks a $\not{P}\not{T}$ interaction from Eq. (6.1), the other vertices representing PT interactions from Eq. (3.24). Only one topology per diagram is shown.

potential consists of diagram 6.2(a) with PT interactions from Eq. (3.24) and $\not{P}\not{T}$ interactions from Eq. (6.1). In momentum space, the expression for the potential is simply

$$\begin{aligned} V_{\not{P}\not{T}}(\vec{k}\,) &= i\frac{g_A\bar{g}_0}{F_\pi^2}\,\boldsymbol{\tau}^{(i)}\cdot\boldsymbol{\tau}^{(j)}\left(\vec{\sigma}^{\,(i)}-\vec{\sigma}^{\,(j)}\right)\cdot\frac{\vec{k}}{\vec{k}^{\,2}+m_\pi^2} \\ &\quad +i\frac{g_A\bar{g}_1}{2F_\pi^2}\Big[\left(\tau_3^{(i)}+\tau_3^{(j)}\right)\left(\vec{\sigma}^{\,(i)}-\vec{\sigma}^{\,(j)}\right) \\ &\quad +\left(\tau_3^{(i)}-\tau_3^{(j)}\right)\left(\vec{\sigma}^{(i)}+\vec{\sigma}^{(j)}\right)\Big]\cdot\frac{\vec{k}}{\vec{k}^{\,2}+m_\pi^2}, \end{aligned} \tag{6.10}$$

where $\vec{\sigma}^{(n)}/2$ ($\boldsymbol{\tau}^{(n)}/2$) is the spin (isospin) vector of nucleon n, and $\vec{k}=\vec{p}_i-\vec{p}_i^{\,\prime}$ is the momentum transferred from nucleon i. In this expression, at LO $\bar{g}_0$ originates from $\bar{\theta}$-term, qCEDM, and FQLR, and $\bar{g}_1$ from qCEDM and FQLR.

In case of χI sources, the scalings in Eq. (6.5) and the power-counting rules outlined above tell us that we need to include both OPE diagrams and short-range NN interactions in the LO potential. Apart from Eq. (6.10), the $\not{P}\not{T}$ potential consists of diagram 6.2(b)

$$V_{\not{P}\not{T}}(\vec{k}\,) = -\frac{i}{2}\left[\bar{C}_1+\bar{C}_2\,\boldsymbol{\tau}^{(i)}\cdot\boldsymbol{\tau}^{(j)}\right]\left(\vec{\sigma}^{\,(i)}-\vec{\sigma}^{\,(j)}\right)\cdot\vec{k}. \tag{6.11}$$

These contact interactions incorporate $\not{P}\not{T}$ effects of short-range, such as single exchanges of the mesons ω and η ($\bar{C}_1$) and ρ ($\bar{C}_2$).

Finally in case of a qEDM the OPE potential gets, apart from Eq. (6.10), additional contributions from the third nonderivative πN coupling $\bar{g}_2$ in Eq. (3.77). Since these πN interactions are suppressed by a factor $\alpha_{\rm em}/4\pi$, by power counting we are forced to add photon-exchange diagrams (diagram 6.2(c)), where one of the vertices originates in the nucleon EDM. Apart from Eq. (6.10), the $\not{P}\not{T}$ potential for the qEDM is given by

$$\begin{aligned} V_{\not{P}\not{T}}(\vec{k}\,) &= i\frac{g_A\bar{g}_2}{F_\pi^2}\left(\tau_3^{(1)}\,\tau_3^{(2)}\right)\left(\vec{\sigma}^{\,(1)}-\vec{\sigma}^{\,(2)}\right)\cdot\frac{\vec{k}}{\vec{k}^{\,2}+m_\pi^2} \\ &\quad -i\frac{e}{2}\left(\bar{d}_0+\bar{d}_1\tau_3^{(1)}\tau_3^{(2)}\right)\left(\vec{\sigma}^{\,(1)}-\vec{\sigma}^{\,(2)}\right)\cdot\frac{\vec{k}}{\vec{k}^{\,2}} \\ &\quad -i\frac{e}{4}\Big[(\bar{d}_0+\bar{d}_1)\left(\tau_3^{(1)}+\tau_3^{(2)}\right)\left(\vec{\sigma}^{\,(1)}-\vec{\sigma}^{\,(2)}\right) \\ &\quad +(\bar{d}_1-\bar{d}_0)\left(\tau_3^{(1)}-\tau_3^{(2)}\right)\left(\vec{\sigma}^{(1)}+\vec{\sigma}^{(2)}\right)\Big]\cdot\frac{\vec{k}}{\vec{k}^{\,2}}. \end{aligned} \tag{6.12}$$

Although the potential in case of the qEDM is very different from the potential of the other sources due to the long-range potential induced by photon exchange and the appearance of $\bar{g}_2$ at LO, this difference has no effect on the EDMs calculated in this chapter. The reason being, as demonstrated by power counting in the previous section, that the nuclear EDMs are dominated by the constituent nucleon EDMs, the potential giving rise to subleading contributions.

In NN scattering, operators that break P and T induce mixing between waves of different parity. At low energy, the most relevant effect is the mixing between S and P waves, and indeed the single momentum in Eqs. (6.10, 6.11, 6.12) can only connect an S to a P wave. In general, one would expect five possible amplitudes connecting S to P waves [81, 101]: three —one for each possible value of $I_3 = 1, 0, -1$— to describe the mixing of the isotriplet ${}^1S_0$ and ${}^3P_0$ waves, one for the mixing of the isosinglet ${}^3S_1$ and ${}^1P_1$ states, and one for the mixing of nucleons in the ${}^3S_1$ configuration with the isotriplet ${}^3P_1$ wave. Since the $\bar{\theta}$ term and isoscalar qCEDM conserve isospin symmetry and only generate $\bar{g}_0$ at LO, they only contribute to ${}^3S_1$–${}^1P_1$ mixing and to ${}^1S_0$–${}^3P_0$ mixing, in equal way for the three I_3 configurations. The ${}^3S_1$–${}^3P_1$ mixing vanishes at leading order, a fact that has important consequences for the estimate of the deuteron EDM. The same holds for the short-range contributions in Eq. (6.11) from χI sources.

The isovector qCEDM, FQLR, and χI sources also contribute through OPE to isospin-breaking $\not{P}\not{T}$ observables at leading order. The first term proportional to $\bar{g}_1$ in Eq. (6.10) depends on third component of the total isospin of the two-nucleon pair, and thus it does contribute to ${}^1S_0$–${}^3P_0$ mixing, but only for $I_3 = \pm 1$. The second term instead is proportional to the total spin of the two nucleons, and it is relevant to ${}^3S_1$–${}^3P_1$ mixing, and, consequently, to the deuteron EDM. Only the qEDM produces full isospin breaking at LO through OPE and photon exchange.

6.3.3 Currents

As we argued above, only one-body currents are necessary at LO. For the $\bar{\theta}$ term, qCEDM, FQLR, and χI sources we need the PT current coming from the proton charge in Eq. (3.24),

$$J^0_{PT} \;=\; \frac{e}{2}\left(1+\tau_3^{(i)}\right)\,, \tag{6.13}$$

where $\boldsymbol{\tau}^{(i)}/2$ is the isospin of the nucleon that couples to the one-body current.

For the qEDM and χI sources we need as well the $\not{P}\not{T}$ current originating from the nucleon EDMs,

$$J^0_{\not{P}\not{T}} \;=\; -i\left(\bar{d}_0+\bar{d}_1\tau_3^{(i)}\right)\vec{\sigma}^{(i)}\cdot\vec{q}\,, \tag{6.14}$$

where $\vec{\sigma}^{(i)}/2$ is the spin of the nucleon that interacts with the photon and $\vec{q}$ is the outgoing photon momentum.

6.4 Ingredients: nuclei with $N = Z$

Although the power counting discussed above holds for general light nuclei, it is possible that a diagram, which is expected to be LO, does not contribute to the EDMs of certain systems. For nuclei of equal neutron and proton number, $N = Z$, *i.e.* the third component of isospin $I_3 = 0$, an insertion of the isoscalar $\not{P}\not{T}$ potential in combination with the LO one-body PT current, *i.e.* Eq. (6.13), does not contribute to the EDM [108]. To see this, consider the EDM operator

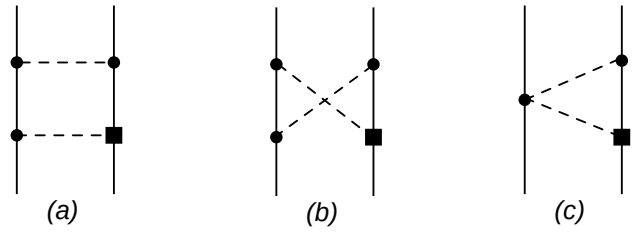

Figure 6.3: Box, crossed and triangle TPE diagrams contributing to the subleading $\not{P}\not{T}$ *NN* potential. The notation is as in Fig. 6.2. Only one topology per diagram is shown.

resulting from the LO one-body PT current, which takes the simple expression

$$\vec{D}^{(1)}_{PT} = \frac{e}{2}\sum_{i=1}^{A}\left(1+\tau_3^{(i)}\right)\vec{\xi}_i = \frac{e}{2}\sum_{i=1}^{A}\tau_3^{(i)}\,\vec{\xi}_i \tag{6.15}$$

in intrinsic coordinates $\vec{\xi}_i$ with $\sum_{i=1}^{A}\vec{\xi}_i = 0$. Since this operator is isovector, *i.e.* $\Delta I = 1$, and conserves I_3, *i.e.* $\Delta I_3 = 0$, it can only yield a nonvanishing moment when the nuclear state of a $(I\,,\, I_3 = 0)$ nucleus acquires some parity admixture with isospin $(I^{'} = I \pm 1\,,\, I^{'}_3 = 0)$. Therefore, one needs isovector components in $V_{\not{P}\not{T}}$ to induce such admixture. The above argument holds in the nonrelativistic limit.

This observation is of no concern for sources where there are other contributions at the same order as those contributions that vanish. The nuclear EDM is then simply dominated by the nonvanishing LO terms. For the $\bar{\theta}$ term however, the LO contribution consists only of an insertion of the isoscalar $\not{P}\not{T}$ potential, such that, for $N = Z$ nuclei, we need to go further down in power counting to find the dominant EDM contributions.

6.4.1 Power counting

Because the formally leading diagram (c) of Fig. 6.1 vanishes for $N = Z$ in the $\bar{\theta}$ term case when both the PT one-body current and the $\not{P}\not{T}$ two-body potential are used, let us first consider corrections in this diagram. It turns out that NLO corrections to the $\not{P}\not{T}$ potential and PT one-body current (both from an insertion from the subleading PT Lagrangian in Eq. (3.25)) still vanish, and the first corrections we need to account for are at NNLO. By looking at the scaling of the LECs for the $\bar{\theta}$ term in Eq. (6.2) and the power counting for the classes of diagrams in Fig. 6.1, we then conclude that the first nonvanishing contributions can come from all classes of diagrams: the LO nucleon EDMs in diagram (a), the LO $\not{P}\not{T}$ two-body currents in diagram (b), the NNLO $\not{P}\not{T}$ two-body potential *or* the NNLO PT one-body current in diagram (c), and the LO PT two-body currents with the LO $\not{P}\not{T}$ two-body potential in diagram (d).

For the other sources only parts of the LO contributions given in the previous section remain. For qCEDM, FQLR, and χI sources we need the $\not{P}\not{T}$ potential from $\bar{g}_1$ OPE. For qEDM and χI sources we also need the isoscalar short-range contribution to the nucleon EDM. The short-range interactions in Eq. (6.11) do not contribute to the deuteron EDM at LO.

6.4.2 The P- and T-odd nucleon-nucleon potential

For qCEDM, FQLR, and χI sources we can use the same potential as in the generic case, but the $\bar{g}_0$ and $\bar{C}_{1,2}$ terms will not contribute. We do not require a $\not{P}\not{T}$ potential for qEDM. For the $\bar{\theta}$ term we need the NNLO $\not{P}\not{T}$ potential, that is, including corrections of $\mathcal{O}(Q^2/M^2_{\rm QCD})$

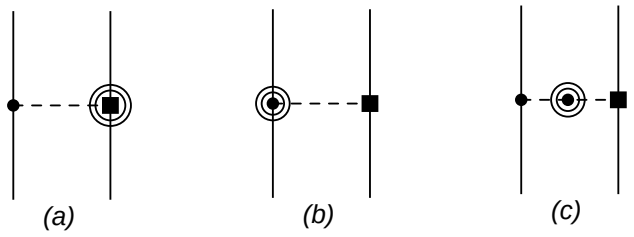

Figure 6.4: OPE corrections to the $\not{P}\not{T}$ NN potential from the $\bar{\theta}$ term. The double circled vertices denote NNLO vertices. The other notation is as in Fig. 6.2. Only one topology per diagram is shown.

with respect to the leading $\not{P}\not{T}$ potential. According to the power-counting rules in Sect. 3.2, corrections at this order come from one-loop diagrams involving LO PT and $\not{P}\not{T}$ interactions only, and from tree diagrams with insertions of higher-order terms. The tree contributions come from the four-nucleon $\not{P}\not{T}$ operators in Eq. (3.85), and from OPE diagrams in which either the PT or the $\not{P}\not{T}$ vertices originate in the power-suppressed Lagrangians. The four-nucleon interactions, however, give rise to a potential of the form given in Eq. (6.11) and they vanish on the deuteron.

The most important loop diagrams are from TPE, depicted in Fig. 6.3. The $\not{P}\not{T}$ πN coupling $\bar{g}_0$ and one of the strong-interaction vertices bring in a factor of $\bar{g}_0 g_A/F_\pi^2$. The other two vertices of the box and crossed diagrams of Fig. 6.3 are strong-interaction πN vertices from Eq. (3.24), and combined with the $(4\pi)^2$ from the loop integration, they yield the suppression factor $g_A^2/(4\pi F_\pi)^2 \sim 1/M_{\rm QCD}^2$. For the triangle diagrams, the seagull vertex is the Weinberg-Tomozawa term also from Eq. (3.24), which brings in a factor of $1/F_\pi^2$ that, combined with the $(4\pi)^2$ from the loop, also leads to a suppression of $1/(4\pi F_\pi)^2 \sim 1/M_{\rm QCD}^2$.

The TPE diagrams in Fig. 6.3 are ultraviolet divergent. Proper renormalization requires that sufficiently many counterterms appear at the same order to compensate for the L and μ dependence of the loops. Indeed, here this dependence can be absorbed by the renormalization of the contact interaction $\bar{C}_2$ from Eq. (3.85).

Once the divergent, short-range part of TPE has been lumped with the contact terms, we are left with the nonanalytic contributions of medium range,

$$V_{\not{P}\not{T},\rm TPE}(\vec{k}) = -i\frac{2\bar{g}_0 g_A}{F_\pi^2}\frac{1}{(2\pi F_\pi)^2}\left[2g_A^2\, B\left(\frac{\vec{k}^{\,2}}{4m_\pi^2}\right) - T\left(\frac{\vec{k}^{\,2}}{4m_\pi^2}\right)\right]\boldsymbol{\tau}^{(i)}\cdot\boldsymbol{\tau}^{(j)}\left(\vec{\sigma}^{(i)} - \vec{\sigma}^{(j)}\right)\cdot\vec{k}, \quad (6.16)$$

in terms of the functions

$$T(x) = \sqrt{\frac{1+x}{x}}\ln\left(\sqrt{x}+\sqrt{1+x}\right) = \frac{1+x}{1+\frac{3}{2}x}B(x). \quad (6.17)$$

As the leading OPE potential, the TPE potential is a function only of the momentum transfer $\vec{k}$. The scale of momentum variation is, as one would expect, $2m_\pi$. More importantly, TPE and leading OPE share the same spin-isospin structure, which means that, just as the OPE potential, the TPE potential in combination with the LO PT one-body current vanishes on the deuteron and we can neglect Eq. (6.16).

A much richer structure arises from the remaining corrections to the $\not{P}\not{T}$ potential, which come from the OPE diagrams depicted in Fig. 6.4. Doubly-circled vertices in the first two diagrams denote $\mathcal{O}(Q^2/M_{QCD}^2)$ corrections to the PT and $\not{P}\not{T}$ πN couplings, given by the operators in

Eqs. (3.25), (3.26), (3.29), (3.58), and (3.62). The last diagram is proportional to corrections to the pion mass in Eqs. (3.26) and (3.29), and to the nucleon mass difference in Eq. (3.29).

The full potential from these terms contain many isoscalar terms, which will not contribute and we do not list them. These terms can be found in Ref. [78]. Here we need only the following terms:

$$\begin{aligned} V_{\not P\not T}(\vec{k},\vec{K},\vec{P}) &= \frac{i}{2F_\pi^2}\left[\left(g_A\bar{g}_1-\frac{\bar{g}_0\beta_1}{2}\right)\left(\tau_3^{(i)}+\tau_3^{(j)}\right)\left(\vec{\sigma}^{(i)}-\vec{\sigma}^{(j)}\right)\right. \\ &\quad \left.+\left(g_A\bar{g}_1+\frac{\bar{g}_0\beta_1}{2}\right)\left(\tau_3^{(i)}-\tau_3^{(j)}\right)\left(\vec{\sigma}^{(i)}+\vec{\sigma}^{(j)}\right)\right]\cdot\frac{\vec{k}}{\vec{k}^{\,2}+m_\pi^2} \\ &\quad +i\,\frac{\bar{g}_0 g_A}{3F_\pi^2}\left[\breve{\delta}m_\pi^2-\delta m_\pi^2-\frac{(\breve{\delta}m_\pi^2)^2}{\vec{k}^2+m_\pi^2}-\delta m_N^2\right]\left(3\,\tau_3^{(i)}\tau_3^{(j)}-\boldsymbol{\tau}^{(i)}\cdot\boldsymbol{\tau}^{(j)}\right) \\ &\quad \times\left(\vec{\sigma}^{(i)}-\vec{\sigma}^{(j)}\right)\cdot\frac{\vec{k}}{(\vec{k}^{\,2}+m_\pi^2)^2}+\frac{\bar{g}_0 g_A}{F_\pi^2}\frac{\delta m_N}{m_N}\left(\boldsymbol{\tau}^{\,(i)}\times\boldsymbol{\tau}^{\,(j)}\right)_3 \\ &\quad \times\left[\left(\vec{\sigma}^{(i)}+\vec{\sigma}^{(j)}\right)\cdot\vec{K}+\left(\vec{\sigma}^{(i)}-\vec{\sigma}^{(j)}\right)\cdot\left(\frac{\vec{P}}{2}+\frac{(\vec{P}\cdot\vec{k})\,\vec{k}}{\vec{k}^{\,2}+m_\pi^2}\right)\right]\frac{1}{\vec{k}^{\,2}+m_\pi^2}\ , \end{aligned} \tag{6.18}$$

where $\vec{P}=\vec{p}_i+\vec{p}_j$ is the center-of-mass (CM) momentum of the nucleon pair and $\vec{K}=(\vec{p}_i+\vec{p}_i^{\,\prime}-\vec{p}_j-\vec{p}_j^{\,\prime})/4$. The first two terms originate in one-pion exchange with $\bar{g}_1$ instead of $\bar{g}_0$ or with β_1 instead of g_A. We have absorbed some small corrections into g_A and $\bar{g}_0$. The next term arises from isospin breaking in the pion and nucleon masses, and it is very small [78]. The last term is due to the isospin-breaking πN vertex. The potential also includes $1/m_N^2$ corrections [78], which we do not include here for the reasons given below.

6.4.3 Currents

For the same reasons that require the NNLO $\not P\not T$ potential we also need the NNLO PT one-body electric current, to be used with the $\bar{\theta}$-term LO potential. Again we do not bother with terms that give a vanishing contribution for $N = Z$ nuclei. The only remaining correction from Eq. (3.31) is given by

$$J^0_{PT} = -\frac{ie}{16m_N^2}\varepsilon^{lmn}\sigma^{(i)l}q^m\left(p_i+p_i'\right)^n\left[1+2\kappa_0+(1+2\kappa_1)\,\tau_3^{(i)}\right]\ , \tag{6.19}$$

which agrees with Ref. [75]. Here $\vec{p}_i$ ($\vec{p}_i^{\,\prime}$) is the momentum of the nucleon that couples to the photon before (after) interaction.

We also need two-body currents, both PT and $\not P\not T$. We use incoming momenta $\vec{p}_i=\vec{P}/2+\vec{p}$ and $\vec{p}_j=\vec{P}/2-\vec{p}$ and outgoing momenta $\vec{p}_i^{\,\prime}=\vec{P}^{\,\prime}/2+\vec{p}^{\,\prime}$ and $\vec{p}_j^{\,\prime}=\vec{P}^{\,\prime}/2-\vec{p}^{\,\prime}$. The photon momentum $\vec{q}=\vec{P}-\vec{P}^{\,\prime}$ is outgoing. For convenience we introduce $\vec{k}=\vec{p}-\vec{p}^{\,\prime}$ as before, $\vec{K}=(\vec{p}+\vec{p}^{\,\prime})/2$, and $\vec{P}_t=(\vec{P}+\vec{P}^{\,\prime})/2$. In the evaluation of the currents at the order we are interested we can use the nucleon on-shell relation $p_n^0=\vec{p}_n^{\,2}/2m_N$, or alternatively $k^0=(\vec{P}_t\cdot\vec{k}-\vec{q}\cdot\vec{K})/2m_N$.

The relevant diagrams for the LO two-body PT electric current, used again in combination with the LO $\not P\not T$ two-body potential, are shown in Fig. 6.5. All interactions come from the PT

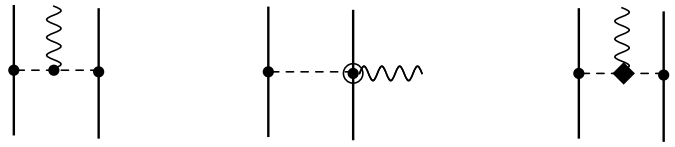

Figure 6.5: Diagrams contributing to the PT two-nucleon electric current. A diamond marks an isospin-breaking PT interaction and the other vertices isospin-conserving PT interactions: leading (filled circles) and subleading (circled circles). The other notation is as in Fig. 6.2. Only one topology per diagram is shown.

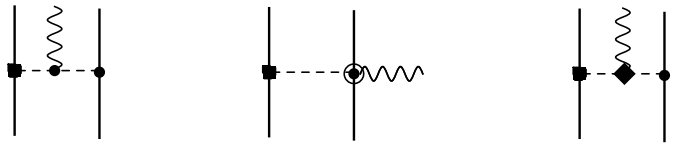

Figure 6.6: Diagrams contributing to the $\not{P}\not{T}$ two-nucleon electric current. A square marks a $\not{P}\not{T}$ interaction; the other notation is as in Fig. 6.2. Only one topology per diagram is shown.

Lagrangian, Eqs. (3.24, 3.25, 3.29). In momentum space the current reads

$$\begin{aligned}
J^0_{PT,a} &= +\frac{2ieg_A^2}{F_\pi^2}\left(\boldsymbol{\tau}^{(i)}\times\boldsymbol{\tau}^{(j)}\right)_3 k^0 \frac{[\vec{\sigma}^{(i)}\cdot(\vec{k}+\vec{q}/2)][\vec{\sigma}^{(j)}\cdot(\vec{k}-\vec{q}/2)]}{[(\vec{k}+\vec{q}/2)^2+m_\pi^2][(\vec{k}-\vec{q}/2)^2+m_\pi^2]}\ , \\
J^0_{PT,b} &= -\frac{ieg_A^2}{2F_\pi^2 m_N}\left(\boldsymbol{\tau}^{(i)}\times\boldsymbol{\tau}^{(j)}\right)_3 \\
&\quad\times\left[\frac{[\vec{\sigma}^{(i)}\cdot(\vec{P}_t+2\vec{K})][\vec{\sigma}^{(j)}\cdot(\vec{k}-\vec{q}/2)]}{(\vec{k}-\vec{q}/2)^2+m_\pi^2}+\frac{[\vec{\sigma}^{(j)}\cdot(\vec{P}_t-2\vec{K})][\vec{\sigma}^{(i)}\cdot(\vec{k}+\vec{q}/2)]}{(\vec{k}+\vec{q}/2)^2+m_\pi^2}\right]\ , \\
J^0_{PT,c} &= -\frac{2eg_A^2}{F_\pi^2}\delta m_N\left(\boldsymbol{\tau}^{(i)}\cdot\boldsymbol{\tau}^{(j)}-\tau_3^{(i)}\tau_3^{(j)}\right)\frac{[\vec{\sigma}^{(i)}\cdot(\vec{k}+\vec{q}/2)][\vec{\sigma}^{(j)}\cdot(\vec{k}-\vec{q}/2)]}{[(\vec{k}+\vec{q}/2)^2+m_\pi^2][(\vec{k}-\vec{q}/2)^2+m_\pi^2]}\ . \qquad (6.20)
\end{aligned}$$

We also need to include the LO two-nucleon $\not{P}\not{T}$ electric current. The diagrams contributing to this current are shown in Fig. 6.6. Here PT interactions come from the PT Lagrangian, Eqs. (3.24, 3.25, 3.29), and the $\not{P}\not{T}$ interaction is the $\bar{g}_0$ vertex in the $\not{P}\not{T}$ Lagrangian, Eq. (6.1). The current is given by

$$\begin{aligned}
J^0_{\not{P}\not{T},a} &= +\frac{2eg_A\bar{g}_0}{F_\pi^2}\left(\boldsymbol{\tau}^{(i)}\times\boldsymbol{\tau}^{(j)}\right)_3 k^0 \frac{(\vec{\sigma}^{(i)}+\vec{\sigma}^{(j)})\cdot\vec{q}/2+(\vec{\sigma}^{(i)}-\vec{\sigma}^{(j)})\cdot\vec{k}}{[(\vec{k}+\vec{q}/2)^2+m_\pi^2][(\vec{k}-\vec{q}/2)^2+m_\pi^2]}\ , \\
J^0_{\not{P}\not{T},b} &= -\frac{eg_A\bar{g}_0}{2F_\pi^2 m_N}\left(\boldsymbol{\tau}^{(i)}\times\boldsymbol{\tau}^{(j)}\right)_3\left[\frac{\vec{\sigma}^{(i)}\cdot(\vec{P}_t+2\vec{K})}{(\vec{k}-\vec{q}/2)^2+m_\pi^2}-\frac{\vec{\sigma}^{(j)}\cdot(\vec{P}_t-2\vec{K})}{(\vec{k}+\vec{q}/2)^2+m_\pi^2}\right]\ , \qquad (6.21) \\
J^0_{\not{P}\not{T},c} &= +\frac{2ieg_A\bar{g}_0}{F_\pi^2}\delta m_N\left(\boldsymbol{\tau}^{(i)}\cdot\boldsymbol{\tau}^{(j)}-\tau_3^{(i)}\tau_3^{(j)}\right)\frac{(\vec{\sigma}^{(i)}+\vec{\sigma}^{(j)})\cdot\vec{q}/2+(\vec{\sigma}^{(i)}-\vec{\sigma}^{(j)})\cdot\vec{k}}{[(\vec{k}+\vec{q}/2)^2+m_\pi^2][(\vec{k}-\vec{q}/2)^2+m_\pi^2]}\ .
\end{aligned}$$

6.5 EDM of the deuteron

We are now in position to calculate the EDM of the deuteron, which provides the simplest example of an $N=Z$ nucleus. The ground state of the deuteron is mainly a ${}^3S_1$ state. The

deuteron obtains a ${}^1P_1$ component after a $\bar{g}_0$ pion exchange or an insertion of $\bar{C}_{1,2}$. Since the LO PT one-nucleon current is spin independent, this cannot bring the deuteron wave function from ${}^1P_1$ to ${}^3S_1$, therefore these contributions vanish for the deuteron, as anticipated on more general grounds in the previous section.

The deuteron EDM has been studied before in the meson-exchange picture [80, 81, 97, 98, 99], with various degrees of sophistication in the treatments of the P- and T-conserving interaction H_{PT}. Using modern high-quality phenomenological potentials [102, 103], Ref. [81] found that the model dependence of H_{PT} is rather small for a deuteron EDM generated by the OPE sector of the $\not{P}\not{T}$ interaction. The detailed study in Ref. [99] confirmed this point. Since our new EFT scheme shows that the leading-order contribution from various $\not{P}\not{T}$ sources to the deuteron EDM also comes from the long-range terms in $V_{\not{P}\not{T}}$, we take advantage of the existing calculation scheme of Ref. [81] to obtain wave functions $|\Psi_{^2\mathrm{H}}\rangle$ and $|\widetilde{\Psi}_{^2\mathrm{H}}\rangle$. The calculation is performed in coordinate space using the $\not{P}\not{T}$ potentials and currents from App. D. Of course, a fully consistent treatment would involve using the PT interaction H_{PT} derived from the complete chiral Lagrangian, instead of a phenomenological potential. At present, unfortunately, such a consistent potential does not exist beyond LO [66]. It would include relativistic corrections as well, which are absent in the phenomenological potentials we use. For this reason, we neglect relativistic corrections in the $\not{P}\not{T}$ potential and currents as well. We expect that the results from a fully consistent calculation will not deviate significantly from the results we obtain here. The numbers below correspond to the Argonne v_{18} potential [103], but results for the Reid93 and Nijmegen II potential [102] agree within 5%. This is less than the error of order $m_\pi/M_{\mathrm{QCD}} \sim 20\%$ intrinsic to χPT in lowest order.

The simplest contribution to the deuteron EDM comes from the constituent EDMs. The LO $J^0_{\not{P}\not{T}}$, given in Eq. (6.14), yields a one-body EDM operator

$$\vec{D}^{(1)}_{\not{P}\not{T}} = \sum_{i=1}^{A} \left(\bar{d}_0 + \bar{d}_1\, \tau_3^{(i)}\right) \vec{\sigma}^{(i)} \ . \tag{6.22}$$

For the deuteron, an isoscalar ($I = 0$) and spin-triplet ($S = 1$) state, one simply gets

$$\frac{1}{\sqrt{6}} \left\langle \Psi_{^2\mathrm{H}} \left|\left| \vec{D}^{(1)}_{\not{P}\not{T}} \right|\right| \Psi_{^2\mathrm{H}} \right\rangle = d_n + d_p \ . \tag{6.23}$$

In order for $\vec{D}^{(1)}_{PT}$, a purely isovector operator as discussed earlier, to yield a nonzero contribution in the deuteron, it is obvious that the parity admixture $|\widetilde{\Psi}_{^2\mathrm{H}}\rangle$ has to be a ${}^3P_1$ state. Among the various terms in the LO $\not{P}\not{T}$ potential, Eqs. (6.10) and (6.11), only the one with the isospin-spin operator $(\tau_3^{(1)} - \tau_3^{(2)})(\vec{\sigma}^{(1)} + \vec{\sigma}^{(2)})$ can contribute. The result is

$$\frac{2}{\sqrt{6}} \left\langle \Psi_{^2\mathrm{H}} \left|\left| \vec{D}^{(1)}_{PT} \right|\right| \widetilde{\Psi}_{^2\mathrm{H}}({}^3P_1) \right\rangle = -0.19\, \frac{\bar{g}_1}{F_\pi}\, e\,\mathrm{fm} \ . \tag{6.24}$$

However, when it comes to the $\bar{\theta}$ term, because the LO contribution vanishes as argued in the previous section, the leading contribution is in fact NNLO. Among the higher-order interactions identified in Sect. 6.4.2, the terms with coupling constants $(g_A\bar{g}_1 + \bar{g}_0\beta_1/2)$ and $g_A\bar{g}_0\delta m_N$ in Eq. (6.18) can contribute, by isospin and spin selection rules. Except for the coupling constants, the operator structures of the former are the same as the one in Eq. (6.10), so the matrix element can simply be obtained by replacing

$$\bar{g}_1 \to \bar{g}_1 + \frac{\beta_1}{2g_A}\bar{g}_0 \tag{6.25}$$

in Eq. (6.24). Combining this with the contribution from the isospin-breaking πN vertex, we find the matrix element

$$\frac{2}{\sqrt{6}}\left\langle \Psi_{^2\mathrm{H}}\left|\left|\vec{D}^{(1)}_{PT}\right|\right|\widetilde{\Psi}_{^2\mathrm{H}}(^3P_1)\right\rangle = -\left[0.19\left(\frac{\bar{g}_1}{F_\pi}+\frac{\beta_1}{2g_A}\frac{\bar{g}_0}{F_\pi}\right)+5.8\cdot10^{-4}\,\frac{\bar{g}_0}{F_\pi}\right]e\,\mathrm{fm} \tag{6.26}$$

for the $\bar{\theta}$ term.

For the $\bar{\theta}$ term, there are in addition NNLO currents to be taken into account. For the $\not{P}\not{T}$ currents, as the corresponding EDM operators are sandwiched between two isoscalar states, they must be isoscalar to contribute. Among the NNLO $\not{P}\not{T}$ currents identified in Sec. 6.4.3, only the third current in Eq. (6.21), $J^0_{\not{P}\not{T},c}$, meets the requirement and leads to a two-body EDM operator (see App. D)

$$\vec{D}^{(2)}_{\not{P}\not{T}} = -e\,\frac{g_A\,\bar{g}_0}{F_\pi^2}\,\delta m_N\,\left(\boldsymbol{\tau}^{(1)}\cdot\boldsymbol{\tau}^{(2)}-\tau_3^{(1)}\,\tau_3^{(2)}\right)\left[\vec{\sigma}^{(1)}\cdot\vec{\nabla}_1+\vec{\sigma}^{(2)}\cdot\vec{\nabla}_2\,,\,(\vec{x}_1+\vec{x}_2)\,\frac{e^{-m_\pi|\vec{x}_1-\vec{x}_2|}}{8\,\pi\,m_\pi}\right] \tag{6.27}$$

in terms of the positions $\vec{x}_1$ and $\vec{x}_2$ of the two nucleons and the derivatives $\vec{\nabla}_1$ and $\vec{\nabla}_2$ with respect to them. This results in the matrix element

$$\frac{1}{\sqrt{6}}\left\langle \Psi_{^2\mathrm{H}}\left|\left|\vec{D}^{(2)}_{\not{P}\not{T}}\right|\right|\Psi_{^2\mathrm{H}}\right\rangle = 1.1\cdot10^{-3}\,\frac{\bar{g}_0}{F_\pi}\,e\,\mathrm{fm} \tag{6.28}$$

for the deuteron EDM. The contributions of two-body PT currents to the EDM have again to be coupled with the parity admixture generated by the LO $V_{\not{P}\not{T}}$, which is purely isoscalar when $\bar{\theta}$ is the $\not{P}\not{T}$ source. The only PT current with an isoscalar component, among those identified in Sec. 6.4.3, is the third current in Eq. (6.20), $J^0_{PT,c}$. It gives a two-body EDM operator

$$\vec{D}^{(2)}_{PT} = -e\,\frac{g_A^2}{F_\pi^2}\,\delta m_N\,\left(\boldsymbol{\tau}^{(1)}\cdot\boldsymbol{\tau}^{(2)}-\tau_3^{(1)}\,\tau_3^{(2)}\right)\left[(\vec{\sigma}^{(1)}\cdot\vec{\nabla}_1)(\vec{\sigma}^{(2)}\cdot\vec{\nabla}_2)\,,\,(\vec{x}_1+\vec{x}_2)\,\frac{e^{-m_\pi|\vec{x}_1-\vec{x}_2|}}{8\,\pi\,m_\pi}\right]\,. \tag{6.29}$$

Since the isoscalar parity admixture $|\widetilde{\Psi}_{^2\mathrm{H}}\rangle$ can only be a $^1P_1$ state, this current gives a matrix element

$$\frac{2}{\sqrt{6}}\left\langle \Psi_{^2\mathrm{H}}\left|\left|\vec{D}^{(2)}_{PT}\right|\right|\widetilde{\Psi}_{^2\mathrm{H}}(^1P_1)\right\rangle = -3.3\cdot10^{-4}\,\frac{\bar{g}_0}{F_\pi}\,e\,\mathrm{fm}\,. \tag{6.30}$$

In total the deuteron EDM can be written as a function of three $\not{P}\not{T}$ LECs,

$$d_{^2\mathrm{H}} = d_p + d_n + \left[-0.19\,\frac{\bar{g}_1}{F_\pi}+\left(0.2-0.7\cdot10^2\,\beta_1\right)\cdot10^{-3}\,\frac{\bar{g}_0}{F_\pi}\right]e\,\mathrm{fm}\,, \tag{6.31}$$

where $d_{p,n}$ should be included for $\bar{\theta}$, qEDM, and χI; $\bar{g}_1$ for $\bar{\theta}$, qCEDM, FQLR, and χI; and $\bar{g}_0$ for $\bar{\theta}$ only.

This result can be compared, for each of the sources, with the calculation where OPE is treated perturbatively in Chapter 5. For qCEDM, FQLR, and qEDM the nonperturbative-pion approach adopted here agrees very well with the perturbative calculation. In the case of the qCEDM or FQLR, it was also found that the deuteron EDM is dominated by $\bar{g}_1$ pion exchange and given by

$$d_{^2\mathrm{H}}(\mathrm{qCEDM,FQLR})|_{pert} = -\frac{eg_A\bar{g}_1m_N}{6\pi F_\pi^2m_\pi}\,\frac{1+\gamma/m_\pi}{(1+2\gamma/m_\pi)^2} = -0.23\,\frac{\bar{g}_1}{F_\pi}\,e\,\mathrm{fm}\,, \tag{6.32}$$

where $\gamma \simeq 45$ MeV is the binding momentum of the deuteron. This result agrees exactly with a zero-range model [80] and is 22% larger than the result from the qCEDM calculation with nonperturbative OPE [81] given above,

$$d_{^2\mathrm{H}}(\mathrm{qCEDM}, \mathrm{FQLR}) = -0.19\, \frac{\bar{g}_1}{F_\pi}\, e\,\mathrm{fm}\ . \tag{6.33}$$

Since the estimated error in the perturbative calculation is of order $Q/M_{NN} \sim 30\%$ (as demonstrated by the size of the NLO corrections in Sec. 5.5), the calculations agree within their uncertainty. Likewise, for qEDM the conclusions of Chapter 5 do not change once we treat OPE nonperturbatively. The deuteron EDM is in this case simply the sum of the neutron and proton EDM,

$$d_{^2\mathrm{H}}(\mathrm{qEDM}) = 2\bar{d}_0\ . \tag{6.34}$$

The comparison is more subtle for $\bar{\theta}$ and χI $\not{P}\not{T}$ sources. For both of these sources, the deuteron EDM is expected in the perturbative-pion approach to be dominated by the isoscalar nucleon EDM, since pion exchange is further suppressed in the Q/M_{NN} expansion. In the nonperturbative power counting $\not{P}\not{T}$ pion exchange is a dominant effect as well. In order to compare the two effects —nucleon EDMs and pion exchange— in the nonperturbative calculation we can look at the estimated scaling of the LECs. For χI sources,

$$d_{^2\mathrm{H}}(\chi\mathrm{I}) = 2\bar{d}_0 - 0.19\, \frac{\bar{g}_1}{F_\pi}\, e\,\mathrm{fm}\ . \tag{6.35}$$

From Eq. (6.5) we infer that $F_\pi \bar{d}_0/\bar{g}_1 = \mathcal{O}(eF_\pi/\varepsilon m_\pi^2) \sim 5\ e\,\mathrm{fm}$. Thus, although formally $\bar{g}_1$ exchange is LO, because of a combination of ε suppression and the relatively small factor of 0.19 in Eq. (6.31), it actually is expected to contribute only at the $\sim 5\%$ level to the deuteron EDM. For $\bar{\theta}$ there are additional contributions from $\bar{g}_0$,

$$d_{^2\mathrm{H}}(\bar{\theta}) = 2\bar{d}_0 + \left[-0.19\, \frac{\bar{g}_1}{F_\pi} + \left(0.2 - 0.7 \cdot 10^2\, \beta_1\right) \cdot 10^{-3}\, \frac{\bar{g}_0}{F_\pi}\right] e\,\mathrm{fm}\ . \tag{6.36}$$

The contributions from the $\not{P}\not{T}$ and PT two-body currents, Eqs. (6.27) and (6.29) respectively, are of similar size. The NN data constraint [70] on β_1 shows that the contribution from the $\not{P}\not{T}$ potential is no larger, and the full $\bar{g}_0$ term is $\lesssim 0.9 \cdot 10^{-3} (\bar{g}_0/F_\pi)\, e\,\mathrm{fm}$. From Eq. (6.2) we expect that $\bar{g}_1/\bar{g}_0 = \mathcal{O}(\varepsilon m_\pi^2/M_{\mathrm{QCD}}^2) \sim 10^{-2}$, so the $\bar{g}_1/F_\pi$ contribution should be comparable to these small $\bar{g}_0/F_\pi$ contributions. In contrast, we expect a larger weight from the pion cloud around each nucleon, which for $\bar{d}_0$ enters at NLO and gives Eq. (4.17) $\bar{d}_0 \geq 0.01 (\bar{g}_0/F_\pi)\, e\,\mathrm{fm}$. Thus again, although pion-exchange contributions in the potential and currents are formally LO, ε suppression and relatively small numerical factors in the deuteron make them likely no more than $\sim 10\%$ of the nucleon EDM contribution.

The fact that pion-exchange contributions are expected to be smaller in the deuteron than assumed in χPT power counting confirms that the power counting of Chapter 5, where pion exchange comes in at NLO, works better for a loosely bound nucleus. The χPT power counting should become more accurate as we consider heavier, denser nuclei, the simplest of which we tackle next.

6.6 EDM of the helion and the triton

In this section we investigate the EDMs of ^{3}He and ^{3}H. No particular cancellations are expected, so the framework of Sect. 6.3 applies.

The EDM of ^{3}He was studied in Ref. [82], where two $\not{P}\not{T}$ mechanisms were considered: nucleon EDMs and a $\not{P}\not{T}$ NN potential containing the most general nonderivative, single π-, ρ-, and ω-meson exchanges. The nuclear wave function was calculated with the no-core shell model (NCSM) [109], where a PT nuclear potential is solved within a model space made from appropriately symmetrized combinations [110] of N_{max} harmonic-oscillator wave functions of frequency Ω. In Ref. [82] both Argonne $v18$ [103] and EFT-inspired [104] potentials, including the Coulomb interaction, were used. At large enough N_{max} results become independent of Ω.

Here we adapt this calculation to the $\not{P}\not{T}$ ingredients from chiral EFT, and calculate the EDM of ^{3}H for the first time. As argued in Sect. 6.3, power counting for generic light nuclei tells us that for all $\not{P}\not{T}$ sources of dimension up to six, the EDM is indeed expected to come mostly from the nucleon EDM and from the two-nucleon $\not{P}\not{T}$ potential, as assumed in Ref. [82]. The only difference is that the EFT potential contains, in addition to OPE, also two LECs ($\bar{C}_1$ and $\bar{C}_2$) representing shorter-range interactions. This potential in coordinate space is given in App. D. The OPE terms were included in Ref. [82], while $\bar{C}_1$ and $\bar{C}_2$ can be thought of as originating from, respectively, ω and ρ exchanges, also considered there. The relation can be made quite explicit if we choose to regularize the delta functions with Yukawa functions, following a strategy successfully employed before to study the effects of the EFT $\not{P}PT$ potential [107]:

$$\frac{m_1^2\bar{C}_1}{4\pi r}e^{-m_1 r} \;\to\; \bar{C}_1\delta^{(3)}(\vec{r}) \;, \tag{6.37}$$

$$\frac{m_2^2\bar{C}_2}{4\pi r}e^{-m_2 r} \;\to\; \bar{C}_2\delta^{(3)}(\vec{r}) \;, \tag{6.38}$$

as $m_{1,2}\to\infty$. When $m_1 = m_\omega$ ($m_2 = m_\rho$) and $\bar{C}_1$ ($\bar{C}_2$) is an appropriate combination of ω (ρ) couplings [78], the expressions on the left-hand side coincide with those in Ref. [82]. Here we recalculate these contributions for values of $m_{1,2}$ up to 2.5 GeV. For uniformity with Sec. 6.5 we again display numbers obtained with the Argonne $v18$ potential. In Ref. [82] it was found that for helion the contributions from nucleon EDMs ($\bar{d}_{0,1}$) and from pion exchange ($\bar{g}_{0,1}$) change with PT potential by no more than $\sim 25\%$. We have verified that the same is true for triton. Unfortunately the situation is different for the short-range two-body contributions ($\bar{C}_{1,2}$), which are much more sensitive to the PT potential, as we discuss shortly.

The nucleon EDM contributions are found to be

$$\frac{1}{\sqrt{6}}\left\langle\Psi_{^3\mathrm{He}}\left|\left|\vec{D}^{(1)}_{\not{P}\not{T}}\right|\right|\Psi_{^3\mathrm{He}}\right\rangle \;=\; 0.88\,d_n - 0.047\,d_p \;, \tag{6.39}$$

$$\frac{1}{\sqrt{6}}\left\langle\Psi_{^3\mathrm{H}}\left|\left|\vec{D}^{(1)}_{\not{P}\not{T}}\right|\right|\Psi_{^3\mathrm{H}}\right\rangle \;=\; -0.050\,d_n + 0.90\,d_p \;. \tag{6.40}$$

As expected, the helion (triton) EDM is mostly sensitive to the neutron (proton) EDM [82].

For the contribution from the $\not{P}\not{T}$ potential, our results for triton are very similar in magnitude to those for helion, in the case of OPE already obtained in Ref. [82]. The contribution of $\bar{C}_{1,2}$ as a function of $m_{1,2}$ is given in Fig. 6.7 for Argonne $v18$. For each regulator mass, we perform calculations at four values of $\Omega = 20, 30, 40, 50$ MeV, up to $N_{max} = 50$. We observe convergence and estimate a 10% error from the spread of results with Ω. (See Fig. 1 of Ref. [82] for a generic convergence pattern.) As it can be seen from Fig. 6.7, the results become approximately $m_{1,2}$ independent at large masses, implying that $\bar{C}_{1,2}$ approach constants in this limit. Results are very different for the EFT-inspired potential. Within the region of masses studied, we found an approximately linear dependence on the regulator mass, always larger in magnitude than for Argonne $v18$. While for $m_1 = m_\omega$ and $m_2 = m_\rho$ the contributions to the tri-nucleon EDMs differ by a factor ~ 2 [82], the difference first increases and then decreases as $m_{1,2}$ increases, but

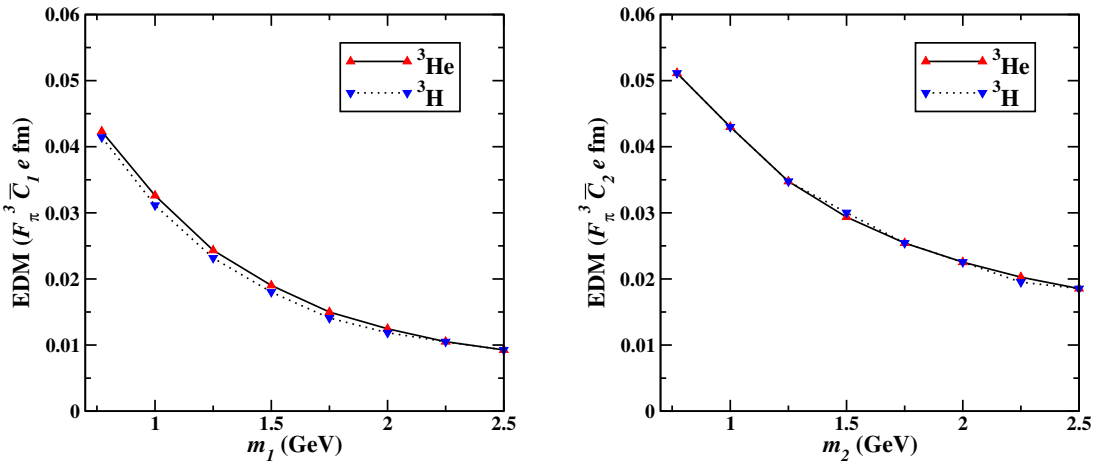

Figure 6.7: Magnitude of the tri-nucleon EDMs in units of $F_\pi^3 \bar{C}_i e$ fm, as function of the regulator mass in GeV: $i = 1$ (left panel) and $i = 2$ (right panel). The solid (dashed) curve is for helion (triton).

it is still a factor of ~ 5 at 2.5 GeV. The linear regulator dependence could indicate a different running of $\bar{C}_{1,2}$, or simply a very slow convergence. However, calculations with this potential are more computationally intensive and we have been limited to $N_{max} = 40$, which increases the error. In any case, there is clearly a much stronger dependence of these short-range contributions on the potential, and more solid numbers have to await a fully consistent calculation. We quote here the Argonne $v18$ numbers at 2.5 GeV, but we emphasize that they represents only an order of magnitude estimate. We obtain

$$\frac{2}{\sqrt{6}} \left\langle \Psi_{^3\mathrm{He}} \left|\left| \vec{D}^{(1)}_{PT} \right|\right| \widetilde{\Psi}_{^3\mathrm{He}} \right\rangle = \left(-0.15 \frac{\bar{g}_0}{F_\pi} - 0.28 \frac{\bar{g}_1}{F_\pi} - 0.01 F_\pi^3 \bar{C}_1 + 0.02 F_\pi^3 \bar{C}_2 \right) e\,\mathrm{fm}\ , \quad (6.41)$$

$$\frac{2}{\sqrt{6}} \left\langle \Psi_{^3\mathrm{H}} \left|\left| \vec{D}^{(1)}_{PT} \right|\right| \widetilde{\Psi}_{^3\mathrm{H}} \right\rangle = \left(0.15 \frac{\bar{g}_0}{F_\pi} - 0.28 \frac{\bar{g}_1}{F_\pi} + 0.01 F_\pi^3 \bar{C}_1 - 0.02 F_\pi^3 \bar{C}_2 \right) e\,\mathrm{fm}\ . \quad (6.42)$$

In total, then, as anticipated in Sects. 6.2 and 6.3, the EDMs of helion and triton (as the EDMs of light nuclei in general) are functions of six $\not{P}\not{T}$ LECs:

$$d_{^3\mathrm{He}} = 0.88\, d_n - 0.047\, d_p - \left(0.15\, \frac{\bar{g}_0}{F_\pi} + 0.28\, \frac{\bar{g}_1}{F_\pi} + 0.01\, F_\pi^3 \bar{C}_1 - 0.02\, F_\pi^3 \bar{C}_2 \right) e\,\mathrm{fm} \quad (6.43)$$

and

$$d_{^3\mathrm{H}} = -0.050\, d_n + 0.90\, d_p + \left(0.15\, \frac{\bar{g}_0}{F_\pi} - 0.28\, \frac{\bar{g}_1}{F_\pi} + 0.01\, F_\pi^3 \bar{C}_1 - 0.02\, F_\pi^3 \bar{C}_2 \right) e\,\mathrm{fm}\ , \quad (6.44)$$

where $\bar{g}_0$ applies for $\bar{\theta}$, qCEDM, FQLR and χI; $\bar{g}_1$ for qCEDM, FQLR, and χI; $d_{n,p}$ for qEDM and χI; and $\bar{C}_{1,2}$ for χI only.

Only in the case of the qEDM do we expect the tri-nucleon EDMs to be dominated by the nucleon EDMs. Not surprisingly, the helion (triton) EDM should be approximately equal to the neutron (proton) EDM. The nucleon EDM for the dimension-six sources was calculated

in Chapter 4 and it was found that for qEDM the EDMs were dominated by the short-range contributions in Eqs. (4.27) and (4.28). In this case,

$$d_{^3\mathrm{He}}(\mathrm{qEDM}) = 0.83\,\bar{d}_0 - 0.93\,\bar{d}_1\ , \tag{6.45}$$

$$d_{^3\mathrm{H}}(\mathrm{qEDM}) = 0.85\,\bar{d}_0 + 0.95\,\bar{d}_1\ . \tag{6.46}$$

For the $\bar{\theta}$ term, on the other hand, the helion and triton EDMs depend at LO only on $\bar{g}_0$. To check this statement we compare the LO contribution with the contribution from the nucleon EDMs. If we assume the neutron and proton EDMs to be saturated by their long-range part, that is, the chiral log in Eq. (4.14) $\bar{d}_1 \simeq 0.1(\bar{g}_0/F_\pi)\,e\,\mathrm{fm}$ shows that the short-range term is comparable to the pion-exchange contribution. To be on the safe side, it seems better not to neglect the LO nucleon EDMs for the $\bar{\theta}$ term, even though the power counting tells us it should be subleading; then

$$d_{^3\mathrm{He}}(\bar{\theta}) = 0.83\,\bar{d}_0 - 0.93\,\bar{d}_1 - 0.15\,\frac{\bar{g}_0}{F_\pi}\,e\,\mathrm{fm}\ , \tag{6.47}$$

$$d_{^3\mathrm{H}}(\bar{\theta}) = 0.85\,\bar{d}_0 + 0.95\,\bar{d}_1 + 0.15\,\frac{\bar{g}_0}{F_\pi}\,e\,\mathrm{fm}\ . \tag{6.48}$$

This argument holds equally well for the qCEDM and FQLR, except that now also $\bar{g}_1$ contributes:

$$d_{^3\mathrm{He}}(\mathrm{qCEDM,FQLR}) = 0.83\,\bar{d}_0 - 0.93\,\bar{d}_1 - \left(0.15\,\frac{\bar{g}_0}{F_\pi} + 0.28\,\frac{\bar{g}_1}{F_\pi}\right) e\,\mathrm{fm}\ , \tag{6.49}$$

$$d_{^3\mathrm{H}}(\mathrm{qCEDM,FQLR}) = 0.85\,\bar{d}_0 + 0.95\,\bar{d}_1 + \left(0.15\,\frac{\bar{g}_0}{F_\pi} - 0.28\,\frac{\bar{g}_1}{F_\pi}\right) e\,\mathrm{fm}\ . \tag{6.50}$$

Finally in the case of χI, we expect the tri-nucleon EDM to consist of $\bar{g}_{0,1}$ pion exchange, insertions of the $\not{P}\not{T}$ short-range NN interactions, and the contributions from the nucleon EDMs. Similarly to the qEDM, the nucleon EDM from χI is dominated by short-range contributions. All six LECs contribute:

$$d_{^3\mathrm{He}}(\chi\mathrm{I}) = 0.83\,\bar{d}_0 - 0.93\,\bar{d}_1 - \left(0.15\,\frac{\bar{g}_0}{F_\pi} + 0.28\,\frac{\bar{g}_1}{F_\pi} + 0.01\,F_\pi^3\bar{C}_1 - 0.02\,F_\pi^3\bar{C}_2\right) e\,\mathrm{fm}\ , \tag{6.51}$$

$$d_{^3\mathrm{H}}(\chi\mathrm{I}) = 0.85\,\bar{d}_0 + 0.95\,\bar{d}_1 + \left(0.15\,\frac{\bar{g}_0}{F_\pi} - 0.28\,\frac{\bar{g}_1}{F_\pi} + 0.01\,F_\pi^3\bar{C}_1 - 0.02\,F_\pi^3\bar{C}_2\right) e\,\mathrm{fm}\ . \tag{6.52}$$

From Eq. (6.5) we infer $F_\pi\bar{d}_{0,1}/\bar{g}_0 = \mathcal{O}(eF_\pi/m_\pi^2) \sim 2\ e\,\mathrm{fm}$ and $F_\pi^4\bar{C}_{1,2}/\bar{g}_0 = \mathcal{O}(F_\pi^2/m_\pi^2) \sim 2$. We see again that the $\bar{g}_{0,1}$ coefficients are somewhat smaller than expected; moreover, the $\not{P}\not{T}$ short-range NN interactions might contribute even less. However, one should keep in mind the large uncertainty in the $\bar{C}_{1,2}$ coefficients, and that these dimensional-analysis estimates could easily be offset by dimensionless factors in the LECs.

6.7 Discussion

Historically, hadronic EDMs have mostly been discussed in the framework of a one-boson-exchange model. It is assumed that P and T violation is propagated by pions which are parametrized by three $\not{P}\not{T}$ nonderivative interactions. In our notation,

$$\mathcal{L} = -\frac{\bar{g}_0}{F_\pi}\bar{N}\boldsymbol{\tau}\cdot\boldsymbol{\pi}N - \frac{\bar{g}_1}{F_\pi}\bar{N}\pi_3 N - \frac{\bar{g}_2}{F_\pi}\bar{N}\tau_3\pi_3 N \tag{6.53}$$

Table 6.1: Dependence of the EDMs of the neutron, proton, deuteron, helion, and triton on the six relevant $\not{P}\not{T}$ low-energy constants. A "-" denotes that the LEC does not contribute in a model-independent way to the EDM at leading order. Values are for the Argonne $v18$ potential; for the potential-model dependence of the results, see text.

LEC	$\bar{d}_0$	$\bar{d}_1$	$(\bar{g}_0/F_\pi)\, e\,\mathrm{fm}$	$(\bar{g}_1/F_\pi)\, e\,\mathrm{fm}$	$(F_\pi^3\bar{C}_1)\, e\,\mathrm{fm}$	$(F_\pi^3\bar{C}_2)\, e\,\mathrm{fm}$
d_n	1	-1	-	-	-	-
d_p	1	1	-	-	-	-
$d_{^2\mathrm{H}}$	2	0	$0.0002 - 0.07\beta_1$	-0.19	-	-
$d_{^3\mathrm{He}}$	0.83	-0.93	-0.15	-0.28	-0.01	0.02
$d_{^3\mathrm{H}}$	0.85	0.95	$+0.15$	-0.28	0.01	-0.02

(in the nuclear physics literature, where power counting is not emphasized, the coefficients are normally defined without F_π). Hadronic EDMs are calculated as a function of these three parameters. In some cases the effects of heavier bosons are included as well. In this thesis we argue that this model is oversimplified. There is *a priori* no reason not to include $\not{P}\not{T}$ $N\gamma$ and short-range NN interactions at low energies. By studying the chiral properties of the fundamental $\not{P}\not{T}$ sources of dimension up to six at the QCD scale, it is possible to construct a model-independent hadronic $\not{P}\not{T}$ Lagrangian with a definite hierarchy between the different $\not{P}\not{T}$ hadronic interactions. It is found that the OPE model with three LECs is not appropriate for any of these $\not{P}\not{T}$ sources, and in general there are six $\not{P}\not{T}$ hadronic interactions that determine the EDMs of light nuclei. Two of those are in the OPE model as well —$\bar{g}_0$ and $\bar{g}_1$— and the other four are additional interactions that need to be considered when determining hadronic EDMs. The $\bar{g}_2$ interaction is not relevant at LO for any of the fundamental sources. The other four necessary LECs are the isoscalar and isovector components of the neutron and proton EDMs and two isoscalar $\not{P}\not{T}$ NN interactions of short range. The isovector $\not{P}\not{T}$ NN interactions come in at higher order for all sources.

We therefore propose that nuclear EDMs be analyzed on the basis of these six LECs. In the previous sections we discussed EDMs of light nuclei, providing specific examples in the form of the deuteron, helion, and triton. In Table 6.1 the dependence of these various EDMs on the six LECs is summarized. From the table it is clear that using the OPE model gives an oversimplified view. At least six observables are required to identify the six LECs. If other light nuclei become the target of experimental investigation, their EDMs can be calculated along similar lines at the cost of larger computer resources. We hope that EDMs of heavier systems can be also expressed in terms of these six LECs. However, in these cases there could be significant enhancement factors for the $\not{P}\not{T}$ potential contribution [108], making important otherwise subleading terms in the potential [78], such as the third nonderivative πN coupling $\bar{g}_2$.

Once (a subset of) the LECs are determined it is possible to learn something about the more fundamental $\not{P}\not{T}$ sources at the QCD scale. In Table 6.2 we list for the different $\not{P}\not{T}$ sources the expected orders of magnitude of the neutron EDM, d_n, and ratios between the other EDMs considered here and d_n. Although some care is needed when using this table —as we have discussed, the numbers found earlier are not always exactly of the expected size— it does allow some qualitative statements, even if less than six measurements are available.

The simplest scenario is the one where $\not{P}\not{T}$ is dominated by the qEDM, in which case all light nuclear EDMs are essentially given by two LECs only: $\bar{d}_0$ and $\bar{d}_1$. (See Eqs. (4.27), (4.28), (6.34), (6.45), and (6.46).) A measurement of the proton and neutron EDMs would make deuteron and

Table 6.2: Expected orders of magnitude for the neutron EDM (in units of $e/M_{\rm QCD}$), the ratio of proton-to-neutron EDMs, the ratio of deuteron-to-neutron EDMs, the ratio of helion-to-neutron EDMs, and the ratio of triton-to-neutron EDMs, for the $\bar{\theta}$ term and the three dimension-six sources.

Source	$\bar{\theta}$	qCEDM	FQLR	qEDM	χI
$M_{\rm QCD}\, d_n/e$	$\mathcal{O}\left(\bar{\theta}\frac{m_\pi^2}{M_{\rm QCD}^2}\right)$	$\mathcal{O}\left(\tilde{\delta}\frac{m_\pi^2}{M_{\not P\not T}^2}\right)$	$\mathcal{O}\left(\xi\frac{M_{\rm QCD}^2}{M_{\not P\not T}^2}\right)$	$\mathcal{O}\left(\delta\frac{m_\pi^2}{M_{\not P\not T}^2}\right)$	$\mathcal{O}\left(w\frac{M_{\rm QCD}^2}{M_{\not P\not T}^2}\right)$
d_p/d_n	$\mathcal{O}\,(1)$	$\mathcal{O}\,(1)$	$\mathcal{O}\,(1)$	$\mathcal{O}\,(1)$	$\mathcal{O}\,(1)$
$d_{^2\rm H}/d_n$	$\mathcal{O}\,(1)$	$\mathcal{O}\left(\frac{M_{\rm QCD}^2}{m_\pi^2}\right)$	$\mathcal{O}\left(\frac{M_{\rm QCD}^2}{m_\pi^2}\right)$	$\mathcal{O}(1)$	$\mathcal{O}(1)$
$d_{^3\rm He}/d_n$	$\mathcal{O}\left(\frac{M_{\rm QCD}^2}{m_\pi^2}\right)$	$\mathcal{O}\left(\frac{M_{\rm QCD}^2}{m_\pi^2}\right)$	$\mathcal{O}\left(\frac{M_{\rm QCD}^2}{m_\pi^2}\right)$	$\mathcal{O}(1)$	$\mathcal{O}(1)$
$d_{^3\rm H}/d_n$	$\mathcal{O}\left(\frac{M_{\rm QCD}^2}{m_\pi^2}\right)$	$\mathcal{O}\left(\frac{M_{\rm QCD}^2}{m_\pi^2}\right)$	$\mathcal{O}\left(\frac{M_{\rm QCD}^2}{m_\pi^2}\right)$	$\mathcal{O}(1)$	$\mathcal{O}(1)$

tri-nucleon EDMs testable predictions

$$d_{^2\rm H} \simeq d_n + d_p \ , \tag{6.54}$$

$$d_{^3{\rm He}} + d_{^3\rm H} \simeq 0.84(d_n + d_p) \ , \tag{6.55}$$

$$d_{^3{\rm He}} - d_{^3\rm H} \simeq 0.94(d_n - d_p) \ . \tag{6.56}$$

The nucleon Schiff moments (Eq. (4.29)) and the deuteron MQM (Eq. (5.23)) depend on other LECs and cannot be predicted. For light nuclei the effects of the $\not P\not T$ potential from the qEDM are suppressed compared to the nucleon EDMs although enhancements could make them more relevant for heavier nuclei.

$\not P\not T$ from $\bar{\theta}$, qCEDM, and FQLR manifests itself in EDMs of light nuclei that differ significantly from the EDMs of their constituents. For these sources, the EDMs we calculated depend at LO on four of the six LECs —$\bar{g}_0$, $\bar{g}_1$, $\bar{d}_0$, and $\bar{d}_1$— but in different ways. For the qCEDM and FQLR, the distinguishing feature is that the deuteron EDM (6.33) is expected to be significantly larger than the isoscalar nucleon EDM, thanks to $\bar{g}_1$. Thus, a measurement of nucleon and deuteron EDMs could be sufficient to qualitatively pinpoint, or exclude, the qCEDM or FQLR as a dominant $\not P\not T$ source, and to fix the values of $\bar{d}_{0,1}$ and $\bar{g}_1$. Then, the isoscalar combination of helion and triton EDMs, $d_{^3\rm He} + d_{^3\rm H}$, which in LO only depends on $\bar{g}_1$, becomes a falsifiable prediction of the theory,

$$d_{^3{\rm He}} + d_{^3\rm H} \simeq 3 d_{^2\rm H} \ . \tag{6.57}$$

If, to be on the safe side, we keep some subleading terms (the nucleon EDMs) as we did in Eqs. (6.49) and (6.50), then we get (including the subleading term $2\bar{d}_0$ in Eq. (6.33)) an additional $-2.16(d_n + d_p)$ on the right-hand side of Eq. (6.57). Furthermore, $\bar{g}_0$ can then be extracted from $d_{^3\rm He} - d_{^3\rm H}$ (see Eqs. (6.49) and (6.50)), leading to testable predictions for other $\not P\not T$ observables.

Our analysis suggests that the observation of nuclear EDMs alone will not easily allow to separate the effects of the FQLR operator from the isovector qCEDM. On the other hand, important information could be gained in conjunction with the measurement of the T-odd correlation coefficient in β decay, D [40]. Indeed, the Ξ operator in Eq. (2.32), which generates at tree level the FQLR operator, also contributes to an operator that couples right-handed quarks to a left-handed electron and neutrino, with coefficient of $\mathcal{O}(\Xi)$. The qCEDM contributions to the

same operator are proportional to G_F due to need of an additional exchange of a W boson and, because of the need of an extra chirality flip, by an insertion of the light-quark mass. Therefore, the contribution of the qCEDM to the operator scales as $\tilde{d}_{0,3} G_F \bar{m}/4\pi \sim G_F \bar{m}^2 \tilde{\delta}_{0,3}/M_T^2$ and is suppressed by a factor $\bar{m}^2/M_W^2$. The size of the D coefficient with respect to nuclear EDMs is therefore very different for the qCEDM and the FQLR operator. In case that the observation of nucleon and deuteron EDM point to an isospin-breaking $\not{P}\not{T}$ source, a measurement of D could help to discriminate between these two operators.

In contrast, for the SM $\bar{\theta}$ term we do not expect the deuteron EDM to be significantly different from twice the isoscalar nucleon EDM. Although the deuteron EDM (6.36) formally depends on the isoscalar nucleon EDM, and on the πN couplings $\bar{g}_0$ and $\bar{g}_1$, the results of Sec. 6.5 show that the pion-exchange contribution is likely only $\sim 10\%$ of the nucleon EDM. On the other hand, the EDMs of ^{3}He and ^{3}H, Eqs. (6.47) and (6.48), are dominated by $\bar{g}_0$, although they receive important contributions from the neutron and proton EDMs. In particular, we expect the isovector combination $d_{^3\mathrm{He}} - d_{^3\mathrm{H}}$, which is sensitive to $\bar{g}_0$, to differ from the isovector nucleon EDM $\bar{d}_1$, while the isoscalar combination $d_{^3\mathrm{He}} + d_{^3\mathrm{H}}$ should be close to $2\bar{d}_0$:

$$d_{^3He} + d_{^3\mathrm{H}} \simeq 0.84(d_n + d_p) \,, \tag{6.58}$$

$$d_{^3\mathrm{He}} - d_{^3\mathrm{H}} \neq 0.94(d_n - d_p) \,. \tag{6.59}$$

The experimental observation of these relations in nucleon, deuteron, helion, and triton EDM experiments would qualitatively indicate the $\bar{\theta}$ term as the main source responsible for $\not{P}\not{T}$. Quantitatively, the measurement of nucleon, helion, and triton EDM allows extraction of the coupling $\bar{g}_0$, which then can be used to provide testable predictions of other $\not{P}\not{T}$ observables, like the proton Schiff moment (Eq. (4.19)) or the deuteron MQM (Eq. (5.23)), which are not sensitive to the nucleon EDMs.

Finally, in the case of the χI sources the analysis is in principle most complicated, due to the appearance of all six LECs. Like for $\bar{\theta}$, the deuteron EDM (6.35), although formally dependent on $\bar{g}_1$ at LO, is probably dominated by $\bar{d}_0$. The tri-nucleon EDMs (6.51) and (6.52) formally depend on all six LECs, but they are again possibly dominated by $\bar{d}_0$ and $\bar{d}_1$. It might thus be difficult to separate the χI sources from qEDM. For less dilute, but still light, systems we expect different results. For these systems, in the case of qEDM the EDMs are still dominated by $\bar{d}_{0,1}$, but for χI sources we expect the contributions from the $\not{P}\not{T}$ potential to be more significant, implying that measurements on these systems might separate χI sources from qEDM. Of course, more extensive calculations are necessary to verify this claim.

In Chapter 5 it has already been pointed out —basically on the basis of dimensional analysis— that sensitivity to the deuteron EDM at the level hoped for in storage ring experiments [20] would probe scales where new physics is expected. A similar analysis holds for our tri-nucleon results Eqs. (6.43) and (6.44). But our results here go beyond dimensional analysis and suggest that, at least for the lightest nuclei, the contribution of the neutron and proton EDMs are more important than expected by simple power counting. For all sources, they compete with, when they do not dominate, the effects of the $\not{P}\not{T}$ potential. For this reason, other $\not{P}\not{T}$ observables insensitive to the nucleon EDMs, for example higher $\not{P}\not{T}$ electromagnetic moments, could provide important complementary information and a cleaner way to extract πN and NN $\not{P}\not{T}$ couplings. Additionally, it would be interesting if EDMs of heavier systems could be recast in terms of our EFT approach.

6.8 The deuteron magnetic quadrupole moment revisited[2]

The analysis in the previous chapter showed that EDMs of light nuclei are significantly influenced by the EDMs of the constituent nucleons. Since the nucleon EDMs consist for all sources, at least partially, of short-range contributions, it is interesting to study an observable which cleanly probes the $\not{P}\not{T}$ NN interaction, providing important complementary information on the fundamental mechanism of time-reversal violation. In case of the $\bar{\theta}$ term, qCEDM, and FQLR such an observable is the nucleon Schiff moment which, as demonstrated in Chapter 4, is dominated by the $\not{P}\not{T}$ πN couplings.. For the other sources, however, the Schiff moments consist of additional short-range LECs. Furthermore, there is no method available to measure the nucleon Schiff moments. This leads us to study a different candidate; the deuteron magnetic quadrupole moment (MQM).

The deuteron MQM is of interest because the constituent nucleons, being spin-1/2 particles, do not possess an MQM themselves. The deuteron MQM therefore has to depend on $\not{P}\not{T}$ nuclear forces. Additionally, in Chapter 5 we showed that only for the $\bar{\theta}$ term is the deuteron MQM expected to be larger than the deuteron EDM (in appropriate units). For the beyond-the-SM sources, the MQM is expected to be of similar size or somewhat smaller than the EDM. A measurement of the deuteron MQM, if possible, could play a central role in separating the various $\not{P}\not{T}$ sources.

In the previous section we concluded that for the deuteron EDM, the results from EFTs treating pions perturbatively and nonperturbatively are very similar. Here we investigate this for the deuteron MQM as well and we address the question, to what extent a possible measurement of the MQM could be of help to separate the different $\not{P}\not{T}$ sources. We also compare our results to previous studies of the deuteron MQM [80, 81]. In particular, Ref. [81] used traditional meson-exchange NN models and a general $\not{P}\not{T}$ NN interaction [81, 101]. We again use the codes of Ref. [81], but adapt and extend the framework (the $\not{P}\not{T}$ NN potentials and currents) to chiral EFT with nonperturbative pions as we did in the previous sections for the EDMs. In principle our framework can be applied to the calculation of the MQM of other light nuclei as well.

We present here only the terms that are relevant for the LO MQM calculation, which depends on five $\not{P}\not{T}$ interactions

$$\begin{aligned}\mathcal{L}_{\not{P}\not{T}} &= -\frac{1}{F_\pi}\bar{N}\left(\bar{g}_0\,\boldsymbol{\tau}\cdot\boldsymbol{\pi}+\bar{g}_1\pi_3\right)N+\frac{\bar{c}_0}{F_\pi}\varepsilon^{\mu\nu\alpha\beta}v_\alpha\,\bar{N}S_\beta\boldsymbol{\tau}\cdot\boldsymbol{\pi}N\,F_{\mu\nu}\\ &\quad+\bar{C}_1\bar{N}N\partial_\mu(\bar{N}S^\mu N)+\bar{C}_2\bar{N}\boldsymbol{\tau}N\cdot(\bar{N}\boldsymbol{\tau}S\cdot\mathcal{D}_+N)\ . \end{aligned} \tag{6.60}$$

Except for $\bar{c}_0$, these interactions play a role in the calculation of nuclear EDMs as well. The scaling of the LECs appearing in the EDM calculations is given in Eqs. (6.2)-(6.5). The scaling of $\bar{c}_0$ can be found in Chapter 3 and is given by

$$\bar{c}_0=\mathcal{O}\left(e\bar{\theta}\frac{m_\pi^2}{M_{\rm QCD}^3},\,e(\tilde{\delta}_0+\tilde{\delta}_3)\frac{m_\pi^2}{M_{\not{T}}^2M_{\rm QCD}},\,e\xi\frac{M_{\rm QCD}}{M_{\not{T}}^2},\,e(\delta_0+\delta_3)\frac{m_\pi^2}{M_{\not{T}}^2M_{\rm QCD}},\,ew\frac{m_\pi^2}{M_{\not{T}}^2M_{\rm QCD}}\right) \tag{6.61}$$

Just as the deuteron EDM, the calculation of the deuteron MQM can be divided into two contributions. The first contribution comes from an insertion of the $\not{P}\not{T}$ electromagnetic two-body current $\vec{J}_{\not{P}\not{T}}$. The current has to be two-body since the constituent nucleons do not possess an MQM. The second contribution comes from the electromagnetic current $\vec{J}_{PT}$ upon perturbing the wave function of the nucleus with the $\not{P}\not{T}$ potential $V_{\not{P}\not{T}}$, such that the wave function obtains

[2] This section is based on C.-P. Liu, J. de Vries, E. Mereghetti, R. G. E. Timmermans, and U. van Kolck, Phys. Lett. B **713**, 447 (2012)

a $\not{P}\not{T}$ component. This current can be one- or two-body. The required $\not{P}\not{T}$ potential $V_{\not{P}\not{T}}$ is given in Eqs. (6.10)-(6.12) and the current $\vec{J}_{\not{P}\not{T}}$ can be calculated from Eq. (6.60).

To first order in the $\not{P}\not{T}$ sources, the deuteron MQM is thus a sum of two reduced matrix elements,

$$\mathcal{M}_d = \frac{1}{\sqrt{30}} \left(\langle \Psi_d || \widetilde{\boldsymbol{M}} || \Psi_d \rangle + 2 \langle \Psi_d || \boldsymbol{M} || \widetilde{\Psi}_d \rangle \right) . \tag{6.62}$$

The deuteron ground state $|\Psi_d\rangle$ and its parity admixture $|\widetilde{\Psi}_d\rangle$ are the solutions of homogeneous and inhomogeneous Schrödinger equations in Eq. (6.7). The MQM operators $\boldsymbol{M}$ and $\widetilde{\boldsymbol{M}}$ are obtained from the corresponding currents $\vec{J}_{PT}$ and $\vec{J}_{\not{P}\not{T}}$, respectively. The Cartesian component along the z direction, M_{33}, which is proportional to the spherical harmonic Y_2^0, takes the form

$$M_{33} = 2 \int d^3x \, x_3 \, (\vec{x} \times \vec{J}(\vec{x}))_3 \, , \tag{6.63}$$

where $\vec{x}$ is the position where the current density is probed. Given the current in momentum space,

$$\vec{J}(\vec{q}) = \int d^3x \, e^{-i \, \vec{q} \cdot \vec{x}} \, \vec{J}(\vec{x}) \, , \tag{6.64}$$

M_{33} can also be derived as

$$M_{33} = -2 \lim_{\vec{q} \to 0} \left(\nabla_{q_3} \nabla_{q_1} J_2(\vec{q}) - \nabla_{q_3} \nabla_{q_2} J_1(\vec{q}) \right) . \tag{6.65}$$

The three classes of contributions to the deuteron MQM described above are shown in Fig. 6.8. In order to decide which diagrams give the main contribution to the MQM we apply the power-counting rules outlined in Sect. 6.3.1. The PT vertices stem from Eqs. (3.24), (3.25), and (3.30) and the $\not{P}\not{T}$ LO vertices from Eq. (6.60). The iteration of the LO PT potential among nucleons before and after any $\not{P}\not{T}$ insertion builds up the PT wave function, represented in Fig. 6.8 by the triangles. In the following power counting we omit this overall factor. The scaling in terms of the LECs in Eq. (6.60) of diagram (a) is then

$$D_a = \mathcal{O}\left(e \, \frac{\bar{g}_0}{F_\pi^2} \frac{Q^2}{M_{\rm QCD}} \right) + \mathcal{O}\left(\frac{\bar{c}_0 Q^2}{F_\pi^2} \frac{Q^2}{M_{\rm QCD}} \right) + \mathcal{O}\left(e \, \bar{C}_2 F_\pi^2 \frac{Q^2}{M_{\rm QCD}} \right) , \tag{6.66}$$

while diagrams (b) and (c) scale as

$$D_{b,c} = \mathcal{O}\left(e \, \frac{\bar{g}_{0,1}}{F_\pi^2} \frac{Q^2}{M_{\rm QCD}} \right) + \mathcal{O}\left(e \, \bar{C}_{1,2} F_\pi^2 \frac{Q^2}{M_{\rm QCD}} \right) . \tag{6.67}$$

Which contribution dominates depends as usual on the fundamental $\not{P}\not{T}$ source,

- For the $\bar{\theta}$ term, only the isoscalar coupling $\bar{g}_0$ plays a role at LO. The other couplings, $\bar{g}_1$, $\bar{c}_0$ and $\bar{C}_{1,2}$, contribute at subleading orders. Since $\bar{g}_0$ enters in principle through the three classes of diagrams with similar factors, all these classes are equally important.
- For the qCEDM and FQLR, we need both πN interactions, since there is no relative suppression of $\bar{g}_1$. Again, all three classes are, a priori, equally important.
- For the qEDM, the purely hadronic interactions are suppressed by factors of the fine-structure constant, and only $\bar{c}_0$ is important. Thus only diagram (a) matters.

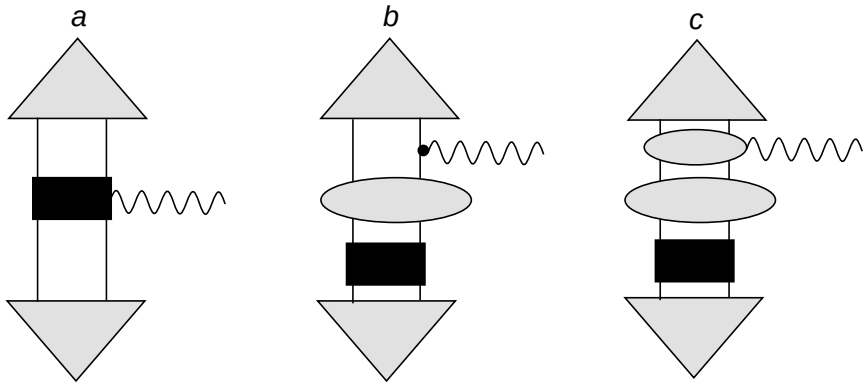

Figure 6.8: The three general classes of diagrams contributing to the deuteron MQM described in the text. Notation as in Fig. 6.1.

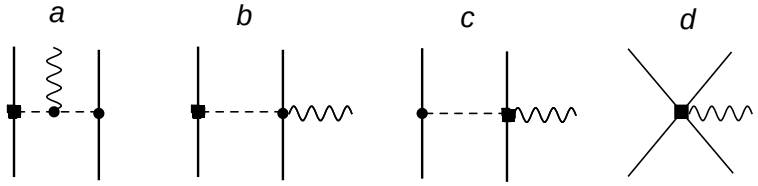

Figure 6.9: Diagrams contributing to the $\not P\not T$ two-nucleon current. Solid, dashed, and wavy lines represent nucleons, pions, and photons. A square marks a $\not P\not T$ interaction and the other vertices PT interactions. Only one topology per diagram is shown.

- For the χI sources the $\not P\not T$ short-range NN interactions are as important as the πN interactions. All three diagrams could be important.

The relevant $\not P\not T$ two-body currents that appear in diagram class (a) of Fig. 6.8 are shown in Fig. 6.9. Since the deuteron wave function is isoscalar, the $\not P\not T$ currents need to be isoscalar as well in order to contribute to the MQM. Only the current in diagram (c), which stems from qEDM, meets this requirement, and we find

$$\vec{J}_{\not P\not T}(\vec{q},\vec{k}) = -\frac{g_A \bar{c}_0}{F_\pi^2}\boldsymbol{\tau}^{(1)}\cdot\boldsymbol{\tau}^{(2)}\left[\vec{\sigma}^{(1)}\times\vec{q}\,\frac{\vec{\sigma}^{(2)}\cdot(\vec{k}-\vec{q}/2)}{(\vec{k}-\vec{q}/2)^2+m_\pi^2} - \vec{\sigma}^{(2)}\times\vec{q}\,\frac{\vec{\sigma}^{(1)}\cdot(\vec{k}+\vec{q}/2)}{(\vec{k}+\vec{q}/2)^2+m_\pi^2}\right]. \quad (6.68)$$

In diagram classes (b) and (c) of Fig. 6.8 the photon interacts instead with a PT current. The PT one-body current in diagram (b) is either the nucleon magnetic moment or the convection current coming from gauging the nucleon kinetic energy in Eq. (3.25),

$$\vec{J}_{PT}(\vec{q},\vec{p}_i) = \frac{e}{4m_N}\left\{\left[1+\kappa_0+(1+\kappa_1)\,\tau_3^{(i)}\right] i\vec{\sigma}^{(i)}\times\vec{q} + \left(1+\tau_3^{(i)}\right)(2\vec{p}_i-\vec{q})\right\}, \quad (6.69)$$

where i is the index of the nucleon that interacts with the photon. In diagram (c) we require the PT two-body currents depicted in Fig. 6.10:

$$\begin{aligned}\vec{J}_{PT}(\vec{q},\vec{k}) &= i\frac{eg_A^2}{F_\pi^2}\left(\boldsymbol{\tau}^{(1)}\times\boldsymbol{\tau}^{(2)}\right)_3\left\{-2\vec{k}\,\frac{\vec{\sigma}^{(1)}\cdot(\vec{k}+\vec{q}/2)}{(\vec{k}+\vec{q}/2)^2+m_\pi^2}\,\frac{\vec{\sigma}^{(2)}\cdot(\vec{k}-\vec{q}/2)}{(\vec{k}-\vec{q}/2)^2+m_\pi^2}\right.\\ &\left. +\vec{\sigma}^{(1)}\,\frac{\vec{\sigma}^{(2)}\cdot(\vec{k}-\vec{q}/2)}{(\vec{k}-\vec{q}/2)^2+m_\pi^2} + \vec{\sigma}^{(2)}\,\frac{\vec{\sigma}^{(1)}\cdot(\vec{k}+\vec{q}/2)}{(\vec{k}+\vec{q}/2)^2+m_\pi^2}\right\}. \quad (6.70)\end{aligned}$$

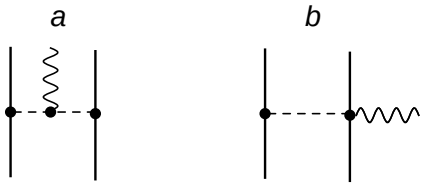

Figure 6.10: Diagrams contributing to the PT two-nucleon current.

With the methods outlined in App. D, these currents can straightforwardly be Fourier transformed to coordinate space, where we denote by $\vec{x}^{(i)}$ the position of nucleon i and by $\vec{r} = \vec{x}^{(1)} - \vec{x}^{(2)}$ the relative position. We also introduce the Yukawa function

$$U(r) = \frac{e^{-m_\pi r}}{4\pi r}\,. \tag{6.71}$$

The MQM operators are, from Eq. (6.68),

$$\begin{aligned}\widetilde{M}_{33} &= 2\,\frac{g_A \bar{c}_0}{F_\pi^2}\boldsymbol{\tau}^{(1)}\cdot\boldsymbol{\tau}^{(2)}\left[\left(3\,\sigma_3^{(1)}x_3^{(1)} - \vec{\sigma}^{(1)}\cdot\vec{x}^{(1)}\right)\vec{\sigma}^{(2)}\right.\\ &\quad\left.-\left(3\,\sigma_3^{(2)}x_3^{(2)} - \vec{\sigma}^{(2)}\cdot\vec{x}^{(2)}\right)\vec{\sigma}^{(1)}\right]\cdot\vec{\nabla}_r U(r)\,,\end{aligned} \tag{6.72}$$

and from Eqs. (6.69) and (6.70),

$$\begin{aligned}M_{33} &= \frac{e}{2m_N}\left\{\left[1+\kappa_0+(1+\kappa_1)\tau_3^{(i)}\right]\left(3\,\sigma_3^{(i)}x_3^{(i)} - \vec{\sigma}^{\,(i)}\cdot\vec{x}^{\,(i)}\right)\right.\\ &\quad\left.+2\left(1+\tau_3^{(i)}\right)\vec{x}_3^{(i)}\,(\vec{x}^{(i)}\times\vec{p}^{(i)})_3\right\}\\ &\quad-\frac{e g_A^2}{2F_\pi^2}\left(\boldsymbol{\tau}^{(1)}\times\boldsymbol{\tau}^{(2)}\right)_3\left\{\left[\sigma_3^{(1)}\left(\vec{\sigma}^{(2)}\times\vec{r}\right)_3 + \sigma_3^{(2)}\left(\vec{\sigma}^{(1)}\times\vec{r}\right)_3\right]\right.\\ &\quad\left.+4\Big[x_3^{(1)}\left(\vec{x}^{(1)}\times\vec{\sigma}^{(1)}\right)_3\vec{\sigma}^{(2)} + x_3^{(2)}\left(\vec{x}^{(2)}\times\vec{\sigma}^{(2)}\right)_3\vec{\sigma}^{(1)}\Big]\cdot\vec{\nabla}_r\right\}U(r)\,,\end{aligned} \tag{6.73}$$

where $\vec{p}^{(i)} = -i\vec{\nabla}_{x^{(i)}}$.

We can now calculate the deuteron MQM from Eq. (6.62). For comparison with the deuteron EDM, we give below numbers corresponding to the Argonne v_{18} (AV18) potential [103]. Differences with results obtained from the NijmII and Reid93 potentials [102] are within a few percent, except for the cases of $\bar{C}_{1,2}$ insertion—for which more details will be provided later.

The ground state of the deuteron is mainly a ${}^3S_1$ state with some ${}^3D_1$ admixture. The matrix element of $\widetilde{\boldsymbol{M}}$ is found to be

$$\frac{1}{\sqrt{30}}\langle\Psi_d||\widetilde{\boldsymbol{M}}||\Psi_d\rangle = 0.07\frac{F_\pi\bar{c}_0}{e}\;e\,\mathrm{fm}^2. \tag{6.74}$$

If the parity admixture comes from a $\bar{g}_1$ pion exchange, the deuteron wave function acquires a ${}^3P_1$ component. In order to get back to the ground state, the deuteron can couple to the photon via the isovector one-body or the two-body currents in Eqs. (6.69) and (6.70), respectively. The result is

$$\frac{2}{\sqrt{30}}\langle\Psi_d||\boldsymbol{M}||\widetilde{\Psi}_d({}^3P_1)\rangle = -\left[0.031(1+\kappa_1) + 0.003 + 0.008\right]\frac{\bar{g}_1}{F_\pi}\;e\,\mathrm{fm}^2, \tag{6.75}$$

where the first and second terms come from the isovector magnetic moment due to the spin and convection current, respectively; and the third term from the PT two-body current.

After a $\bar{g}_0$ pion exchange or an insertion of $\bar{C}_{1,2}$ the deuteron wave function obtains a ${}^1P_1$ component instead. In this case, the deuteron needs to couple to the isoscalar nucleon magnetic moment or an isoscalar two-body current, which is not present at LO. The result is

$$\frac{2}{\sqrt{30}}\langle\Psi_d||\boldsymbol{M}||\widetilde{\Psi}_d({}^1P_1)\rangle = -\left[0.044\,\frac{\bar{g}_0}{F_\pi} + 0.0013F_\pi^3\left(\bar{C}_1 - 3\bar{C}_2\right)\right](1+\kappa_0)\;e\,\mathrm{fm}^2. \tag{6.76}$$

As before, the contact interaction with

$$\bar{C}_0 \equiv \bar{C}_1 - 3\bar{C}_2 \tag{6.77}$$

is simulated by a fictitious heavy-meson (of mass m) exchange, since

$$\frac{m^2\bar{C}_0}{4\pi r}e^{-mr} \quad\to\quad \bar{C}_0\delta^{(3)}(\vec{r}) \tag{6.78}$$

as m goes to infinity. As shown in Fig. 6.11, when m reaches 2.5 GeV, the results converge at about $\lesssim 10\%$ level, so we report the above numbers at this scale. While in this figure one sees good consistency between the AV18 and NijmII results, the Reid93 result is off by a factor of 2. The main reason is that the Reid93 potential generates a deuteron S state whose short-distance wave function is enhanced, leading to more sensitivity to $\bar{C}_0$. The large discrepancy between different potentials suggests that for χI sources, for which $\bar{C}_0$ contributes to the MQM at leading order, a fully consistent calculation of Ψ_d within EFT is necessary if this part of the matrix element needs to be known better than within a factor of 2.

The dependence of the deuteron MQM on $\bar{g}_{0,1}$, $\bar{C}_0$, and $\bar{c}_0$ was studied in Chapter 5 in a framework where pion exchange is treated perturbatively. At LO in that framework, the coefficients in front of $\bar{g}_0(1+\kappa_0)/F_\pi$ and $\bar{g}_1(1+\kappa_1)/F_\pi$ were found to be, respectively, -0.146 and -0.049, in agreement with the results in Ref. [80] where a zero-range approximation for the NN interaction was assumed. Considering the large intrinsic uncertainty ($\sim 30\%$) in the perturbative-pion calculation, the perturbative-pion $\bar{g}_1$ coefficient is in reasonable agreement with Eq. (6.75). A similar agreement was found for the deuteron EDM in Sect. 6.5. On the other hand, the perturbative-pion $\bar{g}_0$ coefficient is three times larger than Eq. (6.76), suggesting that the effects of additional pion exchanges, neglected in the LO perturbative calculation, are larger in the ${}^1P_1$ channel than in the ${}^3P_1$ channel. We have verified that, if the tensor force is ignored and the same strong force is assumed for both the ${}^1P_1$ and ${}^3P_1$ channels, the ratio of the strong parts of the MQM matrix elements due to the isoscalar and isovector one-body currents becomes 3, which is consistent with Eq. (5.23). Preliminary results in Sect. 5.5 of an NLO calculation in the perturbative-pion framework indicate that, indeed, NLO corrections influence the $\bar{g}_0$ coefficient by a larger amount than the $\bar{g}_1$ coefficient.

In the framework of perturbative pions, the PT convection and two-body currents in diagram (b) and (c) of Fig. 6.8 enter at NLO and are expected to be smaller than the contribution from the isovector magnetic moment. This agrees with the numerical results in Eq. (6.75) where the convection and two-body currents only enter at the $\sim 5\%$ level. These currents would have been small ($\sim 30\%$) even if the isovector magnetic moment had been more natural, that is, if $1+\kappa_1$ were $\simeq 1$.

The result for $\bar{c}_0$ in Eq. (6.74) is somewhat smaller than expected from the power-counting estimate in Eq. (6.66), $\mathcal{M}_d(\mathrm{qEDM}) \sim 0.2F_\pi\bar{c}_0\,\mathrm{fm}^2$, and is more in line with the expectation of the perturbative-pion calculation, $\mathcal{O}(\gamma\bar{c}_0/M_{NN}M_{\mathrm{QCD}}) \sim 0.07F_\pi\bar{c}_0\,\mathrm{fm}^2$, where $M_{NN} = 4\pi F_\pi^2/g_A^2 m_N$ is the characteristic scale where pions become nonperturbative [92] and γ the deuteron binding momentum. A more detailed comparison with the perturbative-pion calculation is complicated

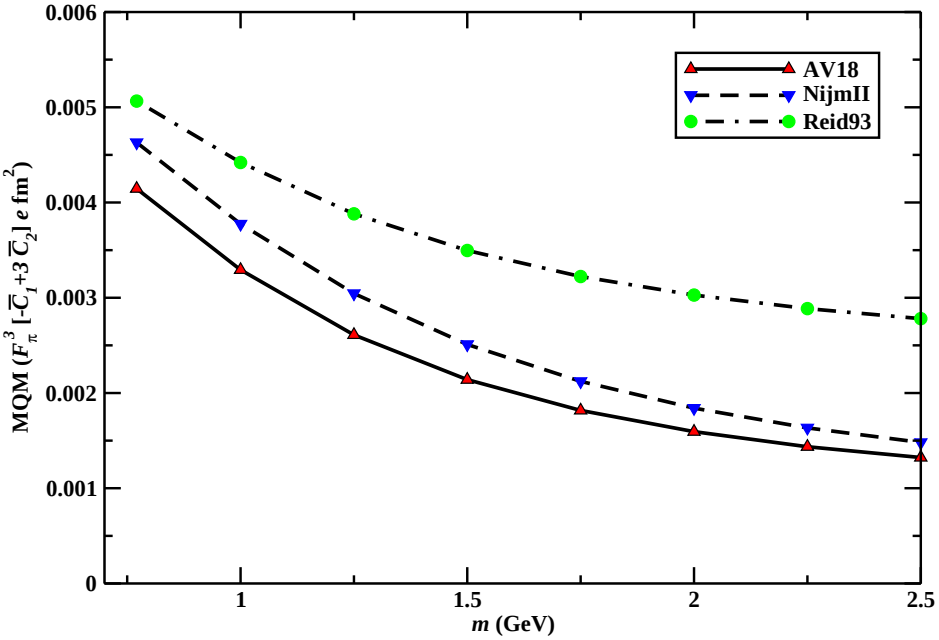

Figure 6.11: Deuteron MQM due to the $F_\pi^3(-\bar{C}_1 + 3\bar{C}_2)$ short-range $\not{P}\not{T}$ interaction as function of a regulating mass m, for various PT Hamiltonians.

by the appearance of a short-range current, which is needed for renormalization purposes. Neglecting the counterterm and using for the renormalization scale $\mu = M_{NN}$ in Eq. (5.23), the perturbative result becomes $0.08 F_\pi \bar{c}_0\,\mathrm{fm}^2$, in good agreement with Eq. (6.74). A comparison between the contributions from the short-range $\not{P}\not{T}$ NN interactions in the perturbative and nonperturbative calculations is not useful because the LEC $\bar{C}_0$ includes different physics and thus has different scalings in the two EFTs.

The deuteron MQM was previously calculated in Refs. [80, 81], in which the deuteron MQM was assumed to be dominated by $\not{P}\not{T}$ one-pion exchange (OPE). Since these calculations did not use the chiral properties of the fundamental $\not{P}\not{T}$ sources, the $\not{P}\not{T}$ πN interactions were assumed to be all of the same size. Our analysis shows that these assumptions only hold in case of a qCEDM or FQLR. For $\bar{g}_0$ and $\bar{g}_1$ OPE we confirm the results in Ref. [81], but our $\bar{g}_0$ result is 3 times smaller than the result in Ref. [80] due the discrepancy discussed above.

We are now in the position to discuss the results for the various $\not{P}\not{T}$ sources. It was noted in Chapter 5 that the observation of a deuteron MQM, together with the nucleon and deuteron EDMs, could provide important clues to separate the various $\not{P}\not{T}$ sources. In particular, it was concluded that only for chiral-symmetry-breaking, but isoscalar, sources like the QCD $\bar{\theta}$ term is the deuteron MQM, in appropriate units, substantially larger than the deuteron EDM. For chiral- and isospin-breaking sources, like the qCEDM and FQLR, the deuteron MQM and EDM are expected to be of the same size, and a measurement of both would fix the couplings $\bar{g}_0$ and $\bar{g}_1$, allowing a prediction of other $\not{P}\not{T}$ observables, like the ^{3}He EDM. For the χI sources and the qEDM, in the perturbative-pion approach the MQM depends on one- and two-body LECs that

do not contribute to the EDM. For these sources the MQM was found to be of the same size, or slightly smaller, than the EDM, but an observation of the MQM would not give us predictive power. These conclusions, based on the perturbative-pion power counting, are confirmed here by the nonperturbative results.

For the QCD $\bar{\theta}$ term, the deuteron EDM is dominated by the isoscalar nucleon EDM, $d_d \sim 2\bar{d}_0$. A naturalness lower bound on the isoscalar nucleon EDM is provided by the nonanalytic terms stemming from the pion cloud in Eq. (4.13), $|\bar{d}_0| \gtrsim 0.01(|\bar{g}_0|/F_\pi)\, e\,\text{fm}$. The deuteron MQM is dominated by the $\bar{g}_0$ piece in Eq. (6.76). Combining the two with the deuteron mass m_d, we find

$$\left|\frac{m_d \mathcal{M}_d}{d_d}\right| \simeq 0.21(1+\kappa_0)\left|\frac{\bar{g}_0}{F_\pi \bar{d}_0}\right| e\,\text{fm} \lesssim 21(1+\kappa_0). \tag{6.79}$$

At LO in the perturbative-pion approach, this ratio is about three times larger, as discussed above. Nonetheless, the nonperturbative calculation confirms that for isoscalar chiral-breaking sources the deuteron MQM is expected to be larger than the EDM in units of m_d.

In case of the qCEDM or FQLR, where $\bar{g}_0$ and $\bar{g}_1$ have similar scalings, both the deuteron EDM and MQM are dominated by pion exchange. At LO, the EDM depends on $\bar{g}_1$ only, and the MQM on the $\bar{g}_{0,1}$ contributions in Eqs. (6.75) and (6.76). The MQM/EDM ratio becomes

$$\frac{m_d \mathcal{M}_d}{d_d} \simeq 1.6(1+\kappa_1) + 2.2(1+\kappa_0)\frac{\bar{g}_0}{\bar{g}_1} + 0.6, \tag{6.80}$$

which formally is $\mathcal{O}(1)$. However, due to the large anomalous isovector magnetic moment, numerically the ratio could be $\mathcal{O}(10)$. This means that the measurement of a large MQM/EDM ratio does not necessarily imply that the $\bar{\theta}$ term is the dominant $\not{P}\not{T}$ mechanism.

If a qEDM is the dominant $\not{P}\not{T}$ source, the MQM is given by Eq. (6.74). It is solely coming from a two-body $\not{P}\not{T}$ current. The EDM is given by the sum of the neutron and the proton EDM, $d_d \simeq 2\bar{d}_0$. Combining these results gives

$$\frac{m_d \mathcal{M}_d}{d_d} \simeq 0.7\frac{\bar{c}_0}{\bar{d}_0}, \tag{6.81}$$

which is $\mathcal{O}(1)$ by NDA. As we observed in the previous discussion, the matrix element of the operator with coefficient $\bar{c}_0$ is smaller than the power-counting estimate, so a more accurate conclusion is that, for $\not{P}\not{T}$ from the qEDM, the deuteron MQM is expected to be slightly smaller than the EDM, in agreement with Chapter 5.

Finally, for χI sources, the MQM is dominated by the sum of Eqs. (6.75) and (6.76). From the NDA estimates in Eq. (6.5), we find $F_\pi^4 \bar{C}_0/\bar{g}_0 = \mathcal{O}(F_\pi^2/m_\pi^2) \simeq 2$, such that the $\bar{C}_0$ contribution only enters at the $\sim 10\%$ level. The deuteron EDM at LO formally depends on $\bar{g}_1$ and the isoscalar nucleon EDM, but numerically the latter is expected to dominate, with pion-exchange corrections at the $\sim 15\%$ level. Ignoring the numerically small convection and two-body currents,

$$\left|\frac{m_d \mathcal{M}_d}{d_d}\right| \simeq \left[0.21(1+\kappa_0)\left|\frac{\bar{g}_0}{F_\pi \bar{d}_0}\right| + 0.15(1+\kappa_1)\left|\frac{\bar{g}_1}{F_\pi \bar{d}_0}\right|\right] e\,\text{fm}. \tag{6.82}$$

By power counting we would expect the ratio to be $\mathcal{O}(1)$, but since the deuteron is weakly bound, pion exchange is smaller than expected. Using the NDA estimate $|\bar{d}_0| \sim 5(|\bar{g}_{0,1}|/F_\pi)\, e\,\text{fm}$, we conclude that for χI sources the deuteron MQM should be smaller than the EDM, in disagreement with Chapter 5 where, purely based on power counting we expected them to be of similar size.

In conclusion, we computed the deuteron MQM for various $\not{P}\not{T}$ sources: the QCD $\bar{\theta}$ term, quark EDM, quark and gluon chromo-EDMs, chiral- and isospin-breaking and chiral-invariant four-quark operators. We performed these computations at leading order in the framework of chiral EFT, with pions treated nonperturbatively. The same parameters as in the corresponding calculation of light-nuclear EDMs appeared here, except for the quark EDM, which involves an independent short-range two-nucleon current. While the results confirm the qualitative conclusions of Chapter 5, there are important quantitative differences. Due to its enhanced sensitivity to the QCD $\bar{\theta}$ term, a potential measurement of the deuteron MQM would be complementary to one of the deuteron EDM.

Chapter 7

Summary, Conclusions, and Outlook

The search for new physics is usually associated with high-energy collider experiments such as the LHC in Geneva. However, certain high-precision experiments performed at low energies are sensitive probes to physics beyond the Standard Model (SM) as well. This thesis is focused on one of these low-energy tests: the search for permanent electric dipole moments (EDMs). EDMs break parity (P) and time-reversal symmetry (T) and, by the CPT theorem, CP symmetry.

In the foreseeable future, a measurement of a nonzero permanent EDM of any particle or system would be an unambiguous sign of new physics, since CP violation due to the quark-mixing matrix predict EDMs orders of magnitude smaller than experimental limits. The SM also contains the QCD vacuum angle $\bar{\theta}$ whose value is unknown but strongly limited by neutron EDM experiments. This smallness leaves room for T violation from physics beyond the SM. In fact, the existence of such a source is well motivated by the universal asymmetry between matter and antimatter. In addition, many extensions of the SM, *e.g.* supersymmetry, include additional T-violating sources and as a consequence predict relatively large EDMs. Such models are strongly constrained by the current null-measurements of EDMs. Of course, the hope is that a nonzero EDM will be found in one of the upcoming experiments. An important open question that remains is whether it will be possible to identify from nonzero EDM measurements, the fundamental, microscopic theory of T and CP violation.

In this thesis a framework based on effective field theories (EFTs) has been developed which can answer this question for measurements of hadronic EDMs. Physics responsible for new T violation originates in a scale considerably higher than the electroweak scale. At the latter scale, the heavy degrees of freedom appearing in the new physics models can be integrated out and their effects can be parametrized by adding to the SM all possible contact interactions in terms of SM fields only and obeying the SM symmetries. The effective T-violating interactions start at dimension six and are suppressed by two powers of a heavy mass scale (typically the mass of the particles appearing in the underlying microscopic theory). In Chapter 2 we list the T-violating dimension-six operators and identify which of them are important for hadronic EDMs. A major advantage of this approach is that we do not need to specify a particular model of new physics, which allows us to work model independently.

In order to calculate EDMs of hadrons and nuclei we have to bring our effective Lagrangian to low-energy scales where the coupling constant of QCD becomes too strong to do perturbation theory. In Chapter 3 we overcome this problem by applying chiral perturbation theory (χPT), an EFT of the strong interaction. By extending χPT to include T violation we recast our effective Lagrangian in terms of quarks and gluons into a chiral Lagrangian involving pions and nucleons. By keeping track of how the different sources of T violation, *i.e* the $\bar{\theta}$ term and the dimension-six operators, transform under chiral symmetry, we derive for each source a unique T-violating

chiral Lagrangian. For example, for sources that break chiral symmetry, such as the $\bar{\theta}$ term and quark chromo-EDM, the most important T-violating interactions are nonderivative pion-nucleon couplings. These interactions give rise to long-range T-violating forces between nucleons which dominate EDMs of light nuclei. For sources such as the gluon chromo-EDM, which are chiral invariant, pion-nucleon interactions are suppressed and local T-violating nucleon-nucleon interactions need to be taken into account. Additionally, for such sources nuclear EDMs obtain important contributions from the EDMs of the constituent nucleons. It is also important to keep track of how certain fundamental sources break chiral symmetry. A quark chromo-EDM breaks isospin symmetry and creates isospin-breaking pion-nucleon interactions, while interactions induced by the $\bar{\theta}$ term are dominantly isospin conserving. These differences are systematically derived in Chapter 3.

The different chiral Lagrangians are put to use in Chapters 4-6, where calculations are performed of T-violating observables in hadronic and nuclear systems. The advantage of our EFT approach is that these calculations are done in a unified and perturbative framework which allows us to estimate theoretical uncertainties and the results can be improved systematically. Chapter 4 focuses on the T-violating electromagnetic properties of the nucleon. We conclude that measurements of the neutron and proton EDM would not be enough to pinpoint the dominant source of T violation. Some additional information can be obtained from measuring the first corrections to the EDMs, the nucleon Schiff moments, however, even full information on these observables would not be sufficient to separate $\bar{\theta}$ from the dimension-six sources.

More promising observables are discussed in Chapter 5, *i.e.* the deuteron electric dipole and magnetic quadrupole moment (MQM). The deuteron EDM is sensitive to isospin-breaking pion-nucleon interactions. Sources that induce such interactions predict a deuteron EDM significantly larger than the proton or neutron EDM. Measuring a large deuteron-to-nucleon EDM ratio would indicate that physics beyond the SM is present, in the shape of a quark chromo-EDM or a particular four-quark interaction. On the other hand, if a deuteron EDM is found and its value lies close to the sum of the nucleon EDMs, we cannot say whether it was due to the SM $\bar{\theta}$ term or due to beyond-the-SM physics. In that case, a measurement of the deuteron MQM could play a pivotal role. Only the $\bar{\theta}$ term predicts the deuteron MQM to be larger than the deuteron EDM, giving an MQM measurement unique sensitivity.

The conclusions on the deuteron T-violating moments are based on a perturbative-pion approach to nuclear EFT, which assumes that pion exchange can be treated perturbatively. In Chapter 6 we relax this assumption and extend our framework to general light nuclei. Within this nonperturbative-pion framework we confirm the conclusions on the deuteron EDM and MQM. Furthermore, we perform explicit calculations of the EDMs of the triton (^{3}H) and helion (^{3}He), giving additional input for separating the different T-violating mechanisms. If other light nuclei, for example lithium isotopes, become the target of experimental investigation, our framework allows their calculation along similar lines.

In conclusion, we have argued that an experimental program to measure nucleon and light nuclear EDMs and higher moments could offer valuable information on yet undiscovered sources of parity and time-reversal violation. Our case is based on some crucial, but relatively general assumptions, such as the validity of the SM with its minimal particle content at the electroweak scale, and the naturalness of interaction strengths.

The work in this thesis can in a natural way be extended in several directions. It would be interesting to extend our EFT approach to heavier nuclei. The EDMs of diamagnetic atoms such as ^{199}Hg and ^{225}Ra are expected to be dominated by the Schiff moment of the nucleus [108]. A many-body nuclear calculation of these moments has recently been performed in terms of the

T-violating nonderivative pion-nucleon interactions and nucleon EDMs [83]. However, short-range NN interactions, important for chiral-invariant sources, were not taken into account. If it is possible to include these interactions in the calculations, we could interpret the EDMs of diamagnetic atoms in a similar way as we have done for the EDMs of light nuclei. One could also think of extending our work to include (semi-)leptonic interactions. The list of dimension-six sources can be supplemented by lepton EDMs, lepton-quark, and four-lepton interactions. At the cost of additional unknown coupling constants, this would, in principle, allow the inclusion of paramagnetic atoms and molecules into our framework. Of course, performing calculations on these complicated systems is a very nontrivial task.

There is also some unfinished business within this thesis which needs to be taken care of. First of all, the calculation of the NLO corrections in Sect. 5.5 needs to be completed, providing an important check of the convergence of the perturbative-pion approach. Additionally, NLO corrections to the deuteron, triton, and helion EDMs in the nonperturbative approach should be calculated, again, in order to check the convergence of the chiral series.

In Chapter 2 we basically performed a tree-level matching between the T-violating Lagrangians at the electroweak and QCD scale. A full matching calculation, including QCD corrections and effects of heavier fields, is needed to accurately interpret the coupling constants in Eq. (2.57) in terms of those appearing at the electroweak scale in Eqs. (2.16)-(2.20). We are working on this matching calculation, but at the moment it is not at a stage fit for including it here. Once the relations between the electroweak and QCD Lagrangian are known, we are in a good position to study specific models beyond the SM. We first match them to the effective Lagrangian at the electroweak scale by integrating out the new heavy fields. We can then match this Lagrangian to the Lagrangian at the QCD scale, then to the chiral Lagrangians in Chapter 3, and finally to the hadronic and nuclear T-violating observables (this flowing of T violation through the different energy scales was schematically depicted in the introduction, see Fig. 1.2). In this way it is possible to quickly and accurately calculate the low-energy EDM predictions of various beyond-the-SM models.

Finally, this work would benefit greatly from lattice-QCD calculations of the low-energy constants appearing in the chiral Lagrangians.

Appendix A

Reparametrization Invariance

In heavy-baryon chiral perturbation theory (HBχPT) [57] the heavy baryons, in our case the nucleons with mass m_N, are described by their velocity v and a residual momentum k,

$$p^\mu = m_N v^\mu + k^\mu. \tag{A.1}$$

The effective theory can be rewritten in heavy fields with a fixed velocity

$$N_v = e^{i m_N v\cdot x} N, \tag{A.2}$$

such that derivatives acting on the heavy fields give powers of the small residual momenta. Since in χPT each additional derivative is associated with one inverse power of $M_{\rm QCD}$, observables can be expanded in powers of k/M_{QCD}. It is convenient to further decompose the fields as

$$N_\pm = \frac{1}{2}(1 \pm \not{v}) N_v. \tag{A.3}$$

The free part of the Lagrangian becomes

$$\begin{aligned} \mathcal{L} &= \bar{N}(i\not{\mathcal{D}} - m_N)N = \bar{N}_v(i\not{\mathcal{D}} - m_N(1-\not{v}))N_v \\ &= \bar{N}_+(iv\cdot\mathcal{D})N_+ - \bar{N}_-(iv\cdot\mathcal{D} + 2m_N)N_m + \bar{N}_+ i\not{\mathcal{D}} N_- + \bar{N}_- i\not{\mathcal{D}} N, \end{aligned} \tag{A.4}$$

from which the propagators of the N_+ field $i/(v\cdot\mathcal{D})$ and the N_- field

$$-\frac{1}{2m_N + iv\cdot\mathcal{D}} = -\frac{1}{2m_N} + \frac{iv\cdot\mathcal{D}}{4m_N^2} + \mathcal{O}\left(\frac{1}{m_N^3}\right), \tag{A.5}$$

can be read off. We see that at LO the mass of N_+ is removed, whereas the N_- field does not propagate. The fields can be interpreted as, respectively, the nucleon and antinucleon field. To apply HBχPT the massive N_- field needs to be integrated out [60].

The decomposition of the nucleon momenta into its velocity and a residual momenta in Eq. (A.1) is somewhat arbitrary in the sense that we can shift the velocity a bit and absorb this into the residual momentum. Our calculations should not depend on these shifts, and therefore our Lagrangian should be invariant under the transformations

$$\begin{aligned} v^\mu &\to v^\mu + \frac{\epsilon^\mu}{m_N}, \\ k^\mu &\to k^\mu - \epsilon^\mu, \end{aligned} \tag{A.6}$$

where $\epsilon \ll m_N$ and $v\cdot\epsilon = \frac{-\epsilon^2}{2m_N}$. This nontrivial requirement on the Lagrangian is known as reparametrization invariance [58]. It can be used to relate coefficients of operators of different order in the Q/M_{QCD} expansion enforcing Lorentz covariance order by order in the expansion. Although the RPI transformations look simple, the transformation of the heavy fields themselves under RPI is more complicated. The proper transformation was derived in Refs. [59, 60] for heavy-quark effective field theory. We briefly rederive the correct transformation by the path-integral method of Ref. [60] and show how to extend this to χPT.

If we ignore NN interactions the most general RPI chiral Lagrangian is given by

$$\mathcal{L} \;=\; \bar{N}_v \left[S + iP\gamma_5 + \not{V} + \not{A}\gamma_5 + T^{\mu\nu}\sigma_{\mu\nu}\right] N_v, \tag{A.7}$$

where S, P, V^μ, A^μ, and $T^{\mu\nu}$ are hermitian gauge-invariant operators build from combinations of nucleon covariant derivatives and v in the combination $v + i\mathcal{D}/m_N$, and (covariant derivatives of) light fields (in our case either pions or photons). The RPI Lagrangian in terms of the light and heavy fields is

$$\begin{aligned}\mathcal{L} \;=\;& \bar{N}_+ \left[S + v\cdot V + 2S^\mu A_\mu + T^{\mu\nu}\sigma_{\mu\nu}\right] N_+ + \bar{N}_- \left[S - v\cdot V - 2S^\mu A_\mu + T^{\mu\nu}\sigma_{\mu\nu}\right] N_- \\ &+ \bar{N}_+ \left[(iP + \not{A})\gamma_5 + \not{V}_\perp + T^{\mu\nu}\sigma_{\mu\nu}\right] N_- + \bar{N}_- \left[(iP + \not{A})\gamma_5 + \not{V}_\perp + T^{\mu\nu}\sigma_{\mu\nu}\right] N_+, \end{aligned}\tag{A.8}$$

where we used [57]

$$\begin{aligned} \bar{N}_\pm \gamma^\mu N_\pm &= \pm v^\mu \bar{N}_\pm N_\pm, \qquad & \bar{N}_\pm \gamma_5 N_\pm &= 0, \\ \bar{N}_\pm \gamma^\mu \gamma_5 N_\pm &= \pm 2 \bar{N}_\pm S^\mu N_\pm, \qquad & \bar{N}_\pm \sigma^{\mu\nu} N_\pm &= -2\varepsilon^{\mu\nu\alpha\beta} v_\alpha \bar{N}_\pm S_\beta N_\pm, \end{aligned}\tag{A.9}$$

with $\epsilon^{0123} = 1$ and the spin operator defined by $[S^\mu, S^\nu] \equiv \frac{i}{2}\sigma^{\mu\nu}$, with $S = (\vec{\sigma}/2, 0)$ in the rest frame $v = (\vec{0}, 1)$, and the properties in d dimensions

$$v\cdot S = 0, \;\; S^2 = \frac{1-d}{4}, \;\; [S^\mu, S^\nu] = -i\varepsilon^{\mu\nu\alpha\beta} v_\alpha S_\beta, \;\; \{S^\mu, S^\nu\} = \frac{1}{2}(v^\mu v^\nu - g^{\mu\nu}). \tag{A.10}$$

We use a subscript $\perp$ to denote the component of a four-vector perpendicular to the velocity,

$$V_\perp^\mu = V^\mu - v^\mu v\cdot V. \tag{A.11}$$

Integrating out N_- in Eq. (A.8) can be done via the antinucleon equation of motion

$$N_- \;=\; -\frac{1}{S - v\cdot V - 2S^\mu A_\mu + T^{\mu\nu}\sigma_{\mu\nu}} \left[(iP + \not{A})\gamma_5 + \not{V}_\perp + T^{\mu\nu}\sigma_{\mu\nu}\right] N_+, \tag{A.12}$$

which, together with Eqs. (A.2) and (A.3), gives the correct RPI transformation of the nucleon field

$$\begin{aligned} v^\mu \;&\to\; v^\mu + \frac{\epsilon^\mu}{m_N}, \\ N_+ \;&\to\; \left(\frac{1+\not{v}}{2} + \frac{\not{\epsilon}}{2m_N}\right) \epsilon^{i\epsilon\cdot x}(N_+ + N_-) \\ &=\; \epsilon^{i\epsilon\cdot x}\left[1 + \frac{\not{\epsilon}}{2m_N}\left(1 - \frac{(iP + \not{A})\gamma_5 + \not{V}_\perp + T^{\mu\nu}\sigma_{\mu\nu}}{S - v\cdot V - 2S^\mu A_\mu + T^{\mu\nu}\sigma_{\mu\nu}}\right)\right] N_+. \end{aligned}\tag{A.13}$$

RPI tells us that a Lagrangian consisting of light fields and N_+ fields only must be invariant under the transformations in Eq. (A.13).

At LO the χPT Lagrangian in terms of the relativistic nucleon field is

$$\begin{aligned}\mathcal{L}^{(0)} &= \bar{N}\left(i\not{\mathcal{D}} - m_N - \frac{g_A}{F_\pi}(\boldsymbol{\tau}\cdot D_\mu\boldsymbol{\pi})\gamma^\mu\gamma_5\right)N \\ &= \bar{N}_v\left(i\not{\mathcal{D}} - m_N(1-\not{v}) - \frac{g_A}{F_\pi}(\boldsymbol{\tau}\cdot D_\mu\boldsymbol{\pi})\gamma^\mu\gamma_5\right)N_v. \end{aligned} \tag{A.14}$$

A comparison with Eq. (A.7) gives the LO identifications

$$S = -m_N, \quad V^\mu = m_N\left(v^\mu + i\frac{\mathcal{D}^\mu}{m_N}\right), \quad A^\mu = -\frac{g_A}{F_\pi}\boldsymbol{\tau}\cdot D^\mu\boldsymbol{\pi}, \quad P = T^{\mu\nu} = 0, \tag{A.15}$$

such that the correct RPI transformation is given by

$$\begin{aligned} v^\mu &\to v^\mu + \frac{\epsilon^\mu}{m_N}, \\ N_+ &\to \epsilon^{i\epsilon\cdot x}\left[1 + \frac{\not{\epsilon}}{2m_N}\left(1 + \frac{i\not{\mathcal{D}}_\perp - (g_A/F_\pi)(\boldsymbol{\tau}\cdot D_\mu\boldsymbol{\pi})\gamma^\mu\gamma_5}{2m_N + iv\cdot\mathcal{D} - (2g_A/F_\pi)(\boldsymbol{\tau}\cdot D_\mu\boldsymbol{\pi})S^\mu}\right)\right]N_+, \\ &= \epsilon^{i\epsilon\cdot x}\left[1 + \frac{\not{\epsilon}}{2m_N} + \frac{i}{4m_N^2}\not{\epsilon}\not{\mathcal{D}}_\perp - \frac{g_A\boldsymbol{\tau}\cdot D_\mu\boldsymbol{\pi}}{4F_\pi m_N^2}\not{\epsilon}\gamma^\mu\gamma^5\right]N_+ + \mathcal{O}\left(\frac{1}{m_N^3}\right). \end{aligned} \tag{A.16}$$

We truncate the expansion at this order, since higher-order corrections require the inclusion of $\mathcal{O}(M_{QCD}^{-1})$ corrections to S, P, V^μ, A^μ, and $T^{\mu\nu}$. The RPI constraints in Eqs. (3.61), (3.74), (3.81), (3.99), (3.103), (3.105), and (3.109) were derived by demanding the Lagrangian to be invariant under Eq. (A.16). In the main text we have dropped the subscript + on the nucleon field.

Appendix B

Naive Dimensional Analysis

In order to estimate the size of the LECs appearing in the chiral Lagrangian we apply a technique called Naive Dimensional Analysis (NDA). This technique was invented by Georgi and Manohar in order to explain the success of the chiral quark model [63]. Here we do not consider this model but use NDA to estimate the LECs appearing in the $\not{P}\not{T}$ chiral Lagrangian. To illustrate the idea of NDA consider the pion kinetic term for massless QCD, which is of the form

$$\mathcal{L} \;=\; \frac{1}{2}(D_\mu \boldsymbol{\pi})^2 = \frac{1}{2}(\partial_\mu \boldsymbol{\pi})^2 - \frac{1}{F_\pi^2}\boldsymbol{\pi}^2(\partial_\mu \boldsymbol{\pi})^2 + \mathcal{O}(\boldsymbol{\pi}^6). \tag{B.1}$$

We can use the four-pion vertex to calculate a simple bubble loop diagram contributing to pion-pion scattering. A particular piece of this diagram has all the derivatives acting on the external pions with momentum p, such that this part is proportional to

$$\frac{p^4}{F_\pi^4}\int \frac{\mathrm{d}^4k}{(2\pi)^4}\left(\frac{1}{k^2}\right)^2 \simeq \frac{p^4}{F_\pi^4}\frac{1}{(2\pi)^2}\log\frac{M_{\mathrm{QCD}}}{\mu}, \tag{B.2}$$

where M_{QCD} is the cutoff and μ the renormalization scale. The μ dependence of the diagrams has to be absorbed by a counterterm, which is simply one of the higher-dimensional operators appearing in the Lagrangian. In this case we need an operator involving 4 pions with a derivative acting on all of them

$$\mathcal{L}_{\mathrm{counterterm}} \;=\; \frac{c}{F_\pi^2}(D_\mu \boldsymbol{\pi})^2(D_\nu \boldsymbol{\pi})^2, \tag{B.3}$$

where c is some LEC. The contribution to the pion-pion scattering amplitude is now of the form

$$\frac{p^4}{F_\pi^2}\left(\frac{1}{(2\pi F_\pi)^2}\log\frac{M_{\mathrm{QCD}}}{\mu} + c\right). \tag{B.4}$$

If the theory is natural we would expect that c should be at least as large as the change in the amplitude that occurs if we alter μ by an amount such that the change in the log is of $\mathcal{O}(1)$. This implies

$$c \;\simeq\; \mathcal{O}\left(\frac{1}{(2\pi F_\pi)^2}\right). \tag{B.5}$$

In an EFT we expect that nonrenormalizable interactions are suppressed by the breakdown scale of the EFT and we identify $M_{\mathrm{QCD}} = 2\pi F_\pi \simeq 1.2\,\mathrm{GeV}$ as the scale where χPT can no longer be applied.

Georgi and Manohar used similar techniques to estimate the size of LECs of general interactions involving strongly interacting particles [63]. The NDA rules are most easily summarized by using "reduced" coupling constants [33]. A coupling constant c of an interaction of dimension D involving N fields has a reduced coupling

$$c^R = \Lambda^{D-4}(4\pi)^{2-N}c, \tag{B.6}$$

where Λ is the high-energy scale, in our case $\Lambda = M_{\rm QCD}$. The rule is that the reduced coupling of an operator below $M_{\rm QCD}$ is of the order of the product of the reduced couplings of the operators that appear above $M_{\rm QCD}$, which induce the operator below $M_{\rm QCD}$. This is a complicated sentence, so let us look at some examples. Consider the chiral-invariant part of the χPT Lagrangian, in particular the πN pseudovector coupling

$$\mathcal{L} = -\frac{2g_A}{F_\pi}\bar{N}S^\mu(\boldsymbol{\tau}\cdot D_\mu\boldsymbol{\pi})N. \tag{B.7}$$

The reduced coupling of the LEC is $(g_A/F_\pi)^R = (g_A/F_\pi)(M_{\rm QCD}/4\pi) \simeq g_A$ where we used $M_{\rm QCD} = 2\pi F_\pi$ (in these NDA estimates we do not care about factors of two). According to the rules this should be equal to the product of the reduced couplings appearing in the high-energy Lagrangian, *i.e.* the chiral-invariant part of the QCD Lagrangian where the reduced couplings are $\mathcal{O}(1)$. That is $(g_A/F_\pi)^R = g_A = \mathcal{O}(1)$, in good agreement with the experimental value $g_A \simeq 1.27$.

LECs of operators that break chiral symmetry also depend on the size of the chiral-breaking parameter in the high-energy theory. Take, for example, the pion mass

$$\mathcal{L} = -\frac{m_\pi^2}{2D}\boldsymbol{\pi}^2, \tag{B.8}$$

with reduced coupling $(m_\pi^2)^R = (m_\pi^2)/M_{\rm QCD}^2$. This should be equal to the reduced coupling of the fundamental source of chiral symmetry breaking, *i.e* the reduced quark mass $(\bar{m})^R = \bar{m}M_{\rm QCD}$. Relating the two gives the well-known result $m_\pi^2 = \mathcal{O}(\bar{m}M_{\rm QCD})$. Similarly, we can estimate the contribution to the pion-mass splitting due to electromagnetism in Eq. (3.27). The reduced coupling is again given by $(\breve{\delta}m_\pi^2)^R = (\breve{\delta}m_\pi^2)/M_{\rm QCD}^2$. The pion-mass splitting arises due to the exchange of a hard photon which requires two insertions of a quark-photon interaction. The reduced coupling is given by $(e)^R(e)^R = \alpha_{\rm em}/4\pi$, such that $\breve{\delta}m_\pi^2 = \mathcal{O}(M_{\rm QCD}^2\alpha_{\rm em}/4\pi)$. By NDA this is expected to be larger than the contribution from the quark-mass difference. Numerically the estimate becomes $\breve{\delta}m_\pi^2 \simeq (30\text{ MeV})^2$, very close to the observed pion-mass splitting $m_{\pi^\pm}^2 - m_{\pi^0}^2 = (35.5\text{ MeV})^2$ [67]. This estimate works remarkably well, but in general we expect the NDA estimates to hold within a factor of a few.

We apply the same techniques to estimate the size of the $\not{P}\not{T}$ LECs in terms of the dimension-four and -six operators. For example, look at a $\not{P}\not{T}$ pion-nucleon interaction and a short-range contribution to the nucleon EDM

$$\mathcal{L} \;=\; -\frac{\bar{g}_0}{F_\pi}\bar{N}\boldsymbol{\tau}\cdot\boldsymbol{\pi}N - \bar{d}_0\bar{N}S^\mu N\,v^\nu F_{\mu\nu}, \tag{B.9}$$

with reduced couplings $(\bar{g}_0/F_\pi)^R = \bar{g}_0/M_{\rm QCD}$ and $(\bar{d}_0)^R = \bar{d}_0(M_{\rm QCD}/4\pi)$. These operators are induced by the operators at the quark-gluon level in Eq. (2.57). Consider, for example the $\bar{\theta}$ term with reduced coupling $(\bar{m}\bar{\theta})^R = \bar{m}\bar{\theta}/M_{\rm QCD}$. The $\bar{\theta}$ term can induce $\bar{g}_0$ by itself such that we estimate $\bar{g}_0 = \mathcal{O}(\bar{m}\bar{\theta}) = \mathcal{O}(\bar{\theta}m_\pi^2/M_{\rm QCD})$. For $\bar{d}_0$, an additional insertion of the quark charge is needed such that $\bar{d}_0 = \mathcal{O}((4\pi/M_{\rm QCD})(e/4\pi)(\bar{m}\bar{\theta}/M_{\rm QCD})) = \mathcal{O}(e\bar{\theta}m_\pi^2/M_{\rm QCD}^3)$.

Similarly, for the isoscalar qCEDM with reduced coupling $(\tilde{d}_0)^R = \tilde{d}_0 M_{\rm QCD}/4\pi$, we estimate $\bar{g}_0 = \mathcal{O}(\tilde{d}_0\, M_{\rm QCD}^2/4\pi) = \mathcal{O}(\tilde{\delta}_0\, m_\pi^2 M_{\rm QCD}/M_{\not T}^2)$, and $\bar{d}_0 = \mathcal{O}(e\tilde{d}_0/4\pi) = \mathcal{O}(e\tilde{\delta}_0 m_\pi^2/M_{\not T}^2 M_{\rm QCD})$ where in the last steps we used Eq. (2.58). The scaling of all the LECs appearing in Chapter 3 are obtained in this way. Ideally, in the future these NDA estimates will be replaced by lattice-QCD calculations.

Finally, we look at the LECs appearing in the perturbative-pion calculations of the deuteron $\not P\not T$ moment in Chapter 5. Consider, for example, the $\not P\not T$ NN interactions

$$\mathcal{L} \;=\; \bar{C}_1 \bar{N} N\, \partial_\mu (\bar{N} S^\mu N). \tag{B.10}$$

The normal NDA rules above give $\bar{C}_1 = \mathcal{O}(\bar{\theta} m_\pi^2/F_\pi^2 M_{\rm QCD}^3)$ which is the scaling given in Chapter 3. In the KSW framework the high-energy scaling is not $M_{\rm QCD}$, but the scale where pion exchange becomes nonperturbative $M_{NN} = 4\pi F_\pi^2/m_N \simeq M_{\rm QCD}/\pi$. To get the scalings of the LECs at this scale we perform another NDA matching. This time both the high-energy and low-energy theory are described by χPT, however the low-energy theory does not contain pions with momenta higher than M_{NN}.

We can generate $\bar{C}_1$ through a high-energy pion exchange between two nucleons with one vertex originating in g_A and the other in $\bar{g}_0$. Effectively, we are integrating out the nonperturbative, high-energy part of pion exchange between nucleons. The reduced couplings are now $(\bar{C}_1)^R = \bar{C}_1 M_{NN}^3/(4\pi)^2$ (on the low-energy side) and $(g_A/F_\pi)^R(\bar{g}_0/F_\pi)^R = g_A \bar{g}_0 M_{NN}/M_{\rm QCD}^2$ (on the high-energy side). Relating the two gives $\bar{C}_1 = \mathcal{O}(g_A \bar{g}_0\, 4\pi/M_{NN}^3 M_{\rm QCD})$. Finally, the operator in Eq. (B.10) connects an S wave to a P wave and, as explained in Sect. 5.2, is renormalized on one side by the LO PT S-wave NN interactions in Eq. (5.2). This renormalization enhances the scaling of the LEC by a factor M_{NN}/Q [92]. So the scaling of the LEC in the perturbative-pion framework is $\bar{C}_1 = \mathcal{O}(\bar{g}_0\, 4\pi/Q M_{NN}^2 M_{\rm QCD})$. Finally, we can plug in the scaling of $\bar{g}_0$ for a particular source. For example, for the $\bar{\theta}$ term we get $\bar{C}_1 = \mathcal{O}(\bar{\theta}\, 4\pi m_\pi^2/Q M_{NN}^2 M_{\rm QCD}^2)$ which is the scaling giving in Eq. (5.5).

Not for all sources is the use of $\bar{g}_0$ the most efficient way to create $\bar{C}_1$ at low energies. For the χI sources, we find a larger estimate by using $\bar{\imath}_1$ in Eq. (3.79). Going through the same analysis again gives $\bar{C}_1 = \mathcal{O}(\bar{\imath}_1\, 4\pi/Q M_{\rm QCD}) = \mathcal{O}(w\, 4\pi/Q M_{\not T}^2)$, given in Eq. (5.6).

The LECs of the $NN\gamma$ interactions in Eq. (5.8) are obtained in similar fashion. These operators connect two S waves and are enhanced by a a factor $(M_{NN}/Q)^2$.

Appendix C

Integration Techniques

Many results in this thesis depend on the calculation of loop diagrams. In this Appendix we list some tricks used to solve the integrals. The easiest integrals encountered are the one-loop diagrams in Chapters 3 and 4 contributing to the $\not{PT}$ pion-nucleon FF and nucleon EDFF. These diagrams, apart from vertices, consist of a product of nucleon and pion propagators where the nucleon poles can always be avoided since they all lie in the same half plane. A typical integral is given by

$$I = \int \frac{\mathrm{d}^d k}{(2\pi)^d} \frac{1}{(-v\cdot k)+i\epsilon} \frac{1}{[k^2-m_\pi^2+i\epsilon]} \frac{1}{[(k+q)^2-m_\pi^2+i\epsilon]}. \tag{C.1}$$

The pion propagators can be combined with standard Feynman parameters. Combining the nucleon propagator with the pion propagators is done via

$$\frac{1}{a^r b^s} = 2^s \frac{\Gamma(r+s)}{\Gamma(r)\Gamma(s)} \int_0^\infty \mathrm{d}\lambda\, \lambda^{s-1} \frac{1}{(a+2\lambda b)^{r+s}}, \tag{C.2}$$

such that our example becomes

$$I = 4\int_0^1 \mathrm{d}x \int_0^\infty \mathrm{d}\lambda \int \frac{\mathrm{d}^d k}{(2\pi)^d} \frac{1}{[k^2-m_\pi^2+2xk\cdot q+xq^2-2\lambda v\cdot k+i\epsilon]^3}. \tag{C.3}$$

After completing the square in the denominator, the k integral becomes trivial. The λ integral can be performed by

$$\int_0^\infty \mathrm{d}\lambda \lambda^{2m+1}(\lambda^2+a)^{n-\epsilon} = \frac{1}{2}\frac{\Gamma(m+1)\Gamma(-m-n-1+\epsilon)}{\Gamma(\epsilon-n)}(a)^{1+m+n-\epsilon}, \tag{C.4}$$

where the ϵ dependence is given in case of ultraviolet divergent integrals. Our example is finite and becomes

$$I = -\frac{i\pi}{(4\pi)^2}\int_0^1 \mathrm{d}x \left[m_\pi^2 - x(1-x)q^2\right]^{-\frac{1}{2}} = -\frac{2i\pi}{(4\pi)^2}\frac{1}{|Q|}\arctan\left(\frac{|Q|}{2m_\pi}\right), \tag{C.5}$$

where we defined $Q^2=-q^2$. These techniques are sufficient to calculate all integrals required in Chapters 3 and 4.

More complicated are the diagrams appearing in Chapter 5. These diagrams involve loops with two intermediate nucleon propagators and the nucleon pole cannot be avoided. A simple example is given by diagram 5.3(a) which represent the nucleon EDFF contribution to the

deuteron EDFF. Before (after) coupling to the photon, the incoming (outgoing) nucleon pair has energy $\bar{E} = E - \vec{p}^{\,2}/4m_N$ ($\bar{E}' = E - q^0 - (\vec{p}-\vec{q})^2/4m_N$). We split the incoming energy and corresponding momenta among the top and bottom nucleon propagators of the diagram. Additionally there is momenta associated with the loop. Focusing only on the propagator structure, the diagram can be written as

$$\begin{aligned} I &= \int \frac{d^4k}{(2\pi)^4} \frac{i}{[\frac{1}{2}E + k^0 - \frac{1}{2m_N}(\frac{1}{2}\vec{p}+\vec{k})^2 + i\epsilon]} \\ &\quad \times \frac{(i)^2}{[\frac{1}{2}E - k^0 - \frac{1}{2m_N}(\frac{1}{2}\vec{p}-\vec{k})^2 + i\epsilon][\frac{1}{2}E - q^0 - k^0 - \frac{1}{2m_N}(\frac{1}{2}\vec{p}-\vec{q}-\vec{k})^2] + i\epsilon}. \end{aligned} \quad \text{(C.6)}$$

Clearly when integrating over the energy we encounter nucleon poles in both the upper and lower half plane. In this example, it is easiest to close the contour in the lower half plane,

$$I = -\int \frac{d^3k}{(2\pi)^3} \frac{1}{[E - \frac{\vec{p}^2}{4m_N} - \frac{\vec{k}^2}{m_N}]} \frac{1}{[E - q^0 - \frac{(\vec{p}-\vec{q})^2}{4m_N} - \frac{(\vec{k}+\frac{1}{2}\vec{q})^2}{m_N}]}. \quad \text{(C.7)}$$

Putting the in- and outgoing deuteron on-shell, $\bar{E}, \bar{E}' \to -B$ with $B = -\gamma^2/m_N$, the deuteron binding energy, gives

$$\begin{aligned} I &= -m_N^2 \int \frac{d^3k}{(2\pi)^3} \frac{1}{\vec{k}^2 + \gamma^2} \frac{1}{(\vec{k} + \frac{1}{2}\vec{q})^2 + \gamma^2} \\ &= -\frac{m_N^2}{2\pi|\vec{q}|} \arctan\left(\frac{|\vec{q}|}{4\gamma}\right). \end{aligned} \quad \text{(C.8)}$$

Diagrams involving one- or more-pion exchanges involve more complicated integrals. Here we give an example of a three-loop integral. Two-loop integrals can be obtained with the same techniques. We consider

$$I = \int \frac{\mathrm{d}^3k \mathrm{d}^3l \mathrm{d}^3t}{(2\pi)^9} \frac{1}{[k^2+\gamma^2]} \frac{1}{[(k+l)^2+\gamma^2]} \frac{1}{[l^2+m_\pi^2]} \frac{1}{[(k+t)^2+m_\pi^2]} \frac{1}{[t^2+\gamma^2]}, \quad \text{(C.9)}$$

where the energy integrals have already been performed. Before starting, each propagator gets a unique parameter

$$I = \int \frac{\mathrm{d}^3k \mathrm{d}^3l \mathrm{d}^3t}{(2\pi)^9} \frac{1}{[k^2+\gamma_k^2]} \frac{1}{[(k+l)^2+\gamma_l^2]} \frac{1}{[l^2+m_l^2]} \frac{1}{[(k+t)^2+m_t^2]} \frac{1}{[t^2+\gamma_t^2]}. \quad \text{(C.10)}$$

The reason for this is simple. If we can do the integral with generic parameters we can easily find, for example, the more complicated integral

$$I_2 = \int \frac{\mathrm{d}^3k \mathrm{d}^3l \mathrm{d}^3t}{(2\pi)^9} \frac{1}{[k^2+\gamma_k^2]} \frac{1}{[(k+l)^2+\gamma_l^2]} \frac{1}{[l^2+m_l^2]} \frac{1}{[(k+t)^2+m_t^2]} \frac{1}{[t^2+\gamma_t^2]^2}, \quad \text{(C.11)}$$

by using

$$I_2 = \frac{-1}{2\gamma_t} \frac{\partial}{\partial \gamma_t} I. \quad \text{(C.12)}$$

To do the integrals we borrow heavily from Ref. [111], although certain steps are done in a slightly different way and we avoid certain mistakes. First the propagators are Fourier transformed

$$\begin{aligned} I &= \int \mathrm{d}^3x\mathrm{d}^3y\mathrm{d}^3z\mathrm{d}^3t\mathrm{d}^3s \times \\ &\quad G_{\gamma_k}(x)G_{\gamma_l}(y)G_{m_l}(z)G_{m_t}(t)G_{\gamma_t}(s)\delta^{(3)}(x+y+t)\delta^{(3)}(y+z)\delta^{(3)}(t+s), \\ G_a(x) &= \frac{1}{4\pi x}e^{-ax}. \end{aligned} \tag{C.13}$$

Using the delta functions this becomes

$$I = \int \mathrm{d}^3x\mathrm{d}^3y G_{\gamma_l}(x)G_{m_l}(x)G_{\gamma_t}(y)G_{m_t}(y)G_{\gamma_k}(x-y). \tag{C.14}$$

We can easily integrate over the two ϕ angles and one θ angle. For the remaining θ angle we use

$$\int_{-1}^{1}\mathrm{d}\cos\theta\frac{1}{|x-y|}e^{-\gamma_k|x-y|} = \frac{1}{\gamma_k}\frac{1}{xy}\left[e^{-\gamma|x-y|}-e^{-\gamma(x+y)}\right], \tag{C.15}$$

which gives for our integral

$$I = \frac{2(2\pi)^2}{(4\pi)^5}\frac{1}{\gamma_k}\int_0^\infty \mathrm{d}x\mathrm{d}y\frac{1}{xy}e^{-(\gamma_l+m_l)x}e^{-(\gamma_t+m_t)y}\left[e^{-\gamma_k|x-y|}-e^{-\gamma_k(x+y)}\right]. \tag{C.16}$$

The factor of $1/(xy)$ is a bit tedious and we remove it by using

$$\int_0^\infty \mathrm{d}x\frac{1}{x}e^{-ax} = -\int_\infty^a \mathrm{d}a\int_0^\infty \mathrm{d}x e^{-ax}, \tag{C.17}$$

for $a>0$. This allows us to write

$$I = \frac{2(2\pi)^2}{(4\pi)^5}\frac{1}{\gamma_k}\int_\infty^a \mathrm{d}a\int_\infty^b \mathrm{d}b\int_0^\infty \mathrm{d}x\mathrm{d}y\; e^{-ax}e^{-by}\left[e^{-\gamma_k|x-y|}-e^{-\gamma_k(x+y)}\right], \tag{C.18}$$

with $a=\gamma_l+m_l$ and $b=\gamma_t+m_t$. There is one difficulty left and that is the absolute value in the exponent. To get rid of it the xy-plane is divided in two parts. One part where $x>y$ ($|x-y|=x-y$) and one part where $y>x$ ($|x-y|=y-x$) giving

$$\begin{aligned} \frac{2(2\pi)^2}{(4\pi)^5}\frac{1}{\gamma_k}\int_\infty^a \mathrm{d}a\int_\infty^b \mathrm{d}b \quad &\left\{\int_0^\infty \mathrm{d}x e^{-(a+\gamma_k)x}\int_0^x \mathrm{d}y\left[e^{-(b-\gamma_k)y}-e^{-(b+\gamma_k)y}\right]\right. \\ &\left.+\int_0^\infty \mathrm{d}y e^{-(b+\gamma_k)y}\int_0^y \mathrm{d}x\left[e^{-(a-\gamma_k)x}-e^{-(a+\gamma_k)x}\right]\right\}. \end{aligned} \tag{C.19}$$

More complicated integrals require integration over the xyz- or $xyzw$-plane. Absolute values in these higher-dimensional planes are treated as in two dimensions. For example

$$\int_0^\infty \mathrm{d}x\mathrm{d}y\mathrm{d}z\; e^{-ax}e^{-by}e^{-cz}\left[e^{-d|x-y|}-e^{-d(x+y)}\right]\left[e^{-e|x-z|}-e^{-e(x+z)}\right]\left[e^{-f|y-z|}-e^{-f(y+z)}\right],$$

is divided into 6 regions with $x>y>z$, $x>z>y$ etc. Continuing with our example

$$\begin{aligned} I &= \frac{2(2\pi)^2}{(4\pi)^5}\frac{1}{\gamma_k}\int_\infty^a \mathrm{d}a\int_\infty^b \mathrm{d}b\frac{2\gamma_k}{(a+b)(a+\gamma_k)(b+\gamma_k)} \\ &= \frac{4(2\pi)^2}{(4\pi)^5}\int_\infty^a \mathrm{d}a\frac{1}{(a+\gamma_k)(a-\gamma_k)}\log\left(\frac{b+\gamma_k}{a+b}\right), \end{aligned} \tag{C.20}$$

which can be done explicitly. The general result is quite complicated but putting γ_k, γ_t, $\gamma_l \to \gamma$ and m_l, $m_t \to m_\pi$ gives the simple result

$$I = \frac{1}{(4\pi)^3}\frac{1}{\gamma}\left[\mathrm{Li}_2\left(\frac{-m_\pi}{\gamma+m_\pi}\right)+\frac{\pi^2}{12}\right]. \tag{C.21}$$

The calculation of the TPE diagrams in Sect. 5.5 requires three-loop integrals with momenta in the numerator. These integrals can be reduced to integrals without momenta in the numerator via standard Passarino-Veltman reduction techniques [112]. The resulting integrals can be calculated with the method described here.

Appendix D

Fourier Transformations

D.1 Potential in coordinate space

In configuration space, the LO potential in Eqs. (6.10) and (6.11) in Sect. 6.2 is given by [78]

$$\begin{aligned} V_{\not\pi\!\!\!/}(\vec{r}) &= -\frac{\bar{g}_0 g_A}{F_\pi^2}\boldsymbol{\tau}^{(i)}\cdot\boldsymbol{\tau}^{(j)}\left(\vec{\sigma}^{\,(i)}-\vec{\sigma}^{\,(j)}\right)\cdot\left(\vec{\nabla}_r\,U(r)\right) \\ &\quad -\frac{\bar{g}_1 g_A}{2F_\pi^2}\left[\left(\tau_3^{(i)}+\tau_3^{(j)}\right)\left(\vec{\sigma}^{(i)}-\vec{\sigma}^{(j)}\right)+\left(\tau_3^{(i)}-\tau_3^{(j)}\right)\left(\vec{\sigma}^{(i)}+\vec{\sigma}^{(j)}\right)\right]\cdot\left(\vec{\nabla}_r U(r)\right) \\ &\quad +\frac{1}{2}\left[\bar{C}_1+\bar{C}_2\boldsymbol{\tau}^{(i)}\cdot\boldsymbol{\tau}^{(j)}\right]\left(\vec{\sigma}^{\,(i)}-\vec{\sigma}^{\,(j)}\right)\cdot\left(\vec{\nabla}_r\,\delta^{(3)}(\vec{r})\right)\ , \end{aligned} \tag{D.1}$$

where $\vec{r}=\vec{x}_i-\vec{x}_j$ is the relative position of the two interacting nucleons and

$$U(r)=\frac{1}{12\pi r}\left[2\exp\left(-m_{\pi^\pm}r\right)+\exp\left(-m_{\pi^0}r\right)\right]\ , \tag{D.2}$$

which reduces to the usual Yukawa function $U(r)=\exp(-m_\pi r)/4\pi r$ when, at LO, we ignore the pion-mass difference.

Analogously, the NNLO potential of Sect. 6.4.2 becomes [78]

$$\begin{aligned} V_{\not\pi\!\!\!/}(\vec{r},\vec{\nabla}_r,\vec{\nabla}_X\,) &= -\frac{\bar{g}_0 g_A}{2F_\pi^2}\left[\left(\frac{\bar{g}_1}{\bar{g}_0}-\frac{\beta_1}{2g_A}\right)\left(\tau_3^{(i)}+\tau_3^{(j)}\right)\left(\vec{\sigma}^{(i)}-\vec{\sigma}^{(j)}\right)\right. \\ &\quad \left.+\left(\frac{\bar{g}_1}{\bar{g}_0}+\frac{\beta_1}{2g_A}\right)\left(\tau_3^{(i)}-\tau_3^{(j)}\right)\left(\vec{\sigma}^{(i)}+\vec{\sigma}^{(j)}\right)\right]\cdot\left(\vec{\nabla}_r U(r)\right) \\ &\quad +\frac{\bar{g}_0 g_A}{3F_\pi^2}\left(3\tau_3^{(i)}\tau_3^{(j)}-\boldsymbol{\tau}^{(i)}\cdot\boldsymbol{\tau}^{(j)}\right) \\ &\quad \times\left(\vec{\sigma}^{(i)}-\vec{\sigma}^{(j)}\right)\cdot\left[\frac{\delta m_N^2}{2m_\pi}\left(\vec{\nabla}_r\,rU(r)\right)+\left(\vec{\nabla}_r W(r)\right)\right] \\ &\quad -i\frac{\bar{g}_0 g_A}{2F_\pi^2}\frac{\delta m_N}{m_N}\left(\tau^{(i)}\times\tau^{(j)}\right)_3\left\{\left(\vec{\sigma}^{(i)}+\vec{\sigma}^{(j)}\right)\cdot\left\{\vec{\nabla}_r,U(r)\right\}\right. \\ &\quad \left.+\left(\vec{\sigma}^{(i)}-\vec{\sigma}^{(j)}\right)\cdot\left[U(r)\vec{\nabla}_X-\frac{1}{m_\pi}\left(\vec{\nabla}_r\nabla_r^n rU(r)\right)\nabla_X^n\right]\right\}, \end{aligned} \tag{D.3}$$

where $\vec{X}=(\vec{x}_i+\vec{x}_j)/2$ and

$$W(r)=\frac{1}{4\pi r}\left[\exp\left(-m_{\pi^\pm}r\right)-\exp\left(-m_{\pi^0}r\right)\right], \tag{D.4}$$

which is entirely a consequence of isospin breaking.

D.2 Fourier transform of the currents

To evaluate the matrix elements in Sects. 6.5 and 6.8 we need to transform the currents to configuration space. We follow Ref. [113] and transform with respect to the nucleon momenta but not with respect to the photon momentum. In the most general case

$$\begin{aligned} J^0(\vec{x}_i,\vec{x}_i^{\,'},\vec{x}_j,\vec{x}_j^{\,'},\vec{q}) &= \int\frac{\mathrm{d}^3p_i}{(2\pi)^3}\int\frac{\mathrm{d}^3p_i'}{(2\pi)^3}\int\frac{\mathrm{d}^3p_j}{(2\pi)^3}\int\frac{\mathrm{d}^3p_j'}{(2\pi)^3}e^{-i\vec{p}_i\cdot\vec{x}_i}e^{-i\vec{p}_j\cdot\vec{x}_j}e^{i\vec{p}_i^{\,'}\cdot\vec{x}_i^{\,'}}e^{i\vec{p}_j^{\,'}\cdot\vec{x}_j^{\,'}} \\ &\quad (2\pi)^3\delta^{(3)}(\vec{p}_i+\vec{p}_j-\vec{p}_i^{\,'}-\vec{p}_j^{\,'}-\vec{q})J^0(\vec{p}_i,\vec{p}_i^{\,'},\vec{p}_j,\vec{p}_j^{\,'},\vec{q})\ . \end{aligned} \tag{D.5}$$

Introducing the relative configuration-space coordinates $\vec{r}=\vec{x}_i-\vec{x}_j$, $\vec{r}\,'=\vec{x}_i'-\vec{x}_j'$, $\vec{X}=(\vec{x}_i+\vec{x}_j)/2$, and $\vec{X}'=(\vec{x}_i^{\,'}+\vec{x}_j^{\,'})/2$, we rewrite this as

$$\begin{aligned} J^0(\vec{r},\vec{r}\,',\vec{X},\vec{X}',\vec{q}) &= e^{-\frac{i}{2}\vec{q}\cdot(\vec{X}+\vec{X}')}\int\frac{\mathrm{d}^3P_t}{(2\pi)^3}\int\frac{\mathrm{d}^3K}{(2\pi)^3}\int\frac{\mathrm{d}^3k}{(2\pi)^3} \\ &\quad e^{-i\vec{P}_t\cdot(\vec{X}-\vec{X}')}e^{-i\vec{K}\cdot(\vec{r}-\vec{r}\,')}e^{-\frac{i}{2}\vec{k}\cdot(\vec{r}+\vec{r}\,')}J^0(\vec{q},\vec{k},\vec{K},\vec{P}_t)\ . \end{aligned} \tag{D.6}$$

Here we show how to derive the EDM operators in Eqs. (6.27) and (6.29). The MQM operators in Eqs. (6.72) and (6.73)) are obtained in analogous fashion. The currents we need (the third currents in Eqs. (6.20) and (6.21)) depend on $\vec{q}$ and $\vec{k}$ only, such that the expression can be simplified to

$$J^0(\vec{r},\vec{X},\vec{q}) = e^{-i\vec{q}\cdot\vec{X}}\int\frac{\mathrm{d}^3k}{(2\pi)^3}e^{-i\vec{k}\cdot\vec{r}}J^0(\vec{q},\vec{k})\ . \tag{D.7}$$

The Fourier transforms can be done and we find for the required currents

$$\begin{aligned} J^0_{PT,c}(\vec{r},\vec{X},\vec{q}) &= -\frac{2eg_A^2}{F_\pi^2}\delta m_N\left(\boldsymbol{\tau}^{(i)}\cdot\boldsymbol{\tau}^{(j)}-\tau_3^{(i)}\tau_3^{(j)}\right) \\ &\quad\times e^{-i\vec{q}\cdot\vec{X}}\left[\vec{\sigma}^{(i)}\cdot\left(i\vec{\nabla}_r+\frac{\vec{q}}{2}\right)\vec{\sigma}^{(j)}\cdot\left(i\vec{\nabla}_r-\frac{\vec{q}}{2}\right)\right]W(\vec{q},\vec{r})\ , \end{aligned} \tag{D.8}$$

$$\begin{aligned} J^0_{\not PT,c}(\vec{r},\vec{X},\vec{q}) &= \frac{2ieg_A\bar{g}_0}{F_\pi^2}\delta m_N\left(\boldsymbol{\tau}^{(i)}\cdot\boldsymbol{\tau}^{(j)}-\tau_3^{(i)}\tau_3^{(j)}\right) \\ &\quad\times e^{-i\vec{q}\cdot\vec{X}}\left[\left(\vec{\sigma}^{(i)}+\vec{\sigma}^{(j)}\right)\cdot\frac{\vec{q}}{2}+\left(\vec{\sigma}^{(i)}-\vec{\sigma}^{(j)}\right)\cdot\left(i\vec{\nabla}_r\right)\right]W(\vec{q},\vec{r})\ , \end{aligned} \tag{D.9}$$

in terms of the function

$$W(\vec{q},\vec{r}) = \frac{1}{8\pi}\int_0^1\mathrm{d}\alpha\,\exp\left[i\frac{\vec{q}\cdot\vec{r}}{2}(1-2\alpha)\right]\frac{\exp[-r(m_\pi^2+\vec{q}^{\,2}\alpha(1-\alpha))^{1/2}]}{[m_\pi^2+\vec{q}^{\,2}\alpha(1-\alpha)]^{1/2}}\ . \tag{D.10}$$

Before continuing it is convenient to look at the inverse Fourier transform of the current

$$\begin{aligned} J^0(\vec{q}) &= \int\mathrm{d}^3x\ e^{-i\vec{q}\cdot\vec{x}}J^0(\vec{x}) \\ &= \int\mathrm{d}^3x\ J^0(\vec{x})-i\vec{q}\cdot\int\mathrm{d}^3x\ \vec{x}J^0(\vec{x})+\mathcal{O}(\vec{q}^{\,2}) \\ &= Ze-i\vec{q}\cdot\vec{D}+\mathcal{O}(\vec{q}^{\,2})\ , \end{aligned} \tag{D.11}$$

where Ze is the total charge and $\vec{D}$ is the EDM operator used in Sects. 6.5 and 6.6. An easy way to extract the EDM operator is by using

$$\vec{D} \;=\; i \lim_{q\to 0} \vec{\nabla}_q J^0(\vec{q}) \; . \tag{D.12}$$

As an example we consider the EDM operator coming from $J^0_{\not P\not T,c}(\vec{r},\vec{X},\vec{q})$. From Eq. (D.12) we read off

$$\begin{aligned}
\vec{D}_{\not P\not T,c} &= \frac{2ieg_A\bar{g}_0}{F_\pi^2}\delta m_N \left(\boldsymbol{\tau}^{(i)}\cdot\boldsymbol{\tau}^{(j)} - \tau_3^{(i)}\tau_3^{(j)}\right) \\
&\quad \times \left[\frac{i}{2}\left(\vec{\sigma}^{(i)}+\vec{\sigma}^{(j)}\right) + \vec{X}\left(\vec{\sigma}^{(i)}-\vec{\sigma}^{(j)}\right)\cdot\left(i\vec{\nabla}_r\right)\right]\frac{e^{-m_\pi\, r}}{8\pi m_\pi} \\
&= -\frac{eg_A\bar{g}_0}{F_\pi^2}\delta m_N \left(\boldsymbol{\tau}^{(i)}\cdot\boldsymbol{\tau}^{(j)} - \tau_3^{(i)}\tau_3^{(j)}\right) \\
&\quad \times \left[\left(\vec{\sigma}^{(i)}\cdot\vec{\nabla}^{(i)} + \vec{\sigma}^{(j)}\cdot\vec{\nabla}^{(j)}\right)(\vec{x}_i+\vec{x}_j)\,\frac{e^{-m_\pi\,|\vec{x}_i-\vec{x}_j|}}{8\pi m_\pi}\right],
\end{aligned} \tag{D.13}$$

where we used $\lim_{q\to 0}\vec{\nabla}_q W(\vec{q},\vec{r}) = 0$. This is Eq. (6.27). Following similar steps we obtain Eq. (6.29) from $J^0_{PT,c}(\vec{r},\vec{X},\vec{q})$.

Nederlandse Samenvatting

Het lijkt duidelijk dat de symmetrie van tijdsomkering compleet gebroken is in de natuur. In ons dagelijks leven loopt tijd vooruit, niet achteruit, en elke bewering voor een symmetrie tussen de twee klinkt absurd. Als we een film bekijken van, bijvoorbeeld, een instortend huis dan zien we direct of de film vooruit of achteruit wordt afgespeeld en het lijkt dat de natuurwetten een intrinsieke richting van tijd kennen. Echter, belangrijke natuurkundige vergelijkingen, zoals de tweede wet van Newton en de Maxwellvergelijkingen, zijn symmetrisch onder de transformatie $t \to -t$. Hoe het toch kan dat we een duidelijke tijdsrichting waarnemen heeft te maken met statistische wetmatigheden. In ons dagelijks leven hebben we te maken met systemen met grote aantallen deeltjes, oftewel macroscopische systemen. Macroscopische systemen hebben een grotere kans om van een geordende toestand (huis) naar een chaotische toestand (puin) te veranderen, dan andersom. Het omgekeerde proces kan in principe wel gebeuren, maar is extreem onwaarschijnlijk. We nemen dus een richting van de tijd waar, ondanks dat de fundamentele, microscopische natuurwetten die richting niet hebben. Dit kan goed geïllustreerd worden met een voorbeeld uit het snookerspel. Bij het zien van een film van een botsing tussen twee bewegende ballen kunnen we, in tegenstelling tot de film van het instortende huis, niet zien of de film voor- of achteruit afgespeeld wordt. Als we echter de afstoot filmen zal iedereen direct kunnen zeggen wat de juiste afspeelrichting is. Het is immers wel erg onwaarschijnlijk dat na een botsing alle ballen precies in een driehoek terecht komen.

Tijdsomkering (T) is een van de drie belangrijke discrete symmetrieën in de elementaire deeltjesfysica. De andere twee zijn pariteit (P), de omkering van alle ruimtelijke coördinaten ($\vec{x} \to -\vec{x}$), en ladingconjugatie (C) wat de omkering van deeltjes met antideeltjes inhoudt. Lange tijd werd er gedacht dat de fundamentele natuurwetten symmetrisch zijn onder elk van deze symmetrieën. Dat zou, bijvoorbeeld, betekenen dat een botsing tussen twee elektronen precies hetzelfde verloopt als dezelfde botsing tussen twee positronen (een positron is het antideeltje van het elektron). In de vorige eeuw zijn vele experimenten uitgevoerd om de discrete symmetrieën te testen, sommige met opmerkelijke resultaten. Het is gebleken dat C, P, en T goede symmetrieën zijn voor de elektromagnetische en sterke wisselwerking, maar in 1956 bleek dat de zwakke wisselwerking, verantwoordelijk voor radioactief verval, de symmetrieën C and P afzonderlijk breekt. Een tijdje werd er gedacht dat deze breking dusdanig was dat de gecombineerde symmetrie CP behouden zou zijn, maar in 1963 werd gemeten dat de zwakke wisselwerking ook deze symmetrie schendt. Hoe zit het met T-violatie? Volgens het CPT-theorema betekent de meting van CP-violatie in 1963 dat T ook gebroken is. Het CPT-theorema zegt namelijk dat elke kwantumveldentheorie die voldoet aan speciale relativiteitstheorie symmetrisch moet zijn onder de gecombineerde symmetrie CPT. Dat wil zeggen dat de zwakke wisselwerking T dusdanig moet schenden zodat, in combinatie met de gemeten schending van CP, CPT weer behouden is. CP-violatie houdt dus T-violatie in en vice versa.

Dit proefschrift gaat over een zoektocht naar CP-violatie in hadronische en nucleaire systemen, de zoektocht naar elektrische dipoolmomenten (EDMs). Wat zijn EDMs? Simpel gezegd

geven EDMs de interactie weer tussen de kwantummechanische spin van een deeltje en een extern elektrisch veld. Spin kan gezien worden als de rotatie van een deeltje om zijn as (al moet deze analogie niet te ver worden doorgevoerd!) en het is niet moeilijk in te zien dat onder een T-transformatie de spin van teken wisselt (het deeltje roteert andersom om zijn as). Het elektrisch veld daarentegen wordt gecreëerd door statische ladingen en verandert niet onder een T-transformatie. We kunnen concluderen dat een EDM, het product van spin en elektrisch veld, van teken wisselt onder een T-transformatie en dus ook onder een CP-transformatie. Dit kan vergeleken worden met een magnetisch dipoolmoment (MDM) wat de wisselwerking tussen de spin en een magnetisch veld is. Een magnetisch veld, gegenereerd door een elektrische stroom, verandert wel onder een T-transformatie zodat een MDM geen symmetrieën schendt. Waar een MDM een goed gemeten grootheid is, is een EDM tot dusver nog nooit gemeten. Het eerste neutron-EDM-experiment is gedaan in de jaren '50 en ondanks het feit dat de metingen inmiddels een miljoen keer preciezer zijn, is er nog steeds geen EDM gevonden.

Een goede vraag is nu of dit niet in tegenspraak is met het Standaard Model (SM) van de elementaire deeltjesfysica. We weten immers dat de zwakke wisselwerking CP en T schendt. Waarom produceert deze schending dan geen EDMs? Het antwoord op deze vraagt ligt in de structuur van de CP-violatie in het SM. Deze CP-violatie vindt plaats in de beschrijving van de quarks. Quarks zijn de bouwstenen van protonen en neutronen (samen nucleonen genoemd) die weer de bouwstenen zijn van atoomkernen. Nucleonen zijn opgebouwd uit twee soorten quarks, de zogenaamde up en down quarks, en in principe zijn deze twee quarks genoeg om alle atoomkernen te beschrijven. Het kwam dan ook als een verassing dat experimenten in de vorige eeuw aantoonden dat er naast de up en down quarks nog vier andere quarks bestaan. Deze quarks spelen nauwelijks een rol in de beschrijving van atoomkernen, maar zijn van cruciaal belang voor CP-violatie in de zwakke interactie. Het blijkt namelijk onmogelijk te zijn om CP-violatie te hebben als er maar twee soorten quarks zouden bestaan. Er zijn minstens zes, precies het aantal in het SM, quarks nodig om wel CP-violatie te kunnen beschrijven. Voor deze theoretische observatie hebben Kobayashi en Maskawa in 2008 de Nobelprijs voor de natuurkunde gekregen. Nu kunnen we ook begrijpen waarom er, bijvoorbeeld, nog geen neutron-EDM gemeten is. Het neutron bestaat uit up en down quarks wat niet genoeg is voor CP-violatie. Via zogenaamde kwantumcorrecties kunnen de andere vier quarks wel een rol spelen maar dit vereist meerdere zwakke interacties die, zoals de naam suggereert, erg zwak zijn. Het is uit te rekenen dat de SM-voorspelling voor de grootte van het neutron-EDM ongeveer een miljoen keer kleiner is dan de huidige experimentele precisie. EDMs gegenereerd door de zwakke wisselwerking zijn dus echt onmeetbaar klein! We kunnen concluderen dat een observatie van een EDM automatisch betekent dat er nieuwe, nog niet eerder gemeten, T- en CP-violatie gevonden is.

Een EDM-meting betekent echter niet automatisch dat er T-violatie gevonden is die niet door het SM beschreven wordt. Het SM bevat namelijk nog een bron van T-violatie in de theorie van de sterke wisselwerking. Deze wisselwerking zorgt ervoor dat atoomkernen niet uiteen vallen door de afstotende elektromagnetische kracht tussen de geladen protonen. De theorie van de sterke wisselwerking bevat een T-violerende interactie tussen gluonen (gluonen zijn de dragers van de sterke interactie analoog aan hoe lichtdeeltjes, *i.e.* fotonen, de dragers zijn van de elektromagnetische interactie) met een sterkte die weergegeven wordt door een parameter $\bar{\theta}$. In tegenstelling tot T-violatie door de zwakke interactie, is sterke T-violatie zeer geschikt voor het produceren van EDMs. Echter, het feit dat er nog nooit een EDM is gemeten betekent dat $\bar{\theta}$ zeer klein moet zijn. Omdat EDM-experimenten met zeer hoge precisie zijn uitgevoerd is de huidige limiet op $\bar{\theta}$ zeer sterk, $\bar{\theta} < 10^{-10}$. Dit wordt ook wel het "sterke CP-probleem" genoemd omdat het momenteel niet begrepen is waarom $\bar{\theta}$ zo extreem klein (of misschien wel nul) is.

Samengevat kunnen we dus zeggen dat een meting van een EDM betekent dat er ofwel een zeer

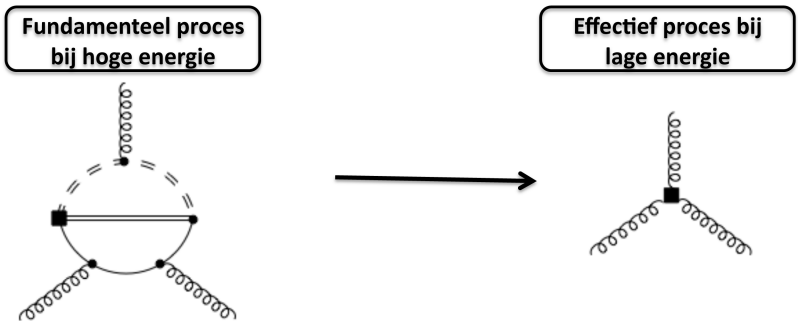

Figure D.1: Een figuur om het idee van een effectieve veldentheorie te illusteren. Het linkerplaatje is een ingewikkeld diagram waarbij zware deeltjes (weergegeven met dubbele hele en gebroken lijnen) worden uitgewisseld die niet in het Standaard Model voorkomen. Het vierkant geeft T-violatie weer. Bij lagere energie kan dit ingewikkelde proces beschreven worden door middel van een lokale interactie tussen deeltjes uit het SM, in dit geval gluonen (weergegeven door gekrulde lijnen).

kleine, maar eindige, waarde voor $\bar{\theta}$ gemeten is ofwel een nieuwe, niet door het SM beschreven bron van CP- en T-violatie. Beide opties zijn ontzettend interessant maar de laatste misschien nog wel het meest vanwege een ander probleem in de natuurkunde: de materie/antimaterie-verhouding in het universum. Deze verhouding kan worden samengevat door te zeggen dat de hoeveelheid antimaterie in het heelal veel kleiner is dan de hoeveelheid materie. Sterker nog, er zijn geen aanwijzingen dat er überhaupt een significante hoeveelheid antimaterie in het heelal aanwezig is. Uitgaande van een oerknalscenario betekent dit gebrek aan antimaterie dat er tijdens de evolutie van het heelal een asymmetrie is ontstaan tussen de hoeveelheid materie en antimaterie. Al in de jaren '60 van de vorige eeuw heeft de Russische natuurkundige Sakharov een aantal condities opgeschreven dat noodzakelijk is voor het ontstaan van deze asymmetrie. Een van deze condities is dat CP geschonden moet zijn. We hebben al beschreven dat de zwakke en sterke wisselwerkingen deze symmetrie breken maar berekeningen tonen aan dat deze schendingen veel te zwak zijn om de materie/antimaterie-asymmetrie te verklaren. Er zijn dus goede redenen om aan te nemen dat er meer CP-violatie in de natuur is dan datgene wat beschreven wordt door het SM. Experimenten die EDMs proberen te meten zijn goede kandidaten om deze nieuwe CP-violatie te vinden.

Er is een interessante tijd aangebroken voor het veld van EDMs. Er zijn nieuwe experimentele methodes voorgesteld om de EDMs van lichte kernen (kernen van de atomen van waterstof, deuterium, helium, etc.) te meten met een duizendmaal betere precisie dan de tot dusver gedane experimenten. Er zijn hoge verwachtingen dat in deze generatie experimenten voor het eerst een EDM gemeten wordt. Een belangrijke vraag die nog open staat is: Stel dat er een EDM of een aantal EDMs gemeten wordt in deze experimenten, kunnen we daaruit het fundamentele mechanisme van T-violatie afleiden? Zijn deze EDMs veroorzaakt door de $\bar{\theta}$ term of is er fundamenteel nieuwe natuurkunde gevonden die niet beschreven wordt door het SM? In het laatste geval, kunnen we ook iets leren over deze nieuwe natuurkunde?

In dit proefschrift worden deze vragen beantwoord met behulp van effectieve veldentheorie (EVT). EVT is gebaseerd op het idee dat natuurkundige processen die plaatsvinden bij lage energie (of volgens het onzekerheidsprincipe van Heisenberg bij grote afstanden) niet afhangen van processen die plaatsvinden bij hoge energie (korte afstanden). Omdat we weten dat het SM zeer goed werkt, kunnen we aannemen dat nieuwe natuurkunde plaatsvindt op een veel hogere energieschaal dan het SM. Dit verschil tussen de energieschalen van het SM en van nieuwe

natuurkunde suggereert dat we het SM niet moeten zien als een fundamentele theorie maar als een effectieve theorie die ongeveer klopt bij relatief lage energie. Bij hogere energie zullen er correcties optreden. Dit wordt geïllustreerd in Figuur D.1. Bij lage energie (de rechterkant van het figuur) kunnen we een T-schendend proces beschrijven als een lokale interactie tussen SM-deeltjes (in dit geval gluonen). Bij hogere energie (de linkerkant), en dus kleinere afstanden, zoomen we in op de lokale interactie en zien we dat de interactie eigenlijk veel ingewikkelder is. EVT zegt nu dat bij lage energie dit ingewikkelde proces accuraat beschreven kan worden met de veel simpelere interactie aan de rechterkant.

Dit idee wordt in detail uitgewerkt in Hoofdstuk 2 van dit proefschrift. Het blijkt dat, vanwege belangrijke wiskundige symmetrie-eisen, er maar een klein aantal T-violerende lokale interacties toegevoegd kan worden aan het SM. Deze interacties parametriseren alle nieuwe T-violerende natuurkunde die mogelijk kan optreden bij hogere energie. Omdat we de fundamentele theorie van nieuwe T-violatie niet kennen voegen we simpelweg alle lokale T-violerende interacties toe die toegestaan zijn. We hoeven dus geen specifiek model van nieuwe natuurkunde te kiezen. Dit is een groot voordeel omdat er vele van dit soort modellen, bijvoorbeeld supersymmetrische modellen, bestaan en het niet duidelijk is welke (als die er tussenzit) de goede is. We werken dus modelonafhankelijk.

Er is nog wel een probleem met deze aanpak. De nieuwe lokale interacties en de SM $\bar{\theta}$ term zijn interacties tussen de elementaire quarks en gluonen. EDM-experimenten vinden echter plaats bij een dusdanig lage energie dat deze deeltjes niet meer vrij voorkomen maar gebonden zijn in samengestelde deeltjes zoals protonen, neutronen en vele andere deeltjes (deze deeltjes worden hadronen genoemd). Dit probleem wordt behandeld in Hoofdstuk 3. Door gebruik te maken van nog meer EVT-technieken vertalen we de T-violerende interaties tussen quarks en gluonen naar interacties tussen hadronen. In de daarop volgende hoofdstukken worden berekeningen gedaan met deze interacties.

In Hoofdstuk 4 tonen we aan dat het meten van zowel het neutron- als het proton-EDM niet genoeg is om te achterhalen wat het fundamentele T-violerende mechanisme is. Zelfs met beide metingen is het niet mogelijk om te zeggen of de $\bar{\theta}$ term verantwoordelijk is of een van de nieuwe effectieve interacties. Het is ook niet mogelijk om de effectieve interacties onderling te scheiden.

Meer belovend is het EDM van het deuteron (de gebonden toestand van een proton en neutron). In Hoofdstuk 5 laten we zien dat de ratio van het deuteron- en het nucleon-EDM een zeer goede indicator is van het fundamentele CP-violerende mechanisme. Als er een deuteron-EDM gemeten wordt die significant groter is dan die van het nucleon, kunnen we concluderen dat $\bar{\theta}$ niet verantwoordelijk is. Er is dan dus natuurkunde buiten het SM gevonden! In dit geval kunnen we zelfs aanwijzen welke van de nieuwe lokale interacties verantwoordelijk is. Dit zou grote implicaties hebben voor de elementaire deeltjesfysica. In het geval dat er een deuteron-EDM gemeten wordt die dicht bij die van het nucleon ligt, kunnen we nog niet zeggen of de $\bar{\theta}$ term verantwoordelijk is of dat er nieuwe fysica is gemeten. In dit geval zou een meting van een exotische eigenschap van het deuteron uitkomst kunnen bieden. Het deuteron heeft namelijk naast een EDM nog een andere T-violerende eigenschap, een zogenaamd magnetisch quadrupoolmoment (MQM). Alleen de $\bar{\theta}$ term voorspelt dat het deuteron-MQM groter is dan het deuteron-EDM, zodat het MQM een unieke gevoeligheid heeft.

De conclusies in Hoofdstuk 5 zijn gebaseerd op een aantal aannames over de interacties tussen nucleonen. In Hoofdstuk 6 worden deze aannames losgelaten. We concluderen dat onze resultaten in Hoofdstuk 5 niet significant veranderen. Ook breiden we onze berekeningen uit naar kernen bestaand uit drie nucleonen: de heliumkern (bestaande uit twee protonen en een neutron) en de tritiumkern (bestaande uit een proton en twee neutronen). Metingen aan de EDMs van deze deeltjes zouden nog meer informatie geven over het mechanisme van T-violatie.

Ons theoretisch raamwerk kan relatief eenvoudig worden uitgebreid naar de EDMs van andere lichte kernen mochten die experimenteel interessant worden.

Concludered kunnen we zeggen dat een experimenteel programma om de EDMs van nucleonen en lichte kernen te meten zeer interessante informatie kan verschaffen over nieuwe, nog niet ontdekte, bronnen van T- en CP-violatie. De resultaten in dit proefschrift dienen als leidraad om de experimentele resultaten te interpreteren. Deze interpretatie kan van groot belang zijn voor openstaande problemen in de natuurkunde zoals de verhouding tussen materie en antimaterie in het universum en het sterke CP-probleem. Ook kan dit proefschrift worden gebruikt om te bepalen welke experimenten prioriteit dienen te krijgen.

Acknowledgements

I did not complete this project by myself despite the single name on the cover. There are quite a lot of people who made very important contributions to this thesis or helped me in other ways during the last years. I would like to thank these people here.

I should start, of course, with my promotor Rob Timmermans who, not by coincidence, was also my adviser for my Master's thesis. I thank you for providing me with interesting research topics and ideas on how to pursue them. I like that you always gave me a lot of freedom to work on whatever I thought was interesting. You have given me many opportunities to develop myself such as my stay in Tucson, talks on conferences, and the Lindau Nobel Laureate meeting. You have been extremely supportive on issues besides physics as well. I am particularly grateful for that. Besides all of this, I always enjoyed our casual interactions, especially our discussions about sports. I am sure that any year now you will beat me in the Tour de France KVI competition.

The second person I would like to thank is Bira van Kolck. You have taught me a lot about physics, in particular about effective field theories. I have always been impressed by your physical insight and your relaxed way of being (your coffee habits spring to mind). From the first mail I sent you about 3 to 4 years ago, you have given me tons of advice (not limited to physics) from which I have benefited a lot. I very much enjoyed the endless discussion sessions about power counting whenever you were in Groningen. I also would like to thank you for hosting my great stay in Tucson and for being in my reading committee. I hope that we will keep collaborating in the future.

I particularly would like to thank Emanuele Mereghetti, with whom I collaborated on almost everything I have worked on in the last years. I very much liked learning and researching effective field theories together. We must have exchanged hundreds of emails even though we only met twice in person. Hopefully, we will keep working together and this will change in the future.

I am grateful to Cheng-Pang Liu for the collaboration on the nonperturbative calculations. I enjoyed the few weeks you spent at KVI when we worked on the light-nuclear EDM paper. I would like to thank Renato Higa, Will Hockings, Claudio Maekewa, and Ionel Stetcu, for working together on various projects.

Last year I spent a week in Jülich to discuss the calculation of electric dipole moments. I would link to thank Christoph Hanhart, Andreas Wirzba, Jan Bsaisou, and Andreas Nogga, for the good time I had. I also enjoyed the EDM storage ring meeting in Bad Honnef. Hopefully this year's meeting will be as good. I am looking forward to joining you in Jülich next year.

I have always liked working at the theory group of the KVI. Thanks to Daniel Boer, Olaf Scholten, and Lex Dieperink, for encouragement and nice discussions about physics. Auke, Daren, Jacob, Keri, Laura, Lotje, Olena, Renato, Sophie, and Wouter, thanks for being great colleagues and friends. I also greatly enjoyed meeting up for lunch, meetings, and football games with the theorists at the university. Of course, besides the theorists there are also other people at the KVI. I would like to thank Klaus Jungmann for encouragement and writing letters of recommendation for me. Ronnie Hoekstra, thanks for all the laughs and all the cynical comments

about me solving integrals and theory in general. I still think you are not too old to learn some real physics. Gerco Onderwater, thanks for being supportive and enthusiastic and always telling the same stories which take half an hour. Hans Beijers thanks for always showing a lot of interest in my work. I would like to thank Ayan, Daniel, David, Duurt, Hans, Joost, Mayerlin, Ola, Olga, Oscar, Stefan, Steven, and Wendy because they made my time at KVI a good one. Bodha, Corine, and Wilbert, thanks for being such good office mates. Amarins, thanks for helping me out so often and for all the chats. I expect you to stay until the end of my party. Thanks to Annet, Carla, Eveline, Grietje, Harry, Hilde, Marjan, Miranda, Robert, and Simone for taking care of many things for me. To all the people who joined in the Friday volleyball games: it was lots of fun.

I would like to thank Eric Bergshoeff and Eric Laenen for being in my reading committee. I am also grateful to Eric Laenen for hosting the monthly (or so) TPP meetings in Amsterdam where I learned lots of new physics and met a lot of fellow theorists of whom many have become friends. Thanks to Irene, Jan, Jan, Jorn, Lisa, Marieke, Reinier, Rob, Sander, Thijs, and Wim for lessening the burden of waking up at six o' clock in the morning to be on time for the first talk at Nikhef. I am impressed that some of you even made the trip to Groningen on a few occasions. Also thanks for the great (but tough) times at the DRSTP schools. In particular, I would like to acknowledge Wilco den Dunnen for being my paranymph and being a good friend. We had great times at many conferences and on our trip to Rio (thanks Ana for hosting us and showing us the city!). In the last four years I got really ill twice, both occasions occurring after spending a week around you. There probably is a correlation with your philosophy that one must never leave a bar if they are still willing to serve (beer). Thanks to Hannah as well for allowing me to spend the night whenever I visited Amsterdam.

Krijn de Vries, thanks for being my paranymph and for being a lousy roommate the last couple of years, one who never cleans up anything. Despite the fact that you support the wrong team, I still consider you to be quite an intelligent guy. Thanks for the good times. The same holds for my friends Henri (a bit better roommate I have to say), Martin, and Stijn.

A big thanks to my group of best friends from Zwolle, in particular to Aiden, A-yong, Erwin, Frank, Ivo, Jeroen, and Vincent. We have stuck together for over ten years now and visited a dozen of countries on dozens of trips. I cannot even begin to imagine how many times we went out together, never mind all the associated stories. Some of which I would gladly forget. I consider you guys very dearly. Thanks to Frank and Vincent for the great time we had living together in Groningen after the first horrible year when I lived with Erwin. Word out to Ivo for designing my cover. Also thanks to Anke, Ilse, Marije, Neri, and Robin for the Zwolle reunions and all the other occasions we met up.

I should say something here about my football team as well. However, the fact that, despite my considerable talent, we never ended up first in the league makes this somewhat difficult. Even though, thanks to AJ, Boelie, Daan, Gerrit, Jos, Kornelis, Steven, Ralph, and Wijbren for all the fun times we had and games we played (lost).

I am very grateful to my parents, my sister (also for our great road trip through Arizona), Roy (and our skiing trips), and my grandmother for the constant support and love during all my life. You have never let me down. Corien, thanks for being such a great girlfriend and for helping me out all the time. Living together this last year has been extremely nice (apart from you waking up absurdly early). Hopefully we can continue to do so in the near future despite that I am moving to Germany.

List of Publications

1. J. de Vries, E. Mereghetti, R. G. E. Timmermans, and U. van Kolck
The Nucleon Electric Dipole Form Factor from Dimension-Six Time-Reversal Violation
Phys. Lett. B **695**, 268 (2011).

2. E. Mereghetti, J. de Vries, W.H. Hockings, C.M. Maekawa, and U. van Kolck
The Electric Dipole Form Factor of the Nucleon in Chiral Perturbation Theory to Subleading Order
Phys. Lett. B **696**, 97 (2011).

3. J. de Vries, E. Mereghetti, R. G. E. Timmermans, and U. van Kolck
The P- and T-odd Form Factors of the Deuteron
Phys. Rev. Lett. **107**, 091804 (2011).

4. C. M. Maekawa, E. Mereghetti, J. de Vries, and U. van Kolck
The Time- Reversal- and Parity-Violating Nuclear Potential in Chiral Effective Theory
Nucl. Phys. A **872**, 117 (2011).

5. J. de Vries, R. Higa, C.-P. Liu, E. Mereghetti, I. Stetcu, R. G. E. Timmermans, and U. van Kolck
The Electric Dipole Moments of Light Nuclei from Chiral Effective Field Theory
Phys. Rev. C **84**, 065501 (2011).

6. C.-P. Liu, J. de Vries, E. Mereghetti, R. G. E. Timmermans, and U. van Kolck
Deuteron Magnetic Quadrupole Moment From Chiral Effective Field Theory
Phys. Lett. B **713**, 447 (2012).

7. J. de Vries
Parity- and Time-Reversal-Violating Moments of Light Nuclei
Contribution to the proceedings of the 5th International Symposium on Symmetries in Subatomic Physics, arXiv:hep-ph/1207.6968 (2012)

8. J. de Vries, E. Mereghetti, R. G. E. Timmermans, and U. van Kolck
The Chiral Lagrangian from Dimension-Six Time-Reversal Violation, in preparation.

9. J. de Vries, E. Mereghetti, R. G. E. Timmermans, and U. van Kolck
The Deuteron P- and T-odd Electromagnetic Form Factors to Subleading Order, in preparation.

10. J. de Vries, C.-P. Liu, and R. G. E. Timmermans
Time-Reversal Violation in Nuclear, Atomic, and Solid State Systems
Commissioned review article for Prog. Part. Nucl. Phys, deadline: 12/2012.

Bibliography

[1] T. D. Lee and C. -N. Yang, Phys. Rev. **104**, 254 (1956).

[2] C. S. Wu, E. Ambler, R. W. Hayward, D. D. Hoppes and R. P. Hudson, Phys. Rev. **105**, 1413 (1957).

[3] J. H. Christenson, J. W. Cronin, V. L. Fitch and R. Turlay, Phys. Rev. Lett. **13**, 138 (1964).

[4] A. Angelopoulos *et al.* [CPLEAR Collaboration], Phys. Lett. B **444**, 43 (1998); C. Cheng [BABAR Collaboration], talk at the Symposium on Symmetries in Subatomic Physics 2012, Groningen, June 2012.

[5] M. Kobayashi and T. Maskawa, Prog. Theor. Phys. **49**, 652 (1973).

[6] G. 't Hooft, Phys. Rev. Lett. **37**, 8 (1976); G. 't Hooft, Phys. Rev. D **14**, 3432 (1976) [Erratum-ibid. D **18**, 2199 (1978)].

[7] E. M. Purcell and N. F. Ramsey, Phys. Rev. **78**, 807 (1950); J. H. Smith, E. M. Purcell and N. F. Ramsey, Phys. Rev. **108**, 120 (1957).

[8] C. A. Baker *et al.*, Phys. Rev. Lett. **97**, 131801 (2006).

[9] M. Pospelov and A. Ritz, Ann. Phys. **318**, 119 (2005).

[10] I. B. Khriplovich and A. R. Zhitnitsky, Phys. Lett. B **109**, 490 (1982).

[11] A. Czarnecki and B. Krause, Phys. Rev. Lett. **78**, 4339 (1997).

[12] A. D. Sakharov, Pisma Zh. Eksp. Teor. Fiz. **5** ,32 (1967) [JETP Lett. **5**, 24 (1967)] [Sov. Phys. Usp. **34**, 392 (1991)] [Usp. Fiz. Nauk **161**, 61 (1991)].

[13] A.G. Cohen, D.B. Kaplan, and A.E. Nelson, Ann. Rev. Nucl. Part. Sci. **43**, 27 (1993); A. Riotto and M. Trodden, Ann. Rev. Nucl. Part. Sci. **49**, 35 (1999).

[14] V. A. Kuzmin, M. E. Shaposhnikov and I. I. Tkachev, Phys. Rev. D **45**, 466 (1992).

[15] T. M. Ito, J. Phys. Conf. Ser. **69**, 012037 (2007); M. G. D. van der Grinten *et al.* [CryoEDM Collaboration], Nucl. Instrum. Meth. A **611**, 129 (2009); I. Altarev, G. Ban, G. Bison, K. Bodek, M. Burghoff, M. Cvijovic, M. Daum and P. Fierlinger *et al.*, Nucl. Instrum. Meth. A **611**, 133 (2009).

[16] W. C. Griffiths *et al.*, Phys. Rev. Lett. **102**, 101601 (2009).

[17] V. F. Dmitriev and R. A. Sen'kov, Phys. Rev. Lett. **91**, 212303 (2003).

[18] B. C. Regan, E. D. Commins, C. J. Schmidt and D. DeMille, Phys. Rev. Lett. **88**, 071805 (2002).

[19] J. J. Hudson, D. M. Kara, I. J. Smallman, B. E. Sauer, M. R. Tarbutt and E. A. Hinds, Nature **473**, 493 (2011).

[20] F. J. M. Farley *et al.*, Phys. Rev. Lett. **93**, 052001 (2004); Y. F. Orlov, W. M. Morse, and Y. K. Semertzidis, Phys. Rev. Lett. **96**, 214802 (2006); C. J. G. Onderwater, J. Phys. Conf. Ser. **295**, 012008 (2011).

[21] G. W. Bennett *et al.* [Muon (g-2) Collaboration], Phys. Rev. D **80**, 052008 (2009).

[22] Y. K. Semertzidis, arXiv:1110.3378; C. J. G. Onderwater, arXiv:1204.2512.

[23] A. C. Vutha, W. C. Campbell, Y. V. Gurevich, N. R. Hutzler, M. Parsons, D. Patterson, E. Petrik and B. Spaun *et al.*, J. Phys. B B **43**, 074007 (2010).

[24] M. E. Pospelov and I. B. Khriplovich, Sov. J. Nucl. Phys. **53**, 638 (1991) [Yad. Fiz. **53**, 1030 (1991)].

[25] A. Adelmann, K. Kirch, C. J. G. Onderwater and T. Schietinger, J. Phys. G G **37**, 085001 (2010).

[26] Y. K. Semertzidis, J. Phys. Conf. Ser. **335**, 012012 (2011).

[27] V. V. Flambaum, I. B. Khriplovich and O. P. Sushkov, Sov. Phys. JETP **60**, 873 (1984); J. F. Donoghue, B. R. Holstein and M. J. Musolf, Phys. Lett. B **196**, 196 (1987); V. M. Khatsimovsky, I. B. Khriplovich and A. S. Yelkhovsky, Annals Phys. **186**, 1 (1988); X. -G. He and B. McKellar, Phys. Rev. D **46**, 2131 (1992).

[28] A. Pich, "Effective field theory: Course," hep-ph/9806303.

[29] D. B. Kaplan, nucl-th/9506035.

[30] G. Aad *et al.* [ATLAS Collaboration], Phys. Lett. B [arXiv:1207.7214 [hep-ex]]; S. Chatrchyan *et al.* [CMS Collaboration], Phys. Lett. B [arXiv:1207.7235 [hep-ex]].

[31] R.J. Crewther, P. Di Vecchia, G. Veneziano, and E. Witten, Phys. Lett. B **88**, 123 (1979); **91**, 487(E) (1980).

[32] W. Buchmuller and D. Wyler, Nucl. Phys. B **268** 621 (1986).

[33] S. Weinberg, Phys. Rev. Lett. **63**, 2333 (1989).

[34] A. De Rújula, M. B. Gavela, O. Pène, and F. J. Vegas, Nucl. Phys. B **357**, 311 (1991).

[35] M. J. Ramsey-Musolf and S. Su, Phys. Rept. **456**, 1 (2008).

[36] B. Grzadkowski, M. Iskrzynski, M. Misiak and J. Rosiek, JHEP **1010**, 085 (2010).

[37] S. Weinberg, Phys. Rev. Lett. **43**, 1566 (1979).

[38] G. Isidori, J. F. Kamenik, Z. Ligeti and G. Perez, Phys. Lett. B **711**, 46 (2012); R. Aaij *et al.* [LHCb Collaboration], Phys. Rev. Lett. **108**, 111602 (2012).

[39] E. Braaten, C. S. Li and T. C. Yuan, Phys. Rev. D **42**, 276 (1990).

[40] J. Ng and S. Tulin, Phys. Rev. D **85**, 033001 (2012).

[41] J. F. Kamenik, M. Papucci and A. Weiler, Phys. Rev. D **85**, 071501 (2012).

[42] A. Cordero-Cid, J. M. Hernandez, G. Tavares-Velasco and J. J. Toscano, J. Phys. G **35**, 025004 (2008).

[43] E. Braaten, C. S. Li and T. C. Yuan, Phys. Rev. Lett. **64**, 1709 (1990); A. De Rujula, M. B. Gavela, O. Pene and F. J. Vegas, Phys. Lett. B **245**, 640 (1990).

[44] G. Degrassi, E. Franco, S. Marchetti and L. Silvestrini, JHEP **0511**, 044 (2005).

[45] H. An, X. Ji and F. Xu, JHEP **1002**, 043 (2010).

[46] K. Fujikawa, Phys. Rev. Lett. **42**, 1195 (1979).

[47] V. Baluni, Phys. Rev. D **19**, 2227 (1979).

[48] E. Mereghetti, W. H. Hockings, and U. van Kolck, Ann. Phys. **325**, 2363 (2010).

[49] F. Xu, H. An and X. Ji, JHEP **1003**, 088 (2010).

[50] R. S. Conti and I. B. Khriplovich, Phys. Rev. Lett. **68**, 3262 (1992); J. Engel, P. H. Frampton and R. P. Springer, Phys. Rev. D **53**, 5112 (1996); M. J. Ramsey-Musolf, Phys. Rev. Lett. **83**, 3997 (1999) [Erratum-ibid. **84**, 5681 (2000)].

[51] C. Jarlskog, Phys. Rev. Lett. **55**, 1039 (1985).

[52] M. E. Pospelov, Phys. Lett. B **328**, 441 (1994).

[53] T. Ibrahim and P. Nath, Rev. Mod. Phys. **80**, 577 (2008).

[54] S. Weinberg, Physica **96A**, 327 (1979); J. Gasser and H. Leutwyler, Ann. Phys. **158**, 142 (1984); Nucl. Phys. **B250**, 465 (1985).

[55] V. Bernard, N. Kaiser, and U.-G Meißner, Int. J. Mod. Phys. E **4**, 193 (1995).

[56] U. van Kolck, Prog. Part. Nucl. Phys. **43** (1999) 337; P.F. Bedaque and U. van Kolck, Ann. Rev. Nucl. Part. Sci. **52** (2002) 339; E. Epelbaum, H.-W. Hammer, and U.-G. Meißner, Rev. Mod. Phys. **81**, 1773 (2009).

[57] E. E. Jenkins and A. V. Manohar, Phys. Lett. B **255**, 558 (1991).

[58] M. E. Luke and A. V. Manohar, Phys. Lett. B **286**, 348 (1992).

[59] W. Kilian and T. Ohl, Phys. Rev. D **50**, 4649 (1994).

[60] R. Sundrum, Phys. Rev. D **59**, 085009 (1999).

[61] S. Weinberg, *The Quantum Theory of Fields*, Vol. 2 (Cambridge University Press, Cambridge, 1996).

[62] U. van Kolck, Ph.D. dissertation, University of Texas (1993); Few Body Syst. Suppl. **9**, 444 (1995).

[63] A. V. Manohar and H. Georgi, Nucl. Phys. B **234**, 189 (1984).

[64] S. Weinberg, Phys. Lett. B **251**, 288 (1990); Nucl. Phys. B **363**, 3 (1991).

[65] A. Nogga, R. G. E. Timmermans, and U. van Kolck, Phys. Rev. C **72**, 054006 (2005);

[66] S. R. Beane, P. F. Bedaque, M. J. Savage, and U. van Kolck, Nucl. Phys. A **700**, 377 (2002); M. C. Birse, Phys. Rev. C **74**, 014003 (2006); **76**, 034002 (2007); M. Pavón Valderrama, Phys. Rev. C **83**, 024003 (2011); B. Long and C. J. Yang, Phys. Rev. C **84**, 057001 (2011).

[67] K. Nakamura [Particle Data Group], J. Phys. G **37**, 075021 (2010).

[68] V. Bernard, N. Kaiser, J. Kambor, and U.-G. Meißner, Nucl. Phys. B **388**, 315 (1992); N. Fettes, U.-G. Meißner, and S. Steininger, Nucl. Phys. A **640**, 199 (1998).

[69] J.L. Friar, U. van Kolck, M.C.M. Rentmeester, and R.G.E. Timmermans, Phys. Rev. C **70**, 044001 (2004).

[70] U. van Kolck, J.L. Friar, and T. Goldman, Phys. Lett. B **371**, 169 (1996).

[71] S.R. Beane, K. Orginos, and M.J. Savage, Nucl. Phys. B **768**, 38 (2007).

[72] U. van Kolck, J.A. Niskanen, and G.A. Miller, Phys. Lett. B **493**, 65 (2000); D.R. Bolton and G.A. Miller, Phys. Rev. C **81**, 014001 (2010); A. Filin *et al.*, Phys. Lett. B **681**, 423 (2009).

[73] J. Gasser and H. Leutwyler, Phys. Rep. **87**, 77 (1982).

[74] U. van Kolck, M.C.M. Rentmeester, J.L. Friar, T. Goldman, and J.J. de Swart, Phys. Rev. Lett. **80**, 4386 (1998); N. Kaiser, Phys. Rev. C **73**, 044001 (2006).

[75] A. V. Manohar, Phys. Rev. D **56**, 230 (1997).

[76] S. D. Thomas, Phys. Rev. D **51**, 3955 (1995).

[77] W. Fischler, S. Paban, and S. Thomas, Phys. Lett. B **289**, 373 (1992).

[78] C. M. Maekawa, E. Mereghetti, J. de Vries, and U. van Kolck, Nucl. Phys. A **872**, 117 (2011).

[79] W. H. Hockings and U. van Kolck, Phys. Lett. B **605**, 273 (2005).

[80] I. B. Khriplovich and R. A. Korkin, Nucl. Phys. A **665**, 365 (2000).

[81] C.-P. Liu and R. G. E. Timmermans, Phys. Rev. C **70**, 055501 (2004).

[82] I. Stetcu, C.-P. Liu, J. L. Friar, A. C. Hayes, and P. Navrátil, Phys. Lett. B **665**, 168 (2008).

[83] V. F. Dmitriev, R. A. Sen'kov and N. Auerbach, Phys. Rev. C **71**, 035501 (2005); J. H. de Jesus and J. Engel, Phys. Rev. C **72**, 045503 (2005); J. Dobaczewski and J. Engel, Phys. Rev. Lett. **94**, 232502 (2005); S. Ban, J. Dobaczewski, J. Engel and A. Shukla, Phys. Rev. C **82**, 015501 (2010).

[84] S. Narison, Phys. Lett. B **666**, 455 (2008); K. Ottnad, B. Kubis, U.-G. Meißner, and F.-K. Guo, Phys. Lett. B **687**, 42 (2010).

[85] V. M. Khatsymovsky and I. B. Khriplovich, Phys. Lett. B **296**, 219 (1992).

[86] V. P. Gudkov, Z. Phys. A **343**, 437 (1992).

[87] R. Arnowitt, J. L. Lopez, and D. V. Nanopoulos, Phys. Rev. D **42**, 2423 (1990); R. Arnowitt, M. J. Duff, and K. S. Stelle, Phys. Rev. D **43**, 3085 (1991).

[88] C. Dib, A. Fäßler, T. Gutsche, S. Kovalenko, J. Kuckei, V. E. Lyubovitskij, and K. Pumsaard, J. Phys. G **32**, 547 (2006).

[89] R. Lewis and N. Mobed, Phys. Rev. D **59**, 073002 (1999); B. Kubis and R. Lewis, Phys. Rev. C **74**, 015204 (2006); V. Bernard, N. Kaiser, J. Kambor, and U.-G. Meißner, Nucl. Phys. B **388**, 315 (1992); V. Bernard, H.W. Fearing, T.R. Hemmert, and U.-G. Meißner, Nucl. Phys. A **635**, 121 (1998), (E) **642**, 563 (1998).

[90] C. M. Maekawa and U. van Kolck, Phys. Lett. B **478**, 73 (2000); C. M. Maekawa, J. S. Veiga, and U. van Kolck, Phys. Lett. B **488**, 167 (2000).

[91] S. R. Beane, P. F. Bedaque, K. Orginos and M. J. Savage, Phys. Rev. Lett. **97**, 012001 (2006).

[92] D. B. Kaplan, M. J. Savage, and M. B. Wise, Nucl. Phys. **B534**, 329 (1998); D. B. Kaplan, M. J. Savage, and M. B. Wise, Phys. Lett. **B424** , 390-396 (1998).

[93] T. Mehen and I. W. Stewart, Phys. Rev. C **59** 2365 (1999).

[94] D.B. Kaplan, M.J. Savage, and M.B. Wise, Phys. Rev. C **59**, 617 (1999).

[95] S. Fleming, T. Mehen, and I.W. Stewart, Nucl. Phys. **A677**, 313 (2000).

[96] O. Lebedev, K.A. Olive, M. Pospelov, and A. Ritz, Phys. Rev. D **70**, 016003 (2004).

[97] O. P. Sushkov, V. V. Flambaum, and I. B. Khriplovich, Sov. Phys. JETP **60**, 873 (1984).

[98] Y. Avishai, Phys. Rev. D **32**, 314 (1985).

[99] I. R. Afnan and B. F. Gibson, Phys. Rev. C **82**, 064002 (2010).

[100] Y. Avishai and M. Fabre de la Ripelle, Phys. Rev. Lett. **56**, 2121 (1986); Nucl. Phys. **A468**, 578 (1987).

[101] P. Herczeg, Nucl. Phys. **75**, 655 (1966); C.-P. Liu and R. G. E. Timmermans, Phys. Lett. B **634**, 488 (2006).

[102] V. G. J. Stoks, R. A. M. Klomp, C. P. F. Terheggen, and J. J. de Swart, Phys. Rev. C **49**, 2950 (1994).

[103] R. B. Wiringa, V. G. J. Stoks, and R. Schiavilla, Phys. Rev. C **51**, 38 (1995).

[104] D. R. Entem and R. Machleidt, Phys. Rev. C **68**, 041001(R) (2003); E. Epelbaum, A. Nogga, W. Glöckle, H. Kamada, U.G. Meißner, and H. Witała, Phys. Rev. C **66**, 064001 (2002).

[105] S. Weinberg, Phys. Lett. B **295**, 114 (1992).

[106] D. R. Phillips, Phys. Lett. B **567**, 12 (2003).

[107] C.-P. Liu, Phys. Rev. C **75**, 065501 (2007).

[108] W.C. Haxton and E.M. Henley, Phys. Rev. Lett. **51**, 1937 (1983).

[109] P. Navrátil, J. P. Vary, and B. R. Barrett, Phys. Rev. Lett. **84**, 5728 (2000); Phys. Rev. C **62**, 054311 (2000).

[110] P. Navrátil, G. Kamuntavicius, and B. R. Barrett, Phys. Rev. C **61**, 044001 (2000).

[111] M. Binger, arXiv:nucl-th/9901012.

[112] G. Passarino and M. J. G. Veltman, Nucl. Phys. B **160**, 151 (1979).

[113] S. Kolling, E. Epelbaum, H. Krebs and U. -G. Meissner, Phys. Rev. C **84**, 054008 (2011).